4

BULLETIN
OF THE
CHEMICAL SOCIETY OF JAPAN

Volume 13

1938

Editor: Yoshiyuki URUSHIBARA

Associate Editors:

Yasuhiko ASAHINA
Keijirō ASŌ
Masumi CHIKASHIGE
Shinkichi HORIBA
Satoyasu IIMORI
Fusao ISHIKAWA
Samuro KAKIUCHI
Masao KATAYAMA
Matsusuke KOBAYASHI
Shigeru KOMATSU
Bennosuke KUBOTA
Rikō MAJIMA
Koichi MATSUBARA
Motooki MATSUI
Shinroku MITSUKURI
Willy NAGAI
Hiroshi NOMURA
Yukichi OSAKA
Jitsusaburo SAMESHIMA
Keita SHIBATA
Yuji SHIBATA
Yoshio TANAKA
Yohei YAMAGUCHI
Isaburo WADA

Published by

The Chemical Society of Japan

c/o Faculty of Science, Imperial University of Tokyo

QD 1
C 54
V.13

OHIO STATE
UNIVERSITY

CONTENTS OF VOLUME 13, 1938.

No. 1. JANUARY.

The papers published in this number are dedicated to Dr. Masao Katayama by his pupils in celebration of his sixtieth birthday.

Professor Masao KATAYAMA (with a Portrait) 1

Hikoichi SHIBA and Shintaro TANABE: Rotatory Dispersion of Sugars in Liquid Ammonia and in Water 3

Kenjiro KIMURA: X-Ray Spectroscopic Determination of Lanthanum, Neodymium and Gadolinium in the Presence of Other Rare Earth Elements 10

Isamu NITTA and Tokunosuké WATANABÉ: X-Ray Investigation of the Cubic Modification of Pentaerythritol, $C(CH_2OH)_4$ 28

Isamu NITTA and Katsuji SUENAGA: On the Thermal Transition in Solid Deuterio-Ammonium Sulphate, $(ND_4)_2SO_4$ 36

Shun-ichi SATOH: The Heat of Formation and the Specific Heat of Silicon Nitride 41

Fumio HIRATA: The Theory on the Constitution of a Thermoreversible Gel 49

Bunnosuke YAMAGUCHI: Constitution and Viscosity Association of High-molecular-weight Hydrocarbons 61

Sunao IMANISHI: On the Use of Interference Spectrographs for the Study of Fine Structures in Molecular Spectra 77

Masao KOIZUMI und Toshizo TITANI: Über den Austausch der Wasserstoffatome zwischen Pyrrol, Indol sowie ihren Methylderivaten und Wasser. I. Austausch der Wasserstoffatome zwischen Pyrrol und Wasser 85

Masao KOIZUMI und Toshizo TITANI: Über den Austausch der Wasserstoffatome zwischen Pyrrol, Indol sowie ihren Methylderivaten und Wasser. II. Austausch der Wasserstoffatome zwischen Thiophen sowie Furan und Wasser. 95

Noriyoshi MORITA, Kokiti GOTO und Toshizo TITANI: Über den Gehalt der Kohlenhydrate an schwerem Sauerstoff 99

Takewo TIKU: Experimental Studies on the Electrochemical Polarisation Produced in the Cylindrical Mass of Litharge. I 110

Isamu SANO: On the Catalytic Decomposition of Hydrogen Peroxide by Colloidal Platinum-carbonyl 118

E05600

Hideo AKAMATU: Studies on the Oiliness of Liquids. V. Lubricants Consisting of Two or Three Chemical Compounds. 127

Tunetaka SASAKI: Studies on the Oiliness of Liquids. VI. Measurements of the Kinetic Friction Coefficients by the Method of Sliding Velocity 134

Monzi TATIMORI: Polymerisation of Tung Oil. I. 142

Takeo IIMORI: A Study of Passivity of Iron Using Electron Diffraction 152

Ken-iti HIGASI: Dipole Moments of Benzil and Stilbene Dichloride. 158

Masaji KUBO: Zur Theorie der Dielektrizitätskonstante des Gases unter hohem Druck. 167

San-ichiro MIZUSHIMA and Masaji KUBO: Quantum Mechanical Resonance and Internal Rotation 174

San-ichiro MIZUSHIMA and Yonezo MORINO: The Motion of Ethylene Halide Molecules in Crystals as Revealed by the Raman Effect. 182

Yonezo MORINO: The Normal Vibrations of Ethylene Halides . . 189

Yukichi GO, Saburo NAGATA und Jiro KAKINOKI: Über die Intensitätsverteilung der Faserdiagramme 198

Juro HORIUTI: On the Statistical Mechanical Treatment of the Absolute Rate of Chemical Reaction 210

Juro HORIUTI and Go OKAMOTO: The Mechanism of the Hydrogen Electrode Process. I. The Catalytic Mechanism 216

Kozo HIROTA and Juro HORIUTI: The Mechanism of the Hydrogen Electrode Process. II. The Electrochemical Mechanism. The Existence of Hydrogen Molecule Ions on the Surface of the Electrode 228

Bunichi TAMAMUSHI: Zur Kenntnis des Aufbaues thixotroper Systeme 234

Eizo KANDA: The Adsorption of Helium on Charcoal below 78°K., and Production and Thermometry of Low Temperatures 241

No. 2. FEBRUARY.

Hideo SHISHIDO: Hofmannscher Abbau von Domesticin-äthern . . 247

Tokuichi TSUMAKI: Nebenvalenzringverbindungen. IV. Über einige innerkomplexe Kobaltsalze der Oxyaldimine 252

Arata IWAMURA: Quantitative Spectral Analysis. IX. Determination of Caesium by Emission-Spectra 260

Arata IWAMURA: Quantitative Spectral Analysis. X. Determination of Lithium by Emission-Spectra 265

Shozo FUKUNAGA and Bennosuke KUBOTA: Synthesis of *l*-Talose. 272

Haruki FUJIMOTO: The Oxidation of Methane 281

Shiro AKABORI und Katuhiko KASIMOTO: Über die chemische Natur der Taka-Amylase. II. Über das Molekulargewicht der Taka-Amylase 291

Masao KOIZUMI und Toshizo TITANI: Über den Austausch der Wasserstoffatome zwischen Pyrrol, Indol sowie ihren Methylderivaten und Wasser. III. Austausch der Wasserstoffatome zwischen *N*-Methylpyrrol und Wasser 298

Masao KOIZUMI und Toshizo TITANI: Polymerisation von Styrol in schwerem Wasser und schwerem Alkohol. (Vorläufige Mitteilung). 304

No. 3. MARCH.

Masao KOIZUMI und Toshizo TITANI: Über den Austausch der Wasserstoffatome zwischen Pyrrol, Indol sowie ihren Methylderivaten und Wasser. IV. Austausch der Wasserstoffatome zwischen Indol und Wasser 307

Masao KOIZUMI und Toshizo TITANI: Austauschreaktion der H-Atome zwischen Nitrophenole und Wasser. I. Austauschreaktion und Wasserstoffbindung 318

Toshizo TITANI, Noriyoshi MORITA und Kokiti GOTO: Ein Versuch zur Austauschreaktion der Sauerstoffatome zwischen Carbonat-Ion und Wasser. (Vorläufige Mitteilung) 329

Yoshiyuki URUSHIBARA and Matsuji TAKEBAYASHI: The Addition of Hydrogen Bromide to Undecenoic Acid in Toluene Solution. I. The Effect of Reduced Nickel 331

No. 4. APRIL.

Yojiro TSUZUKI: Distribution of Diethyl Tartrate between Ether and Aqueous Borate Solution and a Contribution to the Studies on the Equilibrium of the Boro-Diol Complex Formation 337

Buhei SAKURAI: Electrolytic Reduction of *N*-Phenyl-succinimide . . 350

Ryutaro TSUCHIDA: On Experimental Conditions for the Half-shadow Polarimetry . . . . . .

Noriyoshi MORITA und Toshizo TITANI: Der katalytische Isotopenaustausch des gasförmigen Sauerstoffs. I. Die Austauschreaktion der Sauerstoffatome zwischen Sauerstoff und Wasserdampf sowie Kohlendioxyd auf der Oberfläche des Platinschwamms und metallischen Platins 357

Toshio ANDO: Iso-neoergosterol 371

No. 5. MAY.

Taku UÉMURA et Naoichi HIRASAWA: Recherches sur la concentration des ions d'hydrogène contenus dans les solutions aqueuses des ammines-cobaltiques complexes et sur leurs spectres d'absorption. IV. Solutions aqueuses des complexes renfermant la molécule d'éthylènediamine 377

Ryutaro TSUCHIDA: Absorption Spectra of Co-ordination Compounds. I 388

Yoshiyuki URUSHIBARA and Matsuji TAKEBAYASHI: The Addition of Hydrogen Bromide to Allyl Bromide in the Presence of Various Substances. VII. The Effect of Nickel in the Form of Filings, and the Influence of Antioxidants on the Actions of Oxygen and Reduced Nickel 400

Yoshiyuki URUSHIBARA and Matsuji TAKEBAYASHI: The Addition of Hydrogen Bromide to Undecenoic Acid in Toluene Solution. II. The Influence of Antioxidants on the Actions of Oxygen and Reduced Nickel 404

Yoshiyuki URUSHIBARA and Osamu SIMAMURA: The Supposed Activation of Hydrogen Bromide by Oxygen. (Preliminary Note) 407

No. 6. JUNE.

Toshizo TITANI und Noriyoshi MORITA: Die Vergleichung der Dichte des Leitungswassers von Osaka, Japan und von Cambridge, U.S.A. 409

Noriyoshi MORITA und Toshizo TITANI: Wiederbestimmung des Deuterium-Protium-Verhältnisses in gewöhnlichem Wasser . . . 419

Masao KOIZUMI und Toshizo TITANI: Zur Kenntnis der Austauschgeschwindigkeit der Wasserstoffatome zwischen Zucker und Wasser. 427

Ryutaro TSUCHIDA: Absorption Spectra of Co-ordination Compounds. II 436

Hideo SUEDA: On the Relation between the Configuration of Metallic Complex Salts and their Absorption Spectra. II. *cis*-Trinitro-triammine-cobalt 450

Shiro AKABORI und Katuhiko KASIMOTO: Über den „Papain-Amylase-Symplex" (Über die chemische Natur der Taka-Amylase. III.) 453

Hideo AKAMATU: Sedimentation Volume and Thixotropy 456

Masao KOIZUMI und Toshizo TITANI: Austauschreaktion der Sauerstoffatome zwischen Wasser und einigen organischen Verbindungen. (Vorläufige Mitteilung) 463

No. 7. JULY.

Haruomi ÔEDA: On Some 2,5-Dialkyl-piperazines 465

Ryutaro TSUCHIDA and Masahisa KOBAYASHI: Absorption Spectra of Co-ordination Compounds. III. Special Bands of Chromium Complexes 471

Sin'iti KAWAI and Koichi ASHINO: Synthesis of 3,4-Methylene-dioxyphenyl-glyoxal 480

Buhei SAKURAI: Electrolytic Reduction of Glutarimide and Its Derivatives 482

Toshizo ISEMURA: On the Silver Chromate Banding in Silicic Acid Gel 489

Toshizo ISEMURA: On the Calcium Phosphate Banding in Silicic Acid Gel 493

Saburo KOMORI and Sei-ichi UENO: On the Composition of "Akebi" Seed Oil 505

No. 8. AUGUST.

Taku UÉMURA et Yasuo INAMURA: Les spectres d'absorption des hydrocarbures azoïques et l'halochromie 509

Tunetaka SASAKI: On the Nature of Foam. I. Stability of the Foam Produced by the Aqueous Solutions of Alcohols and Acids . 517

Ryutaro TSUCHIDA and Tokuichi TSUMAKI: Absorption Spectra of Salicylaldehyde-ethylenediimine and Related Compounds 527

Shigeo OKUMURA: Über die chemische Natur des Papains. II. Reinigung des Papains durch Taka-Amylase 534

Kazuo YAMASAKI: Absorptionsspektren von Metallkomplexsalzen des 2,2′-Dipyridyls. II 538

Noriyoshi MORITA und Toshizo TITANI: Diffusion des an schwerem Wasserstoff sowie schwerem Sauerstoff angereicherten Wassers durch verdünntes Gelatingel 543

Bunichi TAMAMUSHI and Yaichi SEKIGUCHI: The Thixotropic and Plastic Behaviour of Suspensions of Barium Sulphate with Clay . 556

Yoshiyuki URUSHIBARA and Osamu SIMAMURA: The Isomerization of Isostilbene to Stilbene by Hydrogen Bromide in the Presence of Oxygen and of Ferromagnetic Metals 566

Yoshiyuki URUSHIBARA and Osamu SIMAMURA: On the Reaction of Gaseous Hydrogen Bromide with Reduced Nickel in the Presence of Oxygen 570

Yoshiyuki URUSHIBARA and Matsuji TAKEBAYASHI: The Addition of Hydrogen Bromide to Undecenoic Acid in Toluene Solution. III. The Influence of the Impurities in Undecenoic Acid on the Effects of Oxygen and of Reduced Nickel 574

No. 9. SEPTEMBER.

Tokuichi TSUMAKI: Nebenvalenzringverbindungen. III. Über einige innerkomplexe Eisen- und Mangansalze der Oxyaldimine 579

Tokuichi TSUMAKI: Nebenvalenzringverbindungen. V. Spektrochemische Untersuchungen über die innerkomplexen Metallsalze von Salicylaldehyd-äthylendiimin und seinen verwandten Verbindungen 583

Toshio NAKAI: On Calcio-gadolinite, a New Variety of Gadolinite Found in Tadati Village, Nagano Prefecture 591

Masao KOIZUMI und Toshizo TITANI: Austauschreaktion der Wasserstoffatome zwischen Nitrophenol und Wasser. II. Chemismus der Reaktion 595

Noriyoshi MORITA und Toshizo TITANI: Der katalytische Isotopenaustausch des gasförmigen Sauerstoffs. II. Die Austauschreaktion der Sauerstoffatome zwischen Sauerstoff und Wasserdampf auf der Oberfläche amorphen Siliciumdioxyds, Quarzglases, Asbests sowie Bimssteins 601

Masao KOIZUMI und Toshizo TITANI: Austauschreaktion der Sauerstoffatome zwischen Wasser und einigen organischen Verbindungen. 607

No. 10. OCTOBER.

Ryutaro TSUCHIDA and Masahisa KOBAYASHI: Spectrochemical Study of Microscopic Crystals. I. Application of Microscopes in Spectrography 619

Taku UÉMURA et Yasuo INAMURA: Études spectrochimiques des matières colorantes complexes. I. Sur les complexes métalliques d'*o,o'*-dioxyazobenzène 623

Masao KOIZUMI und Toshizo TITANI: Austauschreaktion der Wasserstoffatome zwischen Nitrophenol und Wasser. II. Chemismus der Reaktion. (*Fortsetzung und Schluss*) 631

Masao KOIZUMI, Yasukuni KOMAKI und Toshizo TITANI: Über den Austausch der Wasserstoffatome zwischen Pyrrol, Indol, sowie ihren Methylderivaten und Wasser. V. Austausch der Wasserstoffatome zwischen *N*-Methylindol und Wasser 643

Tokuro SODA and Fujio EGAMI: On A New Sulphuric Acid Ester in the Mucus of *Charonia lampas* 652

No. 11. NOVEMBER.

Kunio OKAHARA: Eine Bemerkung über den Schmelzpunkt des Psoralens bzw. Ficusins 653

Noriyoshi MORITA und Toshizo TITANI: Der katalytische Isotopenaustausch des gasförmigen Sauerstoffs. III. Die Austauschreaktion der Sauerstoffatome zwischen Sauerstoff und Wasserdampf an der Oberfläche des Kupferoxyds 656

Toshizo TITANI und Kokiti GOTO: Austauschreaktion der Sauerstoffatome zwischen einigen anorganischen Anionen und Wasser. (Vorläufige Mitteilung) 667

No. 12. DECEMBER.

Tunetaka SASAKI: On the Nature of Foam. II. The Foam Formation of Ternary System, Acetic Acid—Ethyl Ether—Water . . . 669

Tutomu KUBOTA: On the Polymerization of Chloroprene as Revealed by the Raman Effect 678

Masao KOIZUMI und Toshizo TITANI: Austauschreaktion der Kernwasserstoffatome des Phenols. I. Austauschreaktion in alkalischer Lösung 681

Author Index to Volume 13 691

Corrections 696

M Katayama

BULLETIN OF THE
CHEMICAL SOCIETY OF JAPAN

Professor Masao KATAYAMA.

Professor Masao Katayama, the second son of Seigo Katayama, was born in Chayamachi near Okayama on September 11, 1877. In 1900 he finished the chemistry course in the Faculty of Science, Tokyo Imperial University, and continued to study as a post-graduate student.

In 1902 he was appointed to a professorship at the Higher Technical School of Tokyo and after three years he was sent to Europe as a Government Research Fellow. He studied there for three years, spending one half of the time in the Laboratory of Professor Lorenz in Zürich and the other half in the Laboratory of Professor Nernst in Berlin. In 1911 he was appointed Professor of Theoretical Chemistry of Tohoku Imperial University in Sendai. In 1919 he was called back to his *alma mater* to succeed Professor Joji Sakurai, now Privy Councillor and the President of the Imperial Academy, in the chair of Physical Chemistry in the Faculty of Science. This chair he has held continuously since then.

Outside the university he is also active as a member of the Imperial Academy and of the National Research Council; as the head of the Katayama Laboratory in the Institute of Physical and Chemical Research in Tokyo; on a committee of the Shanghai Science Institute; and as the Chairman of the Fifth Committee of the Japan Society for the Promotion of Scientific Research.

Professor Katayama's works on physical chemistry cover a notably wide scope, extending over the energetic and atomistic fields. Among them his studies on gas equilibrium and on surface tension are well known and cited in many chemical publications as important researches. The former was carried out with Professor Bodenstein for the dissociation of the vapour of sulphuric acid and nitrogen dioxide, and not only the result of the experiment but also the principle of the measurement was an important contribution to the study of gas equilibrium. The latter refers to the improvement of the Ramsay-Shields equation of surface tension which did not agree with the theory of corresponding states and failed to express the experimental result near the critical point. These two difficulties were overcome by the formula of Professor Katayama who took into consideration the effect of molecular attraction in the vapour phase. Under his direction many interesting researches have been carried out on electrochemistry, equation of state, chemical kinetics, atomic and mole-

CHEMISTRY HALL LIBRARY

cular structures, etc., but many of the results have been published under the names of his pupils. In addition to these brilliant works, Professor Katayama wrote a textbook of physical chemistry named "Kwagaku-Honron", in which the fundamental conceptions of physical chemistry are explained in an original manner and which is indisputably the best written in our language.

The papers published in the present number are dedicated to Professor Katayama by his pupils on the celebration of the sixtieth anniversary of his birthday. It is their heartfelt desire that Professor Katayama may long enjoy good health, and continue his activities on their behalf, as well as for the future development of physical chemistry in Japan.

December, 1937.

San-ichiro MIZUSHIMA.

Rotatory Dispersion of Sugars in Liquid Ammonia and in Water.[1]

By Hikoichi SHIBA and Shintaro TANABE.

(Received January 11, 1938.)

We have attempted to study the nature of sugars in liquid ammonia. In the present paper are reported the results in the preliminary determination of their optical activities at the temperatures below the boiling point of the solvent. The optical rotations of sugars in this medium were measured by Sherry[2] at 20°C. for D-line. We were informed by the abstract that Shatenstein recently carried out polarimetric measurements with saponine at 20°C.

To observe the optical rotations at low temperatures, we constructed a polarimetric tube of fused quartz. It has, as shown in Fig. 1, two double windows of plane parallel plates. Both the chambers of the double windows were well evacuated, so that the disturbance by the frost or dew drops condensed on the window plates from the moisture in air was avoided and the field of view was kept clear even when it was cooled down to −70°C. The temperatures, at which we observed, were in the range from −35 to −70°C. and were kept constant within 1° without difficulty during a series of measurements by immersing the tube in a wooden tank of a sufficiently large capacity filled with alcohol and CO_2 snow and covering it externally with felt. We tried to make such a polarimetric tube of borosilicate glass but the glass plates of the windows had fatal strains for our purposes.

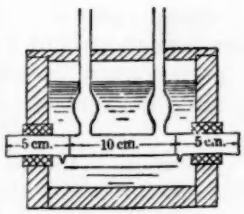

The polarimetric tube.

Fig. 1.

The polarimeter used was the three field type of Schmidt and Haensch with a monochromator as its accessory. For the light source the filament lamp 250 W for kinema projection was used through the monochromater which was calibrated with Hg-lines. Mercury, sodium, and cadmium vapour lamps were also used, being filtered with the monochromator. The sugars and the glucoside used were Kahlbaum's or Merck's products.

(1) This paper was read at the autumnal meeting of the Institute of Physical and Chemical Research (Nov. 21, 1935.)

(2) Sherry, *J. Phys. Chem.*, **11** (1907), 559.

For the comparison and the proof of purity of the materials, we determined accurately the rotatory dispersion in water, using the ordinary polarimetric tube 10 cm. long. The results of the measurements were briefly described in the following.

Aqueous Solutions. We determined the rotatory dispersions of *d*-glucose, *d*-fructose, *d*-galactose, *α*-methyl-*d*-glucoside, saccharose, lactose, and maltose in water with high accuracy. In these cases mercury lines ($\lambda = 0.612\,\mu$, 0.578, 0.546, 0.492, 0.436), cadmium lines ($\lambda = 0.644$, 0.509, 0.480), sodium line ($\lambda = 0.589$) were used except saccharose solutions which were observed with the filament lamp. The concentration of solutions is represented in molarities of anhydrous sugars and the specific rotation is evaluated for unit mass of them. Specific rotations obtained were graphed to test Drude's dispersion formula $[\alpha] = k_0/(\lambda^2 - \lambda_0^2)$ and to compare them with the data given by Grossmann and Bloch and by Wagner-Jauregg.[3] Good agreements were obtained as seen in Fig. 2–8. For saccharose such a comparison was omitted and for maltose the previous data of the dispersion to be utilized was not found.

In the cases where the multirotation was to occur, the measurements were carried out 3 or 4 days after preparing the solution. In the duration of preservation, care was taken not to be interfered by fermentation, avoiding the contact of the solutions with air.

Solutions in Liquid Ammonia. The optical rotations in liquid ammonia were measured with the filament lamp as the light source. The measurements were done in the day of preparation of the solution. The accuracy of the rotation measured in liquid ammonia is less than that in water because of using the special polarimetric tube, as mentioned above, at low temperatures. The fluctuation of the experimental values is within ±1% The sugars and glucoside in liquid ammonia were found to behave in the manner of simple rotatory dispersion, although some deviations are seen in the dispersion curve of lactose. The values of λ_0 and k_0 in Drude's formula were estimated from graphs and tabulated in Table 13. As is seen in Table 9, fructose in liquid ammonia showed small rotations with positive or negative sign. It may be roughly assumed that it has not optical activity under our conditions as well as in Sherry's observation at 20°C. Sherry reported that neither in methylamine nor in ethylamine fructose showed measurable optical activity. Such facts seem to suggest something of chemical change of ketose in these mediums.

(3) "International Critical Tables," Vol. II, 334.

The temperature coefficients of the specific rotation in liquid ammonia were determined for D-line with sodium vapour lamp, as shown in Table 14. We observed also sugars such as glucose, fructose, saccharose, and lactose dissolved in the mixture of water and ethyl alcohol in equal volumes at the room temperature and at low temperatures. The results are shown in Table 15.

Table 1. *d*-Glucose in water.

$^2/_3$ mol, 20-21°C., 3 days after dissolution, Hg-lamp.

λ (μ)	[α]
0.578	53.1
0.546	66.5
0.492	73.9
0.436	120.0

$\lambda_0 = 0.148$ $k_0 = 17.2$

Table 2. *d*-Fructose in water.

$^2/_3$ mol, 20-21°C., the day of dissolution, Hg-, Na-, Cd-lamps.

λ (μ)	[α]
0.644	—
0.612	−83.5
0.589	−93.0
0.578	−98.5
0.546	−110.0
0.509	−127.6
0.492	−128.7
0.480	−145.6
0.436	−181.0

$\lambda_0 = 0.152$ $k_0 = 29.8$

Table 3. *d*-Galactose in water.

$^1/_2$ mol, 21°C., 4 days after dissolution, Hg-, Na-, Cd-lamps.

λ (μ)	[α]
0.644	67.2
0.612	70.6
0.589	79.9
0.578	83.6
0 546	95.2
0.509	112.3
0.492	119.7
0.480	125.2
0.436	154.3

$\lambda_0 = 0.145$ $k_0 = 26.0$

Table 4. *α*-Methyl-*d*-glucoside in water.

$^2/_3$ mol, 20°C., 4 days after dissolution, Hg-, Na-, Cd-lamps.

λ (μ)	[α]
0.644	128.7
0.612	142.6
0.589	158.2
0.578	165.1
0.546	186.0
0.509	218.8
0.492	231.7
0.480	246.7
0.436	308.7

$\lambda_0 = 0.138$ $k_0 = 52.0$

Table 5. Saccharose in water.

0.292 mol, 28.3°C., filament lamp.

λ (μ)	[α]
0.623	57.3
0.589	64.7
0.578	66.4
0.546	76.1
0.517	86.7
0.492	96.4
0.458	105.5
0.436	115.9

1.168 mol, 28°C.

λ (μ)	[α]
0.623	57.8
0.610	60.4
0.600	62.5
0.589	64.8
0.578	67.7
0.565	71.0
0.546	76.6
0.530	81.8
0.510	89.2
0.492	95.7
0.470	105.2
0.450	116.4
0.436	125.0

$\lambda_0 = 0.141$ $k_0 = 21.2$

Table 6. Lactose in water.

1/3 mol, 19°C., 3 days after dissolution, Hg-, Na-, Cd-lamps.

λ (μ)	[α]
0.644	42.4
0.612	46.1
0.589	52.2
0.578	53.8
0.546	60.3
0.509	71.6
0.492	73.6
0.480	78.9
0.436	98 3

$\lambda_0 = 0.145$ $k_0 = 16.6$

Table 7. Maltose in water.

1/2 mol, 16°C., 4 days after dissolution, Hg-, Na-, Cd-lamps.

λ (μ)	[α]
0.644	113.9
0.612	124.6
0.589	138.7
0.578	144.7
0.546	164.4
0.509	191.8
0.492	205.0
0.480	216.5
0.436	271.0

$\lambda_0 = 0.173$ $k_0 = 43.6$

Table 8.
d-Glucose in liquid ammonia.

0.48 mol, −35°C., filament lamp.

λ (μ)	[α]
0.644	62.7
0.612	62.7
0.589	77.3
0.578	74.8
0.546	86.0
0.509	108.0
0.492	114.5
0.480	135.7
0.436	153.0

$\lambda_0 = 0.258$ $k_0 = 20.6$

Table 9.
d-Fructose in liquid ammonia.

0.46 mol, −36°C., filament lamp.

λ (μ)	[α]
0.612	+0.09
0.578	−4.18
0.546	−6.11
0.492	+5.47
0.436	−4.39

Table 10. *α*-Methyl-*d*-glucoside in liquid ammonia.

0.34 mol, −36°C., filament lamp.

λ (μ)	[α]
0.644	140.4
0.612	152.4
0.589	168.2
0.578	180.9
0.546	203.4
0.509	238.5
0.492	259.8
0.480	272.4
0.436	325.1

$\lambda_0 = 0.152$ $k_0 = 55.2$

Table 11.

Saccharose in liquid ammonia.

0.21 mol, −43°C., filament lamp.

λ (μ)	[α]
0.644	63.0
0.612	65.5
0.589	84.6
0.578	83.9
0.546	101.4
0.509	117.3
0.492	125.0
0.480	129.0
0.436	171.0

$\lambda_0 = 0.247$ $k_0 = 22.0$

Table 12.

Lactose in liquid ammonia.

0.19 mol, −51°C, filament lamp.

λ (μ)	[α]
0.644	40.4
0.612	59.0
0.589	62.1
0·578	71.0
0.546	83.4
0.509	96.3
0.492	104.5
0.480	107.0
0.436	122.7

$\lambda_0 = 0.214$ $k_0 = 19.6$

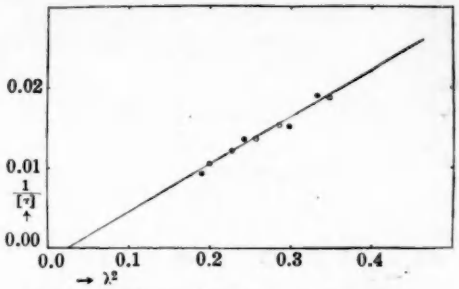

Fig. 2. *d*-Glucose in water. ○ Grossmann and Bloch. 20–21°C.

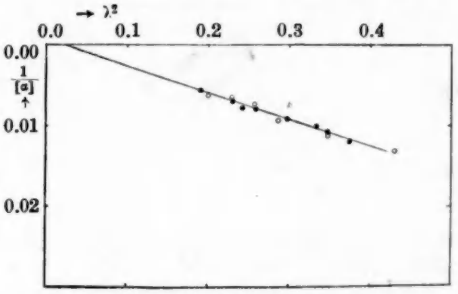

Fig. 3. *d*-Fructose in water. ○ Grossmann and Bloch. 20–21°C.

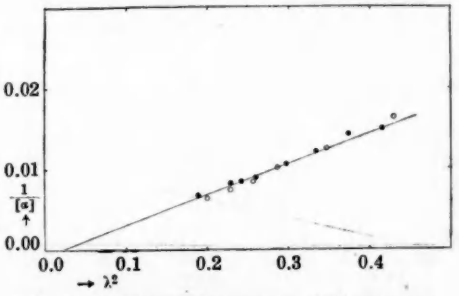

Fig. 4. *d*-Galactose in water. ○ Grossmann and Bloch. 21°C.

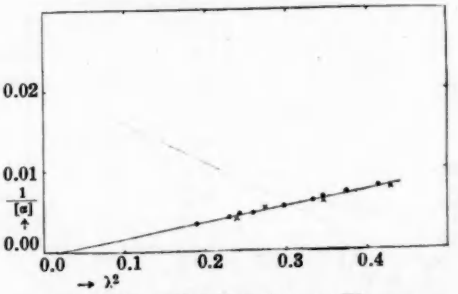

Fig. 5. α-Methyl-*d*-glucoside in water. 20°C. × Wagner-Jauregg.

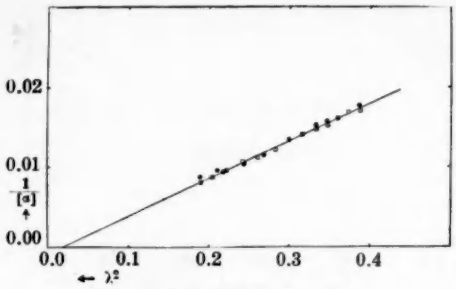

Fig. 6. Saccharose in water.
● 0.292 mol, 28.3°C. □ 1.168 mol, 28.0°C.

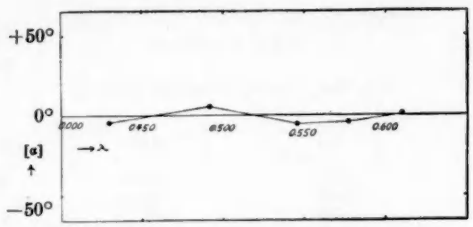

Fig. 10. *d*-Fructose in liquid NH_3, 0.46 mol, −36°C., filament lamp.

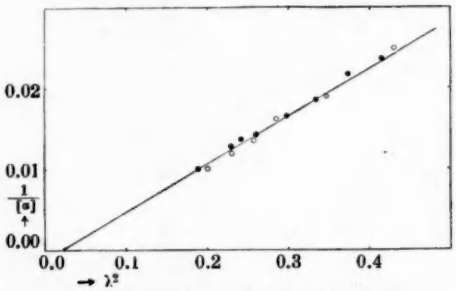

Fig. 7. Lactose in water. ○ Grossmann and Bloch. −19°C.

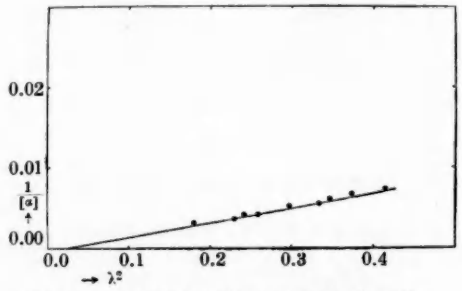

Fig. 11. α-Methyl-*d*-glucoside, in liquid NH_3, 0.34 mol, −36°C., filament lamp.

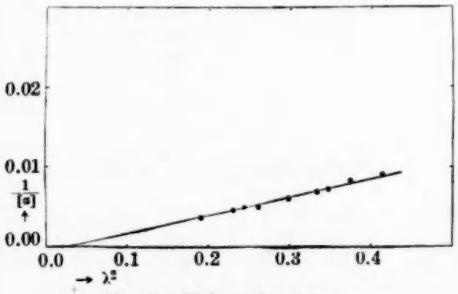

Fig. 8. Moltose in water. 16°C.

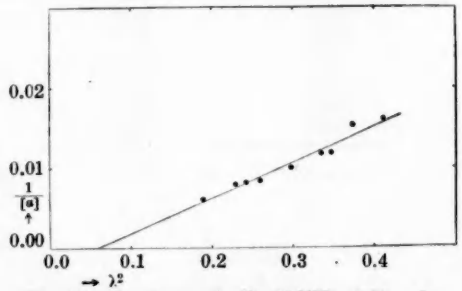

Fig. 12. Saccharose in liquid NH_3, 0.21 mol, −43°C., filament lamp.

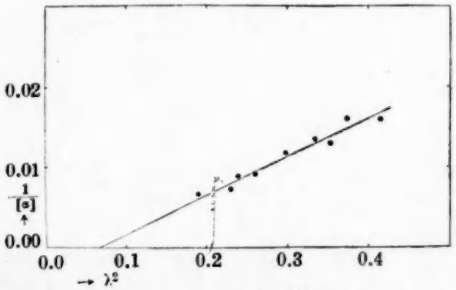

Fig. 9. *d*-Glucose in liquid NH_3, 0.48 mol, −35°C., filament lamp.

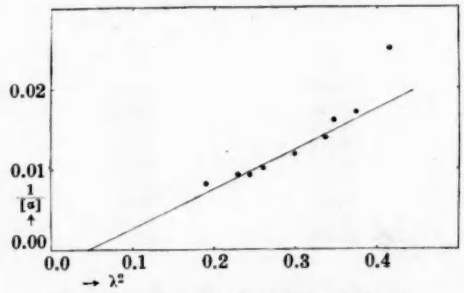

Fig. 13. Lactose in liquid NH_3, 0.19 mol, −51°C., filament lamp.

Table 13. Values of λ_0 and k_0 ($[\alpha] = k_0/(\lambda^2-\lambda_0^2)$).

	Aqueous solution			Solution in liquid NH_3		
	t °C.	λ_0 (μ)	k_0	t °C.	λ_0 (μ)	k_0
d-Glucose	21	0.148	17.2	−35	0.258	20.6
d-Fructose	20–21	0.152	29.8	−36	—	—
d-Galactose	21	0.145	26.0	—	—	—
α-Methyl-*d*-glucoside	20	0.138	52.0	−36	0.152	55.2
Saccharose	28	0.141	21.2	−43	0.247	22.0
Lactose	19	0.145	16.6	−51	0.214	19.6
Maltose	16	0.173	43.6	—	—	—

Table 14. Temperature coefficient of $[\alpha]_D$ in liquid ammonia.

	Concentration	t °C.	$[\alpha]_D$	$\frac{\Delta[\alpha]_D}{\Delta t}$	
d-Glucose	0.48 mol	−35	77.3	−0.26	
	0.48 mol	−62	84.2		
	3.5 g. in 100 c.c. solution	20	56.1		Sherry
	27.8 g. in 100 c.c. solution	20	55.3		Sherry
d-Fructose	0.46 mol	−36	[0]		
	—	20	0		Sherry
α-Methyl-*d*-glucoside	0.34 mol	−36	168.2	−0.31	
	0.34 mol	−54	173.6		
Saccharose	0.21 mol	−43	84.6	−0.20	
	0.21 mol	−63	88.6		
	8.2 g. in 100 c.c solution	20	76.0		Sherry
	48.8 g. in 100 c.c solution	20	73.6		Sherry
Lactose	0.19 mol	−42	60.5	−0.18	
	0.19 mol	−51	62.1		
	7.0 g. in 100 c.c. solution	20	33.2		Sherry
	27.8 g. in 100 c.c solution	20	32.5		Sherry

Table 15. Temperature coefficient of $[\alpha]_D$ in the mixture of water and ethyl alcohol (equal volumes).

	Concentration	t °C.	$[\alpha]_D$	$\frac{\Delta[\alpha]}{\Delta t}$
d-Glucose	0.5 g. in 100 c.c. solution	23 67	59.6 71.6	−0.13
d-Fructose	1 g. in 100 c.c. solution	23 −67.5	−64.8 −76.5	0.13
Saccharose	5 g. in 100 c.c. solution	20 −45	66.5 80.0	−0.20
Lactose	0.2 g. in 100 c.c. solution	23 −67.5	49.1 93.7	−0.53

Institute of Physical and Chemical Research, Tokyo.

X-Ray Spectroscopic Determination of Lanthanum, Neodymium and Gadolinium in the Presence of Other Rare Earth Elements.

By Kenjiro KIMURA.

(Received January 10, 1938.)

As is known, the separation of the rare earth elements from one another is, except cerium, so difficult and tedious that the usual chemical methods of analysis fail entirely when applied to the quantitative determination of each component in a rare earth mixture. Although some indirect methods proposed may be used for the analysis of a rare earth mixture of only a few components, most of them can not be applied to a complex mixture of the rare earths such as extracted from a natural mineral. The only reliable one that can be used even in such a case may be probably the X-ray spectroscopic method.(1)

(1) cf. A. Hadding, *Z. anorg. allgem. Chem.*, **122** (1922), 195; V.M. Goldschmidt and L. Thomassen, "Geochemische Verteilungsgesetze der Elemente," III, Kristiania (1924); P. Günther and G. Wilcke, *Z. physik. Chem.*, **119** (1926), 219; H. Schreiber, *Z. Physik*, **58** (1929), 619; P. Günther, A. Kotowski, and H. Lehl, *Z. anorg. allgem. Chem.*, **200** (1931), 287; I. Noddack, *Z. anorg. allgem. Chem.*, **225** (1935), 337; E. Minami, *Nachr. Ges. Wiss. Göttingen, Math.-physik. Klasse*, Fachgruppe IV, N.F. **1** (1935), 155.

The present author intends to estimate the amount of each of the rare earth elements in their mixture by comparing the intensity of their X-ray spectral lines with that of the reference elements. The method is in its principle quite similar to the one which was first proposed and investigated by G. von Hevesy, D. Coster, Y. Nishina and others[2] for the determination of hafnium content in zirconia-hafnia mixtures. The experimental results obtained with lanthanum, neodymium and gadolinium will be given in the present report.

The Determination of Lanthanum.[3]

For the determination of lanthanum in a mixture of the rare earths, the intensity of the $L\beta_2$ line of lanthanum is compared with that of the $L\beta_3$ line of cerium which is taken as the reference element. As the wavelength difference of the said two lines is only 8 X-Units, which corresponds to about 0.5 mm. on the photographic plate, the error of the estimation of the relative intensities due to the wrong exposure is practically eliminated.

Although cerium is an element that belongs to the rare earth group, it is comparatively easy to separate cerium alone from other rare earth elements by some chemical methods,[4] and there is no difficulty in ascertaining its amount present in a given sample, or in preparing a sample free from it. Since cerium can be completely precipitated from a solution with other rare earth elements in the form of hydroxide or oxalate, thorough mixing of the sample with the added reference substance can be easily attained without that tedious procedure of weighing and grinding which we have to follow when an element of quite different chemical properties is taken as the reference.

To a given sample of rare earth mixture is added a known quantity of cerium oxide, or lanthanum oxide if the cerium line of the original sample is stronger. The quantity added is to be varied until the two lines under consideration show an equal intensity on the photographic plate. If we know the concentration ratio CeO_2/La_2O_3 which makes the said two lines equally intense, we can easily calculate the amount of lanthana in the original sample from that of ceria present.

The actual procedure followed is given below.

(2) Hevesy and Coster, *Nature*, **111** (1923), 182; Coster, *Chem. News*, **127** (1923), 65; Coster and Nishina, *ibid.*, **130** (1925), 149; Kimura, *Z. physik. Chem.*, **128** (1927), 394.

(3) Read before the Chemical Society of Japan, April 3, 1930 and July 11, 1931, and published in Japanese in *J. Chem. Soc. Japan*, **54** (1933), 213.

(4) e.g. C. James and L. A. Pratt, *J. Am. Chem. Soc.*, **33** (1911), 1326; Paul H.M.-P. Brinton and C. James, *ibid.*, **41** (1919), 1080.

Materials and Experimental Procedure. The intensity of the lanthanum $L\beta_2$ line was compared with that of the cerium $L\beta_3$ line by using the oxide mixtures of lanthanum and cerium. The mixtures were prepared from cerium chloride and lanthanum chloride, which had been carefully purified, the former by the bromate method, the latter by the fractionation.

The high purity of the cerium salt used was shown by the X-ray spectroscopic analysis. It did not contain the detectable amount of any of other lanthanide elements.

It was also revealed by the X-ray method that the lanthanum salt prepared was free from neodymide elements. Although a few spectral lines of cerium and praseodymium were observed very faintly on the plate, the $L\beta_3$ line of cerium was not detected under the same experimental conditions that were followed in the case of the comparison of the relative intensities of the said two lines. Besides, the absorption bands due to some other rare earth elements were not observed with the concentrated solution of the lanthanum chloride used. Both the hydrogen peroxide test and the iodate test failed also to show the presence of cerium in it. Therefore, for the present purpose, the material may be assumed to be a pure lanthanum salt.

Solutions with appropriate known concentrations of lanthanum chloride and of cerium chloride were prepared. The proper volumes of each solution were pipetted and mixed thoroughly. By the addition of ammonium chloride and ammonia, the hydroxides of lanthanum and cerium were precipitated from the solution, filtered off, and ignited to oxides, which were used as a standard sample for the comparison of the relative intensities of the lanthanum $L\beta_2$ and the cerium $L\beta_3$ lines.

When a sample to be analysed was given, a mixture that could be used for the X-ray analysis was prepared from it by the following procedure. The original sample, if it consisted of rare earths only, was dissolved in dilute hydrochloric acid after fusion with sodium bisulphate if necessary, and a solution with the known concentration was prepared. But, if it contained some other elements which were precipitated with ammonia, the rare earths should be first extracted from it. By precipitation with oxalic acid, the rare earth elements and thorium could be separated from the other members of the analytical group of ammonia, such as iron, aluminium, zirconium, uranium, etc. Thorium in the oxalate precipitate was removed by applying the hydrogen peroxide method and thus a solution which contained the rare earth elements only was obtained. After the determination of the contents of cerium and total rare earth elements of the solution thus prepared, a definite volume of it was pipetted. To

it was added a known amount of the solution of cerium chloride, or that of lanthanum chloride according to the ratio CeO_2/La_2O_3 of the original sample. From this solution, the hydroxides of the rare earth elements were precipitated by the addition of ammonia, filtered off, and ignited to oxides.

With the oxide mixture thus prepared, the lanthanum $L\beta_2$ and the cerium $L\beta_3$ lines were photographed, using a metal X-ray tube and a vacuum spectrograph of Siegbahn's type. Calcite was used as the crystal. The width of the slit of the spectrograph was about 0.1 mm. The sample was put on the copper plate of the anticathode, which had been changed before each exposure. The X-ray lines were excited by cathode rays from the hot cathode of tungsten wire. The photograph was taken by 41 minutes' exposure at the applied tension of 15 kilo-volts (effective) and the current of about 2 milliamperes. During the exposure, the crystal was slowly rotated through an angle of 0.2 degree.

The spectral lines on the plates were examined under the magnifying glass. Instead of estimating the intensity ratio of the two lines under consideration, the quantity of the element added was varied until the said two lines became equally intense.

The photograph was taken repeatedly with the same sample, and the reproducibility of experiments was confirmed.

Experimental Results. (a) The relative intensities of the lanthanum $L\beta_2$ and the cerium $L\beta_3$ lines were compared by using $La_2O_3 - CeO_2$ mixtures as the samples. In Table 1 are given the results obtained, from which we know that the two lines under consideration show an equal intensity when the ratio CeO_2/La_2O_3 in weight is equal to 2.5(5).

(b) The presence of other rare earth elements might have some effects on the value of the balance ratio which was just determined to be 2.55 in the case of the mixture of lanthanum oxide and cerium oxide.

For the disturbing effects of a third element present in a sample, the following four cases were mentioned by G. von Hevesy[5]: (i) the case when a third element present has a stronger absorption effect on the line of longer wave-length; (ii) the case when a third element present has an absorption edge situated between the two lines to be compared; (iii) the case when a line of a third element present is situated between the absorption edges which correspond respectively to the two lines under comparison; (iv) the case when a line of a third element present lies near and on the short wave-length side of the absorption edges above mentioned.

(5) Hevesy, "Chemical Analysis by X-Rays and its Applications," 117, New York (1932).

In the present case there is no element of the rare earth group which has the absorption effects mentioned in (i) and (ii). As the wave-length difference of the absorption edges corresponding to the two lines to be compared is fairly large, some rare earth elements which have the excitation effects mentioned in (iii) and (iv) may come into consideration. But, as is seen in the following examples, these disturbing effects, if there be any, are generally very small and may be neglected in actual analyses.

Table 1.

CeO_2/La_2O_3 in weight	Intensity of La $L\beta_2$ compared with Ce $L\beta_3$
3.69	Weaker
3.06	Weaker
2.92	Weaker
2.81	Weaker
2.70	Weaker
2.65	Weaker
2.61	A little weaker
2.60	A little weaker
2.59	A little weaker
2.55	Nearly equal
2.54	Nearly equal
2.50	A little stronger
2.45	Stronger
2.39	Stronger
2.37	Stronger
2.20	Stronger
1.97	Stronger
1.80	Stronger
1.79	Stronger
0.87	Stronger

(c) As the examples, the amount of lanthanum oxide in several samples was determined. Sample No. 1 mainly consisted of the oxides of lanthanide elements of lower atomic numbers and was free from ceria. Sample No. 2 was a mixture of cerium earths, rich in neodymium and praseodymium. The amount of ceria in it was determined to be 29.35%. Sample No. 3 contained 49.6% of ceria, and less than 10% of yttrium earths; the remainder was cerium earths rich in neodymium. Sample No. 4 was a mixture of the rare earths; it contained 22.2% of ceria and about 10% of yttrium earths. It was rich in samaria.

Cerium oxide was added to Samples No. 1, No. 2, and No. 4, while lanthanum oxide was added to Sample No. 3 which was already rich in ceria. The relative intensities of the lanthanum $L\beta_2$ and the cerium $L\beta_3$ lines were compared with the results shown in Table 2.

Table 2.

(1) Sample No. 1.

$\frac{CeO_2 \text{ added}}{\text{Sample taken}}$ (%)	Intensity of La $L\beta_2$ compared with Ce $L\beta_3$
114	Stronger
120	Stronger
128	Nearly equal
137	Weaker
139	Weaker

(2) Sample No. 2.

$\frac{CeO_2 \text{ added}}{\text{Sample taken}}$ (%)	Intensity of La $L\beta_2$ compared with Ce $L\beta_3$
8.6	Weaker
7.7	Nearly equal
5.45	Nearly equal
3.9	Nearly equal
2.8	Stronger
2.5	Stronger
0.0	Stronger

(3) Sample No. 3.

$\frac{La_2O_3 \text{ added}}{\text{Sample taken}}$ (%)	Intensity of La $L\beta_2$ compared with Ce $L\beta_3$
44.3	Stronger
22.2	Stronger
17.7	Nearly equal (a little stronger)
15.5	Nearly equal
8.2	Weaker
4.4	Weaker
0.0	Weaker

(4) Sample No. 4.

$\frac{CeO_2 \text{ added}}{\text{Sample taken}}$ (%)	Intensity of La $L\beta_2$ compared with Ce $L\beta_3$
0.0	Stronger
2.29	Weaker
4.57	Weaker

If the balance ratio 2.55 which was determined with $La_2O_3-CeO_2$ mixtures also held true of these samples, the amount of the lanthanum oxide present in them might be easily calculated. Thus, the amount of the lanthanum oxide present in Sample No. 1 would be $128/2.55\%$, that in Sample No. 2, $(5.45 + 29.35)/2.55\%$, that in Sample No. 3, $(49.6/2.55 - 16)\%$, that in Sample No. 4, $(22.2 + 2.29/2)/2.55\%$. But, if the presence of other rare earths had some disturbing effects, the value of the balance ratio which could be used for each sample respectively should be determined.

To know the effects of the other rare earth elements present and to determine the balance ratio for each sample, the following method which was similar to the one proposed by the present author[6] in the case of

(6) Kimura, *Z. physik. Chem.*, **128** (1927), 394.

the determination of hafnia in a mixture of the oxides of the elements precipitated by ammonia was tried.

Let x denote the percentage of lanthanum oxide to be determined, then

$$\frac{a}{x} = k \qquad (1),$$

where a is the amount of cerium oxide required to make the two lines under comparison equally intense, and k is the balance ratio CeO_2/La_2O_3 yet unknown.

To the sample is added first a known quantity of lanthanum oxide, and then cerium oxide is added until the lanthanum $L\beta_2$ and the cerium $L\beta_3$ lines again show an equal intensity. Let b denote the amount of lanthanum oxide added to the sample, and c, the amount of cerium oxide required to make the said two lines equally intense after the addition of b of lanthana. Then,

$$\frac{c}{x+b} = k \qquad (2).$$

From (1) and (2), we get

$$k = \frac{c-a}{b} \qquad (3).$$

If the value of k thus obtained were equal to or nearly equal to 2.55, i.e. the balance ratio determined with the oxide mixture of lanthanum and cerium, then the effects of the other rare earth elements in the sample should be negligible. If the value of k from (3) were different from 2.55, then we could use that value as the balance ratio special to the sample and thus the effects of the other rare earths could be eliminated automatically.

The value of k thus obtained for each sample is shown in Table 3.

Table 3.

Sample	a (%)	b (%)	c (%)	k found
No. 1	128	33.0	214	2.61
No. 2	34.8	9.9	59.7	2.52
No. 3*	49.6*	10.6*	76.2	2.51
No. 4	23.4	6.0	38.2	2.48

* Instead of x, $x+16$ was used.

As was seen from Table 3, the value of k thus found agreed with the balance ratio previously obtained for the mixtures of lanthanum oxide and cerium oxide within the error of experiments. Thus, the disturbing effects were almost negligible in these cases.

The amount of lanthanum oxide found by using the value of the balance ratio, k, obtained for each sample was given in Table 4 together with the amount determined by assuming it to be 2.55.

Table 4.

Sample	k	La_2O_3 (%)	La_2O_3 (%)$_{k=2.55}$
No. 1	2.61	49	50
No. 2	2.52	13.8	13.6
No. 3	2.51	3.8	3.5
No. 4	2.48	9.4	9.2

The Determination of Neodymium.[7]

For the determination of neodymium in a mixture of the rare earths, the intensity of the $L\alpha_1$ line of neodymium is compared with that of the $L\beta_1$ line of cerium, which is taken as the reference element. As the wavelength difference of the said two lines is only 14 X-Units, which corresponds to about 0.9 mm. on the photographic plate, the error of the estimation of the relative intensities due to the wrong exposure is practically eliminated.

Materials and Experimental Procedure. The relative intensities of the neodymium $L\alpha_1$ and the cerium $L\beta_1$ lines were compared by using the oxide mixtures of neodymium and cerium, which were prepared from their chlorides.

The solution of the cerium chloride which was prepared for the experiments with lanthanum was also used here. As for neodymium salt, two different samples were used, the one contained no lanthanide element except the negligible amount of lanthanum and cerium, the other, no lanthanide element except a trace of praseodymium. The amount of impurities was so small in both cases that they might be assumed for the present purpose to be pure neodymium salts.

(7) Read before the Chemical Society of Japan, June 14, 1930 and July 11, 1931, and published in Japanese in *J. Chem. Soc. Japan*, **54** (1933), 220.

As the procedure to prepare a sample to be put on the anticathode was quite similar to the one given already in the part of lanthanum of this report, its description will be omitted here. It must be mentioned only that the mixtures of the rare earths free from thoria and other oxides were used as the samples throughout this work.

The experimental conditions for the exposure were also the same as in the previous case, i.e. the photograph was taken by 41 minutes' exposure at the applied tension of 15 kilo-volts (effective) and the current of about 2 milliamperes.

Experimental Results. (a) With the oxide mixtures of neodymium and cerium, the relative intensities of the neodymium $L\alpha_1$ and the cerium $L\beta_1$ lines were compared. In Table 5 are shown the results obtained, from which we know that the two lines under consideration become equally intense when the ratio CeO_2/Nd_2O_3 in weight is equal to 0.71.[8]

Table 5.

CeO_2/Nd_2O_3 in weight	Intensity of Nd $L\alpha_1$ compared with Ce $L\beta_1$
1.98	Weaker
1.85	Weaker
1.76	Weaker
1.13	Weaker
0.99	Weaker
0.895	Weaker
0.804	Weaker
0.802	Weaker
0.710	Nearly equal
0.708	Nearly equal
0.702	Nearly equal
0.607	Stronger
0.503	Stronger
0.496	Stronger
0.401	Stronger

(b) It is somewhat peculiar that the balance ratio is less than unity. According to the experiments carried out by Y. Nishina and the

(8) The intensity ratio of the said two lines was also estimated by a microphotometer. In this case a little higher value 0.78 was obtained as the balance ratio CeO_2/Nd_2O_3.

present author, in which the intensity of the $L\beta_1$ line of a rare earth element of even atomic number was compared with that of the $L\alpha_1$ line of the element of atomic number higher by two by using the mixtures of the oxides of the two elements under consideration, the amount of the former element was generally greater than that of the latter when the said two lines showed an equal intensity. For examples, the balance ratio Gd_2O_3/Dy_2O_3 was equal to 2.1 for the gadolinium $L\beta_1$ and the dysprosium $L\alpha_1$ lines, the balance ratio Sm_2O_3/Gd_2O_3 was 2.5 for the samarium $L\beta_1$ and the gadolinium $L\alpha_1$ lines, and the balance ratio Nd_2O_3/Sm_2O_3 was 1.8 for the neodymium $L\beta_1$ and the samarium $L\alpha_1$ lines.

Only for the cerium $L\beta_1$ and the neodymium $L\alpha_1$ lines, as was shown by the experiments mentioned above, the balance ratio CeO_2/Nd_2O_3 was less than unity. The origin of this singular result might be traced back to the rapid disappearance of neodymium atoms from the surface layer of the anticathode spot compared with cerium atoms under the bombardment of the cathode rays. To ascertain this, the photographic plates different in time of exposure were compared. The plates taken with the samples remained on the anticathode after the bombardment of the cathode rays were also compared with the regular one. The tendency that the intensity ratio changed in favour of the cerium $L\beta_1$ line with the time of exposure was observed sometimes when the plates quite different in time of exposure were compared. But, the effect was not so clear as seen in the case of the comparison of the relative intensities of the barium $L\alpha_1$ and the titanium $K\alpha_1$ lines, investigated by M. Ishibashi.[9]

(c) The experiments were also carried out to know the effects of the presence of other rare earth elements. The absorption effects are expected by no element of the rare earth group. As for the excitation effects, only samarium and terbium may be mentioned. But as is seen in the following examples these effects are, if there be any, very small.

The following three samples were taken for the examples: Sample No. 5 mainly consisted of the oxides of lanthanide elements of lower atomic numbers and free from ceria; Samples No. 1 and No. 4 were the same as those which were used in the case of lanthanum.

Cerium oxide was added to Samples No. 1 and No. 5, while neodymium oxide was added to Sample No. 4 which was already rich in ceria.

The relative intensities of the neodymium $L\alpha_1$ and the cerium $L\beta_1$ lines were compared with the results shown in Table 6.

If the balance ratio 0.71 which was determined with $Nd_2O_3-CeO_2$ mixtures also held true of these samples, the amount of the neodymium

(9) Ishibashi, *Z. anorg. allgem. Chem.*, **202** (1931), 372.

Table 6.

(1) Sample No. 1.

CeO_2 added / Sample taken (%)	Intensity of Nd $L\alpha_1$ compared with Ce $L\beta_1$
34.19	Weaker
31.63	Weaker
30.74	Weaker
23.09	Weaker
20.70	Nearly equal (a little weaker)
18.89	Nearly equal (a little stronger)
11.40	Stronger

(2) Sample No. 5.

CeO_2 added / Sample taken (%)	Intensity of Nd $L\alpha_1$ compared with Ce $L\beta_1$
32.82	Weaker
26.47	Weaker
25.47	Weaker
22.70	Weaker
20.40	Weaker
18.21	Weaker
18.11	Weaker
16.40	Weaker
15.04	A little weaker
14.29	A little stronger
13.99	Stronger
13.74	Stronger
13.63	Stronger
11.82	Stronger
11.76	Stronger

(3) Sample No. 4.

Nd_2O_3 added / Sample taken (%)	Intensity of Nd $L\alpha_1$ compared with Ce $L\beta_1$
41.2	Stronger
25.5	A little stronger
23.1	A little weaker
20.6	Weaker
16.5	Weaker

oxide in them might be found by simple calculation. Thus, the neodymia content in Sample No. 1 would be $(20.70 + 18.89)/2 \times 0.71\%$, that in Sample No. 5, $(15.04 + 14.29)/2 \times 0.71\%$, and that in Sample No. 4, $\{22.2/0.71 - (25.5 + 23.1)/2\}\%$.

To see the effects of the presence of the other rare earths, the value of the balance ratio was determined for each sample by the method described in the case of lanthanum. The results obtained are shown in Table 7, where a denotes the amount of cerium oxide required to make the two lines under comparison equally intense, b, the amount of neo-

Table 7.

Sample	a(%)	b(%)	c(%)	k found
No. 1	19.8	64.13	66.28	0.73
No. 5	14.7	12.84	23.91	0.72
No. 5	14.7	25.67	32.86	0.71
No. 4*	22.2*	12.0*	30.2	0.67

* Instead of x, $x+24.3$ was used.

dymium oxide added to the sample and c, the amount of cerium oxide required to make the said two lines again equally intense after the addition of b of neodymia.

As was seen from Table 7, the value of k thus found agreed with the balance ratio obtained for the mixtures of neodymium and cerium oxides within the error of experiments.[10] Thus, the disturbing effects of the other rare earths were not observed in these cases. In Table 8, the amount of neodymium oxide found by applying to k the value obtained from the above experiments was compared with that calculated by assuming it to be 0.71.

Table 8.

Sample	k	Nd_2O_3(%)	$Nd_2O_3(\%)_{k=0.71}$
No. 1	0.73	27.	28.
No. 5	0.72	20.	21.
No. 5	0 71	21.	21.
No. 4	0.67	8.8	7.0

The Determination of Gadolinium.[11]

For the determination of gadolinium in a mixture of the rare earths, the intensity of the $L\alpha_1$ line of gadolinium is compared with that of the $L\beta_2$ line of neodymium, which is taken as the reference element. As the wave-length difference of the said two lines is only 10.5 X-Unites, which corresponds to about 0.7 mm. on the photographic plate, the error of the estimation of the relative intensities due to the wrong exposure is practically eliminated.

The neodymium content of a sample given should be previously estimated by the method described already in this report.

Materials and Experimental Procedure. The intensity ratio of the gadolinium $L\alpha_1$ and the neodymium $L\beta_2$ lines was determined with the mixtures of oxides of gadolinium and neodymium, which were prepared from their chlorides. Gadolinium chloride which did not show the presence of other lanthanide elements by the X-ray spectroscopic method was used for this work. The purity of neodymium chloride used was already given in the part of neodymium of the present report.

(10) The relatively low value of k found in the case of Sample No. 4 might be due to the excitation effect of samarium which was richly present in the sample, although it could not be yet confirmed.

(11) In collaboration with Mr. Yoshio Tsunoda. Read before the Chemical Society of Japan, July 14, 1934, and published in Japanese in *J. Chem. Soc. Japan*, **56** (1935), 81.

As the procedure of preparation of a sample to be put on the anti-cathode was quite similar to the one given already in the case of lanthanum, the description of it will be omitted here. It must be only mentioned that the mixtures of the rare earths free from thoria and other oxides were used throughout this work.

The apparatus used was the same as that described before. The photograph was taken by 41 minutes' exposure at the applied tension of 16 kilo-volts (effective) and the current of 2–5 milliamperes. The relative intensities of the lines were compared by a microphotometer with a photo-cell and a string-electrometer. The balance method used in the previous cases was also tried. Both results found agreed with each other.[12]

Experimental Results. (a) By using the mixtures of oxides of gadolinium and neodymium, the intensity of the gadolinium Lα_1 line was compared with that of the neodymium Lβ_2 line. The relative intensities of spectral lines were estimated by microphotometry.

The results obtained are shown in Table 9, where A_b denotes the deflection of the string of the electrometer expressed in divisions of the scale accessory to it at the background of the photographic plate, A_{Gd}, the deflection due to the gadolinium Lα_1 line, and A_{Nd}, that due to the neodymium Lβ_2 line. The density of the gadolinium Lα_1 line, denoted in Table 9 as D_{Gd}, can be expressed by $\log \frac{A_b}{A_{Gd}}$, while that of the neodymium Lβ_2 line, D_{Nd}, by $\log \frac{A_b}{A_{Nd}}$, and the intensity ratio of the said two lines, by D_{Nd}/D_{Gd} or $\log \frac{A_b}{A_{Nd}} : \log \frac{A_b}{A_{Gd}}$.

Table 9.

(1) Exposure at the current of 3 milliamperes.

Nd_2O_3/Gd_2O_3 in weight	A_b	A_{Nd}	A_{Gd}	D_{Nd}/D_{Gd}	D_{Nd}/D_{Gd} (Mean)
4.00	45.2	32.4	29.3	0.77	0.80
	45.2	32.2	30.0	0.83	
4.40	43.2	27.4	26.2	0.91	0.90
	42.7	28.0	26.4	0.88	
4.50	40.7	23.2	24.0	1.06	1.06
	40.7	23.4	24.2	1.06	

(12) In the case of neodymium given in this report and also in some other cases, a slight discrepancy was observed between the value obtained by microphotometry and that by the balance method. This was not the case with gadolinium.

Table 9.—(*Concluded*)

Nd_2O_3/Gd_2O_3 in weight	A_b	A_{Nd}	A_{Gd}	D_{Nd}/D_{Gd}	D_{Nd}/D_{Gd} (Mean)
5.00	41.7	14.4	16.2	1.13	1.13
	42.2	14.6	16.4	1.12	
6.00	36.7	27.2	29.0	1.27	1.27

(2) Exposure at the current of 5 milliamperes.

Nd_2O_3/Gd_2O_3 in weight	A_b	A_{Nd}	A_{Gd}	D_{Nd}/D_{Gd}	D_{Nd}/D_{Gd} (Mean)
4.40	39.8	20.3	19.3	0.93	0.92
	39.7	19.7	18.3	0.91	
4.50	41.3	27.0	29.3	1.24	1.20
	41.8	27.2	28.9	1.16	

(3) Exposure at the current of 2-3 milliamperes.

Nd_2O_3/Gd_2O_3 in weight	A_b	A_{Nd}	A_{Gd}	D_{Nd}/D_{Gd}	D_{Nd}/D_{Gd} (Mean)
4.40*	42.6	36.3	36.0	0.95	0.96
	42.3	35.3	35.1	0.97	
4.50**	42.3	32.3	32.8	1.06	1.07
	42.3	31.5	32.1	1.07	

* The photometer curve is shown in Fig. 1.

** The photometer curve is shown in Fig. 2.

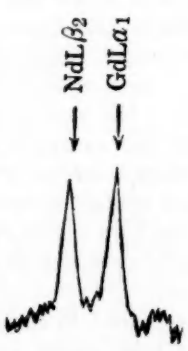

Fig. 1. $Nd_2O_3/Gd_2O_3 = 4.40$.

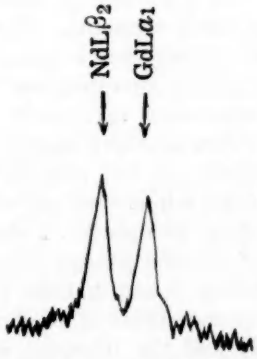

Fig. 2. $Nd_2O_3/Gd_2O_3 = 4.50$.

The balance ratio Nd_2O_3/Gd_2O_3, i.e. the ratio that makes D_{Nd}/D_{Gd} equal to 1.00, was found to be 4.46 from Table 9 (1), 4.43 from Table 9 (2), and 4.44 from Table 9 (3).

The photograph was also taken with the samples that remained on the anticathode after the bombardment of the cathode rays. The results are shown in Table 10. The balance ratio obtained was 4.47 and no sign of the change of the relative intensities was observed.

Table 10.

Nd_2O_3/Gd_2O_3 in weight	A_b	A_{Nd}	A_{Gd}	D_{Nd}/D_{Gd}	D_{Nd}/D_{Gd} (Mean)
4.40	39.9	23.3	21.4	0.86	0.87
	40.8	24.3	22.5	0.87	
4.50	39.8	24.7	25.3	1.05	1.05
	39.8	24.1	24.7	1.05	

From these experiments, the value 4.45 was taken as the balance ratio. A trial experiment with a sample which consisted of neodymium oxide and gadolinium oxide in the proportion of 4.45 to 1.00 showed, as was seen in Table 11, that the value was correct.

Table 11.

Nd_2O_3/Gd_2O_3 in weight	A_b	A_{Nd}	A_{Gd}	D_{Nd}/D_{Gd}	D_{Nd}/D_{Gd} (Mean)
4.45	39.0	26.3	26.6	1.03	1.01
	40.8	31.8	31.8	1.00	

(b) The experiments were also carried out to know the effects of other rare earth elements. The absorption effects are expected by no element of the rare earth group. As the wave-length difference of the absorption edges corresponding to the said two lines under comparison is fairly large, some rare earth elements may have the excitation effects.

The following three samples were used for the examples: Sample No. 6 consisted of the rare earths obtained from so-called gadolinium oxalate on sail which was not naturally pure and contained various rare earth elements; Sample No. 7 was a mixture of the rare earths rich in the elements of yttrium group; Sample No. 8 was the rare earths extracted from gadolinite found in Gihu Prefecture, Japan.

Various quantities of neodymium oxide were added to these samples respectively and the intensity ratio of the two lines under comparison was determined with the results shown in Table 12.

Table 12.

(1) Sample No. 6.

$\frac{Nd_2O_3 \text{ added}}{\text{Sample taken}}$ (%)	A_b	A_{Nd}	A_{Gd}	D_{Nd}/D_{Gd}	D_{Nd}/D_{Gd} (Mean)
0					0.59
11.4	43.5	34.0	36.0	1.30	1.28
	43.2	34.0	36.0	1.25	
9.8	39.8	33.3	33.3	1.00	1.00
	39.8	33.3	33.3	1.00	
8.6	40.5	35.0	34.2	0.86	0.88
	40.5	34.4	33.8	0.90	

(2) Sample No. 7.

$\frac{Nd_2O_3 \text{ added}}{\text{Sample taken}}$ (%)	A_b	A_{Nd}	A_{Gd}	D_{Nd}/D_{Gd}	D_{Nd}/D_{Gd} (Mean)
0					0.75
4.5	42.3	35.3	33.8	0.81	0.79
	41.8	35.1	33.3	0.77	
5.4	39.3	32.5	32.5	1.00	1.00
	38.8	31.3	31.3	1.00	
9.7	43.3	36.8	38.3	1.33	1.31
	43.3	37.5	38.7	1.28	

(3) Sample No. 8.

$\frac{Nd_2O_3 \text{ added}}{\text{Sample taken}}$ (%)	A_b	A_{Nd}	A_{Gd}	D_{Nd}/D_{Gd}	D_{Nd}/D_{Gd} (Mean)
0					0.54
12.2	42.3	34.1	37.3	1.71	1.66
	42.3	34.9	37.3	1.53	
9.2	41.2	33.0	34.4	1.23	1.29
	40.7	32.2	34.2	1.35	
7.4	42.8	38.0	38.1	1.02	1.01
	43.8	37.3	37.3	1.00	
6.1	37.3	27.3	25.8	0.85	0.82
	37.3	27.5	25.3	0.79	

From Table 12 (1), we knew that the addition of 9.4% of neodymium oxide to Sample No. 6 would make the said two lines equally intense. After the addition of this amount of neodymium oxide to the original sample, various quantities of neodymium oxide and gadolinium oxide were added in the proportion, $Nd_2O_3/Gd_2O_3 = 4.45$, and the relative intensities of the said two lines were compared. An example of the results obtained is shown in Table 13 (1).

Samples No. 7 and No. 8 were treated in a similar way. After the addition of 5.4% of neodymium oxide to Sample No. 7 or 7.4% of it to Sample No. 8, various quantities of neodymium oxide and gadolinium oxide were added in the proportion, $Nd_2O_3/Gd_2O_3 = 4.45$, respectively, and the relative intensities of the said two lines were compared. An example for each case is shown in Table 13 (2) and in Table 13 (3) respectively.

Table 13.

(1) Sample No. 6.

A_b	A_{Nd}	A_{Gd}	D_{Nd}/D_{Gd}	D_{Nd}/D_{Gd} (Mean)
37.8	27.3	27.7	1.05	1.01
37.8	26.9	26.7	0.98	

(2) Sample No. 7.

A_b	A_{Nd}	A_{Gd}	D_{Nd}/D_{Gd}	D_{Nd}/D_{Gd} (Mean)
30.3	25.7	25.9	1.03	1.01
30.3	24.5	24.5	1.00	

(3) Sample No. 8.

A_b	A_{Nd}	A_{Gd}	D_{Nd}/D_{Gd}	D_{Nd}/D_{Gd} (Mean)
40.3	24.6	26.0	1.13	1.13
40.3	24.6	26.0	1.13	

From the above experiments, we knew that the balance ratio 4.45 which was determined with the mixture of gadolinium and neodymium oxides also held true of Samples No. 6 and No. 7, and the effects of the other rare earth elements were not observed in these cases. A little low value 4.4 was obtained for Sample No. 8.[13] As the content of neodymium

(13) This might be due to the excitation effect of dysprosium richly present in the sample, although it could not yet be confirmed.

oxide in this sample was estimated to be 19.4% by the method described in the previous part of this report, the content of gadolinium oxide would be 6.1% if we took 4.4 for the balance ratio. It would be 6.0% if we assumed the balance ratio to be 4.45.

Table 14.

Allanite from Oyama.

MgO	1.29%
CaO	10.42
MnO	1.22
FeO	4.76
Fe_2O_3	9.70
Al_2O_3	16.03
La_2O_3	0.63
Ce_2O_3	5.96
Pr_2O_3	0.57
Nd_2O_3	3.80
Sm_2O_3	1.92
Gd_2O_3	1.02
Y_2O_3 etc.	4.19
ThO_2	2.11
SiO_2	34.65
H_2O	1.58
Total	99.85%

Applications.

These methods, combined with the other methods,[14] were applied in this laboratory to the analyses of chemical preparations as well as of minerals containing rare earth elements. As an example, the result of the analysis of allanite found in Oyama, Ehime Prefecture, Japan is given in Table 14.[15]

Summary.

(1) Lanthanum in a rare earth mixture can be determined by comparing the intensity of its $L\beta_2$ line with that of the cerium $L\beta_3$ line.

(2) Neodymium in a rare earth mixture can be determined by comparing the intensity of its $L\alpha_1$ line with that of the cerium $L\beta_1$ line.

(3) Gadolinium in a rare earth mixture can be determined by comparing the intensity of its $L\alpha_1$ line with that of the neodymium $L\beta_2$ line.

In conclusion, the author wishes to express his hearty thanks to Professor M. Katayama and to Professor Y. Shibata for their kind interests during the work. It is also the author's pleasant duty to acknowledge the valuable advice offered by Dr. Y. Nishina.

A part of the cost of this investigation was defrayed from the grant of the Nippon Gakujutsu Shinko-kwai (the Japan Society for the Promotion of Scientific Research) for which also the present author wishes to record his thanks.

Laboratory of Analytical Chemistry,
Chemical Institute, Faculty of Science,
Imperial University of Tokyo.

(14) For the determination of praseodymium, the intensity of the praseodymium $L\beta_2$ line was compared with that of the neodymium $L\beta_3$ line; vid. S. Shinoda, *J. Chem. Soc. Japan*, **56** (1935), 76. For the determination of samarium and also of neodymium, the intensity of the samarium $L\alpha_1$ line was compared with that of the neodymium $L\beta_1$ line by the wedge method proposed by S. Shinoda of this laboratory; vid. S. Shinoda, *J. Chem. Soc. Japan*, **56** (1935), 1483; *ibid.*, **58** (1937), 989.

(15) M. Ikawa, *J. Chem. Soc. Japan*, **58** (1937), 1261.

X-Ray Investigation of the Cubic Modification of Pentaerythritol, $C(CH_2OH)_4$.

By Isamu NITTA and Tokunosuké WATANABÉ.

(Received December 28, 1937.)

It has been reported by L. Ebert,[1] that pentaerythritol, $C(CH_2OH)_4$, shows in the temperature range between 179.5 and 260.5°C., its melting point, another crystalline modification, which is optically isotropic, and that the heat of transition is estimated from the cooling curve to be several times as large as the heat of fusion. Now that the structure of the ordinary tetragonal modification has been determined independently by the present authors[2] and by Llewellyn, Cox, and Goodwin,[3] it will be of interest to make an X-ray investigation of the cubic modification to see if there exist some close relationships between the two structures.

The important features of the determined tetragonal structure may be summarized as follows: If the hydrogen atoms of the OH groups are not taken into consideration, the molecule $C(CH_2OH)_4$ in the crystal possesses approximately the symmetry of D_{2d}–$\bar{4}2m$, precisely S_4–$\bar{4}$, with one pair of primary alcohol radicals puckered upwards and the other downwards, namely,

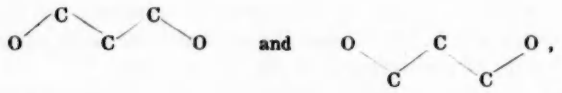

all the bond angles of these atoms being approximately tetrahedral (Fig. 1). The molecules are arranged flat in a sheet parallel to the crystallographic c-plane, and the whole crystal is made up of such molecular layers. The linkage between neighbouring molecules in a layer is more or less firm by the interaction of the hydroxyl groups. The geometrical aspect of this linkage is such that four hydroxyl oxygen atoms, one out of each adjoining molecule, constitute a square, of which every side is presumably bridged over by a hydrogen atom (Fig. 2).

(1) L. Ebert, *Ber.*, **64** (1931), 114. See also K. Weissenberg, *Naturwissenschaften*, **15** (1927), 996; W. M. Cohn, *Z. Physik*, **50** (1928), 134.

(2) I. Nitta and T. Watanabé, *Nature*, **140** (1937), 365.

(3) F. J. Llewellyn, E. G. Cox, and T. H. Goodwin, *J. Chem. Soc.*, **1937**, 883.

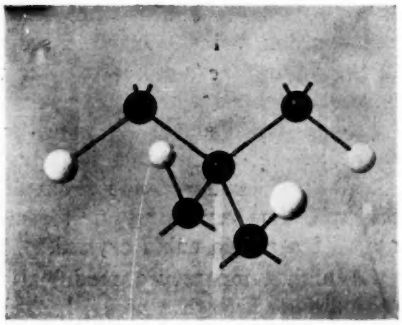

Fig. 1. Atomic configuration in tetragonal pentaerythritol, with C atoms shown as black and O atoms as white balls.

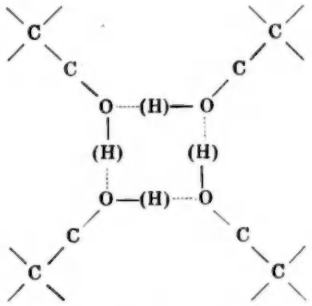

Fig. 2. Hydrogen bridges in tetragonal pentaerythritol.

In such closed hydrogen bridges, the "synchronized oscillations" may, according to Huggins,[4] cause an increased stability of the intermolecular linkage.

In the present experiment, material from Schering-Kahlbaum A. G. was fractionally crystallized from aqueous solution. The melting point of the sample was 257°C. Although the same sample was ascertained to melt, after sublimation, at a temperature higher than 260°C. as Ebert describes, such sublimate was not used.[5]

Since the old crystallographic choice of the principal axes of tetragonal pentaerythritol gives the value $c/a = 1.0236$ at a room temperature,[6] it was first examined by the Laue photographic method if the ratio c/a tends to unity as the temperature approaches to the transition point so that the transformation from tetragonal to cubic takes place rather continuously. Several Laue photographs were prepared at various temperatures up to 179.5°C. with the incident X-ray beam normal to the crystal slice cleaved along (001). The change of the ratio c/a was not found in the sense to decrease to unity. For example, the observed value was $c/a = 1.043$ at a temperature a little below the transition point. It was also found that the dissymmetrical intensity distribution of the Laue spots, (hkl) and (khl) in pairs, remains almost unaltered over the whole examined range of temperatures below 179.5°C. This implies that any torsional change of the atomic arrangement around a tetragonal axis does not sensibly occur. In other words, the molecular shape itself and the

(4) M. L. Huggins, *Nature*, **139** (1937), 550.

(5) For the ordinary and microscopic determination of the melting point our thanks are due to Mr. Z. Kochi at the Osaka Pharmaceutical College.

(6) P. Groth, "Chemische Krystallographie," Part III, 385.

relative orientation of the molecules in a (001) layer undergo practically no change up to the vicinity of the transition point. Thus it seems probable that the observed increase in the value of c/a is mainly due to the enlargement of the spacing $c/2$ between successive molecular layers. When the temperature of the crystal slice is raised above the transition point, the characteristic Laue pattern of the tetragonal modification is replaced by an assembly of a large number of smaller Laue spots distributed quite irregularly on the photograph, thus rendering our attempt unsuccessful to obtain Laue photographs of a single cubic crystal.

Debye-Scherrer photographs of the high temperature modification were made with the copper K radiation filtered through a nickel foil, the camera radius being 100 mm. and the angular range of the film ca. 70°. The temperature of the rotating sample was kept at 230°C. approximately. The films were protected by a paper screen in front of them from heat radiation of the electrical furnace, in which the sample was placed, and they were also water-cooled on the back side in order to prevent difficulties, such as their deformation and fogging, which will be caused by the elevation of the film temperature. It took about ten times as much time of exposure to obtain photographs with the appearance of the first seven lines as that necessary for good photographs of the tetragonal modification at ordinary temperatures. The obtained data are given in Table 1. It may be remarked here that Cohn[7] has already shown in his paper three powder photographs of pentaerythritol taken at 20, 140 and 230°C. respectively, of which he made no analysis of the obtained lines. Perhaps he regarded the third one of his photographs as solely due to the high temperature modification. However, it is now obvious from our present experiment that this is not a pure one but a mixed photograph due to both of the two modifications, indicating that his sample was not kept constantly at a temperature above the transition point.

As shown in Table 1, all the lines on the photographs are very well accounted for by a cubic face-centered lattice, the side of the unit cube being $a = 8.963$ A. at 230°C. Taking the number of molecules contained in the unit as four, the density of the crystal is computed to be $\rho = 1.255$ at 230°C., which is much lower than the value $\rho = 1.398$ at 25°C. for the tetragonal modification. As the volume increase of this tetragonal modification in the range from room temperatures to the transition point is estimated to be not much more than one per cent, the transformation should be accompanied by a considerable expansion of volume, and this is actually in accord with Ebert's and our observations. As for the re-

(7) W. M. Cohn, *Z. Physik*, **50** (1928), 134.

Table 1. Powder photographic data of cubic pentaerythritol.

l (mm.)	θ	$\sin\theta$	d (A.)	hkl	a (A.)
29.8	8°32′	0.1484	5.18_5	111	8.98_0
34.5	9°52′	0.1713	4.49_2	200	8.96_4
49.0	14° 4′	0.2431	3.16_5	220	8.95_1
60.4	17°18′	0.2974	2.58_7	222	8.96_1
70.1	20° 5′	0.3434	2.24_1	400	8.96_4
76.7	21°58′	0.3741	2.05_7	331	8.96_8
78.8	22°35′	0.3839	2.00_4	420	8.96_2
					mean 8.96_3

maining possible units for the crystal, it will be shown that either they contradict with the observed facts or they can be looked upon as improbable.

It is now required to arrange four molecules of $C(CH_2OH)_4$ in the face-centered cubic unit so as to furnish the crystal as a whole with the symmetry characteristic of the cubic system. However, such high symmetry cannot be afforded by the usual manner of arranging the four molecules of the symmetry S_4-$\bar{4}$, which is found in the case of tetragonal pentaerythritol. Thus it comes into question if the unit chosen above is wrong. In order, for the molecule of the symmetry S_4-$\bar{4}$, to yield a unit of cubic symmetry, their number in such unit must be some multiples of 3. After elimination on account of absurd values for the density of the crystal, there remains only one unit containing 12 molecules to be taken into consideration. In this case the side of such a unit becomes 12.67 A. and the underlying lattice simple or body-centered. However, the number of lines actually observed is too few to be accounted for in a natural way by such simple or body-centered lattice. Thus the unit of twelve molecules may also be eliminated. Returning to the original cubic face-centered unit containing four molecules, there arises a second question how it is possible to explain this peculiarity in the symmetry consideration. As in the cases of certain crystal structures,[8] a statistical explanation can be given to such phenomena; i.e. acquisition of higher molecular symmetry by some statistical means. In the present case of pentaerythritol, there will be three ways possible to realize such acquisi-

(8) See, for example, S. B. Hendricks and L. Pauling, *J. Am. Chem. Soc.*, **47** (1925), 2904; S. B. Hendricks, *Z. Krist.*, **74** (1930), 29; L. Pauling, *Phys. Rev.*, **36** (1930), 430; S. B. Hendricks, *Z. Krist.*, **84** (1932), 85; I. Nitta and T. Watanabé, *Sci. Papers Inst. Phys Chem. Research* (Tokyo), **26** (1935), 164.

tion. In the first one, the molecule is considered to keep the symmetry of S_4-$\bar{4}$; in the second, it is regarded to be non-rigid owing to the rotation about the single C–C bonds, of which the four directions from the central carbon atom are in angles of 109°28′; and in the third, both the molecular shape and the mutual orientation of the molecules are to be changed. All of these three possible ways will be taken into the following considerations to see which will give the best account for the observed intensities, the atomic separations in the molecule being assumed to be 1.54 A. for the C–C and 1.46 A. for the C–O bonds and the valency angles of the carbon atoms to be 109°28′.

On the assumption of the rigid molecule possessing the symmetry of S_4-$\bar{4}$, there are two extreme cases conceivable, in which the cubic symmetry of the statistical molecule is attained. The one case is that in which free spatial rotation of the molecule sets in so as to furnish it with the spherical symmetry (Case I). Then the corresponding space group is O_h^5-$Fm3m$ in the statistical sense. In the other case, which is rather statical, the whole crystal is constituted by a random distribution of three kinds of molecules, in equal concentration, the molecular $\bar{4}$-axis of each kind being parallel to each of the principal axes of the crystal (Case II). The space group is now statistically T_d^2-$F\bar{4}3m$. Intermediate of the above two, there is another important case, in which half of the molecules in Case II are rotated about the molecular axis through the angle of 90° (Case III). By the addition of these new orientations, the crystal acquires the cubic holohedral symmetry, the space group being again O_h^5-$Fm3m$. Among these three cases, it was found that Cases II and III account for the observed intensities fairly well, while Case I does not. The calculation of the intensities was made by assuming the molecular symmetry to be T_d-$43m$.

The second possibility of non-rigid molecule gives following important cases worth consideration, the four methylenic carbon atoms being assumed in all these cases as lying on the trigonal axes of the crystal. It is first conceivable that the hydroxyl groups rotate freely around the C–C bonds (Case IV, Fig. 3). Such arrangement corresponds to the space group T_d^2-$F\bar{4}3m$. However, this does not explain the observed intensity data. Next come two rather statical cases (Cases V and VI), in which each of the hydroxyl groups statistically take such three-fold positions, around the directions of the C–C bonds and at the same time in the planes defined by pairs of these C–C bonds, that the molecule may possess the symmetry of T_d-$\bar{4}3m$ (Fig. 4; black circles in Case V and open circles in Case VI). An atomic configuration of the molecule in Case V is closely related to Case II, followingly also to the original molecular shape, and

the calculated intensities are the same for both cases. The space groups in Cases V and VI are T_d^2-$F\bar{4}3m$. Though not satisfactorily, Case V explains the observed intensities much better than Case VI. Besides these,

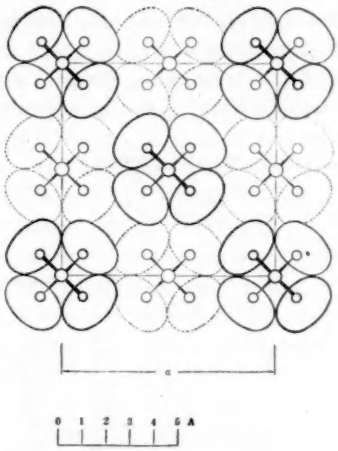

Fig. 3. Molecular arrangement of pentaerythritol in cubic form, corresponding to Case IV.

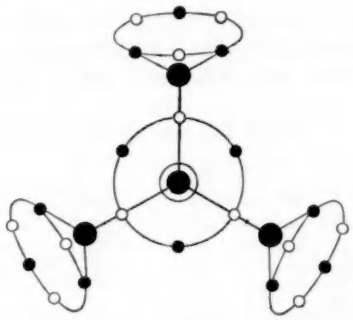

Fig. 4. Statistical atomic configurations of cubic pentaerythritol, $C(CH_2OH)_4$. The largest circle represents the central C, black circles the methylenic C atoms, and small circles the hydroxyl O atoms (black for Case V and white for Case VI).

there will be also another possible molecular symmetry of T-23. This seems, however, rather improbable in the present case of internal motions of non-rigid molecule.

The third possibility of non-fixed orientation of non-rigid molecules will now be discussed. In the first place, the spherical rotation of the molecule with freely rotating hydroxyl groups. This, however, does not seem to correspond to the observation. There comes next another case, in which half of the molecules of Case IV are rotated about the molecular axis through the angle of 90° as in Case III (Case VII). The mean molecular symmetry and the space group are O_h-$m3m$ and O_h^5-$Fm3m$ respectively. This case also does not explain the observed intensities. The same kind of change in the molecular orientations produces from Cases V and VI two new cases (Cases VIII and IX), to which the same molecular symmetry and the same space group as above can be given. The calculated intensities in Case VIII are the same as in Case III and explain the observed intensities fairly well, while Case IX fails. Perhaps it will be superfluous to note that the symmetry properties of Cases VII, VIII, and IX can be effected also by the rotations of molecular axes in azimuth.

After all these considerations, of which the resulting intensities are brought together in Table 2, following conclusions may be regarded as probable. Above the transition point, 179.5°C., pentaerythritol gives a cubic form, in which the central carbon atoms are arranged to build a cubic face-centered lattice, the distance between nearest molecular centers being calculated to be 6.338 A. from the side $a = 8.963$ A. of the unit. In this cubic modification, the layer structure of the tetragonal form is not retained any more, although fairly weakened hydrogen bonds seem to

Table 2. Calculated intensities for various possible cases.

hkl	I	II, V	III, VIII	IV	VI	VII	IX	X	$I_{obs.}$
111	206	327	306	262	280	260	220	287	v.v.s.
200	97.5	11.2	11.2	31	57.3	31	57.3	19.7	v.s.
220	62 3	1.8	1.8	1.8	1.2	1.8	1.2	1.8	—
311	49.5	3.1	2.2	5.0	11.0	0.7	1.2	1.3	v.v.w.
222	13.0	20.0	20.0	2.7	3.3	1.4	3.4	7.9	m.
400	4.0	0.0	0.0	0.3	2.2	0.3	2.2	0.0	v.v.w.
331	9.8	4.8	1.9	4.3	3.0	1.2	0.8	1.6	v.w.
420	8.2	2.2	2.2	0.0	1.5	0.0	1.5	0.7	v.w.
422	5.5	2.5	0.8	3.0	2.7	1.9	1.5	1.3	—
333 511	4.8	3.8 0.3	3.1 0.1	0.6 1.1	1.1 1.3	0.6 0.5	0.1 0.6	1.6 0.4	—

exist still. The molecule becomes non-rigid on account of rotation about the C–C bonds. This rotation, however, is not at all free, and the probability for the existence, accordingly the stability, of the atomic configuration, which corresponds to that observed in the molecule of the tetragonal modification, is outstandingly great among other possible configurations. By virtue of this rotation the orientation of the molecular $\bar{4}$-axis for such most stable atomic configuration can now and then be interchanged with each of the two directions, which are perpendicular to the original one. At the same time as the molecule becomes non-rigid, rotations of the molecule as a whole set in, but these are also not quite free. The most stable molecular orientations together with the most stable atomic configuration of the molecules are probably represented by what is described as Case VIII. Indeed, the actual motions in and of the molecules within the crystal will be very complicated and it will not be satisfactory to try to explain with any one of such models, rather statical in a certain sense, as above. Thus in order to make a better fit to the

observed intensities, it is necessary to take into account more cases in addition to Case VIII; for example, a weighted mean of Cases VIII and VII (Case X in Table 2). It will be added that, from the physical point of view, Case III does not probably represent the actual state of matter, though this can explain the intensities as well as Case VIII.

Perhaps it is interesting to notice that the molecular state in the cubic modification already approaches very much to that of the liquid state. This is fairly obvious from the very small heat of fusion.[1] The thermal vibrations of the molecular centers in the cubic crystal must be considerable chiefly because of the non-rigidity of the molecules. This is shown in the strong decrease of the intensity distribution with increasing angle on the powder photographs. In fact, a temperature factor $\exp(-B\sin^2\theta)$ with so large a constant B as 6.7 was used in the calculation of the intensities (Table 2).

It is well-known that the molecule of pentaerythritol was found in the molecular beam experiment of Estermann[9] to possess a dipole moment of approximately 2×10^{-18} E.S.U. Since a molecule of the symmetry of S_4-$\bar{4}$ cannot have a dipole moment, some intramolecular motions should be assumed in the molecule of pentaerythritol.[10] In this respect the non-rigidity of the molecule found in the present experiment may be looked upon as giving a concrete ground for this assumption, if in the molecular beam investigation above mentioned the temperature, not given in the paper of Estermann, is supposed to be enough high. On the other hand, no moment of pentaerythritol tetrabromide, of which the molecular structure in the gaseous state was determined by the electron diffraction study of de Laszlo[11] to be similar to that of the tetragonal pentaerythritol, will be interpreted by the non-rotation of the C–C bonds owing to the large volume and mass of the bromine atoms.

In conclusion, we wish to express our thanks to the Hattori Hôkôkwai for a grant.

Laboratory of Physical Chemistry, Faculty of Science,
Osaka Imperial University.

---

(9) J. Estermann, *Z. physik. Chem.*, B, **2**(1929), 287.
(10) Refer, for example, to L. Ebert, "Leipziger Vorträge," **1929**, p. 44.
(11) H. de Laszlo, *Compt. rend.*, **198** (1934), 2235.

On the Thermal Transition in Solid Deuterio-Ammonium Sulphate, $(ND_4)_2SO_4$.

By Isamu NITTA and Katsuji SUENAGA.

(Received December 28, 1937.)

In a previous paper[1] it has been reported that deuterio-ammonium chloride, ND_4Cl, shows like ordinary one the phenomenon of excessive specific heat with a discontinuity at about $-24°C.$, this being roughly by six degrees higher than the corresponding transition temperature of ordinary ammonium chloride. The work had been carried out in an attempt to get some closer informations concerning the nature of such peculiar kind of thermal transitions, which, according to the rather qualitative explanation of Pauling,[2] are due to the onset of rotations of the atomic groups in crystals. As a continuation of the investigation, thermal and dilatometrical measurements of the transition of deuterio-ammonium sulphate, $(ND_4)_2SO_4$, have now been made, of which an account will be given in the present paper.

The material used in the present experiment was prepared in the following way. The starting substances of the preparation were deuterium oxide from Norsk Hydro-Electrisk Kvaelstofaktieselskab, magnesium metal from Schering-Kahlbaum A. G., potassium nitrite, ammonium chloride and sulphur trioxide, the last three being pure chemicals of E. Merck. Using magnesium powder and chemical nitrogen from potassium nitrite and ammonium chloride, magnesium nitride, Mg_3N_2, was first produced. By the reaction of this nitride with deuterium oxide, heavy ammonia, ND_3, was then obtained and this was led into heavy sulphuric acid, D_2SO_4, from D_2O and SO_3, to produce the final material $(ND_4)_2SO_4$, the whole procedure being carried out in an evacuated system. The sample thus obtained was determined to contain 93.5 per cent of deuterium. A Debye-Scherrer photograph of this sample showed that the crystal structure is the same as that of ordinary ammonium sulphate, having the unit of practically the same dimensions.

By use of a micro-dilatometer of ordinary type, measurements were made with ordinary and heavy sulphates in a temperature range from

(1) I. Nitta and K. Suenaga, *Sci. Papers Inst. Phys. Chem. Research* (Tokyo), **32** (1937), 83. See also A. Smits and C. J. Muller, *Nature*, **139** (1937), 804.

(2) L. Pauling, *Phys. Rev.*, **36** (1930), 430.

−55 to −40°C. Carbon disulphide was chosen as the dilatometer liquid for the reason that the molecule of this compound contains no hydrogen atom. It is found from the measurements that both salts show quite similar volume-temperature curves and the transitions are accompanied by abrupt contraction of their volumes as the temperature is being raised, the relative change $\Delta V/V$ being approximately a half per cent for both salts. In the case of the ordinary salt the sudden change in volume occurs at −50.3°C. when the temperature is being lowered and −49.5°C. when raised. For the heavy salt the corresponding temperatures are −49.8 and −49.0°C. From these, the dilatometrical values of the transition temperatures are determined to be −49.9°C. for $(NH_4)_2SO_4$ and −49.4°C. for $(ND_4)_2SO_4$. Besides carbon disulphide, toluene was also used, in another dilatometer, to study the transition of ordinary ammonium sulphate with higher precision, and the result is given in Fig. 1. In spite of the early report that R. Ewald[3] failed to find out dilatometrically the transition of $(NH_4)_2SO_4$, it is certain from the present experiment that it really exists and can be observed by use of a dilatometer, if the temperature intervals are chosen small enough.

In order to confirm these obtained values for the transition points and, at the same time, to determine the heats of transition, cooling and heating curve measurements were also carried out with the aid of the same calorimeter as that used for the specific heat determination, which will be described below. The amount of sample taken was 8.35 g. in the case of the ordinary salt and 8.58 g. in the other. The heating curves were prepared with the energy supply of about 2 calories per minute. The obtained curves are shown in Fig. 2. Ordinary ammonium sulphate exhibits an arrest at −49.5°C. on heating and it shifts to −50.7°C. on cooling. The corresponding temperatures for the heavy ammonium sulphate are −48.9 and −50.2°C. Taking the mean of the both arrests on heating and cooling curves, the transition temperatures are given to be −50.1°C. for $(NH_4)_2SO_4$ and −49.6°C. for $(ND_4)_2SO_4$ in good agreement with the dilatometric values obtained above. From the data of the heating curves the heats of transition were determined for both ordinary and heavy salts. They are 210 at −49.5°C. for the former and 225 at −48.9°C. for the latter in calories per gram-ion of ammonium. These values are very remarkable in such a respect that Crenshaw and Ritter[4] gave from their specific heat measurement as the heat of transition of ordinary ammonium sulphate the value 485 cal./gram-ion, which is more

(3) R. Ewald, *Ann Physik*, **44** (1914), 1223.
(4) J. L. Crenshaw and I. Ritter, *Z. physik. Chem.*, B, **16** (1932), 143.

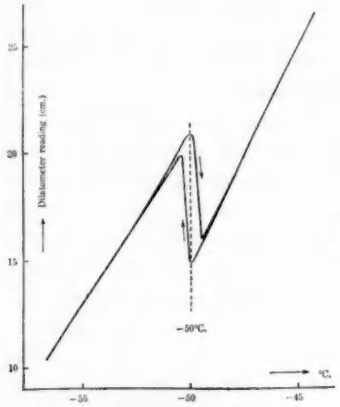

Fig. 1. Dilatometric curve of $(NH_4)_2SO_4$.
The liquid: toluene.
Sample taken: 8.02 g.

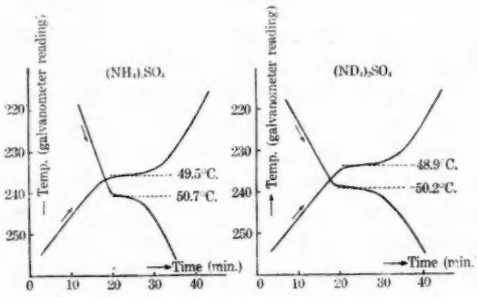

Fig. 2. Cooling and heating curves.

than double as large as the present value 210. This great disagreement seems to be due partly to the difficulty in computation of the heat of transition from the specific heat data and partly to their obtained data themselves, which are always somewhat too high as compared with the values of the present specific heat measurement (Table 1), and also judging from the molecular heat 44.80 cal. at 29°C. obtained by R. Ewald.[3]

The specific heats of ordinary and heavy ammonium sulphates were measured in the range from −180 to +25°C., using an improved vacuum calorimeter of the Nernst type. This calorimeter is made of copper and nickel-plated, its dimensions being 2 cm. in diameter and 4 cm. in height. There are six radial vanes, about 0.2 mm. thick, welded on the inside wall of this calorimeter in order to secure quick and effective conduction of heat into the crystalline sample. Being surrounded by a copper vessel, which is also nickel-plated and whose temperature can be controlled electrically, the calorimeter is put into an enclosed glass system to be evacuated. The samples taken were the same as those used for the cooling and heating curve measurements, viz. 8.35 g. of $(NH_4)_2SO_4$ and 8.58 g. of $(ND_4)_2SO_4$. In each measurement 5 to 20 calories of energy were supplied electrically to the calorimeter and the temperatures were measured by means of copper-constantan thermocouples. The obtained molecular heats C_p are shown in Tables 1 and 2. They are also plotted in form of the molecular heat-temperature curves in Fig. 3. The general

features of the curves are similar to those of ordinary and heavy ammonium chlorides. The discontinuous fall of specific heat begins at $-50°C.$ in the case of ordinary ammonium sulphate and at $-49.5°C.$ in the other. These temperatures of transition agree very well with those found on the volume-temperature and thermal analysis curves. As in

Table 1. Molecular heat of $(NH_4)_2SO_4$.

$t°C.$	Mol. heat	$t°C.$	Mol. heat	$t°C.$	Mol. heat
−180	19.5	−90	38.0	−47.5	42.3
−170	20.9	−80	43.0	−45	40.4
−160	22.6	−70	47.2	−40	40.9
−150	25.2	−60	55.2	−30	42.2
−140	26.8	−55	63.4	−20	43.3
−130	29.2	−52.5	70.7	−10	44.4
−120	31.4	−51.0	80.1	0	44.8
−110	33.6	−50.5	103.	+10	45.5
−100	36.4	−49	53.8	+20	46.0

Table 2. Molecular heat of $(ND_4)_2SO_4$.

$t°C.$	Mol. heat	$t°C.$	Mol. heat	$t°C.$	Mol. heat
−180	23.0	−90	47.2	−47.5	45.9
−170	25.2	−80	50.6	−45	44.8
−160	27.8	−70	54.2	−40	45.8
−150	30.2	−60	60.2	−30	45.9
−140	33.0	−55	67.8	−20	46.4
−130	34.2	−53	75.9	−10	47.2
−120	37.6	−51	92.3	0	48.3
−110	39.6	−50.5	107	+10	49.8
−100	43.2	−48.5	50.2	+20	50.6
				+25	51.5

the case of deuterio-ammonium chloride, the anomalous rise of the specific heat curve of the heavy sulphate begins at a relatively lower temperature as compared with that of the ordinary one. However, it is not certain whether this is characteristic of ND_4 ions, or due to the presence of lighter

components. Besides this peculiarity the curve for the heavy compound lies always higher than that for the ordinary one.

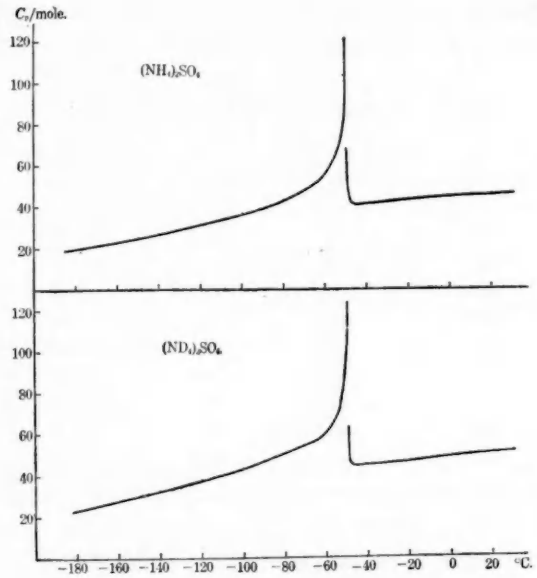

Fig. 3. Molecular heat-temperature curves.

For the reason of analogy, it would be natural from the observations on ordinary and heavy ammonium chlorides to expect that the transition point of heavy ammonium sulphate would be at least a few degrees higher than that of the ordinary sulphate. In the actual case, there was found a temperature shift of not more than a half degree. Perhaps this suggests that the phenomena of such transitions would not be so simple, if one tries to give a quantitative explanation of them. From the point of view of Pauling and Fowler,[5] it seems not impossible to imagine that, in the case of an oxy-acid, the interaction between deuterio-ammonium ion and the surrounding oxygen atoms would be weaker than that in the ordinary ammonium salt and that such effect would cancel out the opposing tendency of raising the transition temperature due to the doubling of the moment of inertia, brought about by the substitution of deuterium

(5) L. Pauling, *loc. cit.*; R. H. Fowler, *Proc. Roy. Soc.* (London), A, **149** (1935), 1; A, **151** (1935), 1; see further his book, "Statistical Mechanics," 2nd Ed., 789 (1936).

in the rotating ammonium ion. Further discussion will be reserved until the investigation is extended to other deuterio-ammonium salts. Only it will be added that, though there are structurally two kinds of ammonium ions in the crystal lattice, the one is surrounded by nine and the other by ten oxygen atoms, there was found single transition point without any observable fine structure in the volume-temperature, thermal analysis, and molecular heat-temperature curves.

In conclusion, we wish to express our thanks to Mr. M. Koizumi for the determination of deuterium content and also to the Hattori Hôkôkwai for a grant.

Laboratory of Physical Chemistry, Faculty of Science,
Osaka Imperial University.

The Heat of Formation and the Specific Heat of Silicon Nitride.

By Shun-ichi SATOH.

(Received November 25, 1937.)

I. **Introduction.** The specific heat of silicon nitride has not yet been determined. Nor has the heat of formation of silicon nitride been measured directly in a calorimeter. The values so far reported in the literature are as follows: C. Matignon[1] obtained the value 159,300 cal. and W. B. Hincke and L. R. Brantley[2] reported the value 176,300 cal. at 1700°K. The object of the present paper is to determine the specific heat and from it the most probable value of the heat of formation of silicon nitride.

II. **Specimen.** (1) *Preparation of specimen.* For the preparation of silicon nitride, the following two methods were adopted: (a) In the first place, silicon amide was prepared by the action of ammonia on silicon tetrachloride:

$$SiCl_4 + 8\,NH_3 = Si(NH_2)_4 + 4\,NH_4Cl\,,$$

(1) C. Matignon, *Bull. soc. chim.*, [4], **13** (1913), 791.
(2) W. B. Hincke and L. R. Brantley, *J. Am. Chem. Soc.*, **52** (1930), 48.

and then it was washed with liquid ammonia to remove ammonium chloride. Silicon amide thus purified was heated in nitrogen to 1200°C. and silicon nitride was obtained as follows[3]:

$$Si(NH_2)_4 \xrightarrow{0°C.} HNSi(NH_2)_2 \xrightarrow{100°C.} NSiNH_2 \xrightarrow{900°C.} HN(SiN)_2 \xrightarrow{1200°C.} Si_3N_4 .$$

Unfortunately, the product obtained in this way did not contain sufficient nitrogen.

(b) In the second place, purified nitrogen was passed over silicon (Kahlbaum) heated at 1300–1400°C. for ten hours (the method of L. Weiss and T. Engelhardt[4]). The silicon nitride thus obtained appeared greyish white and contained Si_2N_3, SiN, SiO_2, and some unchanged silicon. With the object of separating this unchanged silicon, SiN, and Si_2N_3, the nitrides were heated with 20% potassium hydroxide solution for seven hours. By this treatment, SiN was decomposed into silicon and nitrogen, and the silicon thus formed and the unchanged silicon are taken away as silicate. Next, the nitrides thus treated were put in a platinum dish containing 10 c.c. water mixed with 5 c.c. concentrated hydrofluoric acid and 5 c.c. concentrated nitric acid and left there for four days in order to take away Si_2N_3. The nitrides thus purified which contain Si_3N_4 and SiO_2 were washed with water and dried with alcohol and ether.

(2) *Analyses of specimen.* The nitrogen content of the above mentioned specimen was estimated by the method used by A. Dumas. The material to be analysed was intimately mixed with PbO and $PbCrO_4$ of equal quantity. The result thus obtained was 35.07% N. The silicon content was estimated by fusing the specimen with equal mixture of Na_2CO_3 and K_2CO_3. After dissolution in hydrochloric acid, the silica was filtered off and ignited. The result thus obtained was 58.44% Si. From the results shown above, the specimen may be considered to consist of 87.74% Si_3N_4 and 12.26% SiO_2.

III. **The Specific Heat of Silicon Nitride.** The mean specific heat of silicon nitride was measured by means of the ice calorimeter adopted by P. Oberhoffer[5]. The details of the measurement were already described in the measurement of the specific heat of aluminium nitride[6].

---

(3) F. Lengfeld, *Am. Chem. J.*, **21** (1899), 531; Em. Vigoroux and C. Hugot, *Compt. rend.*, **136** (1903), 1670; M. Blix and W. Wirbelauer, *Ber.*, **36** (1903), 4220; A. Stock and F. Zeidler, *Ber.*, **56** (1923), 986.

(4) L. Weiss and T. Engelhardt, *Z. anorg. allgem. Chem.*, **65** (1909), 38.

(5) P. Oberhoffer, "Dissertation Aachen," (1907).

(6) S. Satoh, *Sci. Papers Inst. Phys. Chem. Research* (Tokyo), **29** (1936), 19.

The measurement was carried out over the following three temperature intervals: 0–99.5, 0–316.4, and 0–585°C. The specimen was compressed and put into an aluminium cylinder of 8 mm. diameter and 2–3 mm. height. Over the above temperature intervals, the specific heat of pure aluminium was measured in order to see the correctness of the measurement.

(a) Measurement over the interval 0–99.5°C. Pure aluminium: 0.2193, 0.2171, 0.2175, mean: 0.2179. Specimen: 0.1761, 0.1766, 0.1753, mean: 0.1760.

The value of the mean specific heat of aluminium is in good agreement with that (0.2196) obtained by E. H. Griffiths and E. Griffiths[7]. The mean specific heat of the specimen is 0.1760 and this contains 87.74% Si_3N_4 and 12.26% SiO_2. When the correction was made on the assumption that the mean specific heat of SiO_2 in the specimen is 0.1862[8], the specific heat of pure Si_3N_4 became 0.1746.

(b) Measurement over the interval 0–316.4°C. Pure aluminium: 0.2308, 0.2321, mean: 0.2315. Specimen: 0.1972, 0.1956, mean: 0.1964.

The corresponding value of the mean specific heat of pure aluminium is not found in the literature but it is almost equal to that of the mean specific heat 0.2342 obtained by interpolating the values 0.2336 for 0–300°C. and 0.2374 for 0–400°C. which were determined by F. Wüst[9]. The mean specific heat of the specimen is 0.1964 and the author made the correction, assuming the mean specific heat of SiO_2 to be 0.2183[8], and obtained the mean specific heat of pure Si_3N_4: 0.1933.

(c) Measurement over the interval 0–585°C. Pure aluminium: 0.2440, 0.2434, 0.2448, mean: 0.2441. Specimen: 0.2188, 0.2190, 0.2195, mean: 0.2191.

The mean specific heat of pure aluminium is in accord with the value 0.2445 obtained by interpolating the values 0.2413 for 0–500°C. and 0.2452 for 0–600°C. which were shown by F. Wüst[9]. The mean value of the specimen is 0.2191, and making the correction on the supposition that the mean specific heat of SiO_2 is 0.2517[8], the mean specific heat of pure Si_3N_4 was found to be 0.2145.

The mean specific heat of pure silicon nitride (C_m) can be expressed by the following equation:

$$C_m = 0.1656 + 9.245 \times 10^{-5} t - 1.5 \times 10^{-8} t^2 .$$

(7) E. H. Griffiths and E. Griffiths, *Phil. Trans.*, A, **214** (1914), 319.

(8) "International Critical Tables," Vol. 5, 105.

(9) F. Wüst, A. Meuthen, and R. Durrer, *Forschungsarb. Gebiete Ingenieurw.*, **204** (1918), 42.

If C is the true specific heat and is expressed by the following equation:

$$C = C_0 + \alpha t + \beta t^2 ,$$

by integration, we have

$$\int_0^t C dt = \int_0^t [C_0 + \alpha t + \beta t^2] dt = C_0 t + \frac{1}{2}\alpha t^2 + \frac{1}{3}\beta t^3 = C_m t .$$

Hence $$C = \frac{d(C_m t)}{dt} .$$

Consequently, the true specific heat of pure silicon nitride can be expressed in the following equation:

$$C = 0.1656 + 1.847 \times 10^{-4} t - 4.5 \times 10^{-8} t^2 .$$

IV. **The Specific Heat of Silicon.** The specific heat of silicon was measured by A. Magnus[10]. By introducing $\beta\nu = 712$ into Debye's equation, C_v values can be obtained and C_p values computed from the equation

$$C_p - C_v = 1.42 \times 10^{-5} C_p^2 T$$

give a satisfactory result over a wide temperature range. But in order to simplify the calculation, the variation of the molecular heat of silicon with absolute temperature can be expressed in the following equation:

$$C_p = 3.724 + 4.816 \times 10^{-3} T - 2.186 \times 10^{-6} T^2 .$$

V. **The Heat of Formation of Silicon Nitride.** (1) *From the experimental formula.* From the equilibrium data of the reaction $Si_3N_4 = 3Si + 2N_2$ at high temperatures, the heat of formation of silicon nitride was calculated in the following way: The dissociation pressure of the above reaction at 1600°K. and 1800°K. was measured by W. B. Hincke and L. R. Brantley[2]:

$$\log P_{N_2} = -\frac{19250}{T} + 8.54 .$$

And the free energy equation is expressed as follows:

$$\Delta F^\circ = 176{,}300 - 78.35\, T.$$

Consequently, the heat of reaction at 1700°K. is 176,300 cal.

(10) A. Magnus, *Ann. Physik*, **70** (1923), 303.

As shown in Chapter III, the molecular heat of silicon nitride at 25°C. is 23.85 which can be obtained from the equation:

$$C_p = 0.1656 + 1.847 \times 10^{-4}t - 4.5 \times 10^{-7}t^2 .$$

As shown in Chapter IV, the atomic heat of silicon is expressed in the following equation:

$$C_p = 3.724 + 4.816 \times 10^{-3}T - 2.186 \times 10^{-6}T^2 .$$

According to G. N. Lewis and M. Randall[11], the molecular heat of nitrogen is:

$$C_p = 6.5 + 0.001\,T .$$

Thus in the reactant we have Si_3N_4: 23.85, and in the resultant, we have

$$3\,Si : 11.17 + 1.445 \times 10^{-2}T - 6.558 \times 10^{-6}T^2 ,$$

$$2\,N_2 : 13.00 + 2 \times 10^{-3}T ,$$

$$\therefore\ Si_3N_4 : 24.17 + 1.645 \times 10^{-2}T - 6.558 \times 10^{-6}T^2 .$$

Consequently in the whole system, the terms referring to the specific heats are

$$0.322 + 1.645 \times 10^{-2}T - 6.558 \times 10^{-6}T^2 .$$

Next, by combining the molecular heat terms with ΔH, the equation of the heat of reaction can be expressed as follows:

$$\Delta H = \Delta H_0 + 0.322\,T + 8.225 \times 10^{-3}T^2 - 2.186 \times 10^{-6}T^3 .$$

The free energy equation of the reaction is, therefore,

$$\Delta F^\circ = \Delta H_0 - 0.322T \ln T - 8.225 \times 10^{-3}T^2 + 1.093 \times 10^{-6}T^3 + IT .$$

From the equation $\Delta F^\circ = 176{,}300 - 78.35T$ obtained by W. B. Hincke and L. R. Brantley[2] we find that $\Delta F^\circ = 50{,}940$ at 1600°K. and $\Delta F^\circ = 35{,}270$ at 1800°K.

Introducing these values into the free energy equation, the values ΔH_0 and I can be obtained as shown below:

$$\Delta H_0 = 162{,}204 , \qquad I = -56.84 .$$

Hence, $$\Delta H = 162{,}204 + 0.322\,T + 8.225 \times 10^{-3}T^2 - 2.186 \times 10^{-6}T^3 ,$$

$$\Delta F^\circ = 162{,}204 - 0.322T \ln T - 8.225 \times 10^{-3}T^2 + 1.093 \times 10^{-6}T^3 - 56.84T .$$

(11) G. N. Lewis and M. Randall, "Thermodynamics," 80, (1923).

Consequently the heat of reaction at 25°C. is $\Delta H_{298} = 163{,}024$.
As shown in the above computation, the result obtained is as follows:

$$3Si + 2N_2 = Si_3N_4 + 163{,}024.$$

(2) *From the Nernst's heat theorem.* By the use of the Nernst's heat theorem, the author calculated the heat of formation of silicon nitride as follows: In the reaction $Si_3N_4 = 3Si + 2N_2$, the change of molecular number of the gaseous system is $\Sigma n = 2$.

If Q is the heat of reaction at any temperature and Q_0 is that at absolute zero, Q may be expressed in the following equation by the Nernst's heat theorem:

$$Q = Q_0 + \sum n \cdot 3.5T + aT^2 .$$

Differentiating with respect to T, we obtain

$$\frac{dQ}{dT} = \sum mC_p = 2 \times 3.5 + 2aT .$$

The molecular heat of each substance at 25°C. follows: Si_3N_4: $C_p = 23.85$; Si: $C_p = 4.965$; N_2: $C_p = 6.798$.
Accordingly,

$$a = \frac{3 \times 4.965 + 2 \times 6.798 - 23.85 - 7}{2 \times 298} = -0.003958 .$$

The chemical constant of N_2 is 2.6. So that $\Sigma nI = 2 \times 2.6 = 5.2$, and

$$\log K = -\frac{Q_0}{4.576T} + 3.5 \log T - \frac{0.003958}{4.576} T + 5.2 .$$

According to W. B. Hincke and L. R. Brantley[2]

$$\log P_{N_2} = -\frac{19250}{T} + 8.54 .$$

$$\log P_{N_2} = -3.49 \text{ at } 1600°K.$$

Hence, $\log K = \log P_{N_2}^2 = -\frac{Q_0}{4.576T} + 3.5 \log T - \frac{0.003958}{4.576} T + 5.2$,

$$-3.49 \times 2 = -\frac{Q_0}{4.576 \times 1600} + 3.5 \log 1600 - \frac{0.003958}{4.576} \times 1600 + 5.2 .$$

$$\therefore \quad Q_0 = 161{,}250 , \quad Q = Q_0 + 2 \times 3.5T + aT = 162{,}984 \text{ (at 25°C.)}.$$

This result is tantamount to that obtained by the experimental formula.

(3) C. Matignon[1] measured the equilibrium data of the reaction

$$3SiO_2 + 6C + 2N_2 = Si_3N_4 + 6CO$$

at 1700°K. and by the use of Nernst's approximate formula calculated the heat of formation of silicon nitride at room temperature to be 159,300 cal.

VI. **Discussion of the Result.** As shown above, the most probable value of the heat of formation of silicon nitride is

$$3Si + 2N_2 = Si_3N_4 + 163{,}000.$$

Comparison of the heat of formation of silicon nitride reported in the literature until now is as follows: 176,300 (W. B. Hincke[2]); 163,000 (S. Satoh); 159,300 (C. Matignon[1]).

The heats of formation of the nitrides of the elements: Na, Mg, Al, Si, P, S, and Cl which belong to the second series of the periodic table per one gram atom of nitrogen in the solid or liquid state are indicated in the following table in the order of their atomic numbers.

Atomic number	Nitrides	Heat of formation per one gram of nitrogen (kcal.)
11	(NaN_3)	− 1.7
12	Mg_3N_2	+57.6
13	AlN	+74.7
14	Si_3N_4	+40.7
15	P_3N_5	+16.3
16	SN	−31.9
17	NCl_3	−54.7

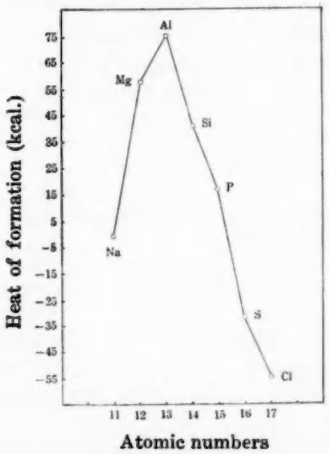

Fig. 1. Relationship between the heat of formation of nitrides of the elements belonging to the second series of the periodic table and their atomic numbers.

The heat of formation of sodium nitride is not yet known but the heat of formation of sodium azide is − 1.7 kcal. per one gram of nitrogen[12].

(12) E. Briner and P. Winkler, *J. chim. phys.*, **20** (1922), 203.

The heat of formation of magnesium nitride is 57.6 kcal.[13] and that of aluminium nitride is 74.7 kcal. as shown in the previous paper[6].

The heat of formation of silicon nitride is 40.7 kcal. as calculated above and that of phosphorus nitride is 16.3 kcal.[14]

The heat of formation of sulphur nitride is −31.9 kcal.[15] and that of nitrogen chloride is −54.7 kcal.[16]

In Fig. 1, the relation between the heats of formation of nitrides per one gram atom of nitrogen and their atomic numbers is shown graphically; the curve shows the maximum for aluminium. This bears a striking resemblance to the appearance of the maximum for beryllium in the curve showing the relationship between the heats of formation of nitrides of the elements belonging to the first series of the periodic table and their atomic numbers, which was reported in my last paper[17].

Summary.

As the specific heat of silicon nitride has not yet been determined, the mean specific heat of silicon nitride was measured by the ice calorimeter over three temperature intervals: 0–99.5, 0–316.4, and 0–585°C., and the equation of the true specific heat was obtained which holds good over the above temperature ranges:

$$C = 0.1656 + 1.847 \times 10^{-4}t - 4.5 \times 10^{-8}t^2 .$$

By using this value, the heat of formation of silicon nitride was computed from the dissociation pressure of silicon nitride at high temperatures. The result obtained is as follows:

$$3Si + 2N_2 = Si_3N_4 + 163{,}000.$$

The relationship between the heats of formation of nitrides of the elements belonging to the second series of the periodic table and their atomic numbers is discussed.

The Institute of Physical and Chemical Research, Tokyo.

---

(13) B. Neumann, C. Kröger, and H. Kunz, *Z. anorg. allgem. Chem.*, **207** (1932), 139.
(14) A. Stock and F. Wrede, *Ber.*, **40** (1907), 2923.
(15) M. Berthelot and Vieille, *Ann. chim. phys.*, [5], **27** (1882), 204.
(16) W. A. Noyes and W. F. Tuley, *J. Am. Chem. Soc.*, **47** (1925), 1336.
(17) S. Satoh, *Sci. Papers Inst. Phys. Chem. Research* (Tokyo), **29** (1936), 53.

The Theory on the Constitution of a Thermoreversible Gel.

By Fumio HIRATA.

(Received December 20, 1937.)

Introduction.

Concerning the constitution of thermoreversible gel, the present author has discussed elsewhere[1] the constitution and the sol-gel transformation of gelatine solution which gives a typical thermoreversible gel. It has been found that the theory of micellar constitution of gel is most adequate to explain the experimental results of the studies on the physicochemical properties of gel of gelatine and that the process of gelation may be explained on an assumption that the cause of gelation is in the fixation of the micelle particle in the system. By assuming that the micelle is of electric constitution and that the origin of rigidity of gel is in the mutually reacting electrostatical forces of these micelles, the experimental results of the measurement of rigidity have been examined, and an experimental equation has been found expressing the existence of a certain relation between the change of rigidity due to temperature and the change of dielectric constant of the intermicellar liquid of the gel due to the change of temperature. Taking into consideration the numerical values of modulus of rigidity and the concentration of the gel, and also the fact that the rigidity shows the maximum value at the isoelectric point of gelatine, it has been concluded that the mutually acting forces of the micelles may be considered to be of electric dipole nature.

In the present paper, the theoretical relation between the rigidity of gel and the dielectric constant of intermicellar liquid is investigated.

I. Consideration on the Constitution of Thermoreversible Gel. Among the theories on the constitution of gel, the theory that a gel is composed of micelles dispersed in a liquid, manifesting the elastic solid mass as a whole, seems to be most acceptable in the case of the gel of gelatine. The results of the studies made by the present author on the scattering of light by sol and gel of gelatine,[2] on the electrolytic conductivity of sol

(1) F. Hirata, *Rev. Phys. Chem.* (Japan), **11** (1937), 262; *Proc. Imp. Acad.* (Tokyo), **33** (1937), 266; *J. Chem. Soc. Japan*, **58** (1937), 1156 et seq.

(2) Duclaux and Hirata, *J. chim. phys.*, **30** (1933), 213.

and gel of gelatine,[3] on the ultrafiltration of sol of gelatine,[4] and on the refractive index of sol and gel of gelatine,[3] suggest that the process of gelation is nothing but the stoppage of the free translational and rotational motion, that is, of the Brownian motion of the micelles. It may be assumed that the direct forces of attraction and repulsion acting at a long distance are in action through the medium between the micelles in both sol and gel states. However, when the system is at high temperature, that is, in the sol state, the kinetic energy due to temperature of the micelles overcomes these forces in its action, and the micelles are free to move and consequently, the whole mass becomes a liquid. At lower temperature, that is, in the gel state, the intermicellar forces become superior in its action and these forces make the micelles take definite positions in the system. It may be said that the micelle is composed of an aggregate of particles of electric charges, and the rigidity of gel is the effect of the electrostatical forces of these micelles, which act through the intermicellar liquid. On the basis of the studies stated above, it may be assumed that the constitution of micelle is not affected by the change of temperature within the range of the present experiments. It follows, therefore, that the cause of the change of the rigidity of gel due to temperature exists not in the micelle itself but in the intermicellar liquid. Since the forces may be assumed to be of the electrostatical nature acting at a long distance through the intermicellar liquid, the change in the intermicellar forces may be ascribed to the change in the intermicellar liquid. If this assumption be correct, there must be a certain quantitative relation between the change of dielectric constant of the intermicellar liquid due to temperature and that of rigidity of the gel due to temperature.

II. **Method and Results of Measurement of Rigidity of Gel.** In order to investigate the constitution of thermoreversible gel, the study of the rigidity of gel, especially the study of the change of rigidity due to temperature must be one of the most important and the most direct process, for the difference between the gel and sol states in the case of thermoreversible gel seems to depend only on the difference of the mechanical rigidity of the colloidal system.

In the investigation of the constitution of gel from its rigidity, it is preferable to use a sample of as low concentration as possible for securing the simplicity of experimental conditions. In measuring the effect of temperature on the rigidity, it is necessary to use the method as ac-

(3) These experiments have been made in the author's laboratory. Cf. *J. Chem. Soc. Japan*, **58** (1937), 1156, et seq.

(4) Duclaux and Hirata, *J. chim. phys.*, **30** (1933), 229.

curate as possible, since the gel loses its rigidity as the temperature rises and turns into liquid in the end. Moreover, the method must be such as will allow the temperature of the sample remain constant and keep it free from desiccation. From these points of view, the method of Michaud[5] seems to be the most satisfactory one.

The method of measurement used by the present author is a modified form of the method of Michaud used in an experimental study on cellulosic solutions by Duclaux and the author.[6]

In this method of measurement[7] the sample is held in a glass capillary tube and the whole is kept in a water thermostat. If a pressure is applied to the sample at one end of the capillary tube, every point of the sample gel will be displaced parallel with the axis of the tube. Let l and R be the length and the radius of the capillary tube, respectively, X_0 be the displacement of the sample at a point on the axis of the capillary tube and μ be the modulus of rigidity of the gel, and the following relation will be obtained theoretically:[7]

$$\mu = PR^2/4lX_0 \qquad (1),$$

where P is the pressure applied.

The results of measurement of P and X_0 for the gel of gelatine at the isoelectric point pH = 4.7 are given in Table 1 to 6. The concentration of this gel was 25.97 g./l. Taking P and X_0 as ordinate and abscissa, respectively, the relations are shown in Fig. 1. In this figure it is

Table 1. $t = 5.80 \pm 0.01$°C.

P (dyne/cm.^{2})	X_0 (cm.)	P/X_0
2.000×10^4	4.104×10^{-4}	4.873×10^7
2.961×10^4	6.156×10^{-4}	4.810×10^7
3.882×10^4	9.234×10^{-4}	4.204×10^7
5.373×10^4	12.31×10^{-4}	4.364×10^7
6.294×10^4	14.36×10^{-4}	4.382×10^7
7.255×10^4	15.39×10^{-4}	4.714×10^7

Table 2. $t = 11.69 \pm 0.01$°C.

P (dyne/cm.^{2})	X_0 (cm.)	P/X_0
1.999×10^4	5.130×10^{-4}	3.897×10^7
2.999×10^4	9.234×10^{-4}	3.248×10^7
3.950×10^4	10.26×10^{-4}	3.859×10^7
5.429×10^4	12.31×10^{-4}	4.410×10^7
6.272×10^4	14.36×10^{-4}	4.367×10^7
7.213×10^4	18.47×10^{-4}	3.906×10^7
8.173×10^4	20.52×10^{-4}	3.983×10^7

(5) Michaud, *Ann. phys.*, [9], **19** (1923), 63.
(6) Duclaux and Hirata, *J. chim. phys.*, **28** (1931), 538.
(7) Hirata, *Rev. Phys. Chem.* (Japan), **11** (1937), 262.

Table 3. $t = 15.00 \pm 0.01$°C.

P (dyne/cm.^{2})	X_0 (cm.)	P/X_0
1.940×10^4	5.130×10^{-4}	3.782×10^7
2.920×10^4	9.234×10^{-4}	3.162×10^7
3.900×10^4	9.234×10^{-4}	4.273×10^7
5.429×10^4	14.36×10^{-4}	3.779×10^7
6.330×10^4	16.42×10^{-4}	3.856×10^7
7.271×10^4	19.50×10^{-4}	3.730×10^7
8.192×10^4	20.52×10^{-4}	3.992×10^7

Table 4. $t = 18.00 \pm 0.01$°C.

P (dyne/cm.^{2})	X_0 (cm.)	P/X_0
2.017×10^4	8.208×10^{-4}	2.458×10^7
2.938×10^4	12.31×10^{-4}	2.386×10^7
3.918×10^4	19.49×10^{-4}	2.009×10^7
5.444×10^4	25.65×10^{-4}	2.123×10^7
6.404×10^4	25.65×10^{-4}	2.440×10^7
7.305×10^4	30.78×10^{-4}	2.373×10^7
8.245×10^4	33.86×10^{-4}	2.455×10^7

Table 5. $t = 20.50 \pm 0.01$°C.

P (dyne/cm.^{2})	X_0 (cm.)	P/X_0
4.895×10^3	5.130×10^{-4}	0.925×10^7
9.790×10^3	8.208×10^{-4}	1.193×10^7
1.469×10^4	14.36×10^{-4}	1.022×10^7
1.978×10^4	18.47×10^{-4}	1.068×10^7
2.428×10^4	20.52×10^{-4}	1.183×10^7
2.820×10^4	26.68×10^{-4}	1.057×10^7
3.290×10^4	31.81×10^{-4}	1.034×10^7
4.229×10^4	41.04×10^{-4}	1.030×10^7
5.189×10^4	48.22×10^{-4}	1.076×10^7
6.089×10^4	59.51×10^{-4}	1.021×10^7
6.931×10^4	68.74×10^{-4}	1.008×10^7
7.842×10^4	76.95×10^{-4}	1.019×10^7

Table 6. $t = 22.60 \pm 0.01$°C.

P (dyne/cm.^{2})	X_0 (cm.)	P/X_0
4.898×10^3	14.36×10^{-4}	3.411×10^6
9.992×10^3	30.76×10^{-4}	3.216×10^6
1.992×10^4	62.59×10^{-4}	3.176×10^6
2.978×10^4	92.34×10^{-4}	3.225×10^6
3.977×10^4	123.1×10^{-4}	3.232×10^6
5.937×10^4	179.6×10^{-4}	3.309×10^6
6.818×10^4	210.3×10^{-4}	3.247×10^6

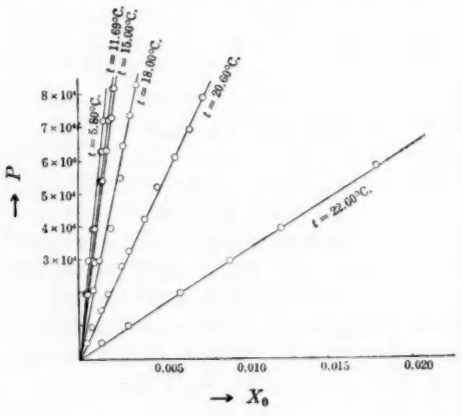

Fig. 1.

represented clearly that the relation between P and X_0 is perfectly linear, that is, the law of elasticity holds strictly within the range of the experimental temperatures and the pressures applied.

III. **Theoretical Relation between X_0 and ε.** As the magnitude of the modulus of rigidity has a direct connection with the displacement X_0, the change of rigidity due to temperature may be expressed in terms of the change of X_0 due to temperature. It is intended here to derive the theoretical relation which will hold between X_0

and ε, the dielectric constant of the intermicellar liquid of the gel for different temperatures.

In order to simplify the calculation, the micellar constitution of the gel of gelatine is assumed as shown in Fig. 2. Each micelle *M* which is supposed to be an electric dipole takes the position of each lattice point of a simple cubic lattice and the space between these micelles is supposed to be filled up by an intermicellar liquid.

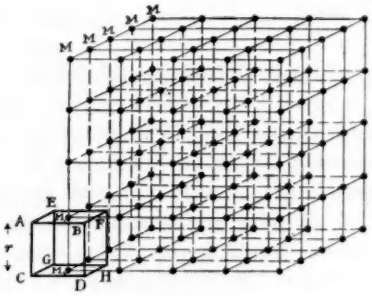

Fig. 2.

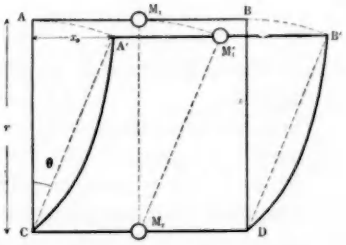

Fig. 3.

When such a gel is subjected to a holizontal shear, all the unit cube in the lattice will be deformed equally. Taking one of those unit cube, let us advance the consideration.

Let a unit cube be ABDC in Fig. 3, in which the cube is indicated by a cross section cut by a plane perpendicular to the side face ACGE of the cube ABCDEFGH in Fig. 2. M_1 and M_2 are the micelles which take the central position of each face shown as AB and CD in Fig. 3. If a pressure is applied at the side face AC, the base CD being fixed, the cube ABDC will be deformed and become the shape like A′B′DC. The micelle M_1 will be displaced to M_1' and the equilibrium of forces will be established. It is supposed that the mutual forces of M_1' and M_2 in the deformed state must produce the reactive elastic force. Let f_i be the direct active force between the micelles M_1' and M_2, and $f_i \sin\theta$ will be its horizontal component which appears in the horizontal direction. This component is nothing but the force which reacts as the rigidity of the cube. As already stated, the direct acting force is caused by the mutual action of the dipole micelles, the direct force between M_1' and M_2 is expressed in the following equation:

$$f_i = \frac{\gamma\sigma_0^2}{\varepsilon\gamma^4} \qquad (2),$$

in which σ_0 represents the dipole moment of M_1' and M_2, γ the factor which is determined by the mutual orientation of the two dipole micelles in the deformed state, ε the dielectric constant of the medium which fills up the space between M_1' and M_2, and r the distance between the two micelles M_1' and M_2. The reactive horizontal force $-f_x$ will be given in the following form:

$$-f_x = -f_l \sin\theta$$

or

$$-f_x = -\frac{\gamma\sigma_0^2}{\varepsilon r^4}\sin\theta \qquad (3),$$

in which the negative sign of f_x indicates that the direction of the force is to the left.

When the temperature of gel changes, this horizontal force, $-f_x$ will be changed in its magnitude; for the rigidity of gel will change when the temperature of gel is changed. In equation (3), σ_0 and r may be assumed to be independent of temperature, but γ, ε and θ are supposed to change with temperature. In order to secure the simplicity of calculation, γ is assumed to be independent of the change of temperature.[8] Consequently, in this case only ε and θ are variable. If the measurement of rigidity, viz., the measurement of X_0 is executed for different temperatures but under a same constant pressure, the above force f_x may be taken as constant for the temperature of measurement. The following equation, therefore, is written for the reactive elastic force in the range of temperature of the measurements:

$$-f_x = k \qquad (4),$$

where k is a constant which is independent of temperature. From equations (4) and (3), we have

$$-\frac{\gamma\sigma_0^2}{\varepsilon r^4}\sin\theta = k \qquad (5).$$

If we summarize all of the constants in equation (5) which are independent of the change of temperature, by b, that is, $kr^4/\gamma\sigma_0^2 = b$, we get the following relation:

$$\sin\theta = -b\cdot\varepsilon \qquad (6).$$

Now we must find the relation between ε and $X_{0\cdot P}$. $X_{0\cdot P}$ means X_0 for a constant pressure P.

(8) As for the value of γ which gives the orientation polarization caused by the stress, it will be treated in a later report.

Next suppose, on the other hand, a cube of homogeneous gel of side length r. This cube is, in the microscopic point of view, is equivalent to the cube which is given in Fig. 1 as ABCDEFGH, but in the present case it is supposed to be an entirely homogeneous, isotropic, elastic mass. Only the dimension of the cubes is assumed to be equal in both cases. This cube is shown as ABDC in Fig. 4 which is shown as the cross section analogous to Fig. 3.

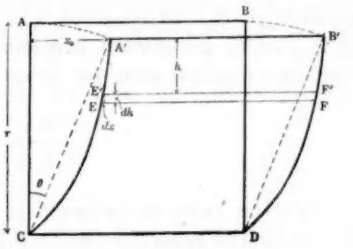

Fig. 4.

If pressure P is applied to the cube from the side face AC, the base CD being fixed, the cube ABDC will be deformed into A′B′DC when the equilibrium will be established. If we represent μ' as the modulus of rigidity of the gel under the deformed state, and consider the equilibrium condition of the acting and reacting forces which act horizontally to the plane E′F′, indicated in Fig. 3, of the infinitely thin gel block EFE′F′, we have the following equation:

$$Phr = -\mu' \frac{dx}{dh} r^2 \qquad (7).$$

The meaning of h, r, dh, dx in this equation is clearly shown in the figure. The left hand side of equation (7) represents the force that acts tangentially on the plane E′F′ in the right direction and the right hand side of the equation represents the reactive tangential force produced by the elastic property of the gel block EFF′E′. If we solve the equation (7), taking the limiting condition: $h = \sqrt{r^2 - x_0^2}$, when $x = 0$, we have

$$\frac{P}{2}(h^2 - r^2 + x_0^2) = -\mu' r x \qquad (8).$$

Putting $h = 0$ and $x = x_0$,

$$\frac{P}{2}(x_0^2 - r^2) = -\mu' r x_0 \qquad (9).$$

Rewriting, we have

$$\frac{P}{\mu'} = 2\frac{x_0}{r}\frac{r^2}{r^2 - x_0^2} \qquad (10).$$

We may write this equation in the following form, if we take the value of θ as the function of x_0, i.e., $\sin\theta = x_0/r$; $\cos\theta = \sqrt{r^2 - x_0^2}/r$,

$$\frac{P}{\mu'} = 2\sin\theta / \cos^2\theta \qquad (11).$$

If we express, on the other hand, the modulus of rigidity of the cube ABDC which is not deformed as μ, this modulus of rigidity μ must correspond to the value of μ measured directly by the method stated in paragraph II. In equation (1) of paragraph II, if we measure the value of X_0 under a constant pressure P, X_0 may be represented as $X_{0\cdot P}$. Rewriting equation (1), we have

$$\frac{P}{\mu} = \frac{4lX_{0\cdot P}}{R^2} \qquad (12).$$

To get the relation between μ and μ', it is necessary to determine the nature of the reactive elastic force. As already stated in the introduction of this paper, it may be concluded that the forces which cause the rigidity of gel is the electrostatic force between the dipole micelles of gelatine. Consequently, as the dipolar force are inversely proportional to the fourth power of the mutual distance of the micelles, the relation between μ and μ' may be represented in the following equation:

$$\frac{\mu'}{\mu} = \left(\frac{r}{r\cdot\cos\theta}\right)^4 = \frac{1}{\cos^4\theta} \qquad (13).$$

Combining equations (11) and (13), we have

$$\frac{P}{\mu} = 2\frac{\sin\theta}{\cos^2\theta}\frac{1}{\cos^4\theta} \qquad (14).$$

From equations (12) and (14), the following equation is given

$$\frac{4lX_{0\cdot P}}{R^2} = 2\frac{\sin\theta}{\cos^6\theta} \qquad (15).$$

Changing the form, we get

$$\frac{4lX_{0\cdot P}}{R^2} = 2\frac{\sin\theta}{(1-\sin^2\theta)^3} \qquad (16).$$

Neglecting the higher order of $\sin\theta$ in the denominator, we have

$$\frac{2lX_{0\cdot P}}{R^2} = \frac{\sin\theta}{1-3\sin^2\theta} \qquad (17).$$

Now, putting the value of sin θ expressed in equation (6), equation (17) will be written as

$$\frac{2lX_{0\cdot P}}{R^2} = \frac{-b\cdot\varepsilon}{1-3b^2\varepsilon^2} \qquad (18).$$

This equation represents the relation between the values $X_{0\cdot P}$ and ε, and may be verified by using the results of the direct measurement of the modulus of rigidity.

If we change the form of equation (18), we have the following equation:

$$\frac{X_{0\cdot P}}{\varepsilon} = 3b^2X_{0\cdot P}\cdot\varepsilon - \frac{R^2}{2l}b \qquad (19).$$

If we put

$$3b^2 = \alpha$$

and

$$-b\frac{R^2}{2l} = \beta \qquad (20),$$

we have

$$\frac{X_{0\cdot P}}{\varepsilon} = \alpha\cdot X_{0\cdot P}\cdot\varepsilon + \beta \qquad (21),$$

where α and β are constant which are independent of temperature. This equation tells that, independent of temperature, the linear relation between $X_{0\cdot P}/\varepsilon$ and $X_{0\cdot P}\cdot\varepsilon$ exists for thermoreversible gels. In this form of relation, the result of calculation of the values of $X_{0\cdot P}$ and ε, and that of the observed values may conveniently be examined.

IV. **The Verification of the Relation Expressed by Equation (21).** The numerical data necessary to the verification of equation (21) are given in the following tables.

Table 7.

t	ε	$X_{0\cdot P}$	$X_{0\cdot P}/\varepsilon$	$X_{0\cdot P}\cdot\varepsilon$
5.80	85.73	$1.30_7\times10^{-3}$	$1.52_4\times10^{-5}$	0.112_1
11.69	83.51	$1.46_0\times10^{-3}$	$1.77_3\times10^{-5}$	0.123_6
15.00	82.19	$1.56_1\times10^{-3}$	$1.89_9\times10^{-5}$	0.128_5
18.00	81.07	$2.55_5\times10^{-3}$	$3.15_2\times10^{-5}$	0.206_7
20.50	80.15	$5.80_6\times10^{-3}$	$7.24_4\times10^{-5}$	0.465_3
22.60	79.38	$18.4_2\times10^{-3}$	$23.2_0\times10^{-5}$	1.46_2

Table 8.

t	$X_{0\cdot P}$ (calc.)	$X_{0\cdot P}$ (obs.)
5.80	$1.00_1\times10^{-3}$	$1.30_7\times10^{-3}$
11.69	$1.48_8\times10^{-3}$	$1.46_0\times10^{-3}$
15.00	$2.06_2\times10^{-3}$	$1.56_1\times15^{-3}$
18.00	$3.15_6\times10^{-3}$	$2.55_5\times10^{-3}$
20.50	$5.61_7\times10^{-3}$	$5.80_6\times10^{-3}$
22.60	$16.0_2\times10^{-3}$	$18.4_2\times10^{-3}$

All the values of $X_{0\cdot P}$ in the table are the values determined under the pressure $P = 6 \times 10^4$ dyne/cm.^{2}. As for the values of ε, values of pure water have been adopted by reason that the gel is at its isoelectric point and that the measurement of electrolytic conductivity of the gel gives the values approximately equal to that of pure water. These values have been calculated by Drude's formula: $\varepsilon_t = 81.07[1 - 0.004583(t - 18) + 0.0000117(t - 18)^2]$. Taking the values of $X_{0\cdot P}/\varepsilon$ and $X_{0\cdot P}\cdot\varepsilon$ as the y-axis and the x-axis of co-ordinates respectively, their relation is shown in Fig. 5. It is clear from the figure that the relation represented by equation (21) holds in the region of the experimental temperatures. If we calculate the constants α and β by the method of least square, using the numerical values given in Table 7, the following values are obtained:

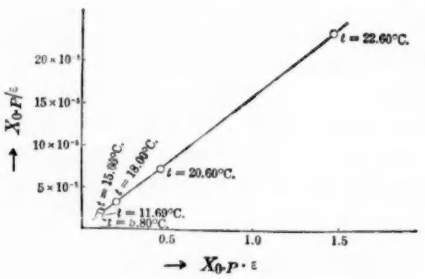

Fig. 5.

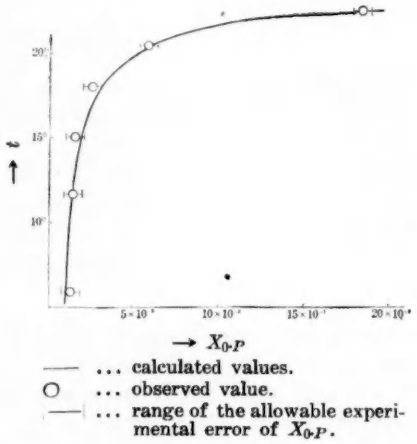

Fig. 6.

$$\alpha = +1.602 \times 10^{-4},$$

$$\beta = -2.082 \times 10^{-6} \qquad (22).$$

Consequently, equation (21) may be written in the following form:

$$\frac{X_{0\cdot P}}{\varepsilon} = 1.602 \times 10^{-4} X_{0\cdot P}\cdot\varepsilon - 2.082 \times 10^{-6} \qquad (23).$$

By this equation and using the numerical values of ε, it is possible to calculate the values of $X_{0\cdot P}$. The result of this calculation is given in Table 8, in which the calculated values are compared with the direct

observed values. In Fig. 6 the calculated values and the observed values of $X_{0.P}$ are plotted as a function of the experimental temperature, t, instead of ε. From the above tables and figures, the validity of equation (21) may be accepted. Next, if we combine equations (6) and (20), the constants α and β of equation (21) may be expressed in the following form:

$$\alpha = \frac{3\sin^2\theta}{\varepsilon^2},$$

$$\beta = \frac{R^2}{2l}\frac{\sin\theta}{\varepsilon} \qquad (24).$$

Consequently, if the values of $\sin\theta$ and ε corresponding to the experimental temperature are known, the constancy of α and β may be examined by the experimental data as follows. If we solve equation (17), the value of $\sin\theta$ will be given by the following equation:

$$\sin\theta = \frac{1}{6}\left(-\frac{R^2}{2lX_{0.P}} + \sqrt{\frac{R^4}{4l^2X_{0.P}^2}+12}\right) \qquad (25).$$

Taking values of R and l (in the present experiment, $R = 0.071$ cm. and $l = 10.01$ cm.)[9] and also that of $X_{0.P}$, the values of $\sin\theta$ for every experimental temperature will be obtained. These values are shown in

Table 9.

t	$\sin\theta$
5.80	0.5460
11.69	0.5497
15.00	0.5511
18.00	0.5612
20.50	0.5702
22.60	0.5750

Table 10.

t	α	β
5.80	$1.21_7\times10^{-4}$	$-1.60_3\times10^{-6}$
11.69	$1.30_2\times10^{-4}$	$-1.66_1\times10^{-6}$
15.00	$1.34_9\times10^{-4}$	$-1.58_3\times10^{-6}$
18.00	$1.43_8\times10^{-4}$	$-1.74_3\times10^{-6}$
20.50	$1.51_9\times10^{-4}$	$-1.79_5\times10^{-6}$
22.60	$1.57_5\times10^{-4}$	$-1.82_4\times10^{-6}$

Table 9. Adopting these values of $\sin\theta$, the numerical values of the constants α and β are computed and are shown in Table 10. If we take into consideration the magnitude of allowable experimental error of the measurement of $X_{0.P}$, it may be said that the calculated values of α and β show a good agreement with the values given in equation (20) and also

(9) F. Hirata, *Rev. Phys. Chem.* (Japan), **11** (1937), 262.

that these values are approximately independent of the change of temperature.

V. Conclusion. Although it is certain that there is a difference between the true configuration of micelles in the gel and the configuration assumed in the present theoretical calculation, the results of the verification described above will allow us to conclude that the assumptions adopted in the course of the theoretical treatment are acceptable, that is to say, the assumptions that the cause of the change of rigidity of gel due to temperature can be ascribed to the change of dielectric constant of intermicellar liquid due to temperature and that the nature of the intermicellar forces which cause the rigidity of gel must be an electric dipolar one.

Summary.

A relation has been derived theoretically between the dielectric constant of the intermicellar liquid and the rigidity of thermoreversible gel and the relation has been examined using the results of measurements of rigidity of the gel of gelatine.

Laboratory of Colloid Chemistry,
Kiriu Higher Technical School.

Constitution and Viscosity Association of High-molecular-weight Hydrocarbons.

By Bunnosuke YAMAGUCHI.

(Received December 4, 1937.)

In his previous paper[1] the author determined for a number of high-molecular-weight liquids a quantity which he called the viscosity association and found the existence of a linear relationship between their viscosity association and their temperature coefficients of viscosity. In the present paper the author attempts to establish by similar studies an empirical equation expressing such a relation, and to calculate by means of the equation the viscosity association of the high-molecular-weight hydrocarbons whose chemical structure and viscosity-temperature coefficients are known, with the object of studying their viscosity association in relation to their chemical structure.

The conception of the viscosity association and the method of its measurement were fully explained in the previous paper, but it will be helpful to give their outlines, as follows:

As indicated by the tangent drawn to the curve in Fig. 1 showing the change in viscosity with concentration of a solution of high-molecular-weight liquid in benzene, viscosity changes always approximately in linear proportion with concentration for dilute solutions not exceeding the concentration C. For higher concentrations the curve bends upward, showing that viscosity increases rapidly with concentration until it finally reaches η_a, which denotes the viscosity of pure solute A when the concentration becomes 100%. If we prolong the tangent qr until it intersects the ordinate at the extreme right, the point of intersection s indicates the viscosity η'_a which the solute would have, provided no special intermolecular forces have acted between the molecules of the solute, and consequently no particular association. Since the ratio η_a/η'_a denotes, as explained in the previous paper, a quantity proportional to that part which association takes in the viscosity of the solute, we express the quantity η_a/η'_a as A_v—viscosity association:

$$A_v = \frac{\eta_a}{\eta'_a} \qquad (1).$$

(1) *Rept. Aeronaut. Research Inst., Tôkyô Imp. Univ.*, No. 102 (1934); *J. Chem. Soc. Japan*, **55** (1934), 353.

In determining the viscosity association, the value of η_a' may be calculated by applying Einstein's equation for the viscosity of a dilute suspensoid to solutions of such high-molecular-weight hydrocarbons as lubricating oils.

Einstein's equation of viscosity is

$$\eta = \eta_0\left(1+k\frac{v}{V}\right) \qquad (2),$$

where V is the total volume of solution, v the volume fraction of solute in the solution, and k a constant whose value, according to Einstein, is 2.5 independent of the size of the solute particles or molecules, provided they are spherical and of uniform size. It is however known from Eisenschitz's viscosity equation[2] and the studies of Kuhn[3] and Staudinger[4] that k depends on the molecular shape or structure of the solute.

If the solution contains g g. of solute and the density of the solute is d_a, equation (2) may be transformed into

$$\frac{\eta}{\eta_0}-1 = \eta_r-1 = k\frac{v}{V} = k\frac{g}{d_aV} = KC \qquad (3),$$

where $C = g\cdot10^3/V$(g./l.), $K = k\cdot10^{-3}/d_a$. Moreover, if the concentration is expressed in percentage C_p, the equation becomes

$$\frac{1}{d}\left(\frac{\eta}{\eta_0}-1\right) = K_pC_p \qquad (4),$$

where d denotes the density of solution and K_p a constant characteristic of the solute, whose value, however, must be independent of the concentration of the solution. Since K_p is proportional to k/d_a, K_pd_a must depend on the structural character of the solute. If we determine the value of K_p for dilute solutions of a high-molecular-weight hydrocarbon to which equation (4) is applicable, the value of η_a' of the hydrocarbon is found by putting $C_p = 100$ in equation (4), seeing that the equation in this case becomes

$$\frac{1}{d_a}\left(\frac{\eta_a'}{\eta_0}-1\right) = K_p\cdot100 \qquad (5),$$

---

(2) *Z. physik. Chem.*, A, **158** (1932), 78.

(3) *Z. physik. Chem.*, A, **161** (1932), 1.

(4) Staudinger, "Die Hochmolekularen Organischen Verbindungen," p. 56 and seq., Berlin.

rendering calculation of η'_a possible, so long as we know the density of the hydrocarbon d_a and the viscosity of the solvent η_0. For certain solutes, such as those having strong polarity and those of highly polymerized molecules, equation (4) is invalid, because it is found that for such compounds, K_p increases with increasing concentration, even though the solutions may be very dilute. As, however, it is possible, even in this case, to determine by the same equation the values of K_p for any solute at different concentrations, the value of K_∞ that K_p assumes at infinite dilution, in which the molecular association of the solute completely disappears, can be approximately determined by graphical extrapolation as described in the previous paper. We can therefore calculate the value of η'_a by inserting the value of K_∞ thus determined, instead of K_p, in equation (5), and accordingly determine the value of A_v.

The Experiment. (1) *Equation expressing the relation between the viscosity association and the viscosity-temperature coefficient of hydrocarbons.* In order to obtain an empirical equation representing the relation between their viscosity association and viscosity-temperature coefficients, careful measurements of viscosities at different temperatures as well as the determination of viscosity association were made of four samples of oils having different chemical compositions and viscosity characteristics. The method of experiment was similar to that used in the previous investigation. The determination of viscosity association was carried out at 25°C., with benzene as the solvent. Its viscosity and density at 25°C. were respectively 0.006043 poise and 0.8731. The results of the experiments are summarized in Table 1, in which the third column shows the relative viscosities of dilute solutions of oils at 25°C. and the fourth column the values of K_p calculated by equation (4). The values of η'_a and A_v, calculated by equations (5) and (1) for the oils, are also shown respectively in the fifth and sixth columns. The last column gives their mean temperature coefficients between 25 and 45°C. of both absolute and kinematic viscosities—$(\Delta\eta/\Delta t)_{25-45°C.}$ and $(\Delta\nu/\Delta t)_{25-45°C.}$. The values of their viscosities measured at various temperatures and their densities at 25°C. are given in Table 2. The result shows that the values of K_p for each oil, calculated for different concentrations of solution, are in every case almost identical, indicating that equation (4) holds good. The relation between the viscosity-temperature coefficient and the viscosity association of the oils is shown in Fig. 2 by circles. Since, in agreement with the results of the previous study, the viscosity-temperature coefficient increases in linear proportion with increase in the value of A_v, a linear relationship exists between them. In Fig. 2, dots, showing the

results for the oils used in the previous study (see Table 3), are found to fall almost on the same straight-line as do the small circles obtained in the present investigation. This straight-line may be expressed by

$$A_v = 4.5+1230\left(\frac{\Delta\eta}{\Delta t}\right)_{25-45^\circ C.} \qquad (6)\ .$$

The seventh column in Table 1 shows the ratio of viscosity association to density at 25°C. for each oil, and since

$$\frac{A_v}{d_a} = \frac{\eta_a}{d_a\eta'_a} = \frac{\nu_a}{\eta'_a} \qquad (1')\ ,$$

the value of the ratio can be obtained by the values of kinematic viscosity ν_a and η'_a at 25°C. As illustrated in Fig. 3, a linear relationship also exists between the ratio of A_v/d_a and the mean temperature coefficient of kinematic viscosity, the relation being expressed by

$$\frac{A_v}{d_a} = 4.5+1230\left(\frac{\Delta\nu}{\Delta t}\right)_{25-45^\circ C.} \qquad (7)\ ,$$

which is found to have the same numerical constants as equation (6).

Although in the foregoing cases, we have taken as the temperature coefficient of viscosity for oils its mean value between 25 and 45°C., it seems more reasonable to study their viscosity-temperature coefficients at 25°C. (if these are calculable) in relation to their viscosity association. As found by S. Erk and H. Eck,[5] the change in viscosity with temperature of mineral oils may be precisely expressed by Walther's equation[6]

$$(\nu+0.8)^{(T^m)} = k_1 \qquad (8)\ ,$$

where ν is the kinematic viscosity in centistokes and T the absolute temperature. As it has been confirmed that equation (8) holds fairly good for the oils used in the present investigation, the writer has used in calculating their viscosity-temperature coefficients at 25°C. the equation

$$\frac{d\nu}{dt} = -m(\log k_1)\frac{\nu+0.8}{T^{m+1}} \qquad (9)\ ,$$

which is derived by differentiating equation (8). In the calculation, the numerical values of the constants m and k_1 for each oil were obtained

(5) *Physik. Z.*, **37** (1936), 113.
(6) *Maschinenbau*, **10** (1931), 671; *Oel Kohle Erdoel Teer*, **12** (1936), 221.

by introducing into equation (8) its viscosities at 25 and 90°C. The results of calculation are given in Table 2. Fig. 4 gives the relation between the viscosity-temperature coefficients thus calculated and the viscosity association of the oils, showing that the relation is also a linear one. In this figure, dots show the results of similar calculations for two of the oils used in the previous study, namely, Aero Shell and Voltol.

(2) *Viscosity characteristics of viscous solutions of polystyrenes.* In order to ascertain on the one hand whether equation (7) holds similarly for viscous solutions of high-molecular-weight hydrocarbons as for liquid hydrocarbons or not, and on the other hand in order to observe the effect of molecular length of high-molecular-weight solutes upon both the viscosity association and the viscosity-temperature coefficient of the solutions, determination of the latter two quantities was carried out for viscous solutions of three polystyrenes that differ markedly in polymerization. In the experiments, the value of K_∞ of each polystyrene was determined by measuring the viscosities of its dilute solutions both in benzene and in ethyl acetate, the results being shown in Table 4, from which it will be seen that the value of K_∞ of each polystyrene differs according as whether benzene or ethyl acetate is used for the solvent in the determination, the value for benzene always greatly exceeding that for ethyl acetate. A similar fact was also found previously by Staudinger and Heuer[7] as well as by the present author,[8] the difference in K_∞ according to solvent being ascribed to difference in degree of solvation, with the conclusion that the molecules of polystyrene are practically not solvated in ethyl acetate, whereas they are greatly solvated in benzene. Therefore in calculating the η'_a of a polystyrene, instead of using its value of K_∞ determined in benzene, we should use that determined in ethyl acetate. As it is known that oils show no appreciable solvation either in benzene or in ethyl acetate, in the foregoing experiments, the values of K_p for oils determined in benzene were used in calculating η'_a, their values of K_p, as the example given in Table 5 shows, not virtually differing whether the solvent used is benzene or ethyl acetate.

In calculating η'_a for viscous polystyrene solutions in benzene, concerning which the relation between viscosity-temperature coefficient and viscosity association is to be studied, the following equation

$$\frac{1}{d_a}\left(\frac{\eta'_a}{\eta_0}-1\right)=K_\infty C_a \qquad (5')$$

(7) *Z. physik. Chem.*, **A, 171** (1934), 129.
(8) *Kolloid-Z.*, **72** (1935), 51.

must be used instead of equation (5), where C_a and d_a respectively denote the concentration (%) and the density of the viscous solution whose η_a is to be obtained. Table 6 shows the values of η'_a and A_v/d_a thus calculated by equations (5′) and (1′) for six different solutions of polystyrenes in benzene, giving also their kinematic viscosities at 25 and 45°C. and their mean viscosity-temperature coefficients between 25 and 45°C. For these solutions, as will be seen from Fig. 5, a linear relationship exists between $(\Delta\nu/\Delta t)_{25-45°C.}$ and A_v/d_a, the straight-line being expressed by equation (7) as for oils. The degree of polymerization of the three polystyrenes used, which differs greatly, is believed to be nearly proportional to their values of K_∞. As will be seen from Table 6, solution No. 1 has a smaller value of A_v/d_a, and consequently a lower viscosity-temperature coefficient than solution No. 5, although the two have nearly the same viscosity at 25°C., the reason for which must be that the molecules of polystyrene I have a much longer structure than those of polystyrene III. Since the difference in viscosity-temperature coefficients between solutions 2 and 6, which have almost the same viscosity at 25°C., can also be explained similarly, it is concluded that for viscous solutions of high-molecular-weight hydrocarbons having the same viscosity at a certain temperature, the longer the molecule of solute, the lower is the temperature coefficient of viscosity. It is of interest, in this connection, to note that the solutions of polystyrene I have an extremely high viscosity index; for example, solution No. 3 shows a viscosity index of 180.

(3) *Constitution and viscosity association of high-molecular-weight hydrocarbons.* As already mentioned, the viscosity-temperature coefficient of a high-molecular-weight hydrocarbon or its solution is definitely related to its A_v value, and since the latter denotes the ratio η_a/η'_a, the former must be a function of η_a and η'_a. For this reason, in order to elucidate the relation between the chemical constitution and the viscosity-temperature coefficient of high-molecular-weight hydrocarbons, it behooves us to study the separate effects of chemical constitution on both η_a and η'_a. As to the effect of chemical structure on viscosity, i.e. η_a, various interesting conclusions have recently been obtained by Mikeska's elaborate investigation[9] on the viscosity characteristics of fifty-two synthetized hydrocarbons and also by Wiggins's study[10] on the constitution and viscosity characteristics of hydrocarbons. Since, as previously stated, $K_v d_a$ is dependent on molecular structure, it is evident from equation (5) that η'_a is likewise affected by chemical constitution. In order

(9) *Ind. Eng. Chem.*, **28** (1936), 970.
(10) *J. Inst. Petroleum Tech.*, **22** (1936), 305.

to study the effect of chemical constitution on $K_p d_a$ and η'_a, we selected twenty-three representative hydrocarbons out of the number which Mikeska synthetized in his investigation, and determined[11] their mean viscosity-temperature coefficients between 25 and 45°C. from his viscosity data, and calculated from the coefficients thus determined their values of $K_p d_a$ and η'_a with the aid of equations (7), (1'), and (5). A similar calculation was made also for 1,1-dicyclohexylhexadecane and 1-cyclohexyl-2-hexahydrobenzylheptadecane from the data of Landa and Čech.[12] The results are given in Table 7(a) and 7(b), from which the following interesting conclusions on the effect of chemical constitution on $K_p d_a$ and η'_a were drawn.

1. *Effect of length of side chain.* (a) A comparison of the results for compounds Nos. 26, 15, and 16 as well as of those for Nos. 1 and 2 leads to the conclusion that, for a given cyclic nucleus with a straight paraffinic side chain, the value of η'_a increases with length of side chain. (Compare also No. 11 with No. 13, No. 37 with No. 38, and No. 12 with No. 14.)

(b) The value of η'_a, as is evident from the results for compounds Nos. 15 and 28, is not appreciably affected by the number of side chains, provided the number of paraffinic carbon atoms attached to a given nucleus remains unchanged.

2. *Effect of straight chains as compared with branched chains.* A comparison of the results for compounds Nos. 2 and 3 as well as of those for Nos. 16 and 17 shows that, for a given number of carbon atoms, straight chains are more effective in increasing the value of η'_a than branched chains. (Compare also No. 12 with No. 13, and No. 38 with No. 39.)

3. *Effect of ring structure.* (a) A comparison of the results for compounds Nos. 1, 15, 40, and 48 indicates that, for a given paraffinic chain, the greater the complexity or the number of the cyclic rings attached to it—in other words, the more effective the cyclic groups in increasing the total length of the molecule, the higher is the value of η'_a. (Compare also No. 11 with No. 37, and No. 13 with No. 38.)

(b) Reduction of the aromatic to the corresponding hydro-aromatic rings slightly increases the value of η'_a. (Compare No. 15 with No. 37, No. 2 with No. 13, No. 3 with No. 12, No. 17 with No. 39, and No. 16 with No. 32 or No. 38.)

---

(11) For the determination, the extra- and inter-polation of their viscosities at 25 and 45°C. were made with the aid of the viscosity-temperature chart of Ubbelohde.

(12) *Collection Czechoslov. Chem. Commun.*, **6** (1934), 423.

4. *Effect of olefinic linkages in the side chain.* As will be seen from the results for compounds Nos. 3 and 5, and also from those for Nos. 17 and 18, an olefinic linkage in the side chain does not appreciably affect the value of η'_a.

5. *Effect of allocation of cyclic nucleus within the molecule.* According to a comparison made of the results for compounds Nos. 48 and 51, the effect of allocation of the cyclic nucleus within the molecule has no appreciable effect on the value of η'_a.

As already mentioned, the viscosity-temperature coefficient of a high-molecular-weight hydrocarbon depends not only on its η'_a, but also on its actual viscosity η_a. Although compounds Nos. 40 and 17 have almost the same value of η'_a, their temperature coefficients of viscosity differ considerably. This must be due to the difference in η_a which the effect of chemical structure brings about. The same may be said in the comparison of the viscosity-temperature coefficients of compounds Nos. 15, 28, and 51 having almost the same value of η'_a. Of these three compounds equally with eighteen paraffinic carbon atoms the one having normal chain has the lowest temperature coefficient of viscosity owing to its lowest viscosity. That compounds Nos. 32, 17, and 51, having nearly the same viscosity at 25°C., also differ much in the viscosity-temperature coefficient, is due to differences in the values of η'_a. As a rule, for such compounds of comparable viscosities, the greater η'_a, the lower the viscosity-temperature coefficient, whence it follows that the longer the molecule, the smaller the temperature coefficient of viscosity.

Since η'_a is related by equations (7) and (1′) to the temperature coefficient of viscosity in the form

$$\frac{1}{1.23\eta'_a} = \frac{1000}{\nu_a}\left[0.00366+\left(\frac{\Delta\nu}{\Delta t}\right)_{25-45°C.}\right] \qquad (7'),$$

an index that is expressed by $\frac{1000}{\nu_a}\left[0.00366+\left(\frac{\Delta\nu}{\Delta t}\right)_{25-45°C.}\right]$, if it be calculated for high-molecular-weight hydrocarbons, must be inversely proportional to their values of η'_a. Therefore, the relation of their chemical structure to their values of this index may at once be found, provided we have complete information on the effects of their chemical structure on their values of η'_a. Fig. 6 shows the variation in $(\Delta\nu/\Delta t)_{25-45°C.}$ and in the index for compounds Nos. 26, 15, and 16 with the number of carbon atoms in the side chain, indicating that the index decreases with length of side chain, whereas $(\Delta\nu/\Delta t)_{25-45°C.}$ increases.

The above mentioned conclusions are in some respects comparable with those made by Mikeska[9] on the relation between the chemical

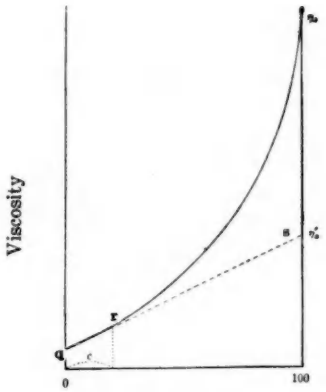

Fig. 1.

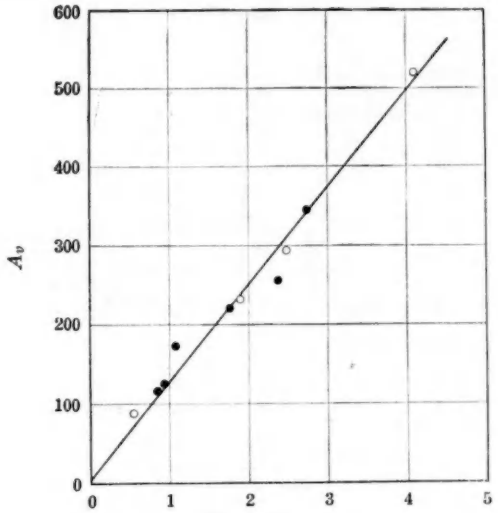

Fig. 2.

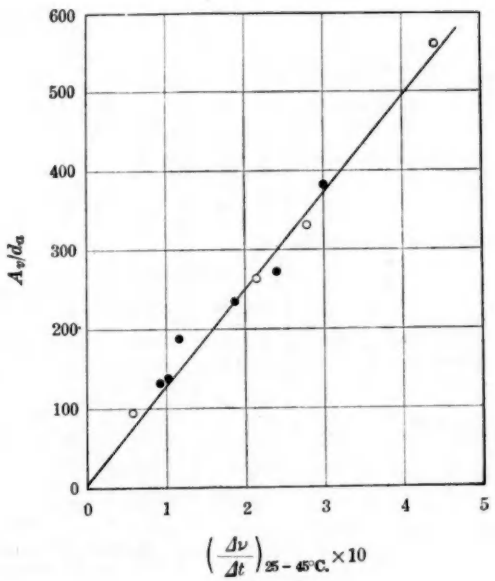

Fig. 3.

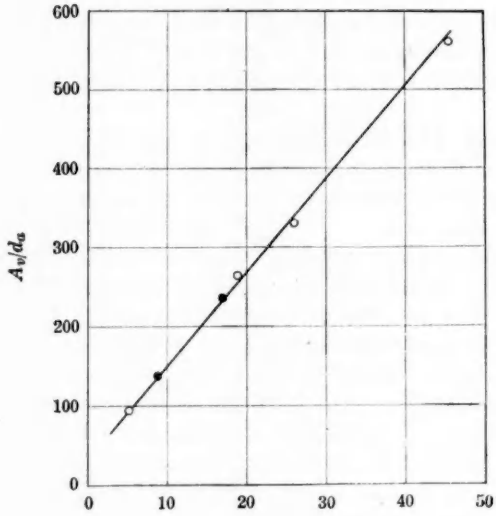

Fig. 4.

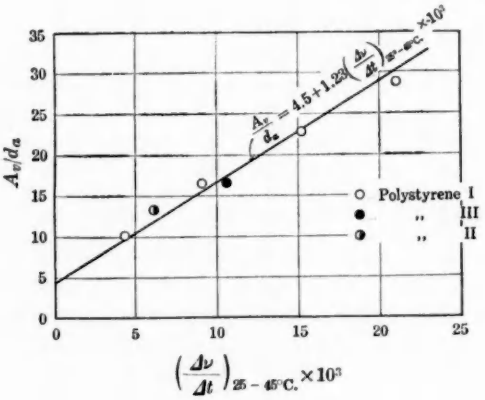

Fig. 5.

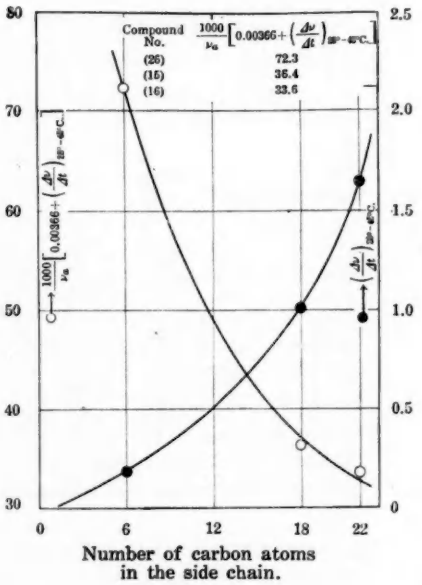

Fig. 6.

Table 1.

Oils	Conc. of benzene solution in % (C_p)	Density (d)	η_r	K_p		η'_a in poises	A_v	$\frac{A_v}{d_a}$	Mean viscosity-temperature coefficient between 25 and 45°C. $\frac{\Delta\eta}{\Delta t}$	Mean viscosity-temperature coefficient between 25 and 45°C. $\frac{\Delta\nu}{\Delta t}$
Mobile Oil S.R.N. (Mixed base)	2.525	0.8743	1.052	0.0238	0.0240	0.0195	520	561	0.410	0.441
	4.183	0.8751	1.087	0.0238						
	4.943	0.8755	1.105	0.0243						
Mobile Oil W. N. (Naphthenic)	2.706	0.8745	1.046	0.0195	0.0195	0.0169	87.9	94.9	0.0536	0.0577
	4.062	0.8752	1.070	0.0197						
Gargoyl Aero. H. (S. A. E. 60) (Paraffinic)	1.282	0 8733	1.035	0.0314	0.032	0.0232	294	331	0.248	0.279
	2.001	0.8734	1.056	0.0322						
	2.873	0.8735	1.083	0.0332						
	4.120	0.8737	1.121	(0.0336)						
Gargoyl Aero. W. (S. A. E. 50) (Paraffinic)	2.112	0.8731	1.054	0.0293	0.0311	0.0226	232	264	0.189	0.214
	3.015	0.8731	1.083	0.0315						
	3.949	0.8731	1.112	0.0325						

Table 2.

Oils	Density at 25°C. (d_a)	Viscosity			Mean viscosity-temperature coefficient between 25 and 45°C.		Constants in Walther's formula		$-\left(\frac{d\nu}{dt}\right)$ at 25°C. in centistokes	Viscosity index
		Temp. (°C.)	Kinematic visc. in stokes (ν)	Absolute visc. in poises (η)	$\frac{\Delta\nu}{\Delta t}$	$\frac{\Delta\eta}{\Delta t}$	m	log k_1		
Mobile Oil S. R. N.	0.9272	25	10.94	10.14	0.441	0.410	4.073	10.56	45.5	14
		45	2.133	1.952						
		90	0.2214	0.1966						
Mobile Oil W. N.	0.9253	25	1.609	1.489	0.0577	0.0536	4.266	10.90	5.13	58
		45	0.456	0.417						
		90	0.0815	0.0723						
Gargoyl Aero. H. (S. A. E. 60)	0.8871	25	7.680	6.813	0.279	0.248	3.427	8.948	26.0	109
		45	2.109	1.847						
		90	0.3043	0.2585						
Gargoyl Aero. W. (S. A. E. 50)	0.8790	25	5.953	5.233	0.214	0.189	3.403	8.864	19.0	97
		45	1.680	1.457						
		90	0.2538	0.2136						

Table 3.

Oils	Density at 25°C.	Kinematic viscosity		Absolute viscosity		$\left(\frac{\Delta\nu}{\Delta t}\right)_{25-45°C.}$	$\left(\frac{\Delta\eta}{\Delta t}\right)_{25-45°C.}$	$-\left(\frac{d\nu}{dt}\right)_{25°C.}$ in centistokes	A_v	$\frac{A_v}{d_a}$
		25°C.	45°C.	25°C.	45°C.					
Shell C. 2A.	0.8867	2.711	0.8663	2.404	0.7580	92.2×10^{-3}	82.3×10^{-3}	—	117	132
Aero Shell	0.9110	2.934	0.8990	2.673	0.8070	102×10^{-3}	93.3×10^{-3}	8.61	126	138
Mobile Oil A.	0.9215	3.212	0.8945	2.960	0.8140	116×10^{-3}	107×10^{-3}	—	174	189
Voltol	0.9359	5.013	1.263	4.692	1.172	187×10^{-3}	176×10^{-3}	16.9	220	235
Flugol	0.9405	6.594	1.800	6.202	1.491	240×10^{-3}	237×10^{-3}	—	256	272
Germ Oil	0.9039	7.755	1.747	7.010	1.560	300×10^{-3}	273×10^{-3}	—	345	382

Table 4.

Polystyrenes	Dilute solution in benzene					Dilute solution in ethyl acetate				
	Conc. in % (C_p)	Density (d)	η_{sr}	K_∞		Conc. in % (C_p)	Density (d)	η_{sr}	K_∞	
No. I	0.0945	0.8737	1.070	0.848	0.84	0.0992	0.8931	1.038	0.429	0.42
	0.1922	0.8738	1.143	0.852		0.2146	0.8934	1.083	0.433	
	0.2459	0.8739	1.178	0.828		0.4018	0.8938	1.157	0.437	
No. II	0.3075	0.8739	1.0961	0.358	0.36	0.2476	0.8935	1.046	0.208	0.20
	0.5056	0.8742	1.153	0.348		0.3981	0.8938	1.080	0.218	
	0.7069	0.8746	1.231	0.374						
No. III	0.4251	0.8746	1.0552	0.149	0.15	0.4943	0.8939	1.047	0.106	0.11
	0.6755	0.8746	1.0901	0.153		0.6630	0.8941	1.066	0.109	
	0.9242	0.8751	1.126	0.155						

Table 5. Comparison of K_p of Mobile Oil S.R.N. in ethyl acetate and benzene.

Solvent	C_p (%)	Density (d)	η_{sr}	K_p	
Ethyl acetate	2.902	0.8931	1.064	0.0247	0.0248
	4.898	0.8932	1.109	0.0249	
Benzene	2.525	0.8743	1.051	0.0238	0.0240
	4.183	0.8751	1.087	0.0238	
	4.943	0.8755	1.105	0.0243	

Table 6. Viscosity characteristics of viscous polystyrene solutions in benzene.

Solution No.	Polystyrenes	Conc. (%)	Density at 25°C. (d_a)	Kinematic viscosity in stokes		$\left(\frac{\Delta\nu}{\Delta t}\right)_{25-45°C.}$	K_∞ in ethyl acetate	η'_a	$\frac{A_v}{d_a}$
				25°C.	45°C.				
1	I	10.83	0.8915	0.3105	0.2244	0.00431	0.42	0.0306	10.2
2		13.82	0.8966	0.6168	0.4350	0.00909		0.0375	16.5
3		16.01	0.9007	0.9722	0.6690	0.0152		0.0426	22.8
4		17.62	0.9035	1.335	0.9147	0.0210		0.0464	28.8
5	III	36.82	0.9352	0.3130	0.1910	0.00610	0.11	0.0235	13.3
6	II	27.92	0.9193	0.6168	0.4043	0.0106	0.20	0.0371	16.6

Table 7 (a). Viscosity characteristics of aromatic hydrocarbons.

Compound No.	Structure	Empirical formula	Densiny at 25°C. (d_4)	Kinematic viscosity*		$\left(\frac{\Delta v}{\Delta t}\right)_{25-45°C.}$	$\frac{A_v}{d_4}$	ν'_4	$K_p \cdot d_4$	Viscosity index
				25°C.	45°C.					
1	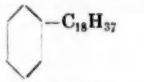	$C_{24}H_{42}$	0.8540*	0.133	0.0770	0.0028	7.94	0.0168	0.0178	196
2	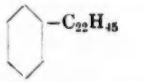	$C_{28}H_{50}$	0.8513	0.197	0.115	0.0041	9.5	0.0207	0.0243	164
3	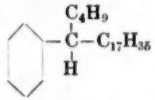	$C_{28}H_{50}$	0.8554	0.274	0.131	0.0073	13.5	0.0203	0.0236	138
5	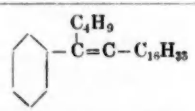	$C_{28}H_{48}$	0.8675	0.228	0.117	0.0056	11.4	0.0200	0.0231	162
15	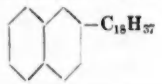	$C_{28}H_{44}$	0.906	0.378	0.177	0.0101	16.9	0.0224	0.0271	140
16	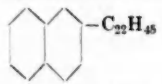	$C_{32}H_{52}$	0.8987	0.599	0.270	0.0165	24.8	0.0242	0.0300	144
17	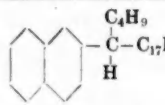	$C_{32}H_{52}$	0.898*	0.630	0.265	0.0183	27.0	0.0233	0.0286	122

* Extrapolated values.

Table 7 (a).—(*Concluded*)

Compound No.	Structure	Empirical formula	Density at 25°C. (d_a)	Kinematic viscosity* 25°C.	Kinematic viscosity* 45°C.	$\left(\frac{\Delta v}{\Delta t}\right)_{25-45°C.}$	$\frac{A_v}{d_a}$	η'_a	$K_p \cdot d_a$	Viscosity index
18	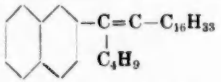	$C_{32}H_{50}$	0.9081	0.555	0.237	0.0159	24.1	0.0230	0.0281	116
26	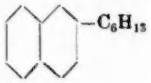	$C_{16}H_{20}$	0.9575	0.0752	0.0396	0.00178	6.69	0.0112	0.0085	−66
28	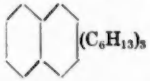	$C_{28}H_{44}$	0.911	0.600	0.241	0.0180	26.6	0.0226	0.0274	98
32	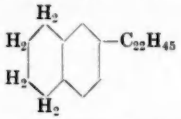	$C_{32}H_{56}$	0.8786	0.629	0.286	0.0172	25.7	0.0245	0.0305	145
40		$C_{30}H_{46}$	0.9138*	0.452	0.213	0.0120	19.3	0.0234	0.0282	131
48	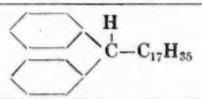	$C_{30}H_{46}$	0.9260*	0.467	0.199	0.0134	21.0	0.0222	0.0267	96
51	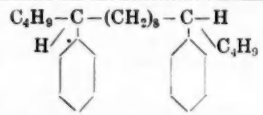	$C_{30}H_{46}$	0.9051	0.630	0.245	0.0193	28.2	0.0223	0.0269	92

Table 7 (b). Viscosity characteristics of naphthenic hydrocarbons.

Table 7 (b). Viscosity characteristics of naphthenic hydrocarbons.

Compound No.	Structure	Empirical formula	Density at 25°C. (d_a)	Kinematic viscosity*		$\left(\frac{\Delta\nu}{\Delta t}\right)_{25-45°C.}$	$\frac{A_\nu}{d_a}$	η'_a	$K_p \cdot d_a$	Viscosity index
				25°C.	45°C.					
11	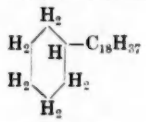	$C_{24}H_{48}$	0.834*	0.204	0.106	0.0049	10.5	0.0194	0.0214	160
12	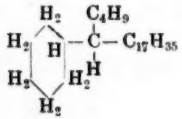	$C_{28}H_{56}$	0.8395	0.322	0.153	0.0085	15.0	0.0215	0.0255	140
13	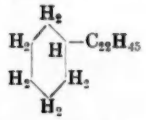	$C_{28}H_{56}$	0.8327	0.313	0.156	0.0079	14.2	0.0220	0.0264	170
14	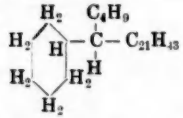	$C_{32}H_{64}$	0.8372	0.462	0.217	0.0123	19.6	0.0236	0.0290	149
37	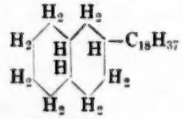	$C_{28}H_{54}$	0.863	0.493	0.230	0.0132	20.7	0.0238	0.0294	144
38	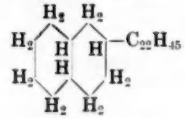	$C_{32}H_{62}$	0.8673	0.772	0.339	0.0217	31.2	0.0247	0.0309	148

* Extrapolated values.

Table 7 (b).—(*Concluded*)

Compound No.	Structure	Empirical formula	Density at 25°C. (d_a)	Kinematic viscosity* 25°C.	Kinematic viscosity* 45°C.	$\left(\frac{\Delta v}{\Delta t}\right)_{25-45°C.}$	$\frac{A_v}{d_a}$	η'_a	$K_p \cdot d_a$	Viscosity index
39	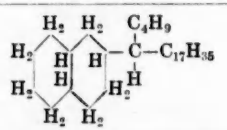	$C_{32}H_{62}$	0.8615	1.00	0.390	0.0305	42.0	0.0238	0.0294	114
46	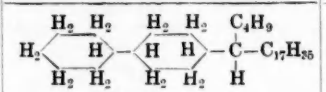	$C_{34}H_{66}$	0.867	1.52	0.541	0.0490	64.8	0.0235	0.0288	110
52	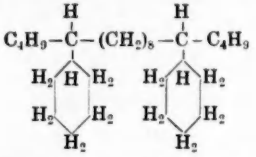	$C_{30}H_{58}$	—	1.033	0.363	0.0335	45.7	0.0226	0.0274	88
53**	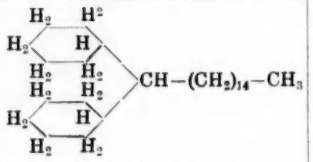	$C_{28}H_{54}$	0.8791 at 20°C.	$\eta_{25°}$ =0.532	$\eta_{145°}$ =0.213	$\left(\frac{\Delta \eta}{\Delta t}\right)_{25-45°C.}$ =0.0160	A_v =24.2	0.0220	0.0264	98
54**	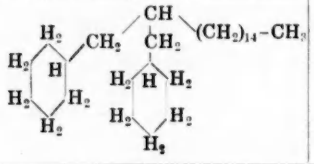	$C_{30}H_{58}$	0.8860 at 20°C.	$\eta_{25°}$ =0.481	$\eta_{145°}$ =0.197	$\left(\frac{\Delta \eta}{\Delta t}\right)_{25-45°C.}$ =0.0142	A_v =22.0	0.0219	0.0262	103

** For the calculation of $\left(\frac{\Delta \eta}{\Delta t}\right)_{25-45°C.}$, η'_a, and $K_p \cdot d_a$ of compounds Nos. 53 and 54, their values of absolute viscosity from Landa and Čech were used.

structure and the viscosity index of hydrocarbons, but none of his conclusions seem possible to explain the fact that compound No. 1, having a shorter side chain than compounds Nos. 2 and 13, is greater in viscosity index, as shown in the last column of Table 7, than the latter, whereas in the case of compounds Nos. 26, 15, 16, the shorter the side chain, the smaller is the viscosity index. No contradiction like this, however, is encountered in considering index $\frac{1000}{\nu_a}\left[0.00366+\left(\frac{\Delta\nu}{\Delta t}\right)_{25-45^\circ C.}\right]$ in relation to their chemical structure, for the reason that in the above two series of compounds η'_a invariably increases with length of side chain.

Aeronautical Research Institute,
Tokyo Imperial University.

On the Use of Interference Spectrographs for the Study of Fine Structures in Molecular Spectra.

By Sunao IMANISHI.

(Received December 13, 1937.)

Introduction. The high resolving powers conveniently obtainable, especially for the visible part of the spectrum, by the use of modern interference instruments may well be utilized for the study of a fine-structure in each rotational line of molecular band spectra, when the latter is suspected, by some reason or other, to be composed of several very closely situated components, or accompanied by satellites in close proximity to the main line. An individual band-line has usually a very small absolute intensity when compared with an atomic line; indeed, the total intensity associated with the emission of a single atomic line may be considered divided up into hundreds or more rotational lines of a whole band system belonging to a single molecular electronic transition. However, apart from the consequent increase in the time of exposure, which implies the necessity of taking much greater precautions against mechanical vibration and changes in the spectrograph due to temperature variation, the technique of photographing a fine-structure pattern of a band-line is the same in principle as with an atomic line.

As is well-known, a Michelson échelon grating or a Lummer-Gehrcke interference plate can magnify only a very small region of the spectrum without being overlapped by patterns of neighbouring "orders". Thus each such instrument has the so-called "range", characteristic of its construction and dependent on the wave-length. Two lines separated in wave-length farther than the range must therefore be resolved by means of an auxiliary or "coarse" dispersing system before or after sending the ray through the high-powered instrument to examine the individual structures. It is convenient, and only practicable for band study, to arrange matters so as to make the two dispersions at right angles to each other on the recording photographic plate, and we get a "crossed" spectrum, or a two-dimensional pattern of interference dots. In the case of a band spectrum each rotational line, at least at some distance from a head, must clearly be resolved from adjacent ones by the aid of this coarse dispersion.

When the region under examination is congested through overlapping of branches, or when treating a branch with very narrowly spaced rotational lines, the "coarse" dispersion may not be so coarse as one would be impressed by the word, since it is often necessary to use for this purpose a long focus plane grating or prism spectrograph, preferably of a small relative aperture to keep the patterns sharply defined; all these requirements pointing to still further prolongation of exposure time.

In the following are given brief descriptions of two studies in which such combined or "crossed" spectrographs were constructed and used.

Electronic Fine Structure in Helium Bands. The diatomic helium molecule, while formed with a very short life, has four electrons, two of which confine themselves in the molecular K-shell, not participating in the emission of visible light. With the remaining two valence electrons the system can have a set of singlet energy levels and a separate set of triplet levels, just like the He atom or the H_2 molecule with their two outer electrons. An inter-combination transition between a singlet and a triplet levels is extremely unlikely to occur in these light atomic or molecular systems, and any observed helium band should be classified either as a singlet-singlet transition with purely single rotational lines, or as a triplet-triplet transition with at least three very closely situated components corresponding to the theoretical spin fine-structures in the levels concerned, quite apart from any multiplication of branches caused by molecular rotation.

All these are very clear in theory and by analogy to other spectra, but, owing to the extreme smallness of spacings characteristic of the lightest atomic systems with their small nuclear charges, no direct experi-

mental evidence had existed as to the multiple nature of lines belonging to those bands classified as "triplets", until R. S. Mulliken and G. S. Monk published a paper[1] dealing with this problem, and found, for the first time, on photographs taken in high orders of a large concave grating spectrograph, a beginning resolution in lines of various bands having the $1s\sigma^2\ 2p\sigma\ 2p\pi\ ^3\Pi$ state either as the upper or the lower electronic level. They also found, in agreement with theoretical expectations, that no other level than the above $2p\pi\ ^3\Pi$ (notations for the inner three electrons will be omitted hereafter) had a fine-structure of measurable magnitude.

At the suggestion of G. H. Dieke, now of Johns Hopkins University, the writer had, independently of Mulliken and Monk, examined the expected fine-structures in the band λ 6400 Å, $3s\sigma\ ^3\Sigma \rightarrow 2p\pi\ ^3\Pi$, $0 \rightarrow 0$, with a 40 plate glass échelon. At λ 6400 Å the échelon had a range $\Delta\lambda_{max}$ of about 0.64 Å and a resolving power $\Delta\lambda/\lambda$ of about 3×10^5. The experimental arrangement for this work is roughly shown in Fig. 1.

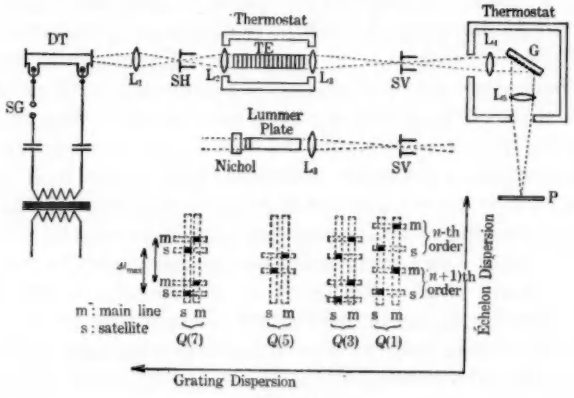

Fig. 1.

The source DT of helium bands is an end-on, sealed pyrex discharge tube of 1 m. length and 2 cm. internal bore, containing pure helium gas at about 4 cm. Hg pressure. A heavy condensed discharge is maintained through the discharge tube and a zinc or aluminium spark gap SG in series. The light from the source is condensed by a lens L_1 on the horizontal échelon slit SH, made parallel by a collimator lens L_2 and passes the échelon TE. The diffracted rays are projected by an achromatic lens L_2 of 1 m. focal length on to the second vertical slit SV of a coarse-analysing spectrograph L_4GL_5 and form here horizontal interference fringes.

(1) *Phys. Rev.*, **34** (1929), 1530.

The latter spectrograph contains a plane grating having 55,100 lines in its 9.3 × 7.6 cm.^{2} ruled area, and a camera lens of 3 m. focal length, giving a dispersion in the first order of about 3.2 Å per mm. on a photographic plate P. Thanks to the stigmatic nature of a plane grating spectrograph the directions of the two dispersions could be made perpendicular to each other as mentioned in the introduction, and the patterns produced on the plate are shown diagrammatically in the same figure, which may be compared with the final photograph obtained for the λ 6400 Å band reproduced in Fig. 3. The band happens to have a *P*-, a *Q*- and an *R*-branch and, fortunately, the λ 6402.246 Å line of neon, which was present in helium as an impurity, appears among the *Q*-lines nearly in a "double order" pattern, supplying a good standard for the determination of $\Delta\lambda_{max}$.

The photograph shows a clear resolution of the one component of the triple structure in several rotational lines at the beginnings of the *Q*- and the *P*-branch as a weak satellite under each thick main line. *R*-lines are too weak at the beginning of the branch to give measurable patterns; each one of them, however, should have the same structure as the corresponding *P*-line labelled with the same rotational quantum number. The main lines themselves are still unresolved doublets, and on the original plate they do show obvious sign of resolution, as their dots are all rhomb-shaped, whereas if they were single the dots would be rectangular, defined by the parpendicular jaws of the two slits, just as the dots for the neon line are. But, as the source was not specially cooled with liquid air to suppress the Doppler effect, which may be quite appreciable with the light helium molecule, no quantitative measurement could be made of the separations in main lines. Result of measurements[(2)] for the resolved components is tabulated below in Table 1. According to H. A. Kramers the upper $3s\sigma\ ^3\Sigma$ state should also have a triple structure, but its spacings are far too smaller than those in the lower $2p\pi\ ^3\Pi$ state, as confirmed by Mulliken and Monk. Therefore the value given in the table under each line-notation can be taken as one of the two spacings in the respective rotational level in the lower $2p\pi\ ^3\Pi$ state. It decreases gradually as the rotational quantum number increases, exactly in accordance with theoretical calculations of the spin fine-structure for the rotating helium molecule. It may here be remarked that owing to special circumstances prevailing in the helium molecule, every other rotational level is lacking in each electronic state. Besides, lower levels for *Q*-lines and those for *P*- or *R*-lines are of different description or symmetry (*c* and *d* respectively). Hence, for this particular band, there is an odd sequence only of

(2) *Nature*, **125** (1930), 529; *Sci. Papers Inst. Phys. Chem. Research* (Tokyo), **14** (1930), 105.

the rotational quantum number for the Q-branch, and an even sequence only for the P- or the R-branch.

Table 1. Band λ 6400 Å

Line	$Q(1)$	$Q(3)$	$Q(5)$	$Q(7)$	$Q(9)$	$Q(11)$	$Q(13)$	$Q(15)$
$\Delta\nu_c$ (cm.$^{-1}$)	0.354	0.281	0.290	0.278	0.266	0.271	0.24	0.21
Line	$P(2)$							
$\Delta\nu_d$ (cm.$^{-1}$)	0.268							

Isotopic Constitution of Gold from Gold Hydride Bands. Early in 1935 gold remained one of a very few elements the isotopic constitution of which had not been determined quantitatively by the mass-spectrograph, owing to the difficulty of producing a suitable positive ion source. Its accepted chemical atomic weight is 197.21, and in analogy to the closely similar elements silver and copper, it seemed highly probable that it would be a mixture of practically only the two isotopes of odd mass-numbers 197 and 199, with an abundance ratio Au^{199}:Au^{197} of 1 to 8.3, or even 1 to 7.0, according as we take for the atomic mass unit $(1/16)O$ or $(1/16)O^{16}$ respectively.

On the other hand, Aston's famous "packing fraction" curve crosses the zero axis near at the mass number 197, and $+11 \times 10^{-4}$ seemed to be too large for the packing effect per proton for the gold atom,[3] a figure which we must assume if we consider this element to be constituted entirely of Au^{197}.

Now, in the domain of diatomic band spectra, we know of the gold hydride, AuH, spectrum, extensively investigated in emission as well as in absorption. It has a system extending from the near ultra-violet down into the visible region, with individual bands of the simplest structure having purely single and comparatively wide-spaced rotational lines. A preliminary calculation, based on the conventional and approximate theory of rotational and vibrational isotope shifts in diatomic bands, showed that if Au^{199} existed in the ratio of about 1 in 7 to Au^{197}, every rotational line near at λ 4000 Å should be accompanied by a satellite at a separation $\Delta\nu$ of about 0.14 cm.$^{-1}$, or $\Delta\lambda$ of about 0.024 Å, on its shorter wave-length side, standing in an intensity relation comparable with that of abundance.

(3) The packing fraction of gold is now obtained by Dempster (a short abstract of a report presented to the Chicago Meeting of the American Physical Society, November, 1937) as $+2.0 \pm 0.4$ ($\times 10^{-4}$), by step-wise comparisons of gold with oxygen via copper[65]. From this the mass-spectrographic atomic weight of Au^{197} appears to be 197.039 ± 0.008.

This appeared a suitable problem for a reflecting échelon spectrograph the writer had for some time assembled out of parts, and an experiment was carried out in the following scheme (Fig. 2).

The light source S is a D.C. arc between gold poles burning in a hydrogen atmosphere of about 20 cm. Hg pressure, contained in a water-cooled metallic chamber. After passing a horizontal slit SH, and deflected by a small 45° prism RP, light enters a Littrow-mounted air-tight reflecting échelon chamber through a lens L_2 of 1.5 m. focus, projected back again by L_2, passes underneath RP, and fringes are formed on a vertical slit of a coarse-analysing prism spectrograph L_3PPL_4, which gives a linear dispersion of about 4 Å per mm. for λ 4000 Å. The reflecting échelon here used is made of 25 plane-parallel plates of fused silica, equal in thickness to about one-eighth of a wave-length, in optical contact, and platinized on its step surfaces. It has the range of about 0.1 Å and a theoretical resolving power of about 10^6 for the region aforementioned.

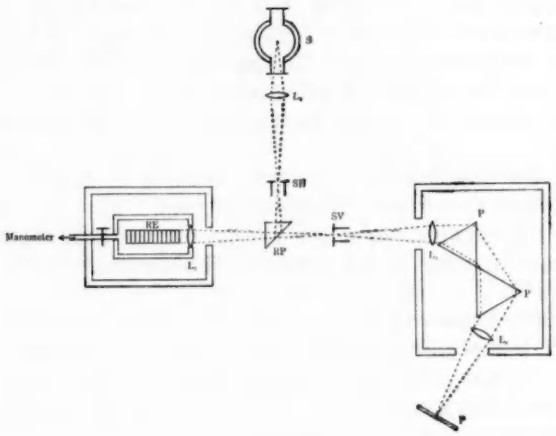

Fig. 2.

A reflecting échelon, first conceived also by Michelson, and constructed with a great precision of modern technique, is in principle no other than a kind of transmission échelon made of air, the steps of which are bounded by very rigid reflecting surfaces; and in passing twice through it, light suffers diffraction to give the enormous resolving power, which nearly matches that of a glass échelon of four times the plate number, with an added advantage of being perfectly free from weakening by absorption. Therefore it is essential to use it in a temperature-controlled air-tight box

to keep the refractive index of the surrounding air constant during an exposure. By a slight change of air pressure diffraction angles change, and we can have the same effect of changing over from the "single order"

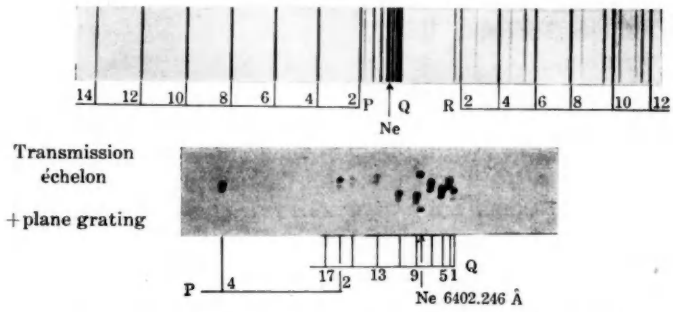

Fig. 3. He_2 band λ 6400 Å, $3s\sigma\,{}^3\Sigma \rightarrow 2p\pi\,{}^3\Pi$, $0 \rightarrow 0$. Plane grating.

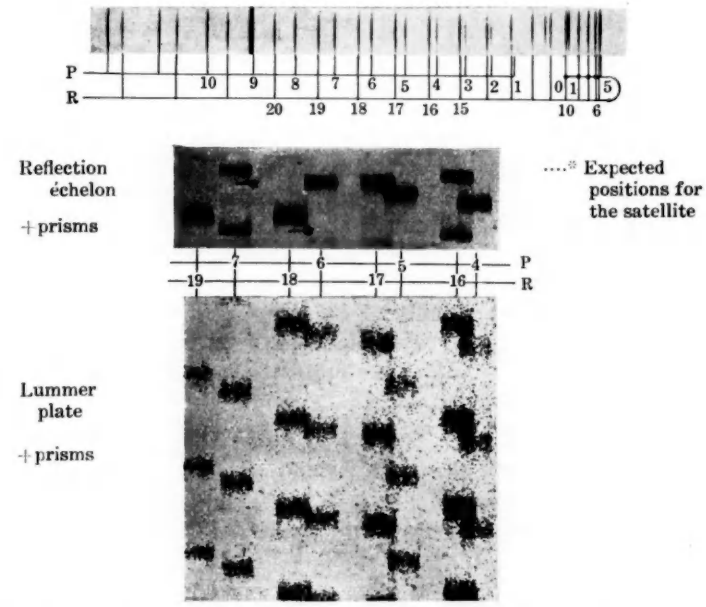
P
R
10 9 8 7 6 5 4 3 2 1 0 1 5
20 19 18 17 16 15 10 6
Reflection échelon
+ prisms
....* Expected positions for the satellite
7 6 5 4 P
19 18 17 16 R
Lummer plate
+ prisms

Fig. 4. AuH band λ 3973 Å, ${}^1\Sigma^* \rightarrow {}^1\Sigma$, $0 \rightarrow 1$. 15-Foot concave grating, 2nd order.

position into the "double order" one for a particular wave-length, just as by tilting an ordinary glass transmission échelon against the direction of incidence to alter path differences.

The final photograph obtained with this arrangement for the 0→1 vibrational band of the AuH $^1\Sigma^*\rightarrow{}^1\Sigma$ system at λ 3973 Å is shown in Fig. 4. Notwithstanding the circumstance that the source used was an ordinary arc only inefficiently cooled by running water, the main line in each pattern for every rotational member is sufficiently sharp to be regarded as purely single, and accompanied by no trace at all of a satellite, which should show up at a separation of about one-fifth of the range or the distance between the fringes of the main line in two consecutive orders, if it had an intensity about one-seventh of that of the latter.

This negative result[4] is quite against the expectation stated at the beginning of this section, but was confirmed by experiments using two alternative arrangements, in which the reflecting échelon was replaced by the 40-plate glass échelon described in the previous section, or a high-resolving quartz Lummer-Gehrcke plate; the patterns by the latter are shown also in the same reproduction (cf. Fig. 1 for the arrangement).

Meanwhile during this work, A. J. Dempster of Chicago University had elaborated a spark source of gold ions for his mass-spectrograph and communicated the same negative result to Nature,[5] stating in a more quantitative way that the ratio of Au^{199}:Au^{197} is much smaller than 1 in 500. Thus the complete agreement of the results obtained by the two quite independent methods, although the band-spectroscopic one is less direct than, and therefore of a supplementary nature to, the mass-spectrographic, confirmed the non-existence of a natural isotope of gold with mass number 199, and the hitherto accepted chemical atomic weight of this element seems, by the reason stated earlier, to need a revision.[3]

In conclusion, the writer wishes to express his most sincere thanks to Prof. M. Katayama of Faculty of Science, Tokyo Imperial University, for unchanging encouragements the writer received throughout his spectroscopic researches after graduation from the Department of Chemistry.

Institute of Physical and Chemical Research, Tokyo.

(4) *Nature*, **136** (1935), 476; *Sci. Papers Inst. Phys. Chem. Research* (Tokyo), **28** (1935), 129.

(5) *Nature*, **135** (1935), 993; also L. Sibaiya, working with hyper-fine structures of atomic gold lines using a Lummer-Gehrcke plate, arrived at the same conclusion, *Proc. Indian Acad. Sci.*, A, **2** (1935), 313.

Über den Austausch der Wasserstoffatome zwischen Pyrrol, Indol sowie ihren Methylderivaten und Wasser. I. Austausch der Wasserstoffatome zwischen Pyrrol und Wasser.[1]

Von Masao KOIZUMI* und Toshizo TITANI.

(Eingegangen am 20. Dezember 1937.)

Inhaltsübersicht. Die Austauschreaktion der H-Atome zwischen Pyrrol und Wasser wurde unter Verwendung des verdünnten schweren Wassers von verschiedenen Wasserstoffionenkonzentrationen untersucht. Die dabei gefundenen Tatsachen kann man kurz wie folgt zusammenfassen.

(1) Solange die H-Ionenkonzentration im verwendeten Wasser von $p\mathrm{H} = 14$ bis 2 bleibt, wird nur ein einziges und höchstwahrscheinlich an N gebundene H-Atom des Pyrrolmoleküls gegen die des Wassers sehr schnell ausgetauscht (die „erste" Austauschreaktion), aber selbst im Verlauf von zehn Stunden bei 30°C. treten keine weiteren H-Atome gegen die des Wassers auf, auch wenn 0.01 N saures schweres Wasser verwendet wird.

(2) Wenn dagegen die H-Ionenkonzentration in schwerem Wasser bis zu $p\mathrm{H} = 2$ bis 1 erhöht wird, setzt ziemlich plötzlich eine neue Art der Austauschreaktion (die „zweite" Austauschreaktion) ein, bei der mehr als ein H-Atom des Pyrrolmoleküls gegen die H-Atome des Wassers ausgetauscht werden. Diese neue „zweite" Austauschreaktion verläuft innerhalb der obenangegebenen pH-Grenzen mit gut messbarer Geschwindigkeit.

(3) Wenn wir aber die H-Ionenkonzentration in schwerem Wasser noch weiter erhöhen und dessen pH unterhalb 1 sinkt, wird die Austauschgeschwindigkeit so gross, dass sie sich fast unmessbar erweist.

(4) Bei Benutzung von fast reinem schwerem Wasser fanden wir, dass in dieser neuen „zweiten" Austauschreaktion die sämtlichen fünf H-Atome des Pyrrolmoleküls gegen die des Wassers austauschbar sind. Daraus folgt, dass der durchschnittliche Verteilungsquotient der D-Atome zwischen dem CH-Radikal des Pyrrolmoleküls und Wasser $k(\mathrm{CH}/\mathrm{H_2O}) = 0.70$ sein muss, wenn man den V.Q. zwischen dem NH-Radikal des Pyrrols und Wasser $k(\mathrm{NH}/\mathrm{H_2O}) = 0.88$ setzt.

Das Auftreten der neuen „zweiten" Austauschreaktion kann man mit der Salzbildung des Pyrrolmoleküls und der daran folgenden tautomerischen Umwandlung desselben erklären.

---

* Früher Masao HARADA.

(1) Vorläufig mitgeteilt in diesem Bulletin, **12** (1937), 107.

Einleitung. Hauptsächlich auf Grund der chemischen Eigenschaften des Pyrrols nimmt man gewöhnlich von dieser Verbindung eine tautomerische Umwadlung an, wie das Schema (1) zeigt:[2]

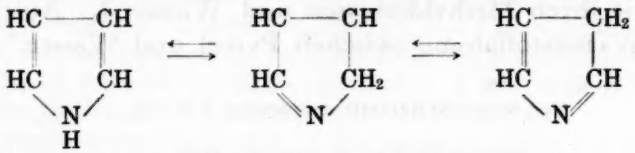

(1)

Sollte eine solche Umwandlung wirklich stattfinden, dann liegt die Möglichkeit nahe, dass die sämtlichen H-Atome des Pyrrolmoleküls gegen die des Wassers ausgetauscht werden können, wenn man die beiden Substanzen zusammenschüttelt, obwohl die direkt an C gebundene H-Atome gewöhnlich nicht direkt austauschbar sind. Gegen diese Erwartung fanden wir aber in unserem früheren Versuch,[3] wo wir Pyrrol zusammen mit neutralem schwerem Wasser schüttelten, dass nur ein einziges und höchstwahrscheinlich an N gebundenes H-Atom des Pyrrolmoleküls gegen D-Atome des schweren Wassers ausgetauscht wurde, es aber selbst nach fünfzig Stunden bei 50°C. zu keinem Austausch weiterer H-Atome des Pyrrolmoleküls gegen die des Wassers kam. Im Anschluss an diesen Versuch führten wir nun einen ähnlichen Versuch nicht aber mit neutralem sondern alkalischem sowie saurem schwerem Wasser aus. Dabei fanden wir, dass die erwartete Austauschreaktion der sämtlichen H-Atome des Pyrrolmoleküls gegen die des Wassers oberhalb einer bestimmten H-Ionenkonzentration im verwendeten Wasser wirklich stattfand.

Austausch der H-Atome zwischen Pyrrol und Wasser bei verschiedenen H-Ionenkonzentrationen im letzteren. Eine genau bestimmte Menge (ca. 5 g.) von Pyrrol wurde zusammen mit einer bestimmten Menge (ca. 2 g.) von alkalischem bzw. saurem verdünntem schwerem Wasser in ein Glasrohr eingeschmolzen und bei bestimmter Temperatur (30°C.) aber verschiedener Länge geschüttelt. Das dazu benutzte alkalische bzw. saure schwere Wasser von bekanntem D-Gehalt sowie bestimmter H-Ionenkonzentration wurde dadurch bereitet, dass wir eine bestimmte Menge von ca. 3-prozentigem schwerem Wasser, dessen Gehalt an D genau bekannt war, mit einer bestimmten Menge von HCl- bzw. KOH-Lösung in gewöhnlichem Wasser versetzten. Nach gründlicher Zusammenschüttelung wurde das Wasser durch Abhebung vom Pyrrol abgetrennt und nach folgender Methode gereinigt. Bei der alkalischen Lösung wurde

(2) Vgl. H. Fisher und H. Orth, „Chemie des Pyrrols," Bd. I, Leipzig (1934).
(3) M. Harada und T. Titani, dies Bulletin, **11** (1936), 465.

das Wasser durch Destillation direkt vom zugesetzten Alkali befreit. Aber bei der sauren Lösung wurde sie zuerst unter Zusatz von kleinen Mengen von CaO neutralisiert und dann abfiltriert. Dabei fanden wir, als wir 1 N HCl-Lösung verwendeten, dass das Pyrrol während der Schüttelung gelb bis orange gefärbt wurde und bei der Neutralisation der damit geschüttelten wässrigen Lösung mit CaO eine weisse Trübung auftrat. Dieselbe Trübung trat auch in Erscheinung, aber in geringerem Masse, bei der Neutralisation von 0.1 N HCl-Lösung, nachdem es mit Pyrrol geschüttelt wurde. In den anderen Fällen blieb aber das Pyrrol während der Schüttelung vollkommen klar und farblos, und bei der Neutralisation der Lösung entstand keine Trübung. Das dadurch von Säure bzw. Alkali befreite Wasser wurde dann von dem darin ein wenig gelösten Pyrrol befreit, indem wir das Wasser zusammen mit gut getrocknetem Äther schüttelten. Der dabei wieder ins Wasser ein wenig gelöste Äther wurde durch die Behandlung des Wassers mittels Pumpenöls vollständig beseitigt.[3] Das so behandelte Wasser wurde dann auf übliche Weise gereinigt, indem wir es zunächst in Dampfform über Rotglut erhitztem CuO leiteten, dann unter Zusatz von Na_2O_2 und $KMnO_4$ in einem geschlossenen Rohr über Nacht erhitzten und zum Schluss im Vakuum zweimal destillierten. Die Dichte des so gereinigten Wassers bestimmten wir nach der Schwebemethode mittels eines kleinen Quarzschwimmers, um daraus die D-Konzentration in demselben kennen zu lernen. Die Reinheit des vom Wasser abgetrennten Pyrrols wurde in einem Fall, wo wir das Pyrrol mit 0.1 N HCl-Lösung schüttelten, durch die Bestimmung seines Siedepunktes geprüft. Dabei erwies er sich genau als derselbe (129–131°C.) wie vor dem Versuch.

Aus den wie oben ausgeführten Experimenten kann man die Zahl der austauschbaren H-Atome in einem Pyrrolmolekül durch Gl. (2) ausrechnen:

$$nk = 2\frac{M_w}{M_P}\frac{D_a - D_e}{D_e} \qquad (2),$$

wo n Zahl der austauschbaren H-Atome in einem Pyrrolmolekül, k Verteilungsquotient (V.Q.) der D-Atome zwischen Pyrrol und Wasser, M_w Molzahl des verwendeten schweren Wassers, M_P Molzahl des verwendeten Pyrrols, und D_a und D_e D-Konzentration im verwendeten schweren Wasser vor und nach dem Experiment ausdrücken. Aber weil die einzelnen H-Atome in einem Molekül streng genommen verschiedene Grösse von V.Q. k besitzen müssen, drückt das aus Gl. (2) ausgerechnete Produkt nk nichts anderes als die Summe derselben der einzelnen Arten von austauschbaren H-Atomen in einem gegebenen Molekül aus, wie Gl. (3) zeigt.

$$nk = \sum n_i k_i \,. \qquad (3).$$

Aus diesem Grund wollen wir das aus Gl. (2) errechnete Produkt nk weiter unten „Austauschäquivalent" eines gegebenen Moleküls nennen.

Das „Austauschäquivalent" nk des Pyrrolmoleküls, das wir unter Verwendung von verschieden alkalischem bzw. saurem schwerem Wasser gefunden haben, geben wir in Tabelle 1 wieder.

Tabelle 1.

Austauschäquivalent nk des Pyrrols bei verschiedenen Wasserstoffionenkonzentrationen.

Versuchsnr.	Normalität des benutzten Wassers	pH	Schüttelungsdauer in Stdn.	nk	Bemerkung
1	1 N KOH	14	1	0.92	
2	„ „	„	5	0.92	
3	neutral	7.00	5–50	0.88[3]	
4	0.01 N HCl	2.00	1	0.90	
5	„ „	„	5	0.88	
6	„ „	„	10	0.90	
7	0.024 N HCl	1.62	1	2.25	
8	„ „	„	3	3.53	
9	0.048 N HCl	1.32	1	3.29	
10	„ „	„	3	3.60	
11	0.1 N HCl	1.00	1	3.64	
12	„ „	„	5	3.74	Pyrrol blieb farblos, aber bei der Neutralisation der Lösung geringe Trübung ?
13	„ „	„	9	3.70	wie oben.
14	1 N HCl	0.00	2/3	3.81	Pyrrol wurde gelb gefärbt und bei der Neutralisation der Lösung trat weisse Trübung auf.
15	„ „	„	2⅙	3.76	wie oben.
16	„ „	„	5	3.64	Pyrrol wurde orange gefärbt, sonst wie oben.

Die Versuchsergebnisse in Tabelle 1 sind auch in der nebenstehenden Abbildung graphisch dargestellt, wo das gefundene nk gegen den pH des verwendeten schweren Wassers aufgetragen ist. Die Nummer bei jedem kleinen Kreis zeigt die Schüttelungsdauer in Stunden. Wie man aus dieser graphischen Darstellung sofort ersieht, hängt die Grösse des „Austauschäquivalents" nk des Pyrrolmoleküls stark von der H-Ionenkon-

zentration des damit geschüttelten Wassers ab. Bleibt nämlich die H-Ionenkonzentration im Wasser kleiner als 0.01 N (pH = 2), so bleibt auch der Wert von nk durchaus konstant und beträgt durchschnittlich 0.88.[4] Wenn dagegen die H-Ionenkonzentration im verwendeten Wasser 0.01 N (pH = 2) überschreitet, setzt plötzlich eine neue Art von Austauschreaktion ein und das Austauschäquivalent nk nimmt sprungweise bis auf 3.7 zu. Dieser letzte Wert bleibt aber wieder konstant bis zur höchsten H-Ionenkonzentration, die wir verwendeten.

Auf diese Weise können wir die Austauschreaktion der H-Atome zwischen Pyrrol und Wasser vorläufig in zwei Arten einteilen. Bei der gewöhnlichen „ersten" Art von Austauschreaktion, die bei kleinen H-Ionenkonzentrationen (pH $\geqq$ 2) im Wasser stattfindet, wird nur ein einziges und höchstwahrscheinlich an N gebundenes H-Atom gegen die des Wassers sehr schnell ausgetauscht. Wenn dagegen die H-Ionenkonzentration im Wasser bis pH $<$ 2 erhöht wird, setzt plötzlich eine neue „zweite" Art von Austauschreaktion ein, bei der mehr als ein H-Atom des Pyrrolmoleküls gegen die H-Atome des Wassers ausgetauscht werden. Diese „zweite" Austauschreaktion verläuft zwischen pH = 2 bis 1 mit gut messbarer Geschwindigkeit. Wenn aber der pH des Wassers unterhalb 1 sinkt, dann wird die Geschwindigkeit dieser „zweiten" Austauschreaktion fast unmessbar gross. Aber bei solchen enormen H-Ionenkonzentrationen im verwendeten Wasser fanden wir zugleich, wie schon oben in Tabelle 1 erwähnt, durch die Färbung des Pyrrols sowie die Trübung der damit geschüttelten Lösung bei der Neutralisation, ein deutliches Anzeichen für das Auftreten der Polymerisation des Pyrrolmoleküls.

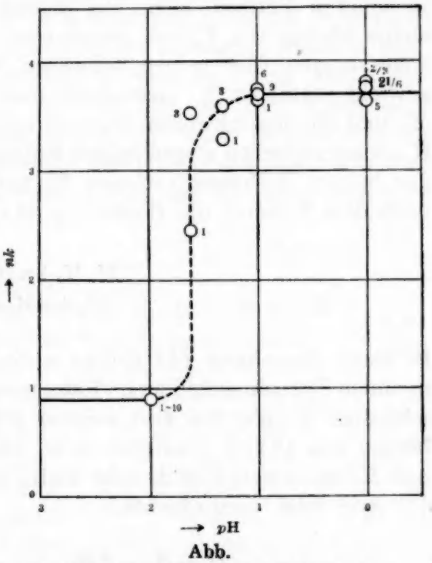

Abb.

Abhängigkeit des Austauschäquivalents nk des Pyrrols auf dem pH des damit geschüttelten Wassers und der Schüttelungsdauer.

(4) Rechnet man bloss aus den vorliegenden Versuchsergebnissen den Mittelwert von nk, dann ergibt er sich als 0.90 statt 0.88. Da aber dieser letztere Wert beim früheren Versuch (Fussnote (3)) nicht nur aus der Abnahme der D-Konzentration im schweren Wasser, sondern auch aus der Zunahme derselben im damit geschüttelten Pyrrol zugleich gerechnet wurde, muss er genauer als der erstere angesehen werden.

Bestimmung der Zahl der austauschbaren H-Atome bei der „zweiten" Austauschreaktion. Aus den oben angegebenen Versuchen fanden wir, dass das Austauschäquivalent des Pyrrolmoleküls bei der gewöhnlichen „ersten" Austauschreaktion $(nk)_1 = 0.88$, während es bei der neuen „zweiten" Austauschreaktion $(nk)_2 = 3.70$ beträgt. Aus diesem ersten Wert $(nk)_1$ darf man wohl schliessen, dass es sich bei der „ersten" Austauschreaktion um ein einziges und höchstwahrscheinlich an N gebundenes H-Atom handelt. Dagegen aus dem zweiten Wert $(nk)_2$ kann man nicht sofort über die Zahl der dabei austauschbaren H-Atome Schlüsse ziehen. Deshalb führten wir, um diese Zahl direkt zu bestimmen, einen besonderen Versuch aus. Bei diesem Versuch liessen wir nämlich eine kleine Menge von Pyrrol gegen eine überschüssige Menge des mit HCl angesauerten fast reinen schweren Wassers bis zum Austauschgleichgewicht reagieren.[5] Bezeichnet man dabei die Molzahl des Pyrrols mit M_P und die des schweren Wassers mit M_w, ferner den mittleren V.Q. der H-Atome zwischen diesen beiden Substanzen mit a, dann besteht zwischen den beiden H-Konzentrationen H_a und H_e im schweren Wasser vor und nach dem Versuch die Beziehung (4):

$$\frac{2M_wH_a+nM_P}{2M_w+nM_Pa} = H_e \qquad (4).$$

In dieser Beziehung (4) drückt n die Zahl der austauschbaren H-Atome in einem Pyrrolmolekül aus. Falls man aber, wie oben erwähnt, eine überschüssige Menge von fast reinem schwerem Wasser gegen eine kleine Menge von Pyrrol reagieren liess, dann sind die H-Konzentrationen H_a und H_e im ersteren beide sehr klein, und deshalb kann man die obige Gl. (4) wie folgt vereinfachen:

$$n = \frac{H_e-H_a}{(1-aH_e)} \cdot \frac{2M_w}{M_P} \fallingdotseq \left(H_e-H_a\right)\frac{2M_w}{M_P} \qquad (5).$$

Mittels dieser Gl. (5) konnten wir die Zahl n der austauschbaren H-Atome in einem Pyrrolmolekül bei der „zweiten" Austauschreaktion experimentell bestimmen. Dazu benutzten wir 99.4%iges schweres Wasser, das mit HCl auf ähnliche Weise wie schon oben erwähnt zu 0.1 bis 1 N angesauert war. Etwa 1 g. von diesem sauren schweren Wasser wurde zusammen mit ca. 0.03 bis 0.05 g. Pyrrol in einem Glasrohr unter Luft-

(5) Vgl. darüber G. Okamoto und S. Abe, *J. Chem. Soc. Japan*, **57** (1937), 1157 (japanisch); G. Okamoto, *J. Faculty Sci., Hokkaido Imp. Univ.*, Ser. III, **2** (1936), 81.

abschluss bei 30°C. etwa zwei Stunden lang geschüttelt, bis das Austauschgleichgewicht zustandekam. Dann wurde das schwere Wasser, auf ähnliche Weise wie schon oben erwähnt, vom Pyrrol geschieden, und die Dichte des so abgetrennten Wassers genau bestimmt, nachdem es neutralisiert und richtig gereinigt worden war. Die Bestimmung der Dichte des schweren Wassers führten wir ebenfalls nach der Schwebemethode mittels eines zu diesem Zweck besonders konstruierten Glasschwimmers aus. Da aber bei dem Blindversuch gefunden wurde, dass die Dichte des benutzten schweren Wassers während des Versuchs durch die Absorption der Feuchtigkeit aus atmosphärischer Luft durchschnittlich um 0.00033 $\pm$ 0.00001 vermindert wurde, und zwar diese Abnahme der Dichte des schweren Wassers der Zunahme des n-Wertes um etwa 0.5 entsprach, addierten wir der direkt gefundenen Dichte des schweren Wassers nach dem Versuch immer den oben angegebenen Wert und erst aus dieser korrigierten Dichte berechneten wir nach Gl. (5) die Zahl n der austauschbaren H-Atome. Die auf diese Weise erhaltenen Resultate geben wir in Tabelle 2 wieder, wo die Abnahme der Dichte des D_2O nach dem Experiment in der vierten Vertikalreihe schon auf die oben erwähnte Weise korrigiert ist.

Tabelle 2. Zahl n der austauschbaren H-Atome in einem Pyrrolmolekül bei der „zweiten" Austauschreaktion.

Versuchsnr.	Molzahl des Pyrrols M_P	Molzahl des D_2O M_w	Abnahme der Dichte des D_2O nach dem Exp.	n
1	0.000442	0.102	0.00135	4.9
2	0.000747	0.0712	0.00329	5.2
3	0.00118	0.0825	0.00454	4.8
4	0.000790	0.0682	0.00392	5.1

Aus diesem Versuch ersieht man sofort, dass bei der „zweiten" Austauschreaktion fünf, nämlich sämtliche, H-Atome des Pyrrolmoleküls gegen die des Wassers austauschbar sind.

Wir haben oben in Gl. (3) darauf hingewiesen, dass das Austauschäquivalent nk eines gegebenen Moleküls nichts anderes als die Summe aus den n_ik_i der einzelnen Arten der austauschbaren H-Atome in diesem Molekül ist. Demgemäss kann man das experimentell gefundene Austauschäquivalent nk des Pyrrolmoleküls wie folgt formulieren:

$$nk = n_Nk_N + n_Ck_C \qquad (6),$$

wo $n_N k_N$ das Austauschäquivalent des an N gebundene H-Atoms und $n_C k_C$ das der an C gebundenen H-Atome im Pyrrolmolekül ausdrückt. Da wir aber bei der „ersten" Austauschreaktion des Pyrrols $(nk)_1 = 0.88$, $n_N = 1$ und $n_C = 0$ gefunden haben, folgt aus Gl. (6) sofort, dass der V.Q. der D-Atome zwischen der NH-Gruppe des Pyrrols und Wasser $k_N = k(NH/H_2O) = 0.88$ liegt. Dagegen haben wir bei der „zweiten" Austauschreaktion $(nk)_2 = 3.7$ und $n_N + n_C = 5$ gefunden. Setzt man nun diese beiden Werte sowie die schon oben gefundene Werte von n_N $(= 1)$ und $k_N (= 0.88)$ in Gl. (6), dann ergibt sich, dass der mittlere V.Q. der D-Atome zwischen der CH-Gruppe im Pyrrol und Wasser

$$k_C = k(CH/H_2O) = \frac{3.70-0.88}{5-1} = 0.70$$

sein muss.

Wir möchten hier bemerken, dass der so gefundene V.Q. $k(CH/H_2O)$ des Pyrrolmoleküls erheblich kleiner als der des Benzolmoleküls ist, der von Koyano[6] bei 100°C. gleich 0.93 gefunden wurde. Daraus ersieht man, dass der V.Q. der D-Atome zwischen der CH-Gruppe, oder im allgemeinen einer bestimmten Atomgruppe, in einem gegebenen Molekül und Wasser ziemlich stark von der Molekülstruktur des ersteren beeinflusst wird.[7]

Diskussion. Eine der massgebenden Bedingungen für das Zustandekommen der „zweiten" Austauschreaktion, bei der alle H-Atome im Pyrrolmolekül gegen die des sauren Wassers ausgetauscht werden, ist ohne Zweifel die H-Ionenkonzentration im letzteren. Je grösser die H-Ionenkonzentration im verwendeten Wasser ist, desto leichter und schneller verläuft die „zweite" Austauschreaktion der H-Atome zwischen Pyrrol und Wasser, und bei genügend grossen H-Ionenkonzentrationen kann sie mit fast unmessbarer Geschwindigkeit verlaufen. Aber in diesem Gebiet der H-Ionenkonzentration tritt zugleich, wie schon oben erwähnt, ein deutliches Anzeichen für die Polymerisation des Pyrrolmoleküls auf. Es ist aber eine wohl bekannte Tatsache, dass das Pyrrol gegen Säuren sehr empfindlich ist. Behandelt man nämlich diese Substanz mit starken Säuren, so entsteht leicht Polymerisation und ergibt ein kompliziertes rot gefärbtes Polymerisationsprodukt (Pyrrolrot). In dem vorliegenden Versuch fanden wir auch, als wir das Pyrrol mit verhältnismässig stark saurer Lösung schüttelten, dass es gelb bis orange

(6) K. Koyano, *J. Chem. Soc. Japan*, **57** (1936), 933.

(7) Vgl. dazu K. Wirtz, *Z. physik. Chem.*, B, **34** (1936), 121; *Z. Elektrochem.*, **43** (1937), 662.

gefärbt und die damit geschüttelte wässrige Lösung bei der Neutralisation mit Kalk weiss getrübt wurde. Alle diese Tatsachen weisen ohne weiteres darauf hin, dass das Pyrrol in diesem Gebiet der H-Ionenkonzentrationen schon merklich polymerisationsfähig geworden war. Aber gerade bei dieser H-Ionenkonzentration trat die „zweite" Austauschreaktion am deutlichsten auf. Aus allen diesen Tatsachen spricht einwandfrei, dass es einen engen Zusammenhang zwischen der „zweiten" Austauschreaktion und Polymerisation des Pyrrolmoleküls geben und der massgebende Vorgang in den beiden Reaktionen die durch Säure bewirkte Lockerung der an C gebundenen H-Atome des Pyrrolmoleküls sein muss.

Aus diesem Grund sowie dem basischen bzw. schwach sauren Charakter der NH-Gruppe des Pyrrolmoleküls nehmen wir an, dass der erste Vorgang bei der „zweiten" Austauschreaktion sowie bei der Polymerisation des Pyrrolmoleküls unter dem Einfluss der Säuren, nichts anderes als die Salzbildung des Pyrrols bzw. die Anlagerung des Protons (bzw. Deuterons) an dem N-Atom desselben ist, wie das Reaktionsschema (7) zeigt:

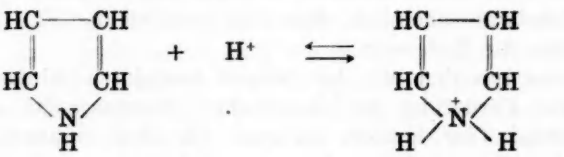

„labilisiertes" Molekül

Durch diese Reaktion wird offenbar die Valenzzahl des N-Atoms von drei auf fünf vermehrt, und zugleich muss die Löslichkeit des Pyrrols im Wasser um einen gewissen Betrag vermehrt werden. Dabei muss man annehmen, dass das so gebildete positive Ion des Pyrrolmoleküls im Vergleich mit dem neutralen normalen Pyrrolmolekül viel reaktionsfähiger ist, oder mit anderen Worten die an C gebundenen H-Atome des Pyrrolmoleküls werden durch die Reaktion (7) mehr oder weniger gelockert. Infolgedessen kann das dadurch gebildete sogenannte „labilisierte" Pyrrolmolekül mittels seiner gelockerten H-Atome die Polymerisation oder die „zweite" Austauschreaktion der H-Atome leicht ausführen.

Was den eigentlichen Chemismus der „zweiten" Austauschreaktion des „labilisierten" Pyrrolmoleküls anbetrifft, so lassen sich noch keine sicheren Angaben machen. Aber allen Umständen nach, besonders infolge der leichten Beweglichkeit der H-Atome dieses Moleküls, liegt die Annahme nahe, dass es sich dabei um die tautomerische Umwandlung des Pyrrolmoleküls handelt. Obwohl die tautomerische Umwandlung des

normalen Pyrrolmoleküls nach dem Schema (1) aus dem vorliegenden Versuch sehr fraglich geworden ist, kann man solche für das bei der Reaktion (7) gebildete „labilisierte" Pyrrolmolekül nicht ganz ausschliessen. Vielmehr besteht die Annahme, dass die tautomerische Umwandlung bzw. Prototropie des „labilisierten" Pyrrolmoleküls nach dem Schema (8) viel leichter als beim normalen Molekül verlaufen kann.

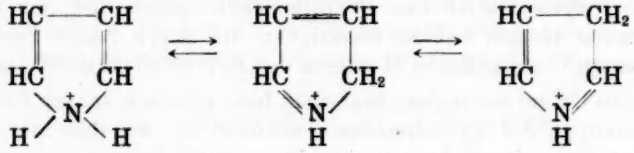

(8)

Die Frage, ob diese Reaktion (8) oder im allgemeinen die „zweite" Austauschreaktion selbst durch die H-Ionen katalysiert wird, lässt sich nicht ohne weiteres beantworten. Aber aus dem Versuch mit Indol, dessen Ergebnisse später in diesem Bulletin veröffentlicht werden sollen, erwies es sich als höchstwahrscheinlich, dass dies wirklich der Fall ist. Doch davon soll später die Rede sein.

Zum Schluss möchten wir der Nippon Gakujutsu-Shinkohkai (der Gesellschaft zur Förderung der japanischen Wissenschaft) sowie der Hattori-Hohkohkai (der Hattori-Stiftung) für ihre finanzielle Unterstützung bei Ausführung der vorliegenden Arbeit unseren besten Dank aussprechen.

Schiomi-Institut für physikalische und chemische Forschung
und
Physikalisch-chemisches Laboratorium der Kaiserlichen Universität zu Osaka.

Über den Austausch der Wasserstoffatome zwischen Pyrrol, Indol sowie ihren Methylderivaten und Wasser.[1] II. Austausch der Wasserstoffatome zwischen Thiophen sowie Furan und Wasser.

Von Masao KOIZUMI und Toshizo TITANI.

(Eingegangen am 20. Dezember 1937.)

Inhaltsübersicht. Thiophen und Furan tauschen nicht ihre H-Atome unter denselben Versuchsbedingungen wie beim Pyrrol, d.h. bei Zimmertemperatur und unter Verwendung sauren Wassers, gegen die des Wassers aus. Die H-Atome dieser beiden Verbindungen können erst dann, wenn man diese Substanzen zusammen mit saurem Wasser unter Zusatz von Platinschwarz als Katalysator bei erhöhter Temperatur schüttelt, langsam gegen die des Wassers ausgetauscht werden. Dabei scheinen alle H-Atome der Verbindungen gegen die des Wassers ausgetauscht werden zu können. Aus diesen Versuchsergebnissen schliessen wir, dass bei der „zweiten" Austauschreaktion des Pyrrols, wo alle H-Atome desselben schnell gegen die des sauren Wassers ausgetauscht werden, nicht nur die Elektronenkonfiguration des Pyrrolmoleküls, sondern auch die chemischen Eigenschaften der NH-Gruppe bzw. des N-Atoms in demselben eine massgebende Rolle spielen.

Einleitung. Es wurde in unserem letzten Versuche,[1] als wir das Pyrrol zusammen mit saurem schwerem Wasser bei Zimmertemperatur schüttelten, gefunden, dass die an C gebundenen H-Atome des Pyrrolmoleküls bei einer bestimmten H-Ionenkonzentration im schweren Wasser ziemlich plötzlich austauschbar und schnell gegen D-Atome des letzteren ausgetauscht werden. Diese „zweite" Austauschreaktion des Pyrrols führten wir auf den chemischen Charakter der NH-Gruppe bzw. des N-Atoms des Pyrrolmoleküls sowie der dadurch bedingten tautomerischen Umwandlung desselben zurück. Aus diesem Grunde untersuchten wir nun die Austauschbarkeit der H-Atome von Thiophen und Furan gegen die des sauren Wassers, weil diese beiden Verbindungen wie bekanntlich mit Pyrrol isoelektronisch sind und ähnliche Elektronenkonfiguration wie dies besitzen.

Versuche mit Thiophen. Das Thiophen wurde chemisch rein von Kahlbaum bezogen und nach einmaliger Destillation direkt zum Versuch

(1) I. Mitteilung, dies Bulletin, **13** (1938), 85.

verwendet. Die sonstige Arbeitsmethode war im grossen und ganzen dieselbe wie im letzten Versuch mit Pyrrol.[1] Aber weil die H-Atome des Thiophens im Vergleich mit denen des Pyrrols sich schwerer austauschbar erwiesen, benutzten wir eine viel stärkere saure Lösung als beim Pyrrol. Jedoch konnten wir unter diesen milden Versuchsbedingungen überhaupt keine Austauschreaktion der H-Atome des Thiophens gegen die des Wassers erzielen, wie aus den Versuchen 1 und 2 in Tabelle 1 ersichtlich ist. Das dabei gefundene negative Austauschäquivalent nk ist selbstverständlich auf den Versuchsfehler zurückzuführen.

Tabelle 1. Versuche mit Thiophen.

Versuchsnr.	Benutzte Lösung	Temp. (°C.)	Schüttelungsdauer in Stdn.	Austauschäquivalent nk
1	1 N HCl	30	5	−0.08
2	3 N HCl	40	5	−0.04
3	1 N HCl + Platinschwarz	100	5	0.33
4	„ + „	150	5	2.11
5	„ + „	150	14	2.22
6	„ + „	150	30	2.80

Da auf diese Weise die unter den ähnlichen Verhältnissen wie beim Pyrrol ausgeführten Versuche 1 und 2 sich ganz negativ erwiesen, führten wir die übrigen Versuche 3 bis 6 unter verhältnismässig stärkeren Graden aus. Bei diesen Experimenten fügten wir nämlich der Lösung eine Menge von Platinschwarz als Katalysator hinzu und erhöhten die Temperatur bis auf 150°C. Die Schüttelung des Thiophens mit dieser Lösung dauerte in einem Fall sogar 30 Stdn. (Versuch 6). Bei dieser verhältnismässig heftigen Behandlung fanden wir erst die H-Atome des Thiophens langsam gegen D-Atome des schweren Wassers sich austauschen, wie aus der Schüttelungsdauer und dem dabei gefundenen Austauschäquivalent des Thiophens in Tabelle 1 ersichtlich ist. Dabei schienen alle H-Atome des Thiophens, nach der Grösse des gefundenen Austauschäquivalents nk zu urteilen, schliesslich ganz gegen D-Atome des schweren Wassers ausgetauscht werden zu können. Aber in diesen Fällen fanden wir schon immer den Beginn einer ziemlich merklichen Zersetzung des Thiophens, wie wir dies aus der Entwicklung des Schwefelwasserstoffs wahrnahmen.

Versuche mit Furan. Das Furan wurde durch die Zersetzung der Brenzschleimsäure unter Erhitzung dieser Verbindung auf 250 bis 270°C. im geschlossenen Rohr hergestellt. Die sonstige Verfahrungsart war

genau dieselbe wie beim Thiophen. Die Versuchsergebnisse geben wir in Tabelle 2 wieder.

Tabelle 2. Versuche mit Furan.

Versuchsnr.	Benutzte Lösung	Temp. (°C.)	Schüttelungsdauer in Stdn.	Austauschäquivalent *nk*
1	1 N HCl	40	5	−0.03
2	3 N HCl	40	5	0.07
3	1 N HCl + Platinschwarz	40	8	−0.02
4	„ + „	100	7	1.29
5	„ + „	100	34	2.72
6	neutrales schweres Wasser	100	20	0.07

Wie man aus Tabelle 2 ersieht, führt das Furan ebenso schwer wie Thiophen die Austauschreaktion der H-Atome aus und erst unter der katalytischen Mitwirkung des Platinschwarzes können die H-Atome des Furans gegen die des Wassers langsam ausgetauscht werden.

Diskussion. Pyrrol, Thiophen und Furan sind untereinander isoelektronisch und nach Pauling[2] können sie im Normalzustand fünf Arten von Elektronenkonfiguration besitzen, wie das folgende Schema zeigt:

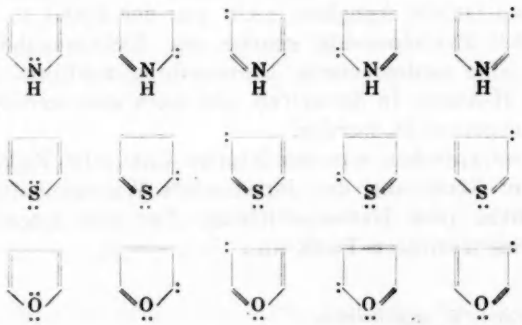

(1)

Schon allein aus diesem Vergleich der Elektronenkonfiguration in drei Arten der Moleküle liegt die Vermutung nahe, dass die H-Atome des Thiophens bzw. Furans ebenso leicht wie die des Pyrrols gegen die des Wassers austauschbar sein müssen. Aber in Wirklichkeit, wie in den

(2) L. Pauling, *J. Chem. Phys.*, **1** (1933), 607.

vorliegenden sowie in den letzten Versuchen gefunden wurde, gibt es einen enorm grossen Unterschied zwischen der Austauschbarkeit der an C gebundenen H-Atome des Pyrrols einerseits und der des Thiophens bzw. Furans anderseits. Dieser Befund weist ohne weiteres darauf hin, dass die Leichtaustauschbarkeit der an C gebundenen H-Atome des Pyrrolmoleküls nicht bloss mit der Elektronenkonfiguration in demselben im Normalzustand erklärt werden kann. Dafür muss man vielmehr den eigentlichen Charakter der NH-Gruppe bzw. des N-Atoms im Pyrrolmolekül in Betracht ziehen, wie wir schon in unserer letzten Mitteilung[1] darauf hingewiesen haben. Dort nahmen wir an, dass der erste massgebende Vorgang bei der „zweiten" Austauschreaktion des Pyrrols gegen saures Wasser die Anlagerung des Protons (bzw. Deuterons) an dem N-Atom des Pyrrolmoleküls und die dadurch bedingte Fünfwertigkeit des N-Atoms ist, wie das Schema (2) zeigt:

„labilisiertes" Molekül

Das durch die Reaktion (2) gebildete „labilisierte" Pyrrolmolekül kann nun ihren an C gebundenen H-Atome gegen die des Wassers leicht austauschen. Dabei ist die Annahme nicht von der Hand zu weisen, dass das „labilisierte" Pyrrolmolekül gemäss der Elektronenkonfigurationsänderung (1) eine tautomerische Umwandlung ausführt und dadurch die sämtlichen H-Atome in demselben eins nach dem anderen gegen die des Wassers ausgetauscht werden.

Zum Schluss sprechen wir der Nippon Gakujutsu-Shinkohkai (Der Gesellschaft zur Förderung der japanischen Wissenschaft) sowie der Hattori-Hohkohkai (der Hattori-Stiftung) für ihre finanzielle Unterstützung unseren wärmsten Dank aus.

Schiomi-Institut für physikalische
und chemische Forschung
und
Physikalisch-chemisches Laboratorium
der Kaiserlichen Universität zu Osaka.

Über den Gehalt der Kohlenhydrate an schwerem Sauerstoff.[1]

Von Noriyoshi MORITA, Kokiti GOTO und Toshizo TITANI.

(Eingegangen am 20. Dezember 1937.)

Inhaltsübersicht. Eine isotopische analytische Methode, nach der der Gehalt des gegebenen Wassers an schwerem Wasserstoff bzw. schwerem Sauerstoff im Vergleich mit gewöhnlichem Wasser ermittelt werden kann, wird angegeben. Nach dieser Methode wurde das Wasser, das bei der Verbrennung von Zucker, Baumwolle und Zedernholz in Luft, sowie von Zucker in elektrolytischem Sauerstoff gebildet worden war, isotopisch analysiert. Daraus fanden wir, dass die grössere Dichtigkeit des Wassers, das bei der Verbrennung dieser Substanzen in Luft gebildet wird, gewöhnlichem Wasser gegenüber fast ausschliesslich von der Anreicherung der schweren Isotope von Sauerstoff im ersteren herrührte. Zugleich wurde gefunden, dass der Wasserstoff im bei der Verbrennung gebildeten Wasser, infolgedessen im Zucker selbst, in der Form von Wasser gemessen, um etwa 1 γ schwerer als gewöhnlicher Wasserstoff ist. Zum Schluss ergab sich aus der isotopischen Analyse des Wassers, das durch die Reduktion des Sauerstoffs im Zucker mittels Wasserstoffs gewonnen wurde, dass der Sauerstoff im Zucker in der Form von Wasser gemessen um 5 ± 1 γ schwerer als gewöhnlicher Wassersauerstoff ist. Um die so aufgefundene Anreicherung der schweren Isotope von Wasserstoff und Sauerstoff im Kohlenhydrat zu deuten, werden einige Möglichkeiten angegeben.

Einleitung. Einige Autoren fanden bei ihren Versuchen, dass das Wasser, das bei der Verbrennung verschiedener Arten von wasserstoffhaltigen Substanzen, wie z.B. Kohlenwasserstoffe[2] und Kohlenhydrate[3] in Luft gebildet wurde, um 5 bis 8 γ dichter als gewöhnliches Wasser war,

(1) Vorläufig mitgeteilt in diesem Bulletin, **11** (1936), 695.

(2) R. D. Snow und H. L. Johnston, *Science*, **80** (1934), 210; C. H. Greene und R. J. Voskuyl, *J. Am. Chem. Soc.*, **56** (1934), 1649; M. Dole, *J. Am. Chem. Soc.*, **56** (1934), 999; *J. Chem. Phys.*, **2** (1934), 337, 548; N. S. Filippova, *J. Chem. Phys.*, **3** (1935), 316; *Compt. rend. acad. sci. U.R.S.S.*, **3** (1935), 29; S. H. Bertram und H. Mendel, *Chem. Weekblad*, **33** (1936), 687; A. Maillard, *Compt. rend.*, **203** (1936), 804.

(3) H. J. Emeléus, F. W. James, A. King, T. G. Pearson, R. H. Purcell und H. V. A. Briscoe, *J. Chem. Soc.*, **1934**, 1207, 1948; T. Titani und M. Harada, dies Bulletin, **10** (1935), 205, 261; K. Okabe und T. Titani, dies Bulletin, **10** (1935), 465.

und führten dies auf die Anreicherung des schweren Wasserstoffs bzw. Sauerstoffs in den untersuchten Verbindungen zurück. Aber diese Schlüsse sind durch den Befund[4] zum mindesten sehr fraglich geworden, dass der Luftsauerstoff um $7 \pm 1\,\gamma$ schwerer als der Wassersauerstoff, d.h. der im Wasser chemisch verbunden vorhandene Sauerstoff, ist. Nach diesem Befund kann das Wasser, das bei der Verbrennung der Substanz, die keinen Sauerstoff in sich enthält, wie z.B. Kohlenwasserstoff, in Luft gebildet wird, immer um einige γ schwerer als gewöhnliches Wasser sein, auch wenn der Wasserstoff in der Substanz gewöhnliche isotopische Zusammensetzung besitzt. Auf diese Möglichkeit haben wir schon in unserer früheren Abhandlung[5] hingewiesen. Aber die Sache liegt etwas anders bei der Verbindung, die Sauerstoff als einen Bestandteil in sich selbst enthält, weil sich in diesem Fall auch dieser Sauerstoff bei der Verbrennung der betreffenden Substanz an der Wasserbildung beteiligen kann. Dies ist z.B. der Fall bei verschiedenen Arten von Kohlenhydraten und kohlenhydrathaltigen Substanzen. Von diesen Substanzen fanden wir bei unseren früheren Versuchen,[6] dass das bei deren Verbrennung in Luft gebildete Wasser immer um 5 bis $8\,\gamma$ schwerer als gewöhnliches Wasser war. Aber bloss aus diesem Befund können wir aus dem eben erwähnten Grund nicht ohne weiteres schliessen, dass es sich dabei in diesen Substanzen um die wirkliche Anreicherung der schweren Isotope des Wasserstoffs bzw. Sauerstoffs handelte. Ebensowenig kann man den Schluss ziehen, dass die grössere Dichtigkeit des zur Verbrennung benutzten Luftsauerstoffs dem Wassersauerstoff gegenüber dabei eine Rolle spielte. Um auf diese Fragen einen sicheren Anhaltspunkt zu gewinnen, haben wir in der vorliegenden Arbeit drei Reihen von Versuchen durchgeführt. Im ersten Versuch wurde das Wasser, das bei der Verbrennung einiger Arten von Kohlenhydrat bzw. kohlenhydrathaltigen Substanzen in Luft gebildet wurde, nach dessen Gehalt an schweren Isotopen des Wasserstoffs und Sauerstoffs isotopisch analysiert. Dann im zweiten Versuch wurde das Wasser, das bei der Verbrennung von Rohrzucker in elektrolytischem Sauerstoff gebildet wurde, ebenfalls isotopisch analysiert. Und zum Schluss im dritten Versuch wurde der Gehalt des Zuckers an schwerem Sauerstoff im Vergleich mit gewöhnlichem Wasser bestimmt,

(4) N. Morita und T. Titani, dies Bulletin, **11** (1936), 36, 414; M. Dole, *J. Am. Chem. Soc.*, **57** (1935), 2731; *J. Chem. Phys.*, **4** (1936), 268; E. R. Smith und H. Matheson, *J. Research Natl. Bur. Standards*, **17** (1936), 625; T. O. Jones und N. F. Hall, *J. Am. Chem. Soc.*, **59** (1937), 259.

(5) N. Morita und T. Titani, dies Bulletin, **11** (1936), 419.

(6) T. Titani und M. Harada, dies Bulletin, **10** (1935), 205, 261; K. Okabe und T. Titani, dies Bulletin, **10** (1935), 465.

indem wir den Sauerstoff im ersteren zunächst durch Reduktion mit Wasserstoff möglichst vollständig in Wasser verwandelten und dessen Gehalt an schwerem Sauerstoff durch die isotopische analytische Methode direkt mit dem des gewöhnlichen Wassers verglichen.

Versuch I. Isotopische Analyse des bei der Verbrennung von Rohrzucker, Baumwolle und Zedernholz in Luft gebildeten Wassers. Bei unseren früheren Versuchen[6] fanden wir, dass die drei Arten von Wasser, die bei der Verbrennung von Rohrzucker (7.4 γ), Baumwolle (5.7 γ) und Zedernholz (4.5 γ) alle in Luft gebildet wurden, um den in den Klammern angegebenen Betrag schwerer als gewöhnliches Wasser waren. Da aber eben diese drei Arten von Wasser seitdem separat in Glasröhren aufbewahrt worden waren, wurden sie je nach deren Gehalt an schwerem Sauerstoff und Wasserstoff im Vergleich mit gewöhnlichem Wasser analysiert. Die analytische Methode besteht darin, dass das Probewasser und das damit zu vergleichende gewöhnliche Wasser beide durch Elektrolyse fast vollständig in ihre Bestandteile gespalten und der dabei entwickelte Sauerstoff separat in überschüssigem Protiumgas, d.h. praktisch deuteriumfreiem Wasserstoff, über erhitztem Platindraht katalytisch bis zu Wasser verbrannt wird.[7] Auf diese Weise erhält man zwei Arten von Protowasser, das eine aus dem Probewasser und das andere aus gewöhnlichem Wasser. Da aber in diesem Protowasser der Sauerstoff des respektiven Wassers als Ganzes enthalten sein muss, lässt sich der geringste Unterschied in der Isotopenzusammensetzung zwischen beiden Arten von Sauerstoff des Probe- und gewöhnlichen Wassers durch den Vergleich der Dichte der so gewonnenen beiden Arten von Protowasser ohne weiteres herausfinden. Falls z.B. das Protowasser aus dem Probewasser um Δs_2 schwerer als das aus gewöhnlichem Wasser wäre, dann muss dieser Dichteüberschuss auf die Anreicherung des schweren Sauerstoffs im untersuchten Probewasser zurückgeführt werden. Wir haben nach dieser Methode die oben angegebenen drei Arten von Wasser nach dessen Gehalt an schwerem Sauerstoff im Vergleich mit gewöhnlichem Wasser untersucht. Die dabei erhaltenen Resultate geben wir in Tabelle 1 wieder.

In dieser Tabelle zeigt Δs_1 in der ersten Vertikalreihe die früher gefundene Dichtezunahme des originalen Probewassers, das direkt bei der Verbrennung der betreffenden Substanz in Luft gebildet wurde, gewöhnlichem Wasser gegenüber. Deshalb muss Δs_1 offenbar von der Anreicherung der beiden schweren Isotope des Sauerstoffs und Wasserstoffs im untersuchten Wasser herrühren. Dagegen zeigt Δs_2 in der zweiten

(7) N. Morita und T. Titani, dies Bulletin, **11** (1936), 403.

Tabelle 1. Die isotopische Analyse des bei der Verbrennung von einigen Kohlenhydraten in Luft gebildeten Wassers.

Substanz	Δs_1 in γ	Δs_2 in γ	$\Delta s_1 - \Delta s_2$ in γ
Rohrzucker	+ 7.4	+ 6.2	+ 1.2
„	+ 7.4	+ 5.8	+ 1.6
Baumwolle	+ 5.7	+ 5.0	+ 0.7
Zedernholz	+ 4.5	+ 3.4	+ 1.1

Vertikalreihe die in dem vorliegenden Versuch gefundene Dichtezunahme des Protowassers, das aus dem betreffenden Probewasser hergestellt wurde, dem gewöhnlichen Protowasser gegenüber, das aus gewöhnlichen Wasser bereitet wurde. Notwendigerweise ist Δs_2 aus dem oben erwähnten Grund ausschliesslich auf die Anreicherung des schweren Sauerstoffs im untersuchten Wasser zurückzuführen. Infolgedessen kann man die Differenz $\Delta s_1 - \Delta s_2$ in der letzten Vertikalreihe der Tabelle als die Dichtezunahme des Probewassers gegen gewöhnliches Wasser wegen der Anreicherung des schweren Wasserstoffs im ersteren, folglich in der verbrannten Substanz selbst, ansehen. Auf diese Weise fanden wir, dass die grössere Dichtigkeit des Wassers, das bei der Verbrennung von Kohlenhydraten bzw. kohlenhydrathaltigen Substanzen in Luft gebildet wird, gewöhnlichem Wasser gegenüber grösstenteils von der Anreicherung des schweren Sauerstoffs im gebildeten Wasser herrührt. Dagegen kann der Wasserstoff in demselben Wasser, also im verbrannten Kohlenhydrat selbst, in der Form von Wasser gemessen nur um etwa 1 γ schwerer als der Wasserstoff in gewöhnlichem Wasser sein.

Versuch II. Isotopische Analyse des bei der Verbrennung von Rohrzucker in elektrolytischem Sauerstoff gebildeten Wassers. In diesem Versuche II haben wir denselben Rohrzucker, den wir im vorhergehenden Versuch I untersuchten, statt in Luft im elektrolytischen Sauerstoff verbrannt und das dabei gebildete Wasser auf dieselbe Weise wie oben isotopisch analysiert. Dazu wird 30 g. Zucker auf einem eisernen Schiffchen in ein Ende des Pyrexglasrohres hineingeschoben. Im anderen Ende des Rohres befindet sich eine Menge von Kupferoxyd, das aus reinem Kupfer und demselben elektrolytischen Sauerstoff, wie zur Verbrennung benutzt wird, hergestellt worden ist. Durch dieses Rohr wird der Sauerstoff, durch die Elektrolyse mit gewöhnlichem Wasser entwickelt, in der Richtung von Zucker nach Kupferoxyd mit einer Geschwindigkeit von ca. 300 c.c.

pro Minute geleitet, und zugleich wird das Rohr von aussen langsam erhitzt. Dadurch entsteht eine allmähliche Verbrennung des Zuckers und das dabei gebildete und abdestillierte Wasser wird in der mit Kohlensäureschneegemisch abgekühlten Flasche kondensiert abgefangen.

Auf diese Weise erhielten wir in zwei Experimenten, die wir beide mit 30 g. Zucker durchführten, jedesmal 15 g. Wasser. Dies entspricht 87% des theoretischen Wertes. Nachdem wir diese beiden Arten von Wasser separat gereinigt hatten, fanden wir das eine um 0.2 γ und das andere 1.0 γ schwerer als gewöhnliches Wasser. Da aber die Menge der beiden Wasser sich als zu wenig erwies, um weitere genauere Messungen auszuführen, wurden sie vereinigt und das so gewonnene Wasser nach dessen Gehalt an schwerem Sauerstoff und Wasserstoff auf dieselbe Weise wie beim Versuch I mit gewöhnlichem Wasser verglichen. Das Resultat ergab, dass das Protowasser aus diesem vereinigten Wasser um 0.2 γ leichter als gewöhnliches Protowasser war, wie in Tabelle 2 angegeben.

Tabelle 2. Die isotopische Analyse des bei der Verbrennung von Rohrzucker im elektrolytischen Sauerstoff gebildeten Wassers.

Substanz	Δs_1 in γ	Δs_2 in γ	$\Delta s_1 - \Delta s_2$ in γ
Rohrzucker	+ 0.2	− 0.2	+ 0.8
„	+ 1.0		

Da aber das untersuchte Wasser als Ganzes um 0.6 γ (= (0.2 + 1.0)/2) schwerer als gewöhnliches Wasser angesehen werden darf, folgt sofort, dass solch ein Anteil des Dichteüberschusses, der auf die Anreicherung des schweren Wasserstoffs im untersuchten Wasser, folglich im verbrannten Zucker selbst, zurückzuführen ist, gleich 0.8 γ (= 0.6 + 0.2) sein muss. Dieser Wert stimmt mit dem im Versuch I gefundenen innerhalb des Messfehlersbereichs sehr gut überein (vgl. Tabelle 1).

Der in diesem Versuch zur Verbrennung des Zuckers benutzte Sauerstoff wurde, wie oben erwähnt, durch die Elektrolyse mit gewöhnlichem Wasser hergestellt. Infolgedessen muss er in der Form von Wasser gemessen um etwa 1.6 γ leichter als gewöhnlicher Wassersauerstoff sein, wenn man den Trennfaktor der Sauerstoffisotope $k = 1.01$[8] setzt. Unter Benutzung dieses spezifisch leichten Sauerstoffs zur Verbrennung des Zuckers fanden wir aber den Sauerstoff im dabei gebildeten Wasser,

(8) N. Morita und T. Titani, dies Bulletin, **11** (1936), 414, 419.

wie oben erwähnt, nur um 0.2 γ leichter oder fast gleich schwer wie gewöhnlicher Wassersauerstoff. Dies weist ohne weiteres darauf hin, dass der Sauerstoff im verbrannten Zucker selbst auch um einige γ schwerer als gewöhnlicher Wassersauerstoff sein konnte. Diese Erwartung wurde tatsächlich im nächsten Versuch III einwandfrei bewiesen.

Versuch III. Isotopische Analyse des bei der Reduktion des Zuckers mittels Wasserstoffs gebildeten Wassers. Eine grosse Menge von Rohrzucker, den wir im Wasserstoffstrom erhitzten, wurde so vollständig zersetzt. Darauf wurde der im Zersetzungsprodukt gebildete Sauerstoff möglichst vollkommen in Wasser verwandelt und dessen Gehalt an schwerem Sauerstoff im Vergleich mit gewöhnlichem Wasser bestimmt. Die zur Zersetzung des Zuckers im Wasserstoffstrom benutzte Apparatur ist in der nebenstehenden Abb. schematisch angegeben. Der Destillierkolben Z, der aus langhalsigen Pyrexglaskolben besteht und den Inhalt von ca. 100 c.c. besitzt, enthält eine kleine Menge (ca. 25 g.) von Zucker, der von aussen langsam erhitzt wird, indem man den Wasserstoff durch das

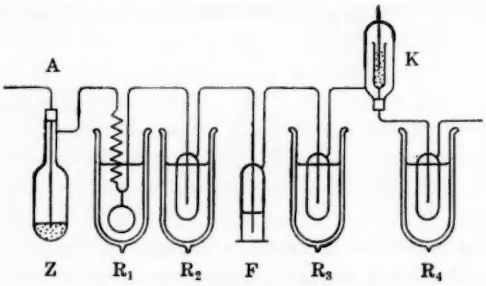

Abb. Zersetzungsapparatur des Zuckers.

Rohr A in den Kolben hineinleitet. Durch diese Prozedur wird der Zucker allmählich zersetzt und die dadurch gebildeten flüchtigen Substanzen, die hauptsächlich aus Wasser, Teer und einigen gasförmigen Verbindungen bestehen, werden zusammen mit dem Wasserstoffgas durch die Kühlflaschen R_1 bis R_4 nacheinander geleitet. Da die erste Flasche R_1 mit Eis und die zweite R_2 mit Kohlensäureschneegemisch je von aussen gut abgekühlt ist, wird dort Wasser und Teer aus dem Zersetzungsprodukt vollständig kondensiert angefangen, und zwar grösstenteils in der ersteren Flasche R_1. Der hier nicht kondensierte gasförmige Anteil des Zersetzungsprodukts, der hauptsächlich aus Kohlendioxyd und -monoxyd zusammen mit dem zugesetzten Wasserstoffgas besteht, wird dann, nachdem das Gasgemisch in der Flasche F mit Benzol gewaschen und von

dessen Dampf in der nächsten mit Kohlensäureschneegemisch abgekühlten Flasche R_3 befreit wird, durch das erhitzte Katalysatorrohr K und die Kühlflasche R_4 nacheinander geleitet. In diesem Katalysatorrohr, das mit Ni-ThO_2-Katalysator gefüllt ist, wird das Kohlendioxyd und -monoxyd mit dem zugleich befindlichen Wasserstoffgas bis zu Wasser reduziert und das so gebildete Wasser wird in der letzten mit Kohlensäureschneegemisch abgekühlten Flasche R_4 ausgefroren.

Am Ende jeder solchen Destillation, die wir immer mit einer Menge von 25 g. Zucker durchführten, fanden wir im Destillierkolben Z 7 bis 8 g. Zuckerkohle, in der Flasche R_1 10 bis 11 g. von gelb gefärbter stinkender Flüssigkeit, in der nächsten Flasche R_2 ebenfalls einige Tropfen von derselben Flüssigkeit, und in der letzten Flasche R_4 ca. 3 g. von fast reinem Wasser. In der Tat wiederholten wir dieselben Destillationen sechs bis elf mal nacheinander und sammelten die aus jeder Destillation erhaltene Flüssigkeit und Wasser zusammen. Die auf diese Weise aus den beiden Flaschen R_1 und R_2 gewonnene Flüssigkeit nennen wir zusammengefasst das Kondensat K_{12} und das Wasser aus der Flasche R_4 das Wasser W_4. Wir erhielten z.B. in einer Reihe von Versuchen, wo wir die Destillationen sechsmal wiederholten und deshalb insgesamt 150 g. Zucker zersetzt wurden, 45 g. Zuckerkohle, 65 g. von K_{12} und 18 g. von W_4.

Da das Wasser W_4 fast reines Wasser war, wurde es unmittelbar zur isotopischen Analyse verwendet. Dagegen, weil das Kondensat K_{12} neben Wasser noch eine beträchtliche Menge von organischen Verbindungen enthielt, wurde es einem weiteren Reinigungsprozess unterworfen. Zu diesem Zweck wird das Kondensat K_{12} unter dem Zusatz von einigen Tropfen von Schwefelsäure angesauert und zwischen Platinelektroden elektrolytisch gespalten. Das dabei entwickelte Knallgas enthält eine beträchtliche Menge von Kohlensäure, die durch die anodische Oxydation der im Kondensat befindlichen organischen Substanzen entsteht. Deshalb wird das Knallgas zuerst durch die Abkühlung mit flüssiger Luft von dieser beigemengten Kohlensäure befreit und dann unter dem Zusatz von einem kleinen Überschuss von Wasserstoff über erhitzter Kupferfolie bis zu Wasser rekombiniert. Das dadurch aus dem Kondensat K_{12} gebildete Wasser nennen wir Wasser W°_{12}. Die bei dieser Elektrolyse aus dem Elektrolyseurgas abgeschiedene Kohlensäure wird für sich auf dem Ni-ThO_2-Katalysator mittels Wasserstoffs bis zu Wasser reduziert. Das so gewonnene Wasser nennen wir Wasser W_{12}. Auf diese Weise erhielten wir, alles zusammen genommen, drei Arten von Wasser aus dem Zucker, nämlich W°_{12}, W_{12} je aus dem Kondensat K_{12} und das in der Flasche R_4 angefangene W_4. Das Mengenverhältnis dieser drei Arten von Wasser bei drei Reihen von Versuchen, die wir je mit 150 g., 280 g. und 250 g.

Zucker durchführten, geben wir in den dritten Vertikalreihen der Tabellen 3 wieder. Wie man daraus ersieht, konnten wir nach der oben angegebenen Methode 69 bis 73% des gesamten Sauerstoffs des Zuckers zu Wasser verwandeln.

Tabelle 3. Die isotopische Analyse des bei der Reduktion des Zuckers mittels Wasserstoffs gebildeten Wassers.

Versuch 1.

1. Menge des Zuckers in g.	2. Menge des Kondensats in g.	3. Menge der Arten von Wasser in g.	4. Δs in γ	5. Mittlerer Δs in γ
150	$K_{12} = 65$	$W^{*}_{12} = 33$ $W_{12} = 12$ $W_{4} = 18$	2.6 4.2 5.9	3.9

Summe = 63 (73% des theoretischen Wertes)

Versuch 2.

1. Menge des Zuckers in g.	2. Menge des Kondensats in g.	3. Menge der Arten von Wasser in g.	4. Δs in γ	5. Mittlerer Δs in γ
280	$K_{12} = 107$	$W^{*}_{12} = 80$ $W_{12} = 19$ $W_{4} = 15$	4.6 8.2 7.6	5.6

Summe = 114 (69% des theoretischen Wertes)

Versuch 3.

1. Menge des Zuckers in g.	2. Menge des Kondensats in g.	3. Menge der Arten von Wasser in g.	4. Δs in γ	5. Mittlerer Δs in γ
250	$K_{12} = -$	$W^{*}_{12} = 71$ $W_{12} = 21$ $W_{4} = 13$	4.1 4.7 5.2	4.4

Summe = 105 (72% des theoretischen Wertes)

Die so gewonnenen drei Arten von Wasser wurden dann separat nach dessen Gehalt an schwerem Sauerstoff isotopisch analysiert. Die analytische Methode war genau dieselbe wie die im vorhergehenden Versuche I und II verwendete. Nämlich das Wasser wird zuerst elektrolytisch fast

vollständig in dessen Bestandteile gespalten und der dabei entwickelte Sauerstoff im überschüssigen Protiumgas bis zu Wasser verbrannt. Das so gewonnene Wasser wird hierauf sorgfältig gereinigt und dessen Dichte mit dem gewöhnlichen Protowasser, das aus gewöhnlichem Wasser auf ähnliche Weise wie oben hergestellt wird, mittels eines Quarzschwimmers verglichen. Auf diese Weise kann man die Dichtezunahme Δs des gegebenen Wassers wegen der Anreicherung des schweren Sauerstoffs in demselben im Vergleich mit gewöhnlichem Wasser finden. Die nach dieser Methode gefundene Dichtezunahme Δs der drei Arten von Wasser W_{12}°, W_{12} und W_4 ist in den vierten Vertikalreihen der Tabellen 3 wiedergegeben. Die dabei leicht ersichtliche grössere Dichtigkeit von W_{12} und W_4, die beide bei der Reduktion der Kohlensäure mittels Wasserstoffs gebildet wurden, im Vergleich mit W_{12}°, das bei der Rekombination des Knallgases erzeugt wurde, kann man dadurch erklären, dass die schweren Isotope des Sauerstoffs beim Austauschgleichgewicht zwischen Wasser und Kohlensäure stets in der letzteren angereichert werden. Aus diesem Grund errechneten wir den Mittelwert von Δs der drei Arten von Wasser W_{12}°, W_{12} und W_4 unter Berücksichtigung ihres Mengenverhältnisses und erhielten dadurch die Werte, die in den letzten fünften Vertikalreihen der Tabellen 3 wiedergegeben sind.

Aus den Ergebnissen der Tabellen 3 ersehen wir, dass der Sauerstoff in den untersuchten Arten von Wasser durchschnittlich um $5 \pm 1\,\gamma$ schwerer als gewöhnlicher Wassersauerstoff ist, falls man beide in der Form von Wasser vergleicht. Aber weil wir in diesen Versuchen, wie unter jeder Tabelle angegeben ist, mehr als zwei Drittel des gesamten Sauerstoffs im Zucker in Wasser verwandeln konnten, darf man wohl schliessen, dass der Sauerstoff im Zucker selbst auch den Dichteüberschuss von mindestens derselben Grössenordnung wie dem oben gefundenen gewöhnlichem Wassersauerstoff gegenüber besitzen muss.

Diskussion. *Wir haben aus den Versuchen I und II den Wasserstoff im Zucker um etwa 1 γ, dagegen aus dem Versuch III den Sauerstoff in demselben um etwa 5 γ, beide in der Form von Wasser gemessen, schwerer als der Wasserstoff bzw. Sauerstoff in gewöhnlichem Wasser gefunden.* Um diese Anreicherung der schweren Isotope des Wasserstoffs und Sauerstoffs im Zucker zu deuten, gibt es offenbar viele Erklärungsmöglichkeiten. Eine der wahrscheinlichsten Ursachen für die Anreicherung des schweren Wasserstoffs im Zucker ist, dass schwerer Wasserstoff durch den Isotopenaustausch zwischen Zucker und Wasser im ersteren akkumuliert wird. Harada[9] fand nämlich, dass beim Austauschgleichgewicht

(9) M. Harada, *J. Chem. Soc. Japan*, **57** (1936), 391.

des schweren Wasserstoffs zwischen Zucker und Wasser dieser um einen kleinen Betrag im Zucker angereichert wird, und der Verteilungsquotient der D-Atome zwischen den Hydroxylgruppen des Zuckers und Wasser $k = 1.10 \pm 0.1$ ist. Nach diesem Befund muss der gesamte Wasserstoff im Zucker in der Form von Wasser gemessen durchschnittlich um $0.7\,\gamma$ schwerer als der Wasserstoff in gewöhnlichem Wasser sein, wenn die beiden Substanzen sich im Isotopenaustauschgleichgewicht befinden. Dieser Wert ($0.7\,\gamma$) stimmt mit dem in den Versuchen I und II gefundenen Dichteüberschuss des Wasserstoffs im Zucker dem gewöhnlichen Wasserstoff gegenüber ($1\,\gamma$) hinreichend gut überein. Auf die Frage, ob man die grössere Dichtigkeit des Sauerstoffs im Zucker im Vergleich mit dem gewöhnlichen Wassersauerstoff auf ähnliche Weise wie oben mit der Austauschreaktion von O-Atome zwischen Zucker und Wasser deuten kann, können wir nicht sofort unumwunden antworten. In diesem Fall liegt auch die Möglichkeit vor, dass schwerer Sauerstoff bei der Assimilation der Kohlensäure von Pflanzen im gebildeten Kohlenhydrat angereichert wird.

Diese letzte Möglichkeit wurde auch schon von Greene und Voskuyl[10] angenommen, um die grössere Dichtigkeit des Luftsauerstoffs dem Wassersauerstoff gegenüber zu deuten. Die beiden Autoren nahmen an, dass atmosphärische Kohlensäure sich mit Wasser im Austauschgleichgewicht befindet, so dass der Sauerstoff in der ersteren um $10 \pm 1\,\gamma$ schwerer als gewöhnlicher Wassersauerstoff ist. Weiter nahmen sie an, dass die Pflanzen bei der Assimilation zwei O-Atome von CO_2 und ein O-Atome von H_2O aufnehmen und daraus ein Molekül von Sauerstoff an die Atmosphäre zurückgeben, so dass das übriggebliebene eine Sauerstoffatom in der Pflanzensubstanz Verwertung findet. Die Assimilationsreaktion verläuft demnach gemäss dem Schema (1).

$$\overset{*}{C}O_2 + H_2O = CH_2(2/3\ \overset{*}{O} + 1/3\ O) + (2/3\ \overset{*}{O} + 1/3\ O)_2 \qquad (1)$$

Unter dieser Annahme ergibt sich sofort, dass sowohl der Sauerstoff im gebildeten Kohlenhydrat (CH_2O) als auch im abgegebenen Sauerstoffmolekül (O_2) schwerer als gewöhnlicher Wassersauerstoff sein muss und zwar beide um $7 \pm 1\,\gamma (= 10 \times 2/3 + 0 \times 1/3)$. Diesen letzten Wert benutzten die beiden Autoren dazu, um den Dichteunterschied zwischen Luft- und Wassersauerstoff ($7\,\gamma$) zu deuten.

Nach dem oben angegebenen Chemismus der Assimilation muss der Sauerstoff im Kohlenhydrat, falls dieser weiter nicht ausgetauscht wird,

(10) C. H. Greene und R. J. Voskuyl, *J. Am. Chem. Soc.*, **58** (1936), 693.

ebenfalls um 7γ schwerer als gewöhnlicher Wassersauerstoff sein. Dagegen fanden wir in der vorliegenden Arbeit den Dichteüberschuss des Sauerstoffs im Zucker gewöhnlichem Wassersauerstoff gegenüber nur $5 \pm 1\gamma$. Die Diskrepanz zwischen diesen beiden Werten kann man eventuell durch den weiteren Austausch der O-Atome im Zucker gegen etwa die des Wassers erklären. Schliesst man aber diese Möglichkeit aus, so lässt sich der Unterschied auch wie folgt erklären: Man könnte z.B. annehmen, dass bei der Assimilation nicht die sämtlichen O-Atome von Kohlensäure und Wasser, sondern nur die Hälfte der O-Atome aus Kohlensäure, dagegen alle O-Atome aus Wasser von den Pflanzen aufgenommen werden, wie das Schema (2) zeigt.[11]

$$\begin{aligned} \overset{*}{C}O_2 + H_2O &= \quad \overset{*}{O} \quad + \quad C\overset{*}{O}\cdot H_2O \\ CO\cdot H_2\overset{*}{O} &= CH_2(1/2\ \overset{*}{O} + 1/2\ O) + (1/2\ \overset{*}{O} + 1/2\ O) \\ \hline \overset{*}{C}O_2 + H_2O &= CH_2(1/2\ \overset{*}{O} + 1/2\ O) + (3/4\ \overset{*}{O} + 1/4\ O)_2 \end{aligned} \qquad (2)$$

Aus diesem Reaktionsschema findet man ohne weiteres, dass der Sauerstoff im gebildeten Kohlenhydrat um $5 \pm 1\gamma (= 10 \times 1/2 + 0 \times 1/2)$, dagegen der im abgegebenen Sauerstoffmolekül um $8 \pm 1\gamma (= 10 \times 3/4 + 0 \times 1/4)$ schwerer als gewöhnlicher Wassersauerstoff sein muss. Der erste Wert stimmt offenbar mit dem im Versuch III von uns für Zucker experimentell gefundenen $(5 \pm 1\gamma)$ und der letztere mit dem bekannten Dichteunterschied $(7 \pm 1\gamma)$ zwischen Luft- und Wassersauerstoff hinreichend gut überein.

Bei der Verbrennung des Kohlenhydrates, der Gegenreaktion der Assimilation, treten dagegen die sämtlichen O-Atome in demselben gleich in der Reaktion ein, wie das Schema (3) zeigt.

$$CH_2\overset{*}{O} + O_2 = C(1/3\ \overset{*}{O} + 2/3\ O)_2 + H_2(1/3\ \overset{*}{O} + 2/3\ O) \qquad (3)$$

Nach diesem Reaktionsschema (3) muss das Wasser, das bei der Verbrennung des Zuckers in Luft gebildet wird, um $7 \pm 1\gamma (= 5 \times 1/3 + 7 \times 2/3 + 1)$ schwerer als gewöhnliches Wasser sein, weil der Sauerstoff im Zucker um 5γ, der in Luft um 7γ und der Wasserstoff in Zucker um 1γ, alles in der Form von Wasser gemessen, schwerer als der Sauerstoff bzw. Wasserstoff in gewöhnlichem Wasser ist. Der so be-

(11) Prinzipiell diesähnlicher Chemismus der Assimilation wurde schon so früh wie 1870 von A. v. Baeyer (*Ber.*, **3** (1870), 63) angegeben. Nach ihm verläuft die Reaktion nach dem folgenden Schema:

$$CO_2 = CO + O,$$
$$CO + H_2O + O = O_2 + H\cdot COH.$$

rechnete Wert ($7 \pm 1\,\gamma$) stimmt mit dem im Versuch I experimentell gefundenen gut überein. Falls man dagegen zur Verbrennung des Zuckers, wie im Versuch II, den elektrolytischen Sauerstoff benutzt, dessen Dichte um 1.6 γ kleiner als gewöhnlicher Wassersauerstoff ist, dann kann das dabei gebildete Wasser nur um etwa $1 \pm 1\,\gamma (= 5 \times 1/3 + (-1.6) \times 2/3 + 1)$ dichter als gewöhnliches Wasser sein. Dieses Resultat stimmt wieder mit dem im Versuch II experimentell gefundenen gut überein.

Zum Schluss sprechen wir der Nippon Gakujutsu-Shinkohkai (der Gesellschaft zur Förderung der japanischen Wissenschaft) sowie der Hattori-Hohkohkai (der Hattori-Stiftung) für ihre finanzielle Unterstützung bei Ausführung dieser Versuche unseren wärmsten Dank aus.

Physikalisch-chemisches Laboratorium
der Kaiserlichen Universität zu Osaka
und
Schiomi-Institut für physikalische
und chemische Forschung.

Experimental Studies on the Electrochemical Polarisation Produced in the Cylindrical Mass of Litharge. I.

By **Takewo TIKU.**

(Received January 4, 1938.)

Introduction. It is well known that the oxides of lead in pasted state applied to the metal grid of lead or lead-antimony alloy are electrolytically transformed into the positive or negative active materials of the lead storage cell in dilute sulphuric acid solution. The above procedure is called the formation of pasted plates. As the negatives are grayish and the positives dark-brown or black, while litharge is yellow, the paste at the initial or final stage of the formation can be easily distinguished. In the intermediate stage of the formation of plates, it is observed that the paste in grids consists of two parts of different colours, displayed by litharge and by the positive or the negative material. The boundary between the two parts is to be regarded as the front of the formation. In the case of the negatives the front progresses from near the surface

of the paste, but in the case of the positives it starts from comparatively deep portion of the paste and reaches the surface at the end. From these features of the progress of the formation, the existence of some definite distribution of the electrochemical condition should be expected in the mass of litharge in the electrode plate.

The author intended to study the electrochemical polarisation in the mass of pasted litharge applying the direct electric potential through it, without using any metal electrodes attached to it.

Method of Producing Polarisation in the Mass of Litharge. In order to produce the positive and negative polarisations of the same kind as in the lead storage cell, the pasted mass of litharge must be placed in dilute sulphuric acid solution between two electrodes leading direct electric current. But, if the two electrodes are bridged with the electrolyte in any way, the portion of electric current passing through the mass of litharge shall be very small and the polarisation can hardly occur in it. In order to avoid this difficulty, a glass tube of moderate length was stuffed in its middle position with the pasted mass of litharge and the cavities at both sides of the mass were filled with dilute sulphuric acid solution, as is shown in Fig. 1. The pasted mass of litharge in the glass

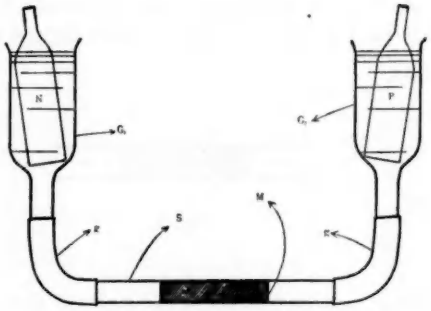

Fig. 1.

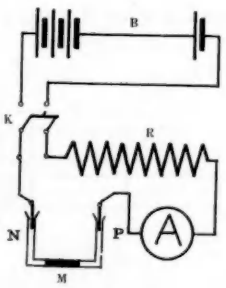

Fig. 2.

tube has a cylindrical form, its two bases being perpendicular to its axis. The length of the cylindrical mass was varied in the range of several centimeters.

In Fig. 1, S is the glass tube mentioned above, which was horizontally supported. M is the pasted mass of litharge. G_1 and G_2 are also glass tubes, supported nearly vertically, and connected to the both ends of S with rubber tubing g. Dilute sulphuric acid was poured into G_1 and G_2 and the small battery plates P and N were introduced as electrodes. The

mass M is thus sandwiched by the electrolyte. Direct electric potential was applied between P and N in the manner as shown in Fig. 2. B is a high tension battery, the voltage (v) of which is applied through the ohmic resistance R(8400 ohms) and the ammeter A when the key K is closed.

The pasted mass was made by mixing litharge powder and distilled water, the water being dropped on the powder till the paste attained the desired degree of stickiness. The consumption of the water was about 10% of the litharge in weight in every case. The litharge was put into the glass tube (the inner diameter about 0.7 cm.) as soon as possible and then the potential was applied. Density of the electrolyte used was about 1.20 at ordinary temperature. The value of v was about 66 volts.

After several hours application of v, chemical changes were observed to develop as follows. Around the positive end of the cylindrical mass several spots of grayish colour appeared in the field of buff colour and then the spots grew to be connected into each other. About this time dark brown and rather diffuse spots appeared at the negative side certain distance apart from the above. Then dendroidal figures began to grow from the former toward the latter and the latter proceeded to spread toward the more negative side. A typical appearance of patterns thus obtained are as drawn in Fig. 3. In Fig. 3, B is the former figure and

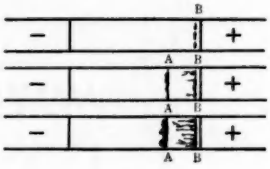

Fig. 3.

Fig. 4.

A the latter. Materials formed at A and B are ascertained to be lead-peroxide and lead respectively. These changes from litharge are of the same nature as in the formation of positive and negative electrodes of the lead storage cell, the electrolysis taking place in the mass itself.

Phenomena Observed before the Polarisation Patterns are Formed. In a few minutes after the application of the potential v, it was found that the colour of the negative end region of the mass turns slightly reddish, and this region spreads toward the positive side (Fig. 4). It was easily observed from the displacement of the boundary $\overline{AA}$ between two regions

of different colours toward the positive side. The average direction of the boundary $\overline{AA}$ appeared almost perpendicularly to the axis of the cylinder.

The velocity of $\overline{AA}$ diminished with time, and the displacement of $\overline{AA}$ became scarcely observable at the position certain distance apart from the positive end of the cylinder. Soon after, the polarisation patterns began to appear and the positive figure of the patterns appeared at the position of $\overline{AA}$, i.e., A in Fig. 3 is the place where $\overline{AA}$ ceased to move.

The current passing through the mass varied with time though the applied voltage v had nearly a constant value. This is shown in Fig. 5, the ordinate being the current, and the abscissa being the time after the application of v. The current gradually decreased with time at the beginning and reached minimum value within 10–90 minutes. At the next increasing stage, the fluctuation of current was so frequent that secure readings can hardly be obtained. It was during this period when

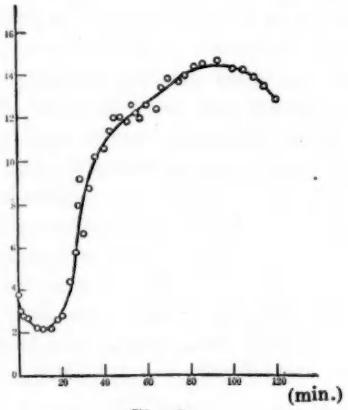

Fig. 5.

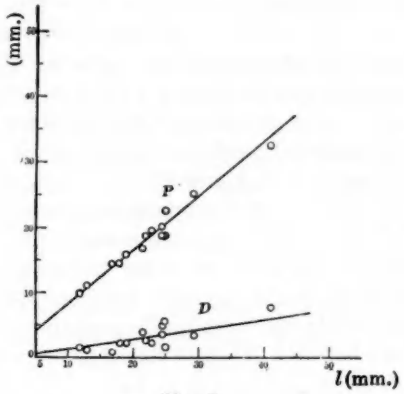

Fig. 6.

the polarisation patterns began to appear. After almost all the patterns shown in Fig. 3 were formed, the current did not change so much and maitained certain values for a while. The order of the currents was about several milliamperes.

On the Polarisation Patterns. It was experimented with several samples of different lengths. Apparent density of the mass in the glass tube before the application of the voltage was about 6.0 in every case. It was found that the position A where the positive figures are formed, was more distant from the positive end of the mass when the length l was larger. While the negative figures were formed at practically same posi-

tion near the positive end, within the range of a millimeter. The relative position of A with respect to l, can be known from Fig. 6. Here, P is the distance of A from the negative end of the mass, and D is the distance between A and B in Fig. 3. From the figure, it may be recognized that points showing P and D respectively distribute on a straight line. The inclinations of the lines for P and D are 0.83 and 0.14 respectively. These are the average values of P/l and D/l which are independent of the length. The above fact shows that the relative position where the positive figure of the polarisation pattern is formed is definite amount apart from the both ends of the cylindrical mass.

The type of the development of positive and negative patterns of the polarisation already described was observed to be similar to that of the Lichtenberg figure. But the dendroidal development of the positive Lichtenberg figure was observed in the negative patterns in our case and the positive patterns were alike the negative Lichtenberg figure. The dendroidal development of the negative patterns corresponds to the phenomenon observed in the negative deposition of metals in electrolysis.

The electrochemical patterns already described are not a superficial phenomenon occurring at the boundary between the mass and the glass tube. The cylindrical sample was cut perpendicularly to the axis and the sectional surface was examined. The results are as follows. (1) In the parts of $\overline{AA}$ and $\overline{BB}$ in Fig. 3, the positive or negative formation was completed over the whole sectional surface. (2) In the part between $\overline{AA}$ and the positive end, the polarity of the formation was positive or negative, and the pattern of either dull-grayish or dark-brown colour was found as spots in the sectional surface. In many cases, the positive was only of single big spot, while the negative was of several small ones. (3) In the part between $\overline{AA}$ and the negative end, no polarisation was found.

Observations with Different Kinds of Litharge and under Varied Conditions. Further experiments on the effects of the modification of litharge, the diameter of the mass, and the terminal voltage V upon the value of P/l were undertaken. The same experimental arrangement as before was used, and in addition to this a voltmeter (resistance 10000 ohms) was shunted between the electrodes to know the value of V. Estimation of P was made as follows in this case. After the polarisation patterns appeared, thin cerophane paper was fastened just around the glass tube and perspective figures of the patterns were drawn on the paper. Then the paper was taken off, spread in a plane and the average value of P was determined by rounding off the irregularities around the mass.

It was noticed that the value of P/l was not always 0.83, but it

varied in wide range under the same experimental conditions, according to the sample used. Litharge is found at ordinary temperature in red, yellow and buff modifications,[1] intermediate ones being often met with in commercial samples. Five different samples were examined in the experiment and the results obtained with them are as shown in Table 1.

Table 1.

Symbols for the different kinds of litharge	Colour of the powder	P/l	Remarks
(D), (C)	light greenish yellow	0.9	
(E)	yellowish red	0.2	
(A)	yellowish brown	0.6	for the battery use
(K)	yellow	0.8	"Bleioxyd–Kahlbaum zur Analyse"

The length and sectional diameter of the pasted cylindrical mass were about 23 mm. and 7 mm. respectively, the applied potential v was 110 – 120 volts. In pasting, 10 g. of the samples were taken and the necessary quantities Q of mixing water dropped into were as follows; 0.7 – 0.8 c.c. for (D) and (C), 1.15 c.c. for (E), 0.85 c.c. for (A), and 1.10 c.c. for (K). The room temperature was about 17 – 20°C. and the relative humidity about 70%. At the above compositions[2] the pastes attained the same degree of stickiness.

The apparent densities of them in the glass tube before the formation were about, 6.5 – 7.0 for (D) and (C), 6.5 for (E), 6.8 – 7.3 for (A), and 6.2 for (K) respectively.

From Table 1 it is known that the value of P/l is comparatively large with rather yellowish litharge, and small with reddish one. And this means that the boundary $\overline{AA}$ does not reach so near the positive end of the mass in the case of the reddish litharge, as for yellowish one. The samples (D) and (C) could not be distinguished by their appearance. The values of P/l for them were roughly 0.9 as shown in the Table 1. Precisely, the value for (C) was about 0.89, for (D) about 0.93, and the polarisation patterns in (C) appeared more elegantly than in (D). The sketches of the figures are shown in the next page.

(1) J.A. Smythe, "Lead," 234, (1923).

(2) In the previous work Q was 10% of the litharge, and the sample was rather reddish or brown.

The differences in the values of P/l for different samples will be considered to be the combined effect of the size of the particle, crystal form, purity and so on.

With the sample (C) described in Table 1, the polarisation phenomena were examined at different lengths and diameters of the mass and at varying series resistances. The composition of the paste was 10 g. of litharge and 0.7–0.85 c.c. of water. Applied voltage v was 110–120 volts.

(1) *Length.* Nineteen specimens of different lengths, 7.5–5.10 mm., were submitted to formation. Glass tubes for them were so chosen as the inner diameters were about 7.0 mm. The apparent densities were about 7.0.

The polarisation figures drawn on cerophane papers are shown in Fig. 7. Numerals in the nineteen figures are the lengths for themselves. The upside of each figure is the positive side. So the upper patterns are of negative and the lower zigzag patterns are of positive in each figure,

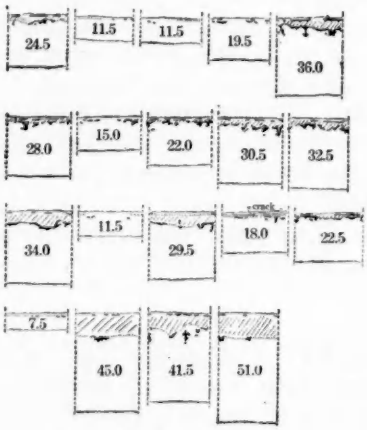

Fig. 7.

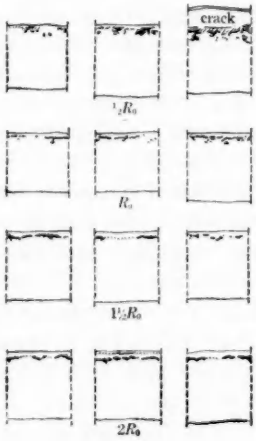

Fig. 8.

and dotted lines are the boundary $\overline{AA}$ where the patterns did not yet appear. The average values of P in these figures are plotted against the length l in Fig. 9. There exists a linear relationship for most points between P and l, which is represented by the straight line (1) in the figure. Several points, however, may be connected with the other straight line (2) also shown in the figure. The above straight lines pass through the origin. P/l estimated from (1) is 0.87, and from (2) is 0.78.

(2) *Thickness.* Thirteen kinds of the glass tube, the inner diameters of which were varied in 2–10 mm., were used to examine the effect of the thickness of the sample. The preparation of the specimens was the same as above. The length was about 25 mm. The value of P/l was about 0.9 or less in the average, and it showed a slight tendency to decrease with diminishing diameter. It would be the effect due to the fact that the apparent densities of the mass were found to diminish with

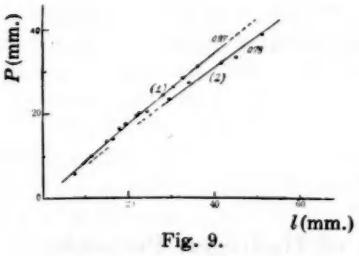

Fig. 9.

Table 2.

Value of series resistance	Time at maximum V (min.)	Maximum value of V (volts)
$\frac{1}{2} R_0$	5–10	80
R_0	15–25	62
$1\frac{1}{2} R_0$	20–30	50
$2R_0$	30–50	40–45

increasing diameter. P/l may be affected by the hardness of the mass.

(3) *Series resistance.* Terminal voltage V and the current through the mass are changed by the value of the external series resistance R. R was 8400 ohms in the above experiments. The four cases when R was $\frac{1}{2}R_0$, R_0, $1\frac{1}{2}R_0$, and $2R_0$ (R_0=8400 ohms) were tested. The lengths and the diameters of the samples were 26–32 mm. and 6.5–6.7 mm. respectively. P/l took nearly the same value, about 0.9, in four cases. The polarisation patterns, however, grew rather finely as seen in Fig. 8 which was drawn in the same manner as Fig. 7 and their progress became slower at higher resistances. It would be due to the lowering of the field in the mass. The characteristic between V and the time changed with the series resistance as shown in Table 2.

Summary.

Litharge powder was mixed with distilled water and turned to pasted form. This was stuffed in glass tubes of moderate length at their middle portions, and direct electric current was passed through the mass. Positive and negative patterns due to electrolytic polarisation was produced in the mass facing each other at definite positions in the axial direction of the cylindrical mass, the position of the negative being near the positive end of the mass. The ratios of the distance P of the positive position from the negative end to the length l of the mass were found to be independent of the length in the average.

The value of P/l is affected by the modification of litharge, but not by the diameter, the length of the mass and the terminal voltage.

In conclusion, the author wishes to express his hearty thanks to Prof. M. Katayama of the Tokyo Imperial University for the interest in this work and the encouragement through the course of the experiment, and to Asst. Prof. D. Nukiyama of the University for his kind advices on this investigation.

Toyoda Research Laboratory, Imperial Invention Society, Shimomeguro, Tokyo.

On the Catalytic Decomposition of Hydrogen Peroxide by Colloidal Platinum-carbonyl.

By Isamu SANO.

(Received November 25, 1937).

There have already been published a number of reports[1] on the catalytic decomposition of hydrogen peroxide by colloidal platinum. In the previous paper,[2] the author described the formation and behaviour of the platinum-carbonyl sol of red colour obtainable from the aqueous solution of chloroplatinic acid by the action of carbon monoxide. The present paper deals with the experiments on the catalytic decomposition of hydrogen peroxide by the colloidal platinum-carbonyl mentioned above and the colloidal platinum obtainable from it.

On passing carbon monoxide through the aqueous solution of chloroplatinic acid at ordinary temperature for some time, the colour of the solution changes from yellow to red, the platinum carbonyl sol being thus obtained. By dialyzing or standing in the air the red sol, it turns black to produce a platinum sol as prepared by Bredig's method.

---

(1) G. Bredig and M. v. Berneck, *Z. physik. Chem.*, **31** (1899), 258; G. Bredig and K. Ikeda, *Z. physik. Chem.*, **37** (1901), 1; T. S. Price and A. D. Denning, *Z. physik. Chem.*, **46** (1903), 89; D. A. MacInnes, *J. Am. Chem. Soc.*, **36** (1914), 878; M. A. Heath and J. H. Walton, *J. Phys. Chem.*, **37** (1933), 977, etc.

(2) I. Sano, this Bulletin, **9** (1934), 320.

Experimental. The hydrogen peroxide solution was obtained from "Oxyfull" by distillation under reduced pressure (50–60 mm. Hg, 85°C.) in a thoroughly steamed hard glass system, diluted with water to 20 times of volume and kept in a Pyrex flask. The reaction was carried out at 30.0°C. in a Erlenmeyer flask which was cleaned and steamed before use. Ninty-five c.c. of the hydrogen peroxide solution was placed in the flask, a definite volume of the red or black sol was added to it, and the solution thoroughly mixed by shaking. At the desired intervals of time, 5 c.c. was taken out from it, added to a mixture of 50 c.c. of water and 10 c.c. of dilute sulphuric acid (1:3), and titrated with a 0.10 N potassium permanganate solution. The sol added as catalyst, red or black, was inferred from calculation to contain 0.075 grams of platinum in one liter.

The results obtained are given in Tables 1, 2, 3, 4 and 5, where t denotes the time elapsed from the beginning in minutes, c the volume of the potassium permanganate solution equivalent to 5 c.c. of the reacting solution at time t in c.c. and k the velocity constant in the formula for unimolecular reaction, $k=(1/t)\log(c_0/c)$, c_0 being the initial concentration. k_p and k_T will be explained later.

Table 1. Five c.c. of red sol was added to 95 c.c. of hydrogen peroxide solution.

t	c	k
0	4.28 (c_0)	—
2	4.39	—
6	4.36	—
10	4.28	—
16.25	4.29	—
23.25	4.28	—
30	4.31	—
45	4.20	—
55	4.15	(0.000236)
60	4.08	(0.000350)
75	3.94	(0.000480)
90	3.82	0.000544
120	3.72	0.000508
150	3.55	0.000540
180	3.38	0.000569
240	3.16	0.000550
270	3.02	0.000559
450	2.39	0.000562

Table 2. Five c.c. of red sol was added to 95 c.c. of hydrogen peroxide solution.

t	c	k
0	4.31 (c_0)	—
2	4.27	—
6	3.37	(0.0178)
10	2.43	0.0249
18	1.53	0.0249
30	0.79	0.0246
45	0.36	0.0240
60	0.15	0.0243

Table 3a. Five c.c. of red sol was added to 95 c.c. of hydrogen peroxide solution.

t	c	k
0	4.25 (c_0)	—
2	4.24	—
5	4.09	(0.00340)
10	3.74	0.00560
15	3.53	0.00540
20	3.28	0.00565
30	2.90	0.00553
45	2.45	0.00531
75	1.71	0.00527

Table 3b. Two c.c. of red sol was added to 95 c.c. of hydrogen peroxide solution.

t	c	k
0	4.39 (c_0)	—
2	4.49	—
5.5	4.37	—
10	4.32	—
20	4.08	(0.00160)
30	3.93	0.00150
51	3.79	0.00124
60	3.70	0.00123
75	3.55	0.00123
90	3.43	0.00118
120	3.15	0.00120

Table 4a. Five c.c. of red sol was added to 95 c.c. of hydrogen peroxide solution.

t	c	k
0	4.27 (c_0)	—
2.17	4.35	—
5	4.25	—
10	4.30	—
15	4.18	—
20	4.08	—
25	3.91	(0.00152)
30	3.69	(0.00210)
35	3.38	(0.00300)
45	3.09	0.00311
60	2.72	0.00327
75	2.38	0.00339
90	2.06	0.00352
120	1.61	0.00353
150	1.32	0.00340
180	1.05	0.00338
210	0.83	0.00338
240	0.67	0.00335

Table 4b. Five c.c. of black sol (not dialyzed) was added to 95 c.c. of hydrogen peroxide solution.

t	c	k	k_p (p: −0.2)	k_T (γ: 0.0706)
0	4.28 (c_0)	—	—	—
2.2	2.91	0.0762	0.136	0.0322
5.3	1.99	0.0627	0.117	0.0322
12	1.00	0.0526	0.105	0.0333
20	0.54	0.0450	0.096	0.0318
30	0.24	0.0417	0.097	0.0322
45	0.08	0.0384	0.101	0.0318

Table 4c. Two c.c. of black sol (not dialyzed) was added to 95 c.c. of hydrogen peroxide solution.

t	c	k	k_p (p: −0.3)	k_T (γ: 0.0730)
0	4.44 (c_0)	—	—	—
2	3.61	0.0450	0.0683	0.0146
5.25	3.14	0.0287	0.0446	0.0106
10	2.58	0.0236	0.0377	0.0100
20	1.74	0.0203	0.0346	0.0105
30	1.24	0.0185	0.0331	0.0107
60	0.50	0.0158	0.0329	0.0110
123	0.11	0 0131	0.0352	0.0105

Table 5a. Five c.c. of red sol was added to 95 c.c. of hydrogen peroxide solution.

t	c	k
0	4.27 (c_0)	—
2	4.40	—
5	4.31	—
10	4.27	—
15	4.10	—
20	3.76	(0.00275)
30	3.02	(0.00500)
45	2.25	0.00618
60	1.74	0.00658
75	1.41	0.00641
90	1.14	0.00637
120	0.70	0.00654
150	0.46	0.00645

Table 5b. Five c.c. of black sol (dialyzed) was added to 95 c.c. of hydrogen peroxide solution.

t	c	k	k_p (p: −0.3)	k_τ (τ: 0.0523)
0	4.28 (c_0)	—	—	—
2.5	2.90	0.0676	0.107	0.0387
5	2.05	0.0639	0.107	0.0406
10.2	1.11	0.0553	0.106	0.0412
20	0.40	0.0515	0.112	0.0413
30	0.21	0.0436	0.106	0.0364

Table 5c. Two c.c. of black sol (dialyzed) was added to 95 c.c. of hydrogen peroxide solution.

t	c	k	k_p (p: −0.4)	k_τ (τ: 0.0719)
0	4.44 (c_0)	—	—	—
2	3.82	0.0327	0.0426	0.0104
5.1	3.22	0.0274	0.0370	0.0102
10	2.60	0.0232	0.0329	0.0100
20	1.80	0.0196	0.0300	0.0101
30	1.29	0.0179	0.0294	0.0103
45	0.80	0.0165	0.0301	0.0107
60	0.59	0.0146	0.0285	0.0100
90	0.29	0.0132	0.0303	0.0099

The red or black sols added as catalysts in the above experiments are summarized in Table 6.

Table 6. Carbon monoxide was passed through a 0.02% aqueous solution of chloroplatinic acid ($H_2PtCl_6 \cdot 6H_2O$) with nearly a constant velocity throughout the experiment. The red sol thus obtained contains 0.075 grams of platinum in one liter as described before.

Number of table	Time duration during which the gas was continually passed through the chloroplatinic acid solution in hours		Time duration during which the red sol was left in the air in hours	Volume of sol added in c.c.	
	before the colour change	after the colour change		red	black
1	0.5	0	2	5	—
2	1	0.5	2.5	5	—
3a	0.5	0.5	3.5	5	—
3b	0.5	0.5	2	2	—
4a	0.5	2.5	0	5	—
4b	0.5	2.5	one night	—	5 (not dialyzed)
4c	0.5	2.5	one night	—	2 (not dialyzed)
5a	0.5	4	0	5	—
5b	0.5	4	one night	—	5 (dialyzed)
5c	0.5	4	one night	—	2 (dialyzed)

Discussion. The above results are graphically represented in terms of the relationship between $\log(c_0/c)$ and t in Fig. 1, 2, 3, 4 and 5. If the catalytic decomposition of hydrogen peroxide by colloidal platinum proceeds in accordance with the formula for unimolecular reaction $-dc/dt = kt$ as exemplified by Bredig and his co-workers, it might be expected, particularly in Fig. 4 and 5, that there should exist a linear relation between $\log(c_0/c)$ and t.

In the case where the red sol is added as catalyst, the apparent concentration of hydrogen peroxide solution remains nearly constant—and sometimes even increases slightly—over a short time of the earlier stage and the reacting solution is of red tint throughout the period, suggesting the sol to exist unchanged. In time, the solution, however, will lose the red colour to become slightly tinged with black, and then, the decomposition reaction begins abruptly and proceeds rapidly. The induction period mentioned above is distinctly shown by the former parts of the curves 1, 2, 3a, 3b, 4a and 5a in Fig. 1, 2, 3, 4 and 5; while the latter

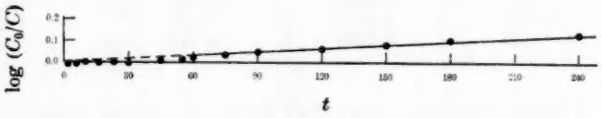

Fig. 1.

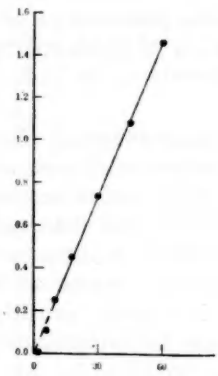

Fig. 2.

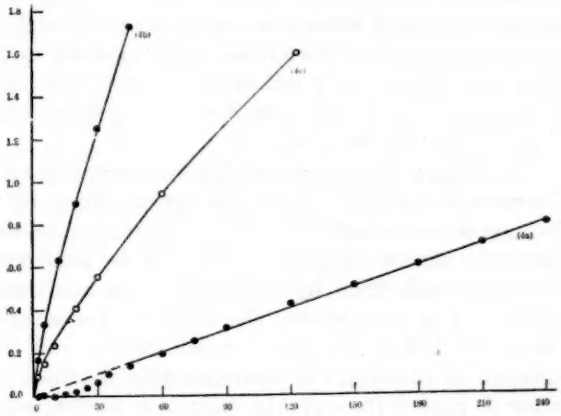

Fig. 4.

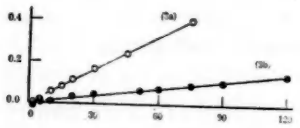

Fig. 3.

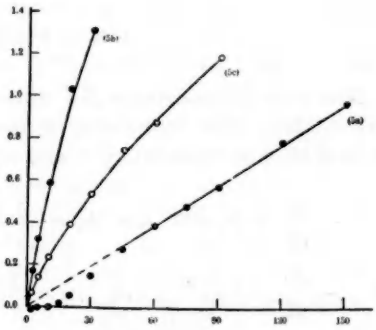

Fig. 5.

parts of these curves are linear and their extension lines passes through the origin, this indicating the reaction to proceed as unimolecular.

On adding the red sol to hydrogen peroxide solution, carbon monoxide considered to be retained in the colloidal particle as its essential constituent may be gradually set free, since the sol is diluted with hydrogen peroxide solution, and on subsequent titration, oxidized with potassium permanganate.[3] The apparent increase in the concentration of hydrogen peroxide solution during the induction period might probably be ac-

(3) J. W. Mellor, "A Comprehensive Treatise on Inorganic and Theoretical Chemistry," Vol. 5, 943.

counted for from such a point of view. Sooner or later, a certain limiting amount of carbon monoxide constituting the particle will be reached, when the particle may be more reasonably regarded as colloidal platinum rather than as colloidal platinum-carbonyl; that is to say, a sol of black colour as prepared by Bredig's method will be formed and hereupon, the induction period will be over.

Carbon monoxide remaining in the particle will, thenceforward, play the part of maintaining the catalytic activity of the colloid unaltered, as it may be considered for the gas either to volatilize from, or to act on oxygen[4] adsorbed by, the surface of the colloidal particle (The influence of oxygen adsorbed by the particle on the catalysis will be discussed below.), and thus render the portion of available surface covered with these free. The fact that, on adding the red sol to hydrogen peroxide solution as catalyst, the decomposition reaction proceeds as unimolecular after it passed through the induction period, may be explained by such a supposition.

In the case where the black sol obtained from the red one is added as catalyst, the decomposition reaction takes place immediately and proceeds rapidly, a curved line, instead of straight, being obtained between $\log(c_0/c)$ and t as shown in Fig. 4 and 5.

The velocity constants for unimolecular reaction k are given in the above tables. The constants, k_p and k_γ, are defined by the formulæ obtained by Freundlich[5] (1) and by the present author (2):

$$-\frac{dc}{dt} = k_p \cdot c^{1-p} \quad \text{or} \quad k_p = \frac{1}{p \cdot t}(c_0^p - c^p) \qquad (p \text{ a constant}) \quad (1),$$

and

$$-\frac{dc}{dt} = k_\gamma \frac{c}{1-\gamma c} \quad \text{or} \quad k_\gamma = \frac{1}{t}\left\{\log\frac{c_0}{c} - \gamma(c_0 - c)\right\} \qquad (\gamma \text{ a constant}) \quad (2).$$

The above-mentioned fact that the reaction deviates from unimolecular may probably be attributed to the retarding influence of oxygen evolved from hydrogen peroxide and subsequently adsorbed by colloidal platinum on the catalysis, subdivided platinum having a definite tendency to absorb oxygen.[6] From this point of view, the above formula (2) has been derived in the following manner: If θ represents the fraction of the available surface covered with molecules of oxygen, it follows,

(4) C. Paal, *Ber.*, **49** (1916), 548.

(5) H. Freundlich, "Kapillarchemie," Vol. 2, (1932).

(6) L. Woehler, *Ber.*, **36** (1903), 3492; C. Paal and C. Amberger, *Ber.*, **40** (1907), 2202; D. O. Shiels, *J. Phys. Chem.*, **33** (1929), 1181, etc.

according to Langmuir,[7] that for equilibrium between the adsorbed layer of molecules of oxygen and those in the surrounding medium, under the assumption that one molecule of oxygen occupies one elementary space of the surface,

$$a\mu(1-\theta) = \nu\theta ,$$

a being the fraction of the number of molecules of oxygen μ striking the surface in unit time which condense and $\nu\theta$ the number of molecules of oxygen which evaporate from the surface in unit time. On the other hand, the rate of decomposition of hydrogen peroxide $-dc/dt$ should be proportional to the number of molecules of hydrogen peroxide μ' striking the surface in unit time; hence

$$-\frac{dc}{dt} = k\mu'(1-\theta) ,$$

k being the velocity constant. Eliminating θ from these, it follows that

$$-\frac{dc}{dt} = \frac{k\mu'\nu}{\nu+a\mu} .$$

Although it might be assumed for μ to be proportional to c_0-c provided the oxygen evolved from hydrogen peroxide was wholly kept in the solution and adsorbed only to a small extent by the particles, the reaction was carried out in an open vessel as described above, and accordingly, it may be assumed for the present under the introduction of a constant β that μ should be proportional to $\beta(c_0-c)$, β being the average fraction of the amount of oxygen evolved which remains in the solution. Considering μ' to be proportional to the concentration of hydrogen peroxide solution c, the velocity of its decomposition should then be given by

$$-\frac{dc}{dt} = k_T\frac{c}{1-\gamma c}$$

which is the formula previously shown. k_T and γ are the constants containing a, β, ν and k.

As seen in Fig. 4 and 5, the catalytic decomposition of hydrogen peroxide proceeds more rapidly with the black sol than with the red one. This fact may be rendered clear by the following consideration: As already described, the red sol turns black on account of the volatilization

(7) I. Langmuir, *J. Am. Chem. Soc.*, **38** (1916), 2286; **40** (1918), 1361.

of carbon monoxide retained in the particles of the sol and becomes catalytically active during the course of an induction period. The colloidal particles of platinum in the black sol thus formed might be considered to be contaminated with carbon monoxide more profoundly than those in the black sol obtainable by standing in the air over-night or dialyzing the red sol; hence, there should be a difference between the areas of active surface available for catalysis, from which may probably result the diversity in the rate of decomposition.

Summary.

(1) The catalytic decomposition of hydrogen peroxide by colloidal platinum-carbonyl as well as colloidal platinum obtainabe from it was examined.

(2) In the former case, the reaction proceeds as unimolecular after it passed through an induction period, while in the latter case, it deviates appreciaiy from unimolecular throughout the course of the reaction concerned.

(3) Some considerations were made on these facts.

The author wishes to express his cordial thanks to Professor J. Sameshima, under whose kind guidance this work has been carried out. The expense of the present experiments has been defrayed from the Committee on Catalysis in the Japan Society for the Promotion of Scientific Research.

Chemical Institute, Faculty of Science,
Imperial University of Tokyo.

Studies on the Oiliness of Liquids. V. Lubricants Consisting of Two or Three Chemical Compounds.

By Hideo AKAMATU.

(Received November 25, 1937.)

In the preceding papers,[1a][1b] the measurements of the coefficients of static friction of glass surfaces were described when some pure chemical compounds were used as lubricants. The present paper records the results when the lubricants consist of mixtures of chemical compounds.

In conclusion, we observed the good much evidence that a selective adsorption takes place on the friction surfaces. The idea of adsorption has already been applied to the boundary lubrication by some investigators, especially W. B. Hardy[2] to whom we owe the fundamental conception that a semi-polar molecule attaches to the friction surface anchoring itself by means of polar group and presenting to the liquid interface non-polar chain, forming a monomolecular orientated layer.

In the practical engineering, a well known patent "germ process" by Wells and Southcombe,[3] depends on the fact that the addition to mineral oil of small percentage of such compounds as fatty acids that lower the interfacial tension between water and oil gives exceptionally good lubricating values.

Wilson and Barnard,[4] W. G. Wilharm,[5] P. Woog,[6] and W. Bachmann[7] have observed the same results and agreed that there takes place adsorption of lubricant on the surfaces.

Most of these works, however, for the practical purposes, were dealing with the oil, the composition of which are very complex, so that it is difficult to postulate any mechanism. The present work deals with some binary or ternary solutions of pure chemical compounds, and the results

(1a) J. Sameshima, M. Kidokoro, and H. Akamatu, this Bulletin, **11** (1936), 659.

(1b) J. Sameshima and Y. Tsubuku, *ibid.*, **12** (1937), 127.

(2) W. B. Hardy and I. Doubleday, *Proc. Roy. Soc.* (London), A, **104** (1923), 25; W. B. Hardy, *Phil. Trans.*, A, **230** (1931), 1; W. B. Hardy and M. Nottage, *Proc. Roy. Soc.* (London), A, **138** (1932), 259.

(3) Wells and Southcombe, *J. Soc. Chem. Ind.*, **39** (1920), 51.

(4) Wilson and Barnard, *Ind. Eng. Chem.*, **14** (1922), 683.

(5) W. G. Wilharm, *ibid.*, **18** (1926), 463.

(6) P. Woog, "Contribution a l'étude du graissage", Paris (1926).

(7) W. Bachmann and Brieger, *Kolloid-Z.*, **36** (1925), 142; **39** (1926), 334.

support the theories described above, suggesting a new point of view on the mechanism.

The method of measuring the static friction and the conditions were the same as described in the preceding paper.[1a] The friction surfaces consisted of a flat glass and a glass with a spherical surface.

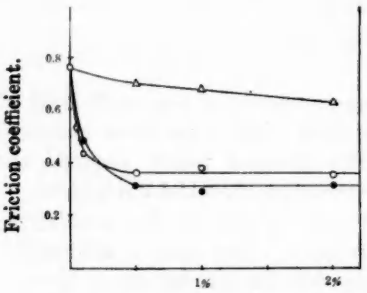

△: *n*-Tetradecyl alcohol/Toluene.
○: Oleic acid/Toluene.
●: Palmitic acid/*m*-Xylene.

Fig. 1.

In carrying out the experiments with several binary solutions, it came to light that there was much evidence for tendency of selective character. This selectivity depends chiefly upon the polarity of the substance, and this appears most clearly when the mixture consists of polar and non-polar compounds. For example, when the lubricant is made by dissolving oleic acid ($\mu = 0.29$) in toluence ($\mu = 0.76$), the friction coefficient is nearly identical with that of pure oleic acid, being independent upon the concentration of oleic acid. Table 1 and Fig. 1 show how small amounts of a polar substance in a non-polar solvent is effective for the reduction of the friction of the solvent.

In the preceding paper,[1a] we have reported that the friction coefficient of hexane and nonane are 0.68 and 0.64 respectively. These data have been revised, since the samples formerly used may contain some unsaturated hydrocarbons as impurities. This time, hexane and nonane were shaken with fuming sulphuric acid for several days, dried over sodium metal and then distilled. With such samples, the friction coefficients are somewhat greater, that is 0.85 for hexane and 0.76 for nonane. It is supposed that heptane and octane have also values of this order. So it seems that the small amount of unsaturated hydrocarbons are still much effective. It is true also that the measurement of friction of a hydrocarbon is rather difficult, for it is readily contaminated while the measurements and the friction steps down gradually. Such a difficulty is little for polar compounds.

It is well known that, the molecules have to take orientation in such a manner as to prevent the abruptness of potential difference between the two neighbouring phases. In other words, the interfacial energy between polar compound and underlying solid surface, such as glass or metal, is smaller than that between a non-polar compound and solid sur-

Table 1. Polar solute and non-polar solvent.

Solute	Solvent	Conc. of solute (wt. %)	Friction coefficient
—	Toluene	—	0.76
—	*m*-Xylene	—	0.76
—	liq. Paraffin	—	0.55
—	*n*-Nonane	—	0.76
Oleic acid	Toluene	2	0.35
,,	,,	1	0.38
,,	,,	0.5	0.36
,,	,,	0.1	0.43
,,	,,	0.05	0.53
Palmitic acid	*m*-Xylene	4	0.32
,,	,,	2	0.31
,,	,,	1	0.29
,,	,,	0.5	0.31
,,	,,	0.1	0.48
Palmitic acid	*n*-Nonane	2	0.31
n-Tetradecyl alcohol	Toluene	2	0.63
,,	,,	1	0.68
,,	,,	0.5	0.70
,,	*n*-Nonane	2	0.54
Tripalmitin	*m*-Xylene	2	0.35
,,	,,	1	0.33
Stearic acid	liq. Paraffin	1 *	0.28
,,	,,	0.2 *	0.25
,,	,,	0.05	0.45
Benzoic acid	*m*-Xylene	2	0.59
Benzophenone	,,	3	0.77

(* This is not a true solution, but a mixture.)

face, so that if such a solution, polar solute and non-polar solvent, be placed on the glass surface (polar) the polar molecules will attach to the surface preferentially with their polar groups facing to the surface, the phenomena will be like that on the water surface. Many investigations[8]

(8) H. N. Holmes and J. B. Thor, "Colloid Symposium Monograph VII," (1930), 213; W. Harkins and Gans, *J. Phys. Chem.*, **36** (1932), 86; J. J. Trillat and R. Vaille, *Compt. rend.*, **202** (1936), 2134.

have been carried out on polar and non-polar adsorption. On the other hand, the experiment on the spreading of liquid on solid surfaces,[9] or the electron diffraction analysis[10] supports this view directly.

It may be said that, in boundary lubrication, the oiliness depends only upon the adsorbed layer and the other part of solution does not impart the friction or oiliness, the non-polar solvent merely furnishing a medium. It seems that oiliness is merely depends on the friction between the surface with such adsorbed layers. Such a adsorption will be a dynamical equilibrium between the solid surface and the liquid in mass, so the orientation of the molecules will not be so complete as that deposited by Blodgett's[11] methods. It is natural, therefore, that the friction of the former is much greater than the latter.[12]

The same idea may be extended to the case when the solvent is also polar, but the phenomena become more complicate. The addition of a small quantity of a fatty substance is not effective generally. The results are shown in Table 2 and Fig. 2.

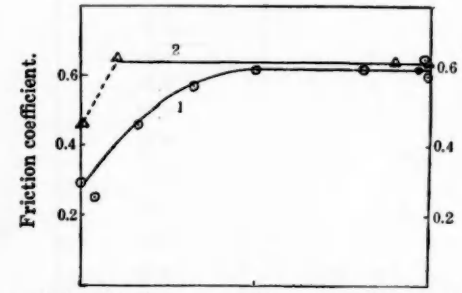

1. Oleic acid.
2. Glycol.

50% Concentration.

1. Acetic acid.
2. *n*-Propyl alcohol.

Fig. 2 (a).

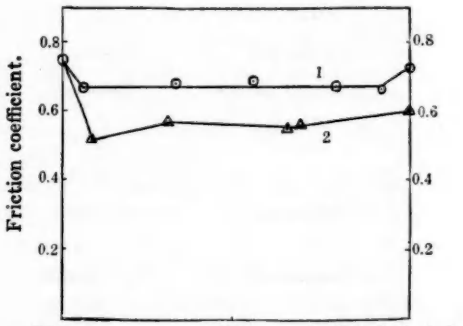

Water.

50% Concentration.

1. Ethyl alcohol.
2. Acetic acid.

Fig. 2 (b).

There are some differences in the adsorbabilities or adhesion forces of molecules with active groups. If the adsorbabilities of the molecules composing the lubricant are alike each other, they will be adsorbed similarly and the value of the friction coefficient will be averaged. If, however, there is any disparity, one of them will be adsorbed preferentially

(9) R. Bulkley and Snyder, *J. Am. Chem. Soc.*, **55** (1933), 194.
(10) L. T. Andrew, *Trans. Faraday Soc.*, **32** (1936), 607.
(11) C. Blodgett, *J. Am. Chem. Soc.*, **57** (1935), 1007.
(12) H. Akamatu and J. Sameshima, this Bulletin, **11** (1936), 791.

Table 2.

Component 1	(wt. %)	Component 2	(wt. %)	Friction coefficient
—	—	Acetic acid	100	0.60
Oleic acid	1	,,	99	0.65
,,	2	,,	98	0.63
,,	3	,,	97	0.62
,,	19	,,	81	0.62
,,	50	,,	50	0.62
,,	6 8	,,	32	0.57
,,	84	,,	16	0.46
,,	96	,,	4	0.25
,,	100	—	—	0.29
Palmitic acid	4	Acetic acid	96	0.6—0.7
,,	2	,,	98	,,
Glycol	10	*n*-Propyl alcohol	90	0.64
,,	90	,,	10	0.65
—	—	*n*-Propyl alcohol	100	0.64
n-Tetradecyl alcohol	1	*n*-Propyl alcohol	99	0.64
,,	2	,,	98	0.66
Benzophenone	1	Glycol	99	.50
Hydroquinone	2	,,	98	0.46
—	—	Glycol	100	0.46
—	—	Dioxane	100	0.61
Palmitic acid	2	,,	98	0.5—0.6
Sebacic acid	2	,,	98	0.62
Ethyl alcohol	100	—	—	0.72
,,	91.6	Water	8.4	0.66
,,	78.8	,,	21.2	0.67
,,	54.7	,,	45.3	0.69
,,	32.4	,,	67.6	0.68
,,	6	,,	94	0.67
Acetic acid	68.4	Water	31.6	0.56
,,	64.6	,,	35.4	0.55
,,	30	,,	70	0.57
,,	8	,,	92	0.52
—	—	Water	100	0.75

and the friction depends on it only. Such a conception may be too simple, since there are many unknown factors affecting the friction. Hardy found, for example, that the temperature coefficient of a mixed lubricant is very complicated, although a single chemical substance has no temperature coefficient of friction. The present experiments were carried out at room temperature, 18–23°C., so the results may be considered as that of the constant temperature.

It has been observed, by some investigators, that the friction would be reduced with the interfacial energy between the lubricant and the friction surfaces, since the film would be stable. Of course, it seems the first essential condition to cover the active surface of the solid by adsorbed molecules. There is found no parallelism, however, between the interfacial energy and the oiliness. Molecules, which have the lower interfacial energy for the friction surface, are adsorbed preferentially by the surface. The friction, therefore, is determined by those surfaces with adsorbed layers, but the order of reducing the friction depends upon the properties of the individual molecules, molecular structure or other unknown properties. If the reducing power of friction is parallel with the stability of the film, the molecules which are adsorbed preferentially, must also be the better lubricant. But the fact is not so. With such a lubricant, as palmitic acid and acetic acid dissolved in *m*-xylene, the friction coefficient is nearly identical with that of acetic acid itself. It seems that acetic acid is adsorbed preferentially, but the molecular structure of acetic acid is not favourable to reduce the friction, in other words, in such a

Table 3. (Solvent: *m*-Xylene)

Solute	(%)	Friction coefficient	Solute	(%)	Friction coefficient
Acetic acid	4	0.49	Benzophenone	2	0.33
Palmitic acid	4		Palmitic acid	2	
Acetic acid	8	0.57	Benzoic acid	2	0.42
Palmitic acid	8		Palmitic acid	2	
Acetic acid	6	0.64	Oleic acid	2	0.64
Palmitic acid	2		Acetic acid	2	
n-Butyric acid	2	0.35	Tripalmitin	4	0.56
Palmitic acid	2		Acetic acid	4	
n-Butyric acid	5	0.31	Tripalmitin	1	0.58
Palmitic acid	5		*n*-Butyric acid	1	

case acetic acid behaves as an inhibitor. When the lubricant is a solution of palmitic acid and butyric acid in *m*-xylene, the friction coefficient is that of palmitic acid itself. When the lubricant consists of tripalmitin and butyric acid dissolved in *m*-xylene, the friction is identical with butyric acid. In those examples, the order of the adsorbability seems as follows; acetic acid, palmitic acid, butyric acid, tripalmitin. Several examples are shown in Table 3.

In conclusion the author wishes to express his gratitude for the kind advices of Prof. J. Sameshima, and for the grant defrayed by Japan Society for the Promotion of Scientific Research.

Summary.

The static boundary frictions were measured when some binary or ternary mixtures were placed on the glass surfaces. The results suggest that: (i) the friction is governed by the surfaces with adsorbed layer of lubricant, and (ii) the reducing power of friction depends upon the individual molecular constitution of the molecules which are adsorbed preferentially by the friction surface, rather than the stability of the film.

Selective adsorption by the glass surface has been investigated, and some examples has been reported.

Chemical Institute, Faculty of Science,
Imperial University of Tokyo.

Studes on the Oiliness of Liquids. VI[1]. Measurements of the Kinetic Friction Coefficients by the Method of Sliding Velocity.

By Tunetaka SASAKI.

(Received December 20th, 1937.)

The present paper describes the measurements of the kinetic friction coefficients by the sliding velocities of a slider on an inclined surface. It is generally accepted, as Amontons's rule, that the frictional force is independent of the contact area of two solids, and is simply proportional to the total pressure or load acting normally to the sliding surfaces. This rule is considered to be applicable to both kinetic and static friction so far as the condition of either dry friction or boundary lubrication is satisfied. In the case of static friction, the conditions of the measurement are relatively simple, while in the case of kinetic friction, it is rather complicated, because the friction is influenced, for instance, by the velocity of a body in motion and temperature rise caused by the friction, etc.

The published results on the influence of velocity on dry friction are rather conflicting. Coulomb pointed out that the velocity has almost no influence upon the dry friction between metals. On the other hand, Galton and Westinghouse,[2] and Smith[3] indicated that the friction decreases profoundly as the velocity increases. Jacob[4] determined the coefficients of kinetic and static frictions from the measurements of the critical angle of the frictional surface and concluded that on the contaminated surfaces the kinetic friction coefficient μ_k differs from the static friction coefficient μ_s considerably and the sliding motion is accelerated, while in the case of clean surfaces, μ_k is equal or nearly equal to μ_s and the motion is uniform.

The reports on the boundary lubrication are also complicated. Deeley,[5] working on boundary lubrication, found that μ_s was independent

(1) The first to fifth reports are published in the following: Sameshima, Kidokoro, and Akamatu, this Bulletin, **11** (1936), 659; Akamatu and Sameshima, *ibid.*, **11** (1936), 791; Sameshima and Miyake, *ibid.*, **12** (1937), 96; Sameshima and Tsubuku, *ibid.*, **12** (1937), 127; Akamatu, *ibid.*, **13** (1938), 127.

(2) Galton and Westinghouse, *Engineering*, **26** (1878), 153.

(3) Smith, Archibutt, and Deeley, "Lubrication and Lubricants," 843, (1927).

(4) Jacob, *Ann. Physik*, **38** (1912), 126.

(5) Deeley, *Proc. Phys. Soc.* (London), **32** (1920), 1s.

of the load and that at slow speeds, μ_k was practically equal to μ_s. On the other hand, Wilson and Barnard,[6] using Deeley's apparatus, observed that μ_k decreased with increasing speed, while Kimball,[7] Jenklin and Ewing[8] showed that at slow speeds μ_k exceeded μ_s and it increased with increasing speeds. Further, Jacob[4] indicated that when the frictional surfaces are separated by oily films, friction obeys the Coulomb's rule, the motion of a body is accelerated on the surface of the inclination exceeding a certain critical angle, and the value of μ_k is independent of the velocity. Recently, Beare and Bowden,[9] using the Deeley machine for measuring μ_k, further studied the problem of friction precisely and determined the constancy of μ_k over the wide range of velocity at various conditions of boundary lubrication.

Apparatus and Measurement. The apparatus employed in the present experiment has been constructed as shown in Fig. 1. In this figure, AB is a glass tube of 3 cm. in diameter and 60 cm. in length. A slider, shown in Fig. 2, has been made of a glass tube of 2 cm. in diameter,

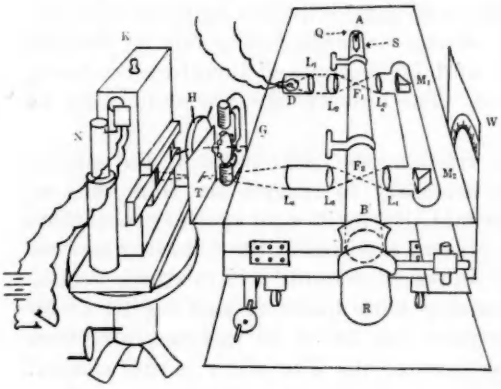

Fig. 1.

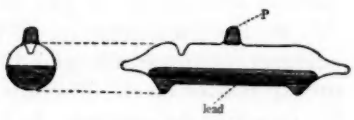

Fig. 2.

which is loaded with lead and carries a small projection P which serves to interrupts the optical paths in the tube AB. Again in Fig. 1, L_1, L_2, L_3, L_4, L_5, L_6, M_1, and M_2 are lenses and total reflexion prisms respectively. By this arrangement, the light from the source D is focussed

(6) Wilson and Barnard, *J. Ind. Eng. Chem.*, **14** (1922), 682.
(7) Kimball, *Am. J. Sci.*, [3], **13** (1877), 353.
(8) Jenklin and Ewing, *Phil. Trans.*, **167** (1877), 509.
(9) Beare and Bowden, *Phil. Trans.*, **234** (1935), 329.

at two points F_1 and F_2 in the tube AB and then, passing through the slit T, interrupted at constant time intervals by the projection H of a cynchronous motor G, it finally enters the time recorder box K, in which a photographic plate is made to slide down vertically, facing the light, with constant speed. The start of the plate is managed by the electromagnet N and a lever. The slider is held by the metal projection Q before its start and it rests, after each run, in the glass tube R containing cotton. The tube is made incline at a desired angle which is subsequently read by the protractor W.

The measurement is carried out as follows. At first the liquid under investigation is poured in the inclined tube, and the lever of the electromagnet N is pressed down to start the photographic plate. Then the slider is set in motion by releasing it from the support Q. Thus, the projection of the slider interrupts, as it runs down, at two points F_1 and F_2 of the optical path from the light source D to the photographic plate. On developing the plate, it gives the image of the line produced by D, having two dark spots caused by the interruption of the slider. At the same time, the cynchronous motor also marks a time scale on the line. Thus the time required for the passage between two points F_1 and F_2 can be measured to the accuracy of 1/50 second and therefore the mean velocity of the slider is calculated. The observations are undertaken at various inclinations of the tube.

In the measurement of the friction, the cleanliness of the sliding surfaces is important and it is necessary to remove the thin films of greasy matter on it. For this account, Hardy[10] paid special precautions for cleaning the surface. In the present experiment the following process has been adopted.[9] The tube is dipped in chromic acid mixture, washed carefully with soap solution, steaming with water vapour for 20 or 30 minutes, further with alcohol vapour for 20 or 30 minutes, and then finally dried by passing dried air through it. The slider is also cleaned by the same process prior to each experiment.

Calculation of the Kinetic Friction. In the present discussion it is assumed that the coefficient of the kinetic friction μ_k is constant and is independent of the sliding velocity, which has been verified in the present investigation. In Fig. 3 and in the following equations S_1 is distance between the starting point Q of the slider and F_1, S_2 distance between Q and F_2, T_1 time required to slide the distance S_1, T_2 time required to slide the distance S_2, m mass of the slider, θ angle of inclina-

(10) S. K. Hardy and W. B. Hardy, *Phil. Mag.*, [6], **38** (1919), 32.

tion of the tube, F driving force acting upon the slider along the tube, $v = 1/(T_2 - T_1)$ the quantity proportional to the mean velocity of the silder, G acceleration of the slider, and g gravity constant.

Then we obtain the following relations:

$$F = mg\sin\theta - \mu_k mg\cos\theta ,$$

$$G = \frac{F}{m} = g\sin\theta - \mu_k g\cos\theta \quad (1),$$

$$S_1 = \frac{1}{2} G T_1^2 \quad (2),$$

$$S_2 = \frac{1}{2} G T_2^2 \quad (3),$$

$$v = \frac{1}{T_2 - T_1} \quad (4).$$

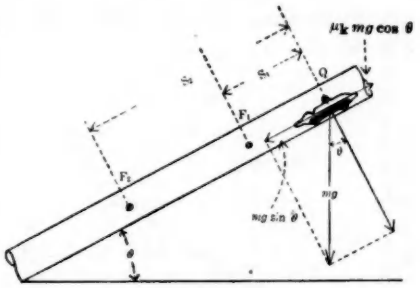

Fig. 3.

Eliminating T_1, T_2, and G from these four equations and expressing μ_k in terms of v and θ, we have the following equation:

$$\tan\theta - \frac{(\sqrt{2S_2} - \sqrt{2S_1})^2}{g} v^2 \sec\theta = \mu_k \quad (5).$$

In this equation the value $(\sqrt{2S_2} - \sqrt{2S_1})^2/g$ is constant and so $\tan\theta$ is linear to $v^2 \sec\theta$. In the figure drawn by plotting $\tan\theta$ against $v^2 \sec\theta$, the point of intersection of the straight line with the axis of $\tan\theta$ gives the value of μ_k.

In order to test the above conclusion several liquids were used to construct the diagram of $\tan\theta$ and $v^2 \sec\theta$. Some typical examples are shown in the following tables and figures. Table 1 and Fig. 4 show the

Table 1. Glycerin.

θ	$\tan\theta$	$T_2 - T_1$ (second)	$v^2 \sec\theta$	θ	$\tan\theta$	$T_2 - T_1$ (second)	$v^2 \sec\theta$
40°	0.838	0.114	100.5	18°	0.324	0.184	31.0
38	0.780	0.112	101.0	16	0.286	0.210	23.5
36	0.726	0.118	88.9	15	0.268	0.216	22.2
34	0.675	0.120	84.8	14	0.249	0.232	20.0
32	0.625	0.124	76.5	13	0.231	0.246	17.0
30	0.575	0.130	68.5	12	0.212	0.278	13.2
28	0.531	0.140	57.9	11	0.194	0.298	11.5
26	0.487	0.140	56 9	10	0.176	0.380	7.0
24	0.445	0.144	52.8	9	0.158	0.420	5.7
22	0.403	0.150	47.9	8	0.140	0.470	4.6
20	0.364	0.166	38.5				

existence of the linear relation between $\tan\theta$ and $v^2 \sec\theta$ as given by equation (5). Most of the other liquids under examination showed the similar results. The angle of inclination of the straight line calculated from equation (5) gives 46°10′ on the scale of diagram employed in Fig. 4. The angles for many liquids range between 40° and 50°. Some liquids deviate from the linear relation, an example of which is shown in Fig. 5.

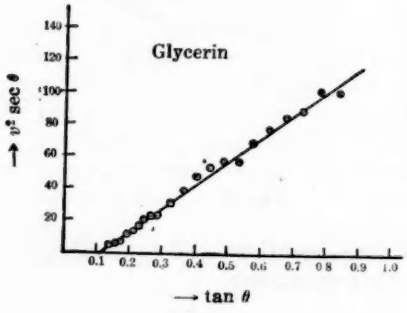

Fig. 4.

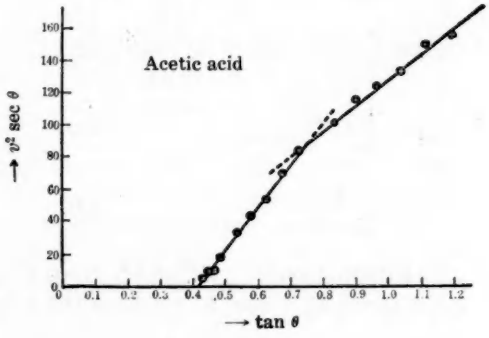

Fig. 5.

Examination of the Experimental Conditions. In order to test the reproducibility and to find the suitable experimental conditions, the following measurements were carried out on glycerin. The results are tabulated in Table 2, which gives the following conclusion. The reproducible value

Table 2.

Experimental conditions	μ_k (Glycerin)
(1) Using new tube of about 1 meter in length and new slider of 76.8 g. in weight.	0.10 0.10 0.09
(2) Using the above tube and slider after both of them have suffered abrasion by repeated experiments.	0.20 — —
(3) Using renewed tube of the same length as in (1) and renewed slider of 60.3 g. in weight.	0.10 — —

Table 2.—(*Concluded*)

Experimental conditions	μ_k (Glycerin)
(4) Using the same renewed tube as in (3) and abrased slider as in (2).	0.10 — —
(5) Using another new tube of 60 cm. in length and the abrased slider.	0.09 0.10 0.11

of μ_k can always be obtained with new tube and new slider, and it is independent of the length of the tube and the weight of the slider ((1), (3), and (5) in Table 2.), as is expected from equation (5). The value of μ_k remains unaltered so far as the glass tube is not abrased. The abrasion of both glass tube and slider increases the value of μ_k. In the present experiment the glass tube was always renewed when the reproducibility of μ_k with standard glycerin failed to exist.

Further it is necessary to start the slider with the force just to overcome the static friction. The excessive force imparts initial velocity to the slider which results the apparent decrease in the value of μ_k as shown in Table 3. In the experiments, pushing forces were controlled by the elastic strength of suitable spring arrangement. Too much force gives even a negative value of μ_k.

Table 3.

Force to overcome the static friction	Apparent μ_k of glycerin
Strongest	—0.03
Strong	0.05
Weak	0.10

Measurement of μ_k. The observed values of μ_k for water, alcohols, hydrocarbons, and fatty acid are tabulated in Table 4.

In the above observations, glycerin sometimes showed convex curves towards $\tan\theta$ axis owing perhaps to its high viscosity. When we plot the values of μ_k for alcohols against the numbers of carbon atoms in their molecules, the gradual decrease of μ_k with increasing numbers of carbon atoms is observed as in Fig. 6. These results may be compared with those of Beare and Bowden[9] or Sameshima and Miyake[1]. The μ_k value of water is large as is expected from the μ_s value of water.[1] The μ_k values

Table 4.

Lubricant	μ_k	Lubricant	μ_k
Glycerin	0.10	Hexane	0.34
Methyl alcohol	0.41	Heptane	0.16
Ethyl alcohol	0.34 (0.39)	Octane	0.24
Propyl alcohol	0.26	Nonane	0.31 (0.27)
Butyl alcohol	0.26 (0.23)	Acetic acid	0.42
Hexyl alcohol	0.15	Water	0.66 (0.69)

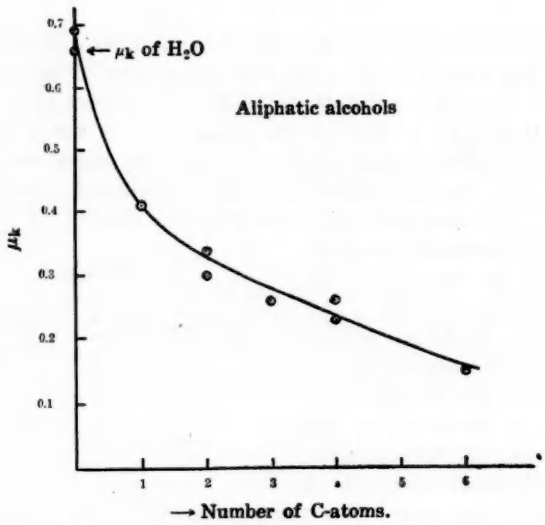

Fig. 6.

of hydrocarbons are irregular with respect to the numbers of carbon atoms in their molecules. Of the μ_k values of fatty acids series, only that of acetic acid was measured.

The author wishes to express his sincere gratitude to Professor J. Sameshima for his kind guidance. The expense for the experiments has been defrayed by a grant given to Professor Sameshima from Nippon Gakujutsu Shinkokwai (Japan Society for the Promotion of Scientific Research), to which the author's thanks are due.

Summary.

(1) Measurements of the kinetic friction coefficient have been made to study the oiliness of liquids. The method consists of the observation of the sliding velocity of a slider on an inclined surface lubricated with the liquid to be tested. Special apparatus has been constructed to measure the sliding velocity.

(2) It is confirmed that the kinetic friction coefficient is generally independent of the velocity over the range of the experiment (up to about 100 cm./sec.), and the following equation holds.

$$\tan\theta - \frac{(\sqrt{2S_2}-\sqrt{2S_1})^2}{g} v^2 \sec\theta = \mu_k$$

where v is the mean velocity of the slider on the surface of the inclination θ. The above equation lacks the viscosity term, so the conditons of the boundary lubrication are considered to be satisfied.

(3) The kinetic friction coefficients of glycerin, aliphatic hydrocarbons, aliphatic alcohols, acetic acid, and water have been measured.

Chemical Institute, Faculty of Science,
Imperial University of Tokyo.

Polymerisation of Tung Oil. I.

By Monzi TATIMORI.

(Received December 4, 1937.)

I. **Introduction.** It is well known that drying oils such as linseed, perilla, and tung oil are used for coating materials after special treatment generally called cooking.

Tung oil[1] is one of the most unsaturated oils and is important in paint and varnish industry. Its iodine value is about 260 as measured by hydrogenation method[2] and its polymerisation velocity is far greater than that of linseed oil. Therefore it has the disadvantage of gelation[3] and there are several devices and patents[4] to avoid it.

Most fatty oils are composed of glycerides of fatty acids such as stearic, oleic, linolic, and linolenic acid and obey the rule of proportionality between iodine value and density.[5] Tung oil, however, is an exception,[6] and it is supposed that the tung oil acids have distinctly different constitutions from that of linseed oil acids. There are many theories[7] on the constitutional formula of *a*-eleostearic acid, the main constituent of the tung oil acids. At present it is generally accepted that its most probable constitutional formula is

$$CH_3\text{-}(CH_2)_3\text{-}CH{=}CH\text{-}CH{=}CH\text{-}CH{=}CH\text{-}(CH_2)_7\text{-}COOH.$$[8]

The cooking of a drying oil at high temperatures in the absence of oxygen is accompanied by an increase in the viscosity, density, and apparent molecular weight of the oil and by a decrease in iodine value

(1) This oil is obtained from the seed of *Aleurites Fordii*, and is called Chinese wood oil.

(2) L. A. Jordan, *J. Soc. Chem. Ind.*, **53** (1934), 1.

(3) Gelation is the phenomenon that an oil solidifies suddenly and becomes an insoluble and unfusible mass.

(4) H. Brendel, *Farbe u. Lack*, **1932**, 145; H. Hardert, *ibid.*, **1928**, 558.

(5) K. Yokota and M. Tatimori, not yet published.

(6) The iodine value of tung oil is ca. 165 by Wijs method and is smaller than that of linseed oil.

(7) M. S. Cloez, *Compt. rend.*, **81** (1875), 469; **82** (1876), 501; **83** (1876), 943; M. L. Maquenne, *ibid.*, **135** (1902), 696; T. Kametaka, *J. Chem. Soc.*, **83** (1903), 1042; Fokin, *J. Russ. Phys.-Chem. Soc.*, **38** (1906), 419; R. Majima, *Ber.*, **42** (1909), 674.

(8) The formula was proposed by Boeseken and Ravensway, *Rec. trav. chim.*, **46** (1927), 619.

and saponification value, unless heat treatment is effected at unusually high temperature. Most authorities agree that these changes are due to the polymerisation of fatty acid radicals, although some investigators propose different hypothesis as to the exact mechanism.[9] According to Rhodes and Welz[10] the polymerisation of tung oil proceeds in the following schema, forming a tetramethylene linkage by the union of a pair of ethenoid groups,

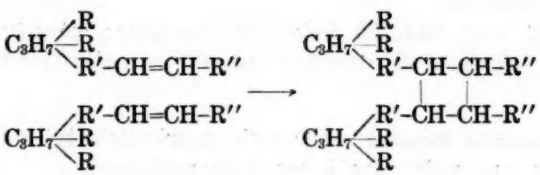

(1).

While Fonrobert[11] supposed that tung oil polymerises after monomolecular reaction as can be concluded from the fact that the decrease in the evolution of heat is too small for bimolecular reaction, when tung oil is diluted by the addition of linseed oil.

It is desirable to study the polymerisation phenomena from the standpoint of chemical kinetics, as few papers have been published along this line. R. H. Kienle[12] studied the kinetics of the baking of tung oil film and found that it proceeds as a first order reaction. While Fuller[13] pointed out that the reaction constant calculated as the first order reaction is not constant, but has a maximum. J. Rinse[14] studied the polymerisation by measuring the refractive index. To compare polymerisation velocity for different temperatures he drew curves of refractive index and temperature, measuring time from the moment when the temperature reached 220°C. neglecting the polymerisation below 220°C. He did not treat the results kinetically. The present author studied the polymerisation of tung oil quantitatively and found that it is a second order reaction.

II. **Experimental Procedure.** An oil bath provided with an electric heater, a stirrer, and a mercury temperature regulator, was filled with

(9) By polymerisation of oil, we mean the result of changes by heating. There may be chances for reactions such as intramolecular and extramolecular polymerisation of glycerides, isomerisations of fatty acid radicals, and cracking and condensation of glycerine radicals.

(10) Rhodes and Welz, *Ind. Eng. Chem.*, **19** (1927), 68.

(11) Fonrobert, *Farben-Ztg.*, **40** (1935), 477, 505, 533, 560, 586.

(12) R. H. Kienle, *Ind. Eng. Chem.*, **22** (1930), 1370.

(13) Fuller, *ibid.*, **23** (193¹), 1458.

(14) J. Rinse, *Rec. trav. chim.*, **51** (1932), 529.

soya bean oil and heated. The temperature was kept constant and a three necked 300 c.c. flask, which contained 250 g. of tung oil, was dipped in it and a gentle stream of carbon dioxide was passed over the surface of the oil. When the required temperature was reached the first 10 c.c. of the oil was taken as a sample in a test tube and chilled quickly by inserting it in cold water. The time was measured from that moment. Samples were withdrawn at suitable intervals and the run was continued until finally the oil gelatinised.

The material used had the following constants: density = 0.9418, refractive index (n_D^{20}) = 1.5191, iodine value (Wijs method) = 166.8, acid value = 1.8.

III. **Experimental Results.** For each sample density, iodine value, relative viscosity, and refractive index were measured.

Increase in density. The density was measured at 15°C. The results are shown in Fig. 1.

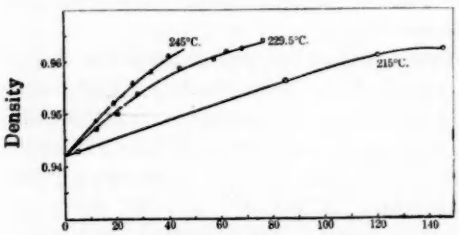

Fig. 1.

Decrease in iodine value. The iodine value is affected by the ratio of halogen solution to oil, by the duration of contact, and by the reaction temperature.

The Wijs reagent used was 0.1 N solution of iodine monochloride, with 2% excess of iodine to chlorine and the temperature was kept exactly at 20°C. during two hours.

If we denote by f the factor of thiosulphate solution for the titration of Wijs solution, by A the number of titration of blank Wijs solution, by B that of actual measurement, and by m the weight of oil, the iodine value is calculated as $(A - B)f/m$ and the ratio Z of halogen solution to oil as Bf/m.

Determinations for each sample were made for two or three values of Z, and the iodine value corrected for $Z = 239.9$ was obtained from the graph of log $[(A - B)f/m]$ versus log Z. The results are shown in Tables 1–3.

Increase in relative viscosity. Samples were dissolved in benzene to 2 and 3% and the viscosity was measured at 30°C. by an Ostwald viscometer described in the previous report.[15] The viscosity constant K_0 was

(15) M. Tatimori, *J. Soc. Chem. Ind., Japan*, **39** (1936), Suppl. binding, 473 B.

Table 1. (206°C.)

Time of heating (min.)	Iodine value
0	—
30	163.7
60	158.1
90	154.3
120	150.4
150	147.9
180	144.9
210	141.1

Table 2. (230°C.)

Time of heating (min.)	Iodine value
0	160.6
8	157.8
16	154.4
24	151.7
32	148.7
40	146.8
48	144.6
56	142.3
64	140.1
72	139.2

Table 3. (245°C.)

Time of heating (min.)	Iodine value
0	164.1
7	160.2
14	154.0
21	150.6
28	146.8
35	143.0
42	140.6

calculated by

$$\eta_{sp} = \frac{\eta_s - \eta_0}{\eta_0} = K_0C + K_1C^2 \qquad (2),$$

where η_{sp} denotes the specific viscosity, η_0 the viscosity of the solvent, η_s that of the solution, C the concentration, and K_0 and K_1 are constants. The author has already[16] discussed the meaning of K_0. For bodied linseed oil K_0 is approximately proportional to molecular weight.

Assuming K_0 to be a constant relating to the molecular weight of the solute, the relative molecular weight, i.e. the ratio of K_0 of bodied oil to that of raw oil, was calculated from the viscosity data and are shown in Fig. 2.

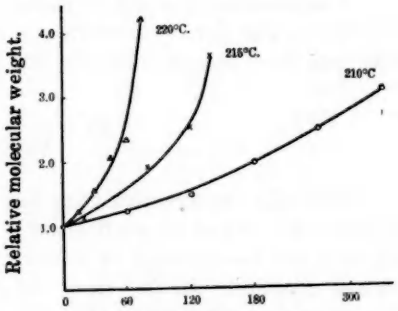

Fig. 2.

Decrease in refractive index. Refractive index was measured by an Abbe refractometer at 20°C. The results are shown in Tables 5–10. The total amount of decrease in refractive index up to gelation is ca. 0.0081 in agreement with the J. Rinse's result.

IV. Kinetics of Polymerisation. *Theoretical consideration.* The molecule of tung oil is composed of three fatty acids, each of which having one active center of polymerisation. Therefore two types of polymerisation are possible, intramolecular polymerisation and extramolecular poly-

(16) M. Tatimori, *J. Soc. Chem. Ind., Japan*, **40** (1937), Suppl. binding, 19 B.

merisation, and it is known[17] that both occur. In this case polymerisation velocity is given by the superposition of the first order and the second order reaction.

From the study of quantities such as iodine value and refractive index, we obtain the concentration of active radicals instead of that of molecules. In this case the concentration of active radicals should be taken into consideration, so that the polymerisation velocity can be expressed by a second order reaction formula,

$$\frac{dx}{dt} = K_2(a-x)^2 \qquad (3),$$

where x denotes the concentration of polymerised active radicals at time t, a the initial concentration of unpolymerised radicals, and K_2 is a reaction constant.

Then we have

$$K_2t = \frac{x}{a(a-x)} \qquad (4).$$

If we denote by n the refractive index at time t, by n_0 that for $t = 0$, and by n_∞ that for $t=\infty$, then $x = K'(n_0 - n)$ and $a = K'(n_0 - n_\infty)$. By inserting these to equation (4), and putting $K = K_2K'$, we have

$$Kt = \frac{n_0-n}{(n_0-n_\infty)(n-n_\infty)} \qquad (5).$$

Generally the reaction constant can be calculated from equation (5). In reactions such as saponification of esters, n_∞ or the quantity corresponding to it can be obtained by raising the temperature or by prolonging the time of reaction. In this case, the gelation occurs before the polymerisation proceeds to the end, so that the measurement of n_∞ is impossible. This is the difficulty in the kinetical treatment of the reaction. Therefore n_∞ must be calculated. A glance at equation (5) shows that, unknown n_∞ being contained in a quadratic form, it is difficult to calculate the most probable value of n_∞ from the experimental data.

By taking reciprocals of both sides, equation (4) can be transformed as follows,

---

(17) As for intramolecular polymerisation see E. Fonrobert and F. Pallauf, *Chem. Umschau Fette, Öle, Wachse Harze*, **33** (1926), 41; E. Rossmann, *Fette u. Seifen*, **44** (1937), 187. For extramolecular polymerisation see Rhodes and Welz, *Ind. Eng. Chem.*, **19** (1927), 68; Nagel and Grüss, *Wiss. Veröffentl. Siemens-Konzern*, **4** (1925), 284.

$$\frac{1}{aK_2t} = \frac{b}{t} = \frac{a}{x} - 1 \qquad (6),$$

in which a and b are constants.

The relation between $1/t$ and $1/x$ is linear, so that in a graph a straight line should be obtained. This is a conventional method to determine whether a reaction proceeds in the schema (1) or not. a and b can be obtained from the relation of $1/t$ versus $1/x$, and K_2 can be calculated by equation (6).

As an illustration of bimolecular reaction, the decrease of iodine value (at 215°C.) and that of refractive index (at 206°C.) are given in Tables 4–5 and Figures 3–4.

Table 4.

Time of heating (min.)	Iodine value	$\frac{1}{t} \times 10^2$	$\frac{1}{x} \times 10^2$
0	162.6	—	—
20	157.4	5.000	19.23
40	153.0	2.500	10.42
60	149.2	1.666	7.462
80	146.7	1.250	6.289
100	144.9	1.000	5.650
120	142.6	0.833	5.000
140	141.3	0.714	4.695

Table 5. (206°C.)

t	n_D^{20}	$\frac{1}{x} \times 10^{-2}$	$\frac{1}{t} \times 10^3$	K
0	1.5183	—	—	—
30	1.5169	7.14	33.33	0.203
60	1.51575	3.92	16.67	0.201
90	1.51465	2.74	11.11	0.209
120	1.5138	2.22	8.33	0.208
150	1.5130	1.89	6.67	0.210
180	1.5123	1.67	5.56	0.212
210	1.51175	1.53	4.76	0.211
240	1.51115	1.40	4.17	0.215
270	1.5110	1.37	3.70	0.198
				Mean 0.2074

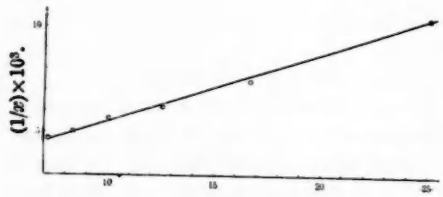

Fig. 3. Relation between reciprocals of iodine value and polymerisation time.

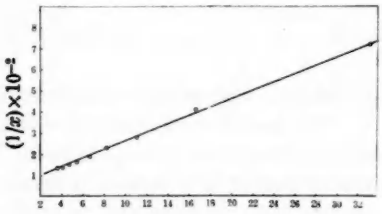

Fig. 4. Relation between reciprocals of refractive index and polymerisation time.

As the accurate measurements of iodine value of polymerised oil are difficult, refractive index is better for the study of the kinetics.

Reaction constants. The changes in refractive index of oils with time at various temperatures can exactly be expressed by equation (6).

Reaction constants were calculated from the refractive index and are given in Tables 5–10.

Table 6. (215°C.)

t	n_D^{20}	$\frac{1}{x} \times 10^{-2}$	$\frac{1}{t} \times 10^{3}$	K
0	1.5159	—	—	—
20	1.5149	10.00	50.00	0.297
40	1.51395	5.13	25.00	0.314
60	1.5131	3.57	16.67	0.324
80	1.5125	2.94	12.50	0.313
100	1.5118	2.44	10.00	0.324
120	1.51125	2.15	8.33	0.326
140	1.5111	2.08	7.14	0.293
				Mean 0.3130

Table 7. (224°C.)

t	n_D^{20}	$\frac{1}{x} \times 10^{-2}$	$\frac{1}{t} \times 10^{3}$	K
0	1.51695	—	—	—
15	1.5157	8.00	66.67	0.432
30	1.5146	4.26	33.33	0.453
46	1.5136	2.99	21.47	0.448
60	1.51275	2.38	16.67	0.466
75	1.5119	1.98	13.33	0.489
91	1.5113	1.77	10.99	0.481
				Mean 0.4614

Table 8. (229.5°C.)

t	n_D^{20}	$\frac{1}{x} \times 10^{-2}$	$\frac{1}{t} \times 10^{3}$	K
0	1.51595	—	—	—
8	1.51505	11.11	125.00	0.658
16	1.51425	5.88	62.50	0.664
24	1.5136	4.26	41.67	0.647
32	1.5130	3.39	31.25	0.644
41	1.5124	2.82	24.39	0.641
45	1.5121	2.60	22.22	0.653
50	1.5119	2.47	20.00	0.632
56	1.5116	2.30	17.86	0.625
64	1.5113	2.15	15.63	(0.605)
				Mean 0.6455

Table 9. (240°C.)

t	n_D^{20}	$\frac{1}{x} \times 10^{-2}$	$\frac{1}{t} \times 10^{3}$	K
0	1.5151	—	—	—
7.5	1.5140	9.09	133.3	0.999
15.0	1.5129	4.55	66.67	1.10
22.5	1.5121	3.33	44.45	1.09
30.25	1.51155	2.78	30.06	1.03
37.5	1.51045	2.41	26.67	1.02
45.0	1.51035	2.11	2.22	1.05
				Mean 1.049

Table 10. (245°C.)

t	n_D^{20}	$\frac{1}{x} \times 10^{-2}$	$\frac{1}{t} \times 10^{3}$	K
0	1.51555	—	—	—
7	1.5142	7.41	142.8	1.26
14	1.51295	3.85	71.43	1.44
21	1.5119	2.74	47.62	1.47
23	1.51115	2.27	35.71	1.41
35	1.5104	1.94	28.57	1.44
4	1.5100	1.80	23.81	1.34
				Mean 1.444

n_∞, n_G, and K are summarised in Table 11, where n_G is the refractive index just before the gelation.

Table 11.

Polymerisation temperature (°C.)	n_∞	n_G	K
245.0	1.5034	1.5100	1.444
240.0	1.5024	1.5104	1.049
229.5	1.5041	1.5113	0.6455
224.0	1.5034	1.5109	0.4505
215.5	1.5026	1.5111	0.3130
210.0	1.5026	1.5111	0.2447
206.0	1.5011	1.5110	0.2074
	Mean 1.5024		

Effect of temperature. The rate of polymerisation was determined at temperatures between 206 and 245°C.

In all cases the whole elapses can be expressed by a bimolecular reaction formula. The relation between reaction constant and temperature is shown in Fig. 5.

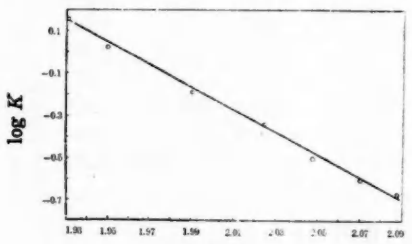

Fig. 5.

Table 12.

t°C.	K	K_1/K_2
240	1.065	1.67
230	0.635	1.62
220	0.392	1.56
210	0.250	

From Fig. 5 it will be seen that a linear relation exists between the logarithm of velocity coefficient and the reciprocal of polymerisation temperature, as can be expressed by the Arrehnius formula,

$$\ln K = C - \frac{Q}{RT} \qquad (7).$$

The values of C and Q were determined as: $C = 5.335$, $Q = 24{,}300$ cal. Temperature coefficient per ten degrees, which has a practical signifi-

cance, was calculated in the temperature range from 240 to 210°C. and is shown in Table 12.

Summary.

(1) Tung oil was polymerised up to gelation at various temperatures from 206 to 245°C. In the course of cooking, density, iodine value, relative viscosity, and refractive index were measured.

(2) Density, iodine value, and refractive index change rather quickly at the beginning but slowly towards the end of polymerisation. The viscosity changes, however, in opposite sense.

(3) The constants of raw oil and of polymerised oil just before the gelation are as follows.

	Raw oil	Polymerised oil
Density	0.9418	0.9631
Iodine value	166.8	140.5
K_0	3.36	13.4
Refractive index	1.5191	1.5109

(4) A new method to obtain the reaction constant is proposed for reactions of the type $A + A \rightarrow A_2$.

(5) This method was applied to the polymerisation of tung oil and the following conclusions were obtained.

(6) The polymerisation is a second order reaction as determined by both refractive index and iodine value.

(7) The polymerisation velocity was calculated between 206 and 245°C.

(8) The heat of activation was found to be ca. 24,000 cal.

(9) The temperature coefficients of the reaction per ten degrees is 1.55–1.67, in the temperature range from 210 to 240°C.

In conclusion, the author wishes to express his sincere thanks to Dr. K. Baba, Mr. T. Yoshioka, and Mr. K. Yokota for their kind guidance.

Laboratory of Hitachi Works, Hitachi Ltd.,
Sukegawa, Ibaraki Prefecture.

A Study of Passivity of Iron Using Electron Diffraction.

By Takeo IIMORI.

(Received December 22, 1937.)

Introduction. Since the discovery of passivity of iron in the eighteenth century, various explanations have been suggested. Lately, through careful experiments and studies, such as the electrolytic isolation of a transparent film by U. R. Evans[1] or the optical observations of L. Tronstad,[2] it has been shown that the phenomenon is definitely associated with a thin protective film on the surface of iron. However, the electron diffration method has not yet given a sufficiently satisfactory result in this study. G. P. Thomson's[3] examination of passive iron in nitric acid does not enable us to determine the composition of the film and the work of E. Rupp[4] merely suggests that the film might be α-Fe_2O_3.

The present author examined iron rendered passive in nitric acid or in a chromate solution by reflective diffraction of electrons from the surface film and also by transmissional diffraction, by first isolating the film. A part of this work has already been reported last year in a paper[5] from the Iitaka Laboratory and the present paper gives further details and also reports on the results of advanced experiments.

The Invisible Film. (a) *Isolation of an invisible film.* The isolation of an invisible film was carried out using the electrolytic method of U. R. Evans. A strip of electrolytic iron (0.15 mm. thick and 1 cm. wide) was cleaned by gentle polishing with emery papers of increasing fineness and then rendered passive by immersing it in a 0.1 N solution of potassium chromate. The passive strip was gently rinsed with water and the end, to be immersed into a 6% solution of sodium chloride contained in an electrolytic cell, was trimmed cross-wise after which it was immersed in the electrolytic bath to the depth of one centimeter. The cell was divided into an anodic and a cathodic section by means of a porous porcelain cylinder. With the passive strip as the anode electrolysis was immediately started, care being taken to maintain the current density constant at 6–7

(1) U. R. Evans, *J. Chem. Soc.*, **127** (1927), 1020.
(2) L. Tronstad, *Nature*, **127** (1931), 127.
(3) G. P. Thomson, *Proc. Roy. Soc.* (London), A, **128** (1930), 657.
(4) E. Rupp, *Kolloid-Z.*, **69** (1934), 375.
(5) I. Iitaka, S. Miyake, and T. Iimori, *Nature*, **139** (1937), 156.

milliamperes per square centimeter throughout the process. And also throughout the electrolysis, fresh sodium chloride solution was continually fed into the cell drop by drop while the excess was overflowed through a siphon. After continuing the electrolysis for some eighteen hours, two transparent, colorless but lustrous films were isolated, one from each side of the strip. The films were carefully scooped up with a piece of fine brass netting and transferred with the netting into water containing a small amount of alcohol and then thoroughly and carefully washed.

(b) *Transmissional electron diffraction by the film.* A piece of the film free from any stain whatsoever was selected, scooped up on a netting and then dipped first into a 50% solution of alcohol and next into a 95% alcohol. After the film was completely dried on a small piece of netting, it was placed with the net into an electron diffraction camera.

The electron beam used was accelerated with about 50 KV. potential (corresponding to about 0.05 Å in wavelength); the exact wavelength was determined from the diffraction pattern of zinc oxide used as a reference, the oxide being placed in the camera always ready for use immediately after each exposure.

In many cases, the films gave diffraction patterns composed up of only two or three vague rings attributable only to nearly amorphous substances; however, as shown in Table 1, in a few cases several rings were distinguished.

Table 1. Diffraction patterns of thin films.

Intensity	Spacing of rings (Å)				Indices of planes	Side of unit cube (Å)
	Exp. 1	Exp. 2	Exp. 3	Exp. 4		
m or *w*			4.5	4.6	(111)	8.0
w				2.96	(200)	8.37
s	2.5	2.53	2.54	2.53	(311)	8.43
s or *m*		2.07	2.09	2.08	(400)	8.32
w				1.63	(333), (511)	8.48
s	1.5	1.48	1.49	1.48	(440)	8.35
w				1.39?	(135)	8.45
					Mean	8.40 Å
			X-ray data[6]		8.380 Å for Fe_3O_4 8.322 Å for γ-Fe_2O_3	

(6) G. Hägg, *Z. physik. Chem.*, B, **29** (1935), 102.

The above table clearly indicates that the thin film is composed of either γ-Fe_2O_3 or Fe_3O_4 and not of α-Fe_2O_3. Many previous investigators, on the contrary, assumed the film to be α-Fe_2O_3. The magnetic property of the film, which is ferromagnetic, confirms without doubt the results as in above and proves that the film is either γ-Fe_2O_3 or Fe_3O_4 and also shows that the previous assumption is erroneous.

(c) *Invisible film on polished iron (not passive).* U. R. Evans[1] first ascertained through experiments that an invisible film similar to the one on passive iron also exists on iron polished in air but in this case the cracks and pores present in the film in countless numbers make it vulnerable to reagents. A piece of non-passive electrolytic iron exposed for several hours to dry air after being polished, also yielded thin films by electrolysis; but in this case, unlike in the passive iron, the film always broke into fragments and were stained badly with rust. It was extremely difficult to select a sufficiently good film for a proper examination of its composition. Diffraction patterns obtained in a few cases were identical with that of Table 1, Exp. 2 or Exp. 1 and show that its composition is the same as that of passive iron.

Reflectional Election Diffraction with Passive Iron. (a) *Iron made passive in concentrated nitric acid.* Examination of iron made passive in concentrated nitric acid gave a result no more revealing than that obtained by G. P. Thomson[3] or E. Rupp.[4] The ring corresponding to 2.6 Å usually showed itself besides the iron pattern and merely indicates the existence of a thin oxide layer of a structure of the type similar to Fe_3O_4. Probably, the oxide layer cannot become any thicker in nitric acid so as to be detectable, because concentrated nitric acid has two properties, that of a strong oxidizer and that of a strong acid. It was observed, as a matter of fact, that iron made passive in a chromate solution after being highly polished, lost its luster and appeared as if etched when left in concentrated nitric acid overnight.

(b) *Iron made passive in potassium chromate solution.* In order to obtain a sufficiently thick protective film for study, potassium chromate solution was selected as the oxidizing reagent which also has the advantage of not dissolving the film. When a polished iron specimen was used, the diffraction pattern indicated no difference from that of non-passive iron; the pattern was identical with that of the invisible film, Table 1, Exps. 1 and 2. On the other hand, when iron etched with concentrated hydrochloric or nitric acid was used, at first a diffraction pattern similar to the one made passive in nitric acid was obtained; but a prolonged immersion in the chromate solution gradually made the iron pattern fainter, finally

turning it into the "Fe_3O_4 pattern". This change took place without any manifestation in the outward appearance of the specimen. (Fig. 2–5).

These results obtained by transmissional and reflectional diffraction of electrons by the protective film clearly indicate that the film on passive iron may be isolated without undergoing any change during the process and that its composition is either γ-Fe_2O_3 or Fe_3O_4.

Supplementary Experiments and Discussion. From examinations made thus far, it can be readily seen that the protective film on passive iron is composed of either γ-Fe_2O_3 or Fe_3O_4 and because the diffraction patterns are similar, it is impossible to make a distinction and consequently some other method must be resorted to in order to make the identification. Hence, the following experiments were carried out:

(a) *Passivity of Fe_3O_4.* When iron coated with Fe_3O_4 by heating in water vapor at 400°C. was immersed in a dilute nitric acid, the oxide coating rapidly dissolved away. On the other hand, when the iron coated with Fe_3O_4 was immersed in concentrated nitric acid, the oxide did not dissolve at all; subsequent immersion in a dilute nitric acid had no effect upon the oxide so treated. Further, treatment of the Fe_3O_4 coating with a chromate solution gave precisely the same result as above. It can therefore be seen that Fe_3O_4 can be rendered passive by treating it with an oxidizing agent. From the diffraction pattern and also from the outward appearance of the oxide film, it is seen that in the above treatment, passivity takes place without visible changes. It naturally follows that the passive state is produced by an oxide having the same diffraction as the superficial layer of Fe_3O_4 previously formed. With due regard of these phenomena, it is conceivable that the protective surface film of passive iron is probably also γ-Fe_2O_3.

(b) *The "unknown primary oxide".* A passive iron giving a good γ-Fe_2O_3 reflection pattern was heated in high vacuum at 600°C. in order to determine whether the oxide will actually transform into α-Fe_2O_3. Instead of this transformation, a very interesting phenomenon took place which is worthy of detailed description here. The heated specimen gave a pattern heretofore unknown among those given by various oxides of iron and in this paper the substance producing the pattern will be referred to as the "unknown primary oxide". This oxide was also obtained in the author's previous work[7] and it was found that its formation took place at a temperature between 200–300°C. or at 500°C. and at a very low pres-

(7) T. Iimori, *Nature*, **140** (1937), 218; *Sci. Papers Inst. Phys. Chem. Research* (Tokyo), **34** (1937), 60.

Fig. 1. The best photograph obtained from a protective film of passive iron.

Fig. 2. Iron.

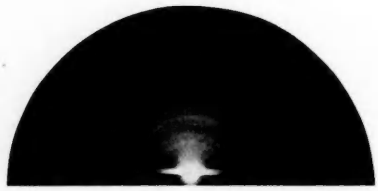

Fig. 5. Passive iron (immersed in a chromate solution 30 days).

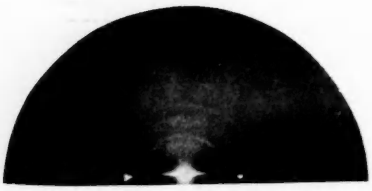

Fig. 3. Passive iron (immersed in a chromate solution 2 hours).

Fig. 6. γ-Fe_2O_3 (formed on etched iron in air at 300°C. and 10 mm.).

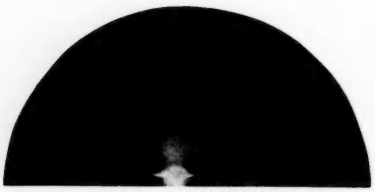

Fig. 4. Passive iron (immersed in a chromate solution 45 hours).

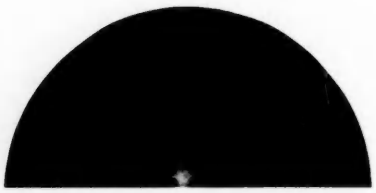

Fig. 7. The "unknown oxide" pattern formed by heating a passive iron at 600°C. in vacuum).

sure. Apparently, the formation of this unknown primary oxide takes place before that of either γ-Fe_2O_3 or Fe_3O_4. In the previous work, the rings obtained were quite vague but in the present case, the pattern was somewhat clearer and the rings identified are shown in Table 2.

Table 2. "Unknown primary oxide."

Spacing of rings (Å)	3.38	2.96	2.53	2.05	1.62	1.48	1.18
Intensity	*s*	*w*	*s*	*s*	*w*	*s*	*m*

Whether the oxide is simple or mixed is yet unknown, moreover, the exact condition favorable to its formation being still quite hazy further consideration cannot be made here. It is supposed, however, that the oxide is formed by the reduction of the protective film by migrating iron atoms.

(c) *Consideration with other experiments.* In the previous paper[7] by the present author, it was reported that the oxide formed on iron at lower temperatures is γ-Fe_2O_3 and the favorable pressure for the formation of Fe_3O_4 approaches that of vacuum as the temperature becomes low. Since the protective film on passive iron is the same as that formed on polished iron by mere exposure to dry air at room temperature, it is obvious that the surface film on passive iron is γ-Fe_2O_3 or, to say the least, some modification of ferric oxide.

Recently, on the basis of electrolytic experiments, U. R. Evans and H. A. Miley[8] are in the opinion that the oxide formed below 200°C. is γ-Fe_2O_3 because although being ferric it seems to be different from α-Fe_2O_3.

W. D. Bancroft and J. D. Porter[9] assumed the protective film on passive iron to be an adsorbed layer of FeO_3 and considered that the transformation from the unstable FeO_3 to the stable Fe_2O_3 occurs during the isolation of the film. But, in view of the fact that diffraction patterns obtained with the isolated film and with the unisolated one are identical, it might follow that the assumption of the existence of a protective film of FeO_3 is superfluous.

In conclusion, the experimental results described above and also their consideration infer that the protective film on passive iron is a layer of γ-Fe_2O_3 forming a perfectly compact covering.

(8) U. R. Evans and H. A. Miley, *J. Chem. Soc.*, **1937**, 1295.
(9) W. D. Bancroft and J. D. Porter, *J. Phys. Chem.*, **40** (1936), 37.

Summary.

The transmissional electron diffraction pattern of the isolated film from passive iron and the reflectional one obtained from iron rendered passive in a chromate solution are in both cases either γ-Fe_2O_3 or Fe_3O_4. Collaborating with the author's previous work and consideration of the passivity of Fe_3O_4, the protective oxide film is believed to be γ-Fe_2O_3.

The author wishes to express his sincere appreciation to Dr. I. Iitaka for his kind guidance and constant encouragement, and to Mr. S. Miyake for his valuable advices and assistance in electron diffraction technique. He also thanks to the Hattori Hôkô Kwai for the financial grant which was used for an improvement of our electron diffraction apparatus.

Iitaka Laboratory,
The Institute of Physical and Chemical Research, Tokyo.

Dipole Moments of Benzil and Stilbene Dichloride.

By **Ken-iti HIGASI.**

(Received December 20, 1937.)

In a famous paper[1] published in 1899, J. Thiele pointed out that benzil might be regarded as having conjugated double bonds. On reduction, its double bonds were supposed to move to the centre, giving an unsaturated glycol, and to prove this view, he succeeded in obtaining the *cis*- and *trans*-forms of the enolic diacetate.

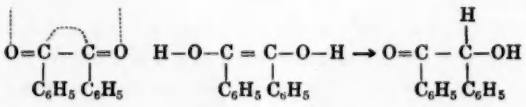

Benzil. Enolic isomer. Benzoin.

Translating this into modern words, the case for benzil may be said as intimately related to single bond-double bond resonance. If the C–C

(1) Thiele, *Ann.*, **306** (1899), 87, 142. See also Waters, "Physical Aspects of Organic Chemistry," 373, London (1935).

single bond aquires a considerable amount of double bond character due to this quantum mechanical resonance, intramolecular rotation should be greatly hindered, and its direct consequence would appear in the temperature independence of dipole moment.[2]

Having this view in mind, the dipole moment of benzil was measured in benzene and carbon tetrachloride at 25 and 50°C. The reason for choosing two different solvents is to check the specific action of solvents.

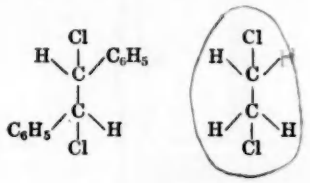

The dipole moment of *a*-stilbene dichloride in benzene and carbon tetrachloride was also studied. This substance resembles $CH_2Cl{\cdot}CH_2Cl$ in structural formula, the only difference being the existence of two C_6H_5 groups instead of two H atoms. From the comparison with the moment of $CH_2Cl{\cdot}CH_2Cl$ in the corresponding solvent, the effect of introducing big phenyl groups was sought.

Preparation of Materials. *Benzil.* Benzoin was first prepared from benzaldehyde and HCN and then was oxidised to benzil. Material thus obtained was recrystallised from alcohol and then from benzene. M.p. 95°C. Benzil was also synthesised from stilbene dichloride, and the dielectric study on it was made for comparison's sake.

a-Stilbene dichloride. This material was obtained by the addition of chlorine to stilbene (purest) of Fränkel and Landau. Recrystallised from alcohol and then from the mixture of benzene and hexane. M.p. 191°C. At first the material recrystallised from alcohol and dried was examined; and the slightly higher moment of 1.50 D was obtained; this seems to be due to the remaining alcohol.

Benzene, hexane, and carbon tetrachloride. Materials from the Schering-Kahlbaum A. G. and the Nippon Zyunyaku Co. were treated as in earlier work.[3]

Experimental Results. As the apparatus and the method of measurement of the dielectric constant were described in a previous paper,[3][4] only some improvements[5] which were made later will be reported here. In the oscillation circuit which contained the dielectric cell, a tetrode

(2) Kozima and Mizushima, *Sci. Papers Inst. Phys. Chem. Research* (Tokyo), **31** (1937), 296.
(3) Higasi, *ibid.*, **24** (1934), 57.
(4) Mizushima, Morino, and Higasi, *ibid.*, **25** (1934), 159.
(5) Cordial thanks are due to Mr. T. Sibata for his kindness in helping the writer in making these improvements.

bulb "Mazda" UY 236 with a screening grid and an indirectly heated cathode, were employed (Fig. 1.). For the switch which connects the dielectric cell to the oscillating circuit, a pen-form one (Fig. 2.) was used

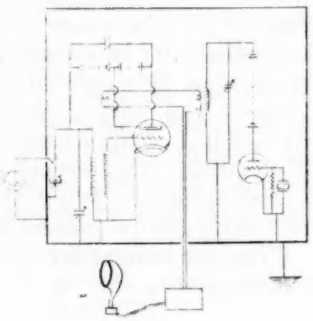

Fig. 1.

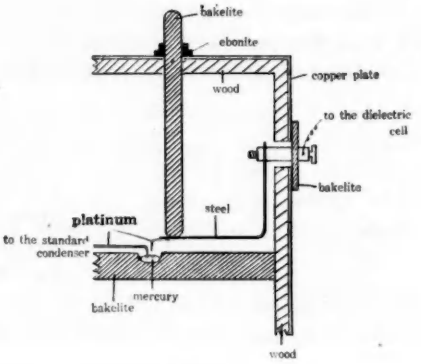

Fig. 2.

in the place of the former. A radio set of ordinary UY 24B, UY 47B, KX 12B type with a slight improvement was satisfactorily utilized for the purpose of amplifying the beat note.

Symbols and formulæ used in this article are as follows:

ω : the concentration of the solute in the gram percentage.
ε, ε_1 : the dielectric constant of the solution and the solvent respectively.
d, d_1 : the density of the solution and the solvent respectively.
p_{12}, p_1 : the specific polarization of the solution and the solvent,

$$p_{12}=\frac{\varepsilon-1}{\varepsilon+2}\cdot\frac{1}{d} \quad \text{and} \quad p_1=\frac{\varepsilon_1-1}{\varepsilon_1+2}\cdot\frac{1}{d_1}, \quad \text{respectively.}$$

P_2 : the molar polarization

$$P_2=M_2\left(p_1+\frac{p_{12}-p_1}{\omega}\right),$$

where M_2 denotes the molecular weight of the solute.

μ : the dipole moment, which is calculated in this article as follows,

$$\mu=0.01273\left[P_{2\infty}-(P_E+P_A)\right]^{\frac{1}{2}}T^{\frac{1}{2}}\fallingdotseq 0.01273(P_{2\infty}-(1+\delta)MR_D)^{\frac{1}{2}}T^{\frac{1}{2}}$$
$$\delta=0.05\sim0.15\,.$$

The estimation of the atomic polarisation in the determination of the dipole moment has been quite arbitrary and sometimes confusing. In the present case where the temperature dependence in moment is to be

examined, the total neglect of the atomic polarisation appears to be much more erratic. In this paper, the atomic polarisation was estimated as 5% of the molecular refraction, MR_D after Groves and Sugden[6] (denoted by μ) and also as 15% after Wolf's school[7] (denoted by μ'). As is clear by the results, the difference in the choice of the atomic polarization hardly affects the temperature dependence (See Table 2).

The results are shown in Table 1. The results on benzil from stilbene dichloride are also recorded in the same table. A glance at it will show that there is no difference in moment in benzene solution between this and the sample from benzaldehyde.

Discussion of Results. The dipole moment of benzil in benzene solution at 25°C. was found as 3.71 D by Hassel and Naeshagen[8] and 3.2 D by Sängewald and Weissberger.[9] The result of the present measurement, $\mu = 3.62$ D lies between them. The moment of α-stilbene dichloride

Table 1.

Benzil (prepared from benzoin).

In benzene at 25°C.

ω	ε	d	p_{12}	p_2	P_2
0.00	2 273	0.87336	0.34112	—	—
0.904	2.3379	0.87525	0.35238	1.587	333
1.610	2.3904	0.87684	0.36117	1.586	333
2.995	2.4951	0.87799	0.37883	1.599	336

$P_{2\infty} = 333$ c.c., $MR_D = 58.92$ c.c.,
$P_A = 5\% MR_D$, $P_E + P_A = 61.87$ c.c., $\mu = 3.62$D
$P_A = 15\% MR_D$, $P_E + P_A = 67.76$ c.c., $\mu' = 3.58$D

In benzene at 50°C.

0.00	2.225	0.84607	0.34269	—	—
0.904	2.2826	0.84824	0.35307	1.491	313
1.610	2.3281	0.84987	0.36106	1.484	312
2.995	2.4176	0.85342	0.37601	1.455	306

$P_{2\infty} = 313$ c.c., $P_E + P_A = 61.87$ c.c., $\mu = 3.62$D
$P_E + P_A = 67.76$ c.c., $\mu' = 3.58$D

(6) Groves and Sugden, *J. Chem. Soc.*, **1935**, 971.
(7) Wolf and Trieschmann, *Z. physik. Chem.*, B, **14** (1931), 346.
(8) Hassel and Naeshagen, *ibid.*, B, **6** (1929), 152.
(9) Sängewald and Weissberger, *Physik. Z.*, **30** (1929), 268.

In carbon tetrachloride at 25°C.

ω	ε	d	γ_{12}	p_2	P_2
0.00	2.232	1.58434	0.18374	—	—
0.6403	2.3094	1.58044	0.19225	1.512	318
0.910	2.3430	1.57888	0.19586	1.516	319
2.096	2.4912	1.57260	0.21114	1.491	314

$P_{2\infty} = 318$ c.c., $P_E + P_A = 61.87$ c.c., $\mu = 3.52$D
$P_E + P_A = 67.76$ c.c., $\mu' = 3.48$D

In carbon tetrachloride at 50°C.

0.00	2.183	1.53501	0.18424	—	—
0.6403	2.2497	1.53217	0.19193	1.385	291
0.910	2.2787	1.53097	0.19520	1.389	292
2.096	2.4104	1.52465	0.20974	1.400	294

$P_{2\infty} = 291$ c.c., $P_E + P_A = 61.87$ c.c., $\mu = 3.46$D
$P_E + P_A = 67.76$ c.c., $\mu' = 3.42$D

Benzil (prepared from stilbene dichloride)

In benzene at 25°C.

0.00	2.273	0.87353	0.34105	—	—
1.150	2.3569	0.87604	0.35551	1.599	336
1.491	2.3817	0.87708	0.35953	1.581	332

$P_{2\infty} = 334$ c.c., $P_E + P_A = 61.87$ c.c., $\mu = 3.63$D
$P_E + P_A = 67.76$ c.c., $\mu' = 3.59$D

In hexane at 25°C.

0.00	1.8871	0.66547	0.34293	—	—
0.524	1.9103	0.66729	0.34886	1.473	309
0.720	1.9182	0.66763	0.35100	1.463	307
1.442	1.9500	0.66966	0.35915	1.467	08

$P_{2\infty} = 308$ c.c., $P_E + P_A = 61.87$ c.c., $\mu = 3.45$D
$P_E + P_A = 67.76$ c.c., $\mu' = 3.41$D

α-Stilbene dichloride.

In benzene at 25°C.

ω	ε	d	p_{12}	p_2	p_2
0.00	2.273	0.87353	0.34105	—	—
0.767	2.2819	0.87548	0.34195	0.4584	115.1
1.254	2.2872	0.87658	0.34252	0.4583	115.1

$P_{2\infty} = 115.1$ c.c., $MR_D = 68.63$ c.c.
$P_A = 5\% MR_D = 3.4$ c.c., $P_E + P_A = 72.0$ c.c., $\mu = 1.45$D

In carbon tetrachloride at 25°C.

0.00	2.225	1.58411	0.18303	—	—
0.1925	2.2286	1.58340	0.18349	0.422	105.8
0.1928	2.2289	1.58339	0.18352	0.437	109.6

$P_{2\infty} = 108$ c.c., $P_E + P_A = 72.0$ c.c., $\mu = 1.32$D

given by Weissberger and Sängewald[10] is recorded as 1.27 D in benzene at 25°C. in contrast to 1.45 D of the present author. The difference between them seems rather large, but on account of the small solubility of this substance in benzene, high accuracy cannot be claimed in an earlier work—in the present case, the accuracy being $\mu = 1.45 \pm 0.06$ D.

Table 2. Dipole moment of benzil.

Solvent / t°C.	C_6H_6		CCl_4	
	μ	μ'	μ	μ'
25	3.62	3.58	3.52	3.48
50	3.62	3.58	3.46	3.42

The result of the present work on benzil is summarised in Table 2. The values of benzene solution are quite independent of temperature, while those in carbon tetrachloride solution slightly decrease with rising temperature.

One must emphasize that this fact is incomprehensible by the ordinary chemical formula of benzil. If the carbon-carbon bond be purely single,

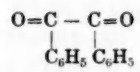

from the analogy of $CH_2Cl{\cdot}CH_2Cl$,[4] it is clear that the stable internal position should correspond to the *trans*-position and measurable increase in moment with rising temperature should result. And if we can attribute the constancy in moment in the benzene solution to the abnormal action

(10) Weissberger and Sängewald, *Z. physik. Chem.*, B, **9** (1930), 133.

of the solvent, how can we explain the result obtained in carbon tetrachloride?

On the other hand, Hassel estimated the moment as 3.78 D, when free rotation occurs, and seemed to consider the agreement with the experimental value to be something more than mere coincidence. But free rotation, which is greatly hindered even in the case of $CH_2Cl{\cdot}CH_2Cl$ (with weaker mutual effect between the rotating groups), is very unlikely to occur.

From the result of Table 2, we may conclude as the following:

(1) The oscillatory rotation of the polar groups near the *trans*-position like that of $CH_2Cl{\cdot}CH_2Cl$ does not occur.

(2) The free rotation of the groups is improbable.

(3) Therefore, the carbon-carbon bond in benzil is different from the pure single bond.

As stated in the introduction, on account of the quantum mechanical resonance the carbon-carbon bond may acquire the double bond character. And the electronic structure of this bond has no longer the axial symmetry and tends to lock the groups either at the *cis*- or the *trans*-position. The dipole moment will be zero at the *trans*-position, while it will be very large at the *cis*-position.

The simplest explanation of the present experiment is to consider the existence of the *cis*-form only, (the *trans*-form having a much larger energy). From this assumption the constancy in the moment follows at once. Then we have to consider that the bond moments of this molecule become very different from the ordinary ones on account of the quantum mechanical resonance.

If, however, we consider the coexistence of the *trans*- and *cis*-configurations, the variation of the moment with temperature should result. And the observable value of the moment should be governed by the Maxwell-Boltzmann's law of distribution. The small decrease in the moment in CCl_4 solution might indicate this effect, but the temperature range of the present research is too small to draw a definite conclusion from it.

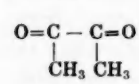

It is very interesting to note that diacetyl is reported to behave just like ethylene dichloride. According to Zahn,[11] its moment increases from 1.25 D at 66° to 1.48 D at 231°. Therefore in spite of its similar structure to benzil, its carbon-carbon bond does not show any marked deviation from the single bond. Although further studies are desirable

(11) Zahn, *Phys. Rev.*, ii, **40** (1932), 291.

to explain it, we should like to point out here that a similar behaviour in dipole moment was recently discovered by Mizushima and Kubo.[12]

Next, we will discuss the moment of α-stilbene dichloride.

Stilbene dichloride has two modifications (I and II of Fig. 3), and α-modification is supposed to be form I.

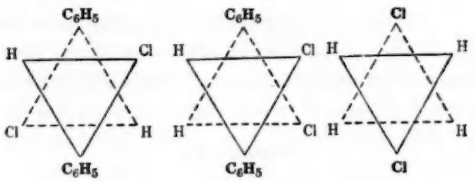

Fig. 3.

In Table 3 the comparison is made of the moments of this substance with those of ethylene dichloride in corresponding solvents.

As benzene is known to exert specific solvent action on ethylene dihalides, the results in carbon tetrachloride are first considered. It is remarkable that α-stilbene dichloride has almost the same moment as ethylene dichloride. As the moment of the rotating group $-CH(C_6H_5)Cl$ is supposed not to be much different from that of $-CH_2Cl$ (the moment of $C_6H_5CH_2Cl$ is 1.85 D in C_6H_6, while that of CH_3Cl is 1.86 D in vapour), this indicates that large phenyl groups do not exert a marked influence on the intramolecular rotation. This is easily understood by the consideration that in form I, the most stable position is the *trans*-position as regards to both phenyl groups and chlorine atoms, and the mutual effect of phenyl groups is not significant owing to large separation.

Table 3. Dipole moment at 25°C.

Solute \ Solvent	CCl_4	C_6H_6
$C_6H_5CHCl \cdot C_6H_5CHCl$	1.32	1.45
$CH_2Cl \cdot CH_2Cl$	1.36[4]	1.75[4]

The moment in benzene is larger than that in carbon tetrachloride. But this tendency is not so strong as it is observed in ethylene dichloride. As an explanation of anomalous behaviour of this substance in benzene, the formation of a loose-complex was proposed in which the mutual posi-

(12) Mizushima and Kubo, this Bulletin, **13** (1938), 174.

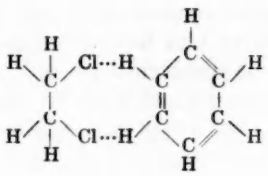

Fig. 4.

tion of two chlorine atoms tends to approach the *cis*-position[4] (Fig. 4.). According to this view, we might consider the case of *a*-stilbene dichloride as follows. This loose complex exists in the benzene solution of stilbene dichloride, too, giving a higher moment. But the two chlorine atoms cannot approach so near as in the case of ethylene dichloride because of the greater repulsion due to two phenyl groups.

Summary.

(1) The dipole moment of benzil was studied in three solvents and its temperature dependence was examined.

(2) The carbon-carbon bond of benzil is not a pure single bond and is probably a hybrid of single and double bonds. This is the result expected from Thiele's old idea of conjugated system and also from the quantum mechanical resonance.

(3) The dipole moment of *a*-stilbene dichloride was also studied in benzene and carbon tetrachloride solution. The result was compared with that of ethylene dichloride.

The research was conducted under the supervision of Professor M. Katayama and the author is specially indebted to Professor S. Mizushima for his guidance. Thanks are also due to Mr. T. Ando for discussions.

The Institute of Physical and Chemical Research,
Hongo, Tokyo.

Zur Theorie der Dielektrizitätskonstante des Gases unter hohem Druck.

Von Masaji KUBO.

(Eingegangen am 20. Dezember 1937.)

Nach der Debyeschen Dipoltheorie,[1] setzt sich die Molekularpolarisation polarer Verbindungen im Gas- oder Dampfzustand aus zwei Teilen, einem konstanten optischen Glied und einem von der Temperatur, aber nicht vom Druck abhängigen Dipolglied, zusammen, nämlich,

$$P = \frac{\varepsilon-1}{\varepsilon+2} V = a + \frac{b}{T},$$

wo P die Molekularpolarisation, ε die Dielektrizitätskonstante, V das Molekularvolumen und T die absolute Temperatur bedeutet. Die für das Material charakteristischen Konstanten a und b sind durch die Molekularkonstanten desselben bestimmt, und zwar

$$a = \frac{4\pi N\alpha}{3}, \qquad b = \frac{4\pi N\mu^2}{9k},$$

wo N die Avogadrosche Zahl, k die Boltzmannsche Konstante und α bzw. μ die Polarisierbarkeit bzw. das Dipolmoment bedeutet. Untersuchungen beim nicht zu hohen Druck haben bestätigt, dass die Debyesche Gleichung sich sehr gut bewährt hat und uns erlaubt, von der Temperaturabhängigkeit der Molekularpolarisation Rückschlüsse auf die Polarisierbarkeit und das Dipolmoment des freien Moleküls zu ziehen. Wir wollen nun über die Abweichung von dem Debyeschen Ausdruck beim hohen Druck diskutieren. Daran schon einige experimentelle Untersuchungen bis zu recht hohem Druck ausgeführt. Dafür ist die theoretische Forschung[2] von grosser Bedeutung, weil sie uns die Kenntnis über die Wechselwirkung der Moleküle untereinander liefert. Im folgenden wird eine Theorie entwickelt, die die Wechselwirkung der Dipole in Betracht zieht.

Wirken gar keine äusseren Kräfte, so ist die Verteilung im Raum der Dipole polarer Gasmoleküle statistisch ganz unregelmässig, d.i. keine

(1) Debye, „Polare Molekeln," (1929).

(2) Darunter ist die Arbeit von Keyes und Kirkwood (*Phys. Rev.*, **37** (1931), 202.) zu nennen. Sie berechneten statistisch den durchschnittlichen inneren Feld in einem Dielektrikum. Vergleiche ferner die Arbeit von Van Vleck (*J. Chem. Phys.*, **5** (1937), 556.).

Richtung in Bezug auf das raumfeste Koordinatensystem ist zur Orientierung des Dipols bevorzugt. Anders ist es beim molekülfesten Koordinatensystem. Wegen der gegenseitigen elektrostatischen Wechselwirkung, sind die Verteilung und die Orientierung der Moleküle nicht mehr unregelmässig, sondern von den Koordinaten abhängen. Es liegt also der Gedanke nahe, dass die von allen anderen Dipolen herrührende elektrische Feldstärke nicht mehr auf dem Anfangspunkt des Koordinatensystems verschwindet und eine kleine Beeinflussung ausübt.

Wir denken uns einen Raum, der polare Gasmoleküle mit dem Dipolmoment m enthält. Ferner wählen wir den Mittelpunkt eines beliebigen Moleküls als den Anfangspunkt der Polarkoordinaten (r, θ, φ), deren Pol oder z-Achse mit der Richtung des Dipols übereinstimmt. Wir bezeichnen mit f_z die z-Komponente der von einem Dipol auf dem Koordinatenanfangspunkt erregten elektrischen Feldstärke, der auf dem Punkt P (r, θ, φ) nach der Richtung (χ, ψ) orientiert ist, wobei χ den Winkel zwischen dem Radiusvektor r und der Richtung des Dipols auf dem Punkt P und ψ die Differenz der Azimute der beiden Dipole um ihre Verbindungslinie bedeutet. Ferner bezeichnen wir das elektrostatische Potential dieser zwei Dipole mit U. Da wir uns nur auf den nicht zu hohen Druck beschränken, ist die Wahrscheinlichkeit, dass mehr als zwei Moleküle gleichzeitig zusammenstossen, äusserst klein. Infolgedessen brauchen wir nur die Wechselwirkung zwischen zwei Dipolen behandeln. Nach dem Maxwell-Boltzmannschen Verteilungsgesetz, ist die Wahrscheinlichkeit, dass ein Molekül sich im Bereich $r \sim r + dr$, $\theta \sim \theta + d\theta$, $\varphi \sim \varphi + d\varphi$, $\chi \sim \chi + d\chi$ und $\psi \sim \psi + d\psi$ befindet, dem Ausdruck $\exp(-U/kT)$ proportional. Daher berechnet sich die von allen anderen Dipolen auf dem Koordinatenanfangspunkt erregte elektrische Feldstärke F_z nach der Formel

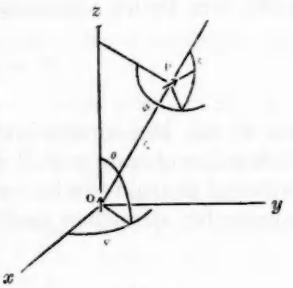

Abb. 1.

$$F = F_z = \int_{2s}^{\infty}\int_0^{\pi}\int_0^{2\pi}\int_0^{\pi}\int_0^{2\pi} f_z C \exp\frac{-U}{kT}\, r^2 \sin\theta \sin\chi\, dr\, d\theta\, d\varphi\, d\chi\, d\psi ,$$

wo C eine Konstante ist. Es ist ohne weiteres klar, dass F_x und F_y nach der Symmetrie verschwinden. Eine einfache Rechnung der Elektrostatik ergibt:

$$f_z = \frac{m}{r^3}(2\cos\theta\cos\chi - \sin\theta\sin\chi\cos\psi) ,$$

$$U = -mf_z = -\frac{m^2}{r^3}(2\cos\theta\cos\chi - \sin\theta\sin\chi\cos\psi) .$$

Wir wollen einfach annehmen, dass der Dipol auf dem Mittelpunkt des kugelförmigen Moleküls[3] liege und eine viel kleinere Ausdehnung als die Wirkungssphäre des Moleküls habe. Ferner nehmen wir an: Das Abstossungspotential, welches stark mit der abnehmenden Entfernung zwischen den zwei Molekülen zunimmt, werde unendlich gross für den Abstand, der kleiner als 2β ist (β = der Halbmesser der Wirkungssphäre des Moleküls), und das Dipolpotential spiele die Hauptrolle in der Wechselwirkung zwischen den beiden Molekülen. Dabei integrieren wir den Ausdruck über den ganzen Raum, ausschliesslich der Kugel, deren Mittelpunkt mit dem Koordinatenanfangspunkt zusammenfällt, und deren Halbmesser gleich 2β ist. Die obere Grenze der Integration nach r kann gleich unendlich gesetzt werden, weil die Ausdehnung des Raums viel grösser als β ist. Wenn man den Ausdruck $\exp(-U/kT)$ nach der Taylorschen Reihe entwickelt und integriert, so bekommt man:

$$F = \frac{4\pi^2 Cm^3}{9kT\beta^3}\left(1 + 1.250\times10^{-3}\frac{m^4}{k^2T^2\beta^6} + 1.156\times10^{-6}\frac{m^8}{k^4T^4\beta^{12}} + \cdots\right).$$

In unserem Fall, wo wir uns nur mit den elektrischen Momenten von der gewöhnlichen Grössenordnung abgeben, werden unter den gewöhnlichen experimentellen Bedingungen das zweite und das dritte Glied usw. gegen das erste vernachlässigt. Um zu zeigen, dass die Näherung genügend genau ist, setzen wir z.B. für Ammoniak bei 150°C. die folgenden numerischen Werte ein, $m = 1.44\times10^{-18}$ e.s.E., $k = 1.37\times10^{-16}$ erg Grad^{-1}, $T = 423$°K. und $\beta = 1.82\times10^{-8}$ cm. Dann beträgt das zweite bzw. das dritte Glied nur zu 4.4×10^{-2} bzw. 1.4×10^{-3} mal das erste, und die obige Formel wird:

$$F = \frac{4\pi^2 Cm^3}{9kT\beta^3} .$$

Um die Konstante C zu bestimmen, berechnen wir die Anzahl der Moleküle, die sich in der Kugel (deren Mittelpunkt mit dem Koordinatenanfangspunkt zusammenfällt) vom Halbmesser l befinden wobei, l eine der Grössenordnung nach mit dem experimentellen Apparat vergleichbare Länge hat. Demnach

(3) Das kugelförmige Molekülmodell wird für Ammoniak gerechtfertigt, dessen drei Protonen sind in der Elektronenwolke des Stickstoffs eingehüllt.

$$1+\int_{2\beta}^{l}\int_0^{\pi}\int_0^{2\pi}\int_0^{\pi}\int_0^{2\pi} C\exp\frac{-U}{kT}r^2\sin\theta\sin\chi\,dr\,d\theta\,d\varphi\,d\chi\,d\psi=\frac{4\pi}{3}l^3n\,,$$

wobei n die Anzahl der Moleküle pro Kubikzentimeter bedeutet. Erinnern wir uns, dass $l^3n\gg 1$ und $l\gg\beta$, so erhalten wir

$$C=\frac{n}{4\pi}\,.$$

Deshalb

$$F=\frac{\pi m^3 n}{9kT\beta^3}\,.$$

Da das Molekül von diesem elektrischen Feld polarisiert wird, wird das elektrische Moment um den Betrag aF vergrössert:

$$m=\mu+aF=\mu\left(1+\frac{\pi a\mu^2 n}{9kT\beta^3}\right),$$

wobei wir m im Korrektionsglied mit μ ersetzen. Beim hohen Druck haben wir anstatt μ (das Dipolmoment des freien Moleküls) m (das wirkliche Dipolmoment unter hohem Druck) in den Debyeschen Ausdruck von P einzusetzen. Wir haben

$$P=\frac{4\pi Na}{3}+\frac{4\pi Nm^2}{9kT}=\frac{4\pi Na}{3}+\frac{4\pi N\mu^2}{9kT}\left(1+\frac{\pi a\mu^2 n}{9kT\beta^3}\right)^2.$$

Da n gleich N/V ist,

$$P=\frac{4\pi Na}{3}+\frac{4\pi N\mu^2}{9kT}\left(1+\frac{2\pi Na\mu^2}{9kT\beta^3 V}\right).$$

oder

$$P=a+\frac{b}{T}+\frac{3ab^2}{8\pi N\beta^3 T^2 V}\,.$$

Das dritte Glied, das als Korrektionsglied zur Debyeschen Gleichung eingesetzt wird, hängt vom Druck ab. Wird P bei konstanter Temperatur als Funktion von $1/V$ aufgetragen, so erwarten wir nach der obigen Gleichung eine gerade Linie, die mit der Abszisse einen endlichen Winkel bildet. Daraus kann man β mittels der Gleichung

$$\beta=\sqrt[3]{\frac{3a(P_\infty-a)^2}{8\pi N\left(\dfrac{\partial P}{\partial(1/V)}\right)_T}}\,.$$

berechnen, wobei P_∞ die zum unendlichen Molekularvolumen extrapolierte Molekularpolarisation ($P_\infty = a + b/T$) bedeutet.

Zunächst wollen wir uns mit den nichtpolaren Gasen beschäftigen. Die Konstanz der Molekularpolarisation, d.h. die Gültigkeit des Clausius-Mosottischen Gesetzes, wurde nach vielen Messungen innerhalb der Messgenauigkeit bis zum sehr hohen Druck an Wasserstoff, an Stickstoff, an Methan und an Luft bestätigt.[4] Dies stimmt mit meiner Theorie gut überein, denn das dritte Glied, welches von dem Druck abhängt, für die nichtpolaren Verbindungen verschwindet.

Für die Molekularpolarisation des Kohlendioxyds fanden Keyes, Kirkwood und Uhlig[5] eine geringe Zunahme mit dem steigenden Druck, während Michels und Michels[6] eine geringe Tendenz zur Abnahme erhielten.[7]

Für Propan fanden Keyes und Oncley[8] eine fast lineare Zunahme der Clausius-Mosottischen Funktion mit der Dichte. Aber der Effekt ist nicht so ausgeprägt wie bei Kohlendioxyd.

Nun wenden wir uns den polaren Gasen zu. Leider ist Ammoniak das einzige, für welches Messungen über das grössere Druckintervall bis jetzt ausgeführt worden sind. Im Gegensatz zu nichtpolaren Gasen fanden Uhlig, Kirkwood und Keyes[5] eine deutliche Zunahme der Molekularpolarisation mit dem Druck. Wie aus der Abbildung 2 ersichtlich, zeigt die Molekularpolarisation bei konstanter Temperatur ein lineares Ansteigen mit $1/V$, was man von meiner Theorie erwartet.[9] Der daraus berechnete Molekularhalbmesser β ist in der Tabelle 1 wiedergegeben. Die dabei notwendige Konstante a wurde aus der zum unendlichen Molekularvolumen extrapolierte Molekularpolarisation P_∞ ermittelt und beträgt

(4) Tangl, *Ann. Physik*, **26** (1908), 59; Occhialini und Bodareu, *Ann. Physik*, **42** (1913), 67; Waibel, *Ann. Physik*, **72** (1923), 161; Broxon, *Phys. Rev.*, **37** (1931), 1338; **38** (1931), 2049; Jordan, Broxon und Walz, *Phys. Rev.*, **46** (1934), 66; Michels und Michels, *Phil. Mag.*, [7], **13** (1932), 1192; Michels, Jaspers und Sanders, *Physica*, **1** (1934), 627; Michels, Sanders und Schipper, *Physica*, **2** (1935), 753; Uhlig, Kirkwood und Keyes, *J. Chem. Phys.*, **1** (1933), 155; McNabney, Moulton und Beuschlein, *Phys. Rev.*, **47** (1935), 695.

(5) Keyes und Kirkwood, *Phys. Rev.*, **36** (1930), 754, 1570; Uhlig, Kirkwood und Keyes, *J. Chem. Phys.*, **1** (1933), 155.

(6) Michels und Michels, *Phil. Trans. Roy. Soc. London*, A, **231** (1933), 409.

(7) John (*Phil. Mag.*, [7], **22** (1936), 274.) versuchte die Dichteabhängigkeit der Clausius-Mosottischen Funktion von Kohlendioxyd durch die Raman-Krishnansche Theorie zu erklären.

(8) Keyes und Oncley, *Chem. Rev.*, **19** (1936), 195.

(9) Da Uhlig, Kirkwood und Keyes das Molekularvolumen von dem Druck nach der experimentell von Beattie und Lawrence (*J. Am. Chem. Soc.*, **52** (1930), 6.) gefundenen Beziehung zwischen Temperatur, Druck und Molekularvolumen berechneten, sind die Werte der Molekularpolarisation vom Fehler frei, der von der Abweichung des nach der Zustandsgleichung berechneten Molekularvolumens von dem wirklichen herrührt.

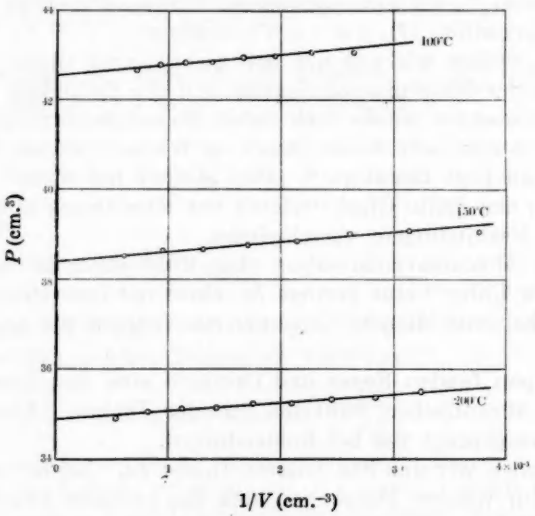

Abb. 2. Molekularpolarisation P von Ammoniak in Abhängigkeit von der Dichte $1/V$ für verschiedene Temperatur.

Tabelle 1.

t(°C.)	P_∞(cm.³)	$\frac{\partial P}{\partial(1/V)}$(cm.⁶)	$\beta \times 10^8$ (cm.)	Mittel	Messungen von
100	41.83	485	1.47	1.45	Keyes und Kirkwood
125	40.05	500	1.41		
150	37.72	410	1.44		
175	36.35	330	1.50		
100	42.55	235	1.90	1.82	Uhlig, Kirkwood und Keyes
150	38.40	225	1.78		
200	34.90	175	1.79		

6.2 cm.³. Zum Vergleich sind in Tabelle 2 die aus den anderen Methoden bestimmten Molekularhalbmesser zusammengestellt. Von den aus der inneren Reibung bestimmten Molekularhalbmessern, wurde der erste aus dem von Rankine und Smith[10] gemessenen gaskinetischen Stossquerschnitt (entnommen dem Tabellenwerk von Landolt-Börnstein), der zweite aus der Sutherlandschen Konstante und der Zähigkeit (Rankine und

(10) Rankine und Smith, *Phil. Mag.*, [6], **42** (1921), 601.

Tabelle 2.

Methode	$\beta \times 10^8$ (cm.)
Druckabhängigkeit der Molekularpolarisation	1.45 1.82
Innere Reibung	1.43 1.48 1.20
Van der Waalssche Zustandsgleichung	1.54

Smith[10] und Vogel,[11] entnommen dem Tabellenwerk von „International Critical Tables") berechnet und der dritte von Braune und Linke[12] gemessen. Auch die van der Waalssche Konstante wurde dem Tabellenwerk von Landolt-Börnstein entnommen. Die Übereinstimmung ist recht gut, wenn man in Betracht zieht, dass eine und dieselbe Messung der inneren Reibung des Gases für den Molekularhalbmesser sogar um 10 Prozent verschiedene Werte ergibt, je nachdem man dazu die Sutherlandsche oder die Reinganumsche Gleichung anwendet.[13]

Diese Theorie wird auch von ganz anderer Seite geprüft. Der elektrooptische Kerr-Effekt hängt eng mit den dielektrischen Eigenschaften zusammen, und zwar hat schon Oka[14] im Anschluss an meine Theorie eine Formel für die Druckabhängigkeit der Kerr-Konstante von Gasen abgeleitet. Auch hier ist das neu eingesetzte Korrektionsglied für nichtpolare Gase gleich Null, so dass bei diesen die bekannte Formel von Langevin und Born gelten muss, wie es auch Messungen an Kohlendioxyd, Methan, Athan und Äthylen bestätigen. Beobachtungen an polaren Gasen innerhalb grösserer Druckintervall sind leider bis heute noch nicht gemacht worden.

Herrn Professor Dr. M. Katayama und Herrn Professor Dr. S. Mizushima danke ich herzlich für ihre wertvollen Ratschläge und Unterstützungen.

Chemisches Institut, Wissenschaftliche Fakultät,
Kaiserliche Universität zu Tokyo.

---

(11) Vogel, *Ann. Physik*, **43** (1914), 1235.
(12) Braune und Linke, *Z. physik. Chem.*, A, **148** (1930), 195.
(13) Vergleiche dazu den Bericht von Titani (*Bull. Chem. Soc. Japan*, **8** (1933), 254.). Im allgemeinen gibt die Reinganumsche Gleichung einen höheren Wert für den Molekularhalbmesser als die Sutherlandsche Gleichung.
(14) Oka, *Proc. Phys.-Math. Soc. Japan*, [3], **19** (1937), 156.

Quantum Mechanical Resonance and Internal Rotation.

By San-ichiro MIZUSHIMA and Masaji KUBO.

(Received December 20, 1937.)

In a series of researches[1][2][3][4] on Raman spectra and electric dipole moments we have discussed the configuration of molecules having an internal degree of freedom. In some cases such as halogenated ethanes,[1] the intramolecular rotation around the C–C single bond is essentially governed by the exchange repulsion, dispersion attraction, and coulombic force between the atoms attached to the different movable groups of the molecule, the electronic structure of the rotation axis giving in itself no preference to any internal configuration. In other cases, however, where the axis acquires partially the character of a double bond due to the quantum mechanical resonance,[2][3][4] the electronic state of the bond has no more the axial symmetry and plays an important rôle in the hindrance of internal rotation,—a phenomenon which is inexplicable, even qualitatively, from the classical chemical theory. As the latter cases are of interest from the standpoint of stereochemistry we want to give further discussion on the resonance effect and especially on carboxylic resonance, supplementing some new experimental data of the dipole moments of the organic vapours.

The complete degeneracy between the two structures $R-C\begin{matrix}O^- \\ \diagdown \\ \diagup \\ O\end{matrix}$ and $R-C\begin{matrix}O \\ \diagdown \\ \diagup \\ O^-\end{matrix}$ in the case of carboxylic ion was treated in our previous communication[3] from the discussion of normal vibration of this ion and especially of the value of force constant for the C···O bond. If we attach a hydrogen atom to one of the two previously equivalent oxygen atoms of carboxylic ion to form acid molecule, the carboxylic resonance is inhibited to some extent and therefore a change in bond character takes place, as can at once be seen from the considerable change in the Raman

(1) Mizushima, Morino, and co-workers, *Physik. Z.*, **35** (1934), 905; **36** (1935), 600; **38** (1937), 459; *Sci. Papers Inst. Phys. Chem. Research* (Tokyo), **25** (1934), 159; **26** (1934), 1; **29** (1936), 63, 111, 188.

(2) Mizushima, Uehara, and Morino, this Bulletin, **12** (1937), 132.

(3) Morino and Mizushima, *Sci. Papers Inst. Phys. Chem. Research* (Tokyo), **32** (1937), 33.

(4) Kubo, Morino, and Mizushima, *Sci. Papers Inst. Phys. Chem. Research* (Tokyo), **32** (1937), 129.

spectrum.[3] We have, however, good reason to believe that the resonance effect is here still large enough as to permit no internal oscillatory rotation of finite amplitude around the C–O axis. For this molecule we can consider the two configurations A and B in Fig. 1 which the resonance effect

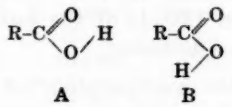

Fig. 1. The two molecular configurations of carboxylic acid.

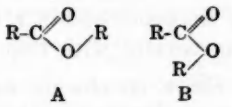

Fig. 2. The two molecular configurations of carboxylic ester.

would allow, but according to the dipole measurement carried out by Zahn[5] almost all the molecules assume the A-form. This must be due to the coulombic attraction between the carbonyl and the hydroxyl bonds, which is superimposed upon the resonance effect, although this electrostatic effect alone is not sufficient to lock the molecule rigidly at the said position. In the case of *o*-chlorophenol the existence of the two molecular forms 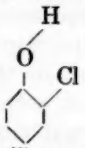 and 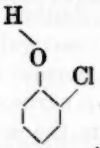 predicted by the assumption of resonance[6] can be shown experimentally by the observation of the infrared absorption spectra, corresponding to the first,[7] second,[2] and third overtones[2] of the O–H vibration (each of them has two absorption maxima corresponding to these two molecular species). For the molecule of acetic acid vapour, however, we[8] have found only one absorption maximum for each of the second (9760 Å) and third overtones (7501 Å), which supplies with another experimental evidence as to the existence of the only one stable form of the carboxylic acid molecule (i.e. form A).

There will be some further inhibiting effect on the carboxylic resonance if we replace the hydrogen atom of the acid molecule by an alkyl radical to form ester molecule. The observed values of ester moments as well as their temperature independence show, however, that the resonance effect is still considerable and the molecules are locked at the position of A in Fig. 2 without performing oscillatory rotation about this

(5) Zahn, *Phys. Rev.*, **37** (1931), 1516; *Trans. Faraday Soc.*, **30** (1934), 804.
(6) Pauling, *J. Am. Chem. Soc.*, **58** (1936), 94.
(7) Wulf and Liddel, *J. Am. Chem. Soc.*, **57** (1935), 1464.
(8) Mizushima, Kubota, and Morino, to be published shortly.

stable position at all ordinary temperatures. So far as we know, such an observation has been carried out only by Zahn[9] and in view of the importance of this conclusion in stereochemistry, we have undertaken the reexamination of the dipole moment of methyl acetate in the vapour state. The result was that over a temperature range of 180° (from 34.5 to 209.2°C.) we could obtain a constant value 1.69_6 D of the ester moment in good agreement with that of Zahn's measurement.

The above conclusion as to the stable configuration of the ester molecule was obtained by comparing the observed value of moment with that calculated by vectorial addition for form A in Fig. 2. Although the quantum mechanical resonance makes the values of bond moments in the actual "mesomeric" molecule more or less different from those of the pure C=O, C−O, and O−R bonds respectively, there would scarcely be doubt that form A is the more stable. In any way the energy difference between the two molecular forms shown in Fig. 2 must be so large that we could almost speak of a normal and an excited state, otherwise we would find an observable temperature dependence of the ester moment according to the Maxwell-Boltzmann distribution. For the more exact treatment of the problem it is desirable to investigate the vibration spectra of esters, although the discussion of the normal vibration in this case must be much more difficult than that for carboxylic acid, whose O–H bond vibration can easily be separated from the other normal vibrations.

It is now very interesting to see to what extent such a resonance effect can hinder the intramolecular rotation, if we make a substitution in the ester molecule. When we replace the hydrogen atom of formic ester by a methyl group to form acetic ester, there is no change in the rigidity of the internal state which reveals itself in the observed value of dipole moment. If, however, we replace it by a methoxyl group to form methyl carbonate, the situation becomes quite different and as we reported in our previous communication,[4] the dipole moment of this vapour increases considerably as the temperature is raised (Compare Table 1),—i.e. while for carbonate ion there is complete degeneracy among the three structures

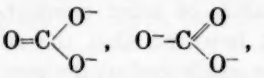

, and

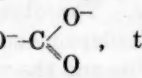

, the electronic state of methyl carbonate can better be approximated by the classical formula

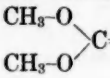

than in the case of carboxylic esters.

(9) Zahn, *Physik. Z.*, **33** (1932), 730.

Instead of methoxyl group we have next chosen chlorine as the substituent atom to study the effect of quantum mechanical resonance on the internal rotation of methyl and ethyl chloroformates. From the result of our dipole measurement in Table 1 it is easily shown that these molecules

Table 1. Dipole moments of several esters in the vapour state.

Dimethyl carbonate (P_E = 18.5 c.c.)		Methyl chloroformate (P_E = 16.7 c.c.)		Ethyl chloroformate (P_E = 21.2 c.c.)	
t(°C.)	m(D)	t(°C.)	m(D)	t(°C.)	m(D)
55.0	0.86	34.6	2.38	35.0	2.56
76.9	0.89	78.0	2.40	76.9	2.47
139.1	0.94	140.2	2.29	137.6	1.79
206.2	1.00_5	207.4	1.68	207.3	1.43

must exert internal oscillatory rotation, the amplitude of which is easily affected by the change of temperature. The C–O bond in the actual "mesomeric" molecule of these substances cannot, therefore, have such an amount of double bond character as in the case of simple carboxylic esters, for which practically the complete inhibition of internal rotation is realized at all ordinary temperatures by the said quantum mechanical force. To determine the stable configuration of these chloroformate molecules we have calculated the resultant moment as the function of the azimuthal angle φ, $\varphi = 0$ corresponding to the closest approach of the alkyl group to the chlorine atom (See Fig. 3). Assuming the values of the bond moments as m(C–Cl) = 1.86 D, m(C=O) = 2.75 D, and m(C–O) = 1.13 D, we obtain the maximum value of the resultant moment of 2.15 D for $\varphi = 0$, which decreases monotonously till it attains the minimum value of 1.58 D at $\varphi = \pi$. By comparing these calculated values with the observed (Table 1), we can easily understand that the stable internal position should correspond to that for $\varphi = 0$, although the quantitative comparison between them may be of small significance, because of the neglect of the mutual effect between bond moments as well as the resonance effect.

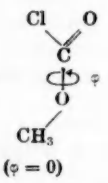

Fig. 3. Intramolecular rotation of methyl chloroformate.

Experimental.

Preparation of materials. Methyl acetate: Kahlbaum's sample "pure" was dehydrated over calcium chloride and subjected to fractional distillation; b.p. 57.2–57.7°C.

Methyl chloroformate: Kahlbaum's sample was purified by fractional distillation; b.p. 71.4–72.4°C.

Ethyl chloroformate: Takeda's sample was dehydrated over calcium chloride and fractionally distilled; b.p. 92.5–93.5°C.

The dielectric constant ε of the vapour was determined with the apparatus previously described[10] and the polarization P was calculated by means of the equation $P=[(\varepsilon-1)/(\varepsilon+2)]V$, in which V is the molar volume. The latter was calculated by using the van der Waals equation of state for methyl acetate. As the greatest deviation from the ideal gas law was less than 0.5% for this substance, we have used this law in evaluating the molar volume of the other two compounds, for which the van der Waals constants have not been reported.

The results of the measurements for methyl acetate are shown in Table 2. The polarization P was found to be a linear function of $1/T$, for which a least squares

Table 2. Dielectric constant ε and molecular polarization P of methyl acetate in the vapour state.

T(°K.)	p(mm.)	$(\varepsilon-1)\times10^6$	V(l.)	P(c.c.)	Mean
307.5	94.9	1126	202.0	75.92	
	131.7	1560	145.6	75.75	
	134.6	1611	142.4	76.55	
	147.8	1765	129.7	76.39	76.15
328.5	90.0	986	227.8	74.86	
	90.5	971	226.3	73.30	
	112.5	1198	182.1	72.78	
	162.6	1731	126.0	72.72	73.41
350.5	146.1	1412	146.8	69.20	
	190.8	1835	112.4	68.82	
	197.4	1898	108.7	68.80	
	208.8	2010	102.7	68.86	68.92
378.1	112.6	940	209.4	65.66	
	139.0	1150	169.7	65.06	
	145.6	1195	162.0	64.62	
	180.7	1489	130.6	64.85	65.05
410.5	171.6	1245	148.8	61.80	
	206.2	1478	123.7	61.00	
	209.9	1530	121.7	62.08	
	242.2	1785	105.3	62.71	61.90
482.2	221.4	1235	135.6	55.81	
	229.4	1229	130.9	53.60	
	234.6	1296	128.0	55.32	
	247.5	1358	121.3	54.93	54.91

(10) Kubo, *Sci. Papers Inst. Phys. Chem. Research* (Tokyo), **26** (1935), 242; **27** (1935), 65; **32** (1937), 26.

solution gives:

$$P = 18.1_5 + 1.785 \times 10^4/T.$$

From the second term of this equation we can calculate the value of dipole moment as 1.69_6 D and from the first that of atomic polarization as 0.6_5 c.c. by subtracting the molar refraction 17.5 c.c. extrapolated to infinite wave length. Thus in the accuracy attainable by the present experiment the dipole moment of this ester remains constant over the above temperature range.

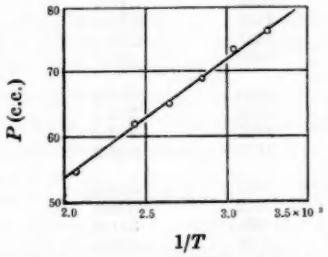

Fig. 4. The molecular polarization of methyl acetate.

The values of molecular polarization obtained by Zahn are in good agreement with those of the present measurement, but as he assumes the sum of electronic and atomic polarizations to be 19.4 c.c., his value of dipole moment decreases slightly with temperature from 1.69 D at 54.2°C. to 1.66 D at 243.3°C. and is equal to 1.67 D in the mean.

The experimental results for the two chloroformates are given in Table 3 and 4 and in Fig. 5. As can be expected for homologous series, the curves for the two

Table 3. Dielectric constant ε and molecular polarization P of methyl chloroformate in the vapour state.

T(°K.)	p(mm.)	$(\varepsilon-1)\times10^6$	V(l.)	P(c.c.)	Mean
307.7	112.9	2384	170.0	135.1	
	123.2	2565	155.7	133.1	
	136.2	2840	140.8	133.3	
	138.5	2813	138.5	130.0	132.9
351.1	125.1	2041	175.0	119.2	
	140.3	2329	156.1	121.1	
	141.0	2335	155.4	121.0	
	151.9	2492	144.3	119.9	120.3
413.3	137.0	1579	188.2	99.0	
	157.2	1769	164.0	96.7	
	157.6	1770	163.6	96.6	
	160.7	1780	160.5	95.2	96.9
480.5	204 5	1042	146.5	51.0	
	212.7	1152	141.0	54.2	
	215.4	1167	139.1	54.1	
	217.1	1201	138.0	55.2	54.6

Table 4. Dielectric constant ε and molecular polarization P of ethyl chloroformate in the vapour state.

T(°K.)	p(mm.)	$(\varepsilon-1)\times10^6$	V(l.)	P(c.c.)	Mean
308.1	56.3	1366	341.6	155.5	
	57.3	1405	335.6	157.2	
	64.5	1581	298.1	155.0	
	67.1	1600	286.6	152.8	155.1
350.0	56.8	1030	384.4	132.0	
	56.8	1016	384.4	130.1	
	58.6	1052	372.7	130.7	
	62.0	1127	352.2	132.4	131.3
410.7	78.7	645	325.6	70.0	
	79.1	672	324.0	72.6	
	79.7	664	321.5	71.2	
	87.5	746	293.0	72.8	71.7
480.4	70.7	354	424.0	50.0	
	73.5	375	407.9	51.0	
	74.2	359	404.0	48.3	
	75.6	377	396.2	49.8	49.8

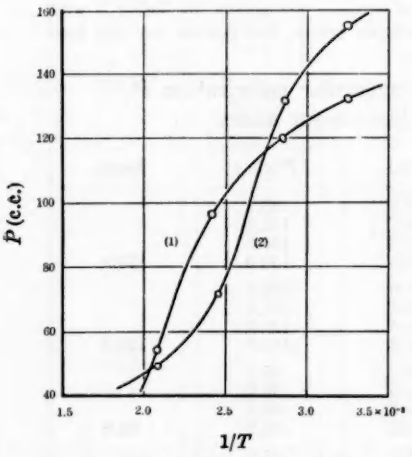

Fig. 5. The molecular polarizations of methyl chloroformate (1) and ethyl chloroformate (2).

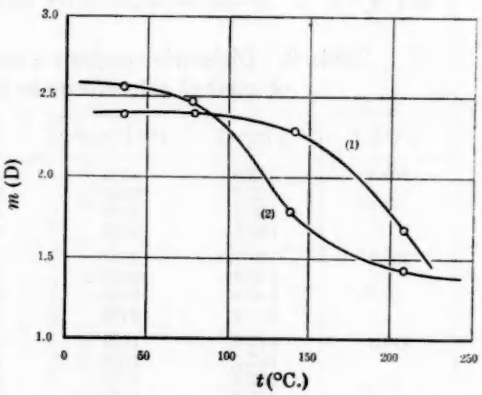

Fig. 6. The dipole moments of methyl chloroformate (1) and ethyl chloroformate (2).

compounds show an analogous behaviour. P is not here a linear function of $1/T$, indicating that the values of dipole moments change with temperature. To ascertain that no appreciable thermal decomposition took place in our measuring condenser we made the following observation in the case of ethyl chloroformate.[11] After the sample was evaporated to an appropriate pressure in the gas condenser previously evacuated, the cock was closed to separate the vapour chamber from the vessel containing the liquid sample, and the variation of pressure was carefully observed. After a few ten seconds the pressure attained a value, which remained constant. If decomposition had been occurring, there would have been the increase of pressure with time. The vapour was at last pumped out and was caught in a vessel cooled by the mixture of solid carbon dioxide and acetone. The colourless liquid, which condensed, showed the specific properties of the substance.

For these substances we have to calculate the dipole moments from the orientation polarization $P_O = P - P_A - P_E$ at each temperature. We assume, for each substance, that the atomic polarization amounts to 10% of the electronic polarization or the molar refraction extrapolated to infinite wave length. The values of dipole moments calculated by means of the usual relation $m = 0.0127\sqrt{P_O T}$ are shown in Table 1 and in Fig. 6. No data for the moment in the vapour state as well as in solution have been found in the literature to be compared with those of our observation on these two compounds.

We thank Prof. M. Katayama for his kind advices. Our thanks are also due to Nippon Gakujutsu-Shinkokai for a grant in aid of this research.

Summary.

The effect of single bond—double bond resonance upon the internal rotation was discussed for carboxylic acids and their derivatives. In acids and esters the strong carboxylic resonance imparts the double bond character to the C–O bond of the actual "mesomeric" molecule to such an extent that practically the complete inhibition of the internal motion is realized at all ordinary temperatures, while the replacement of hydrogen of H–COOR by chlorine or methoxyl group greatly reduces this double bond character, so that the internal oscillatory rotation of finite amplitude can take place about the C–O bond as axis.

Chemical Institute, Faculty of Science,
Tokyo Imperial University.

(11) Ethyl chloroformate decomposes slowly from 250°C. as:
$ClCOOC_2H_5 \rightarrow C_2H_5Cl + CO_2$ (Beilstein).

The Motion of Ethylene Halide Molecules in Crystals as Revealed by the Raman Effect.

By San-ichiro MIZUSHIMA and Yonezo MORINO.

(Received December 20, 1937.)

The conspicuous difference in the Raman spectra of ethylene dihalides between the liquid and solid states reported in our previous paper was explained as due to the considerable change of the intramolecular state upon solidification.[1][2] Below the freezing point the molecules are almost all in the *trans* configuration 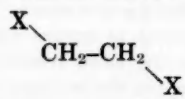 , while in the liquid state or in solutions there is a considerable deviation of the mean internal state from this stable position. (It was shown by our calculation[2] of normal vibrations that the Raman lines observed in the solid state all correspond to the symmetric vibrations to the centre of symmetry of the *trans* form.) The sharp drop of dielectric constant of ethylene chloride and bromide at the freezing point recently observed by White and Morgan is in conformity with our conclusion, which is discussed fully in their communication.[3]

In the vicinity of the unmodified line there seemed to exist other Raman lines which we could not resolve from the primary line in our former measurement. As it is doubtless important for the investigation of intermolecular state to confirm the existence of such low frequency lines, we have reexamined the Raman spectra of ethylene chloride and bromide with a spectrograph of our own construction having a larger dispersion and higher luminocity than the former one (dispersion 10 Å/mm. at 4000 Å). As was expected we could really observe fairly intense Raman lines in the said frequency region both as Stokes and anti-Stokes—for ethylene chloride at −40°C. a diffuse line was observed at 66 cm.$^{-1}$, and for ethylene bromide at 0°C. a line of the same nature at 49 cm.$^{-1}$, while for the latter substance at −40°C. two sharp and fairly intense lines appeared at 41 and 53 cm.$^{-1}$ respectively (see Figs. 1 and 2).

(1) Mizushima, Morino, and Noziri, *Nature*, **137** (1936), 945.

(2) Mizushima, Morino, and Noziri, *Sci. Papers Inst. Phys. Chem. Research* (Tokyo), **29** (1936), 63.

(3) White and Morgan, *J. Chem. Phys.*, **5** (1937), 655.

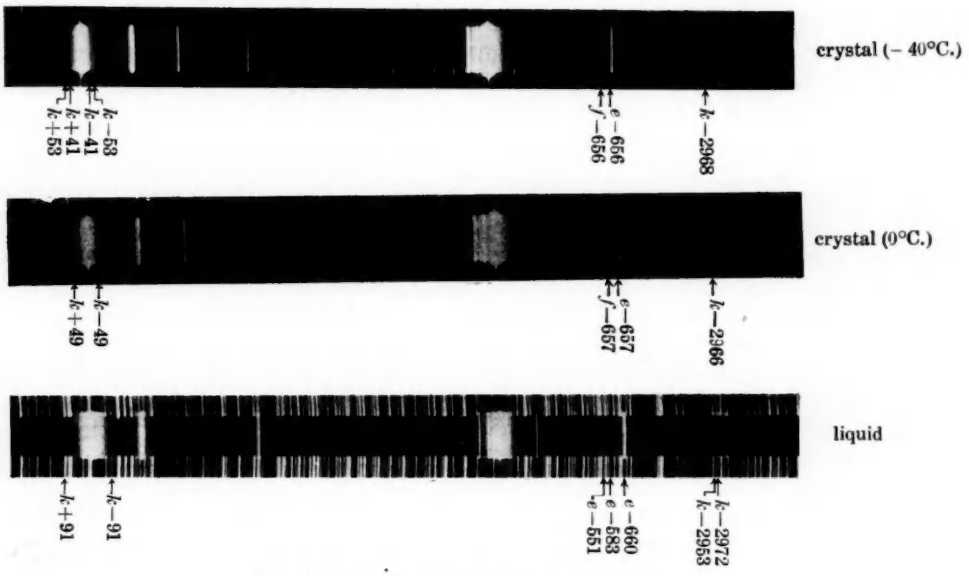

Fig. 1. Raman spectra of ethylene bromide.

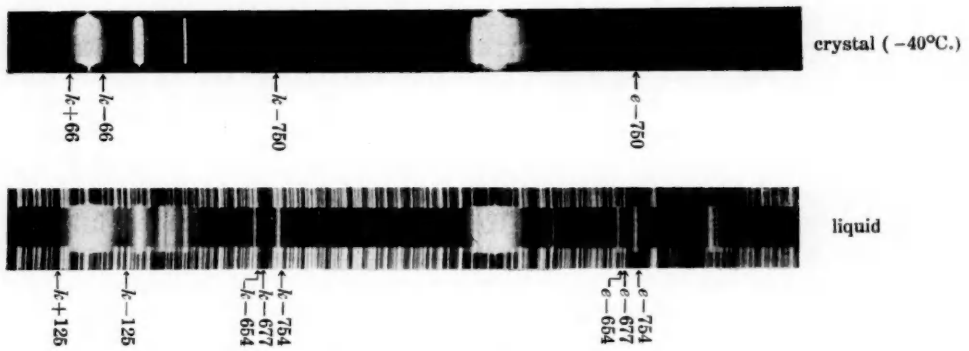

Fig. 2. Raman spectra of ethylene chloride.

It is very interesting to consider the observed change in Raman spectrum of the crystalline ethylene bromide in connection with the thermal transition observed at −24°C. by White and Morgan,[3] from which it may be concluded that these low frequency lines correspond to some motion of a molecule as a whole in the crystal lattice. There are two more reasons which would justify this conclusion: (1) we could observe no line (at least of the comparable intensity) in this frequency region of the liquid spectra, (2) the frequencies of these lines are too low to be identified with any of the internal normal vibrations,[4] as can be seen from our calculation for these molecules.[2]

Let us tentatively assume that these low frequency lines correspond to lattice frequencies and see how far we can treat our interesting experimental results with this assumption. In these crystals the van der Waals force between the halogen atoms would play the leading part in forming the molecular lattice, because of the greater polarizability of these atoms. This is also in conformity with the appearance of these lattice frequencies as the Raman effect, since there can also take place a considerable change in polarizability for the lattice vibration in such a crystal.

Before entering into the detailed discussion of this problem, we have to consider somewhat about the intramolecular state as revealed by the lines of higher frequencies. The values of Raman frequencies observed in the present experiment are no doubt of greater precision than those reported in our previous communication because of the larger dispersion of the spectrograph used. As far as, however, the conclusion given previously[2] is concerned, nothing need be changed. The disappearance of some of the liquid lines in the solid spectrum, which was the most important result of our previous experiment, has acquired further confirmation by the high luminocity of the present apparatus,—e.g. in the solid spectra we could observe distinctly the Raman lines excited by Hg-*f* and Hg-*g*, which correspond to the symmetric C–X vibrations (750 cm.$^{-1}$ for $C_2H_4Cl_2$ and 656 cm.$^{-1}$ for $C_2H_4Br_2$), but could find no trace of strong liquid lines to be found in their vicinity even by Hg-*e* excitation (654 cm.$^{-1}$ for $C_2H_4Cl_2$ and 551 cm.$^{-1}$ for $C_2H_4Br_2$). Thus it is quite sure that below the freezing point the molecule of ethylene halide is in a nearly pure *trans* state and the thermal transition observed for ethylene bromide at −24°C. has no effect on this intramolecular configuration.

(4) The intramolecular oscillatory rotation about the *trans* position (compare footnote (5)), which can have a frequency value of this order of magnitude, is not allowed in the Raman effect for the solid state, since this normal vibration is antisymmetric to the centre of symmetry of the *trans* configuration.

Returning to the problem of intermolecular motion, let us consider that the change in Raman spectrum of crystalline ethylene bromide is caused by the transition observed at −24°C. Then the said change of Raman lines must be due to the change in the molecular lattice. Now many thermal transitions are doubtless caused by the setting-in of molecular rotation in the crystal lattice, for which Pauling[5] first gave a theoretical treatment. The transition observed for ethylene bromide cannot, however, correspond to the onset of three dimensional molecular rotation in the crystal lattice, as can easily be seen from the following discussion. We have already stated that upon solidification the intramolecular rotation about the C–C axis is greatly restricted and the molecule assumes practically the pure *trans* form. This must be explained in terms of crystal forces. Such a specific effect of these forces in fixing the shape of the molecule would not be expected, if it were rotating about three axes. Taking into account our former result in Raman measurement,[1] White and Morgan explained the thermal transition of ethylene bromide observed by them as due to the onset of molecular rotation about only one axis, i.e. that of the zigzag Br–C–C–Br chain. Rotation about this axis does not contradict the existence of the said crystal forces which keep the molecules of the solid in a nearly pure *trans* state and it would not require a large amount of energy which is consistent with the small value of heat of transition estimated by White and Morgan.[3] The commencement of such a molecular rotation necessarily causes a change in the molecular field in the crystal lattice which affects the value of force constant and consequently the frequency of a normal vibration. The small frequency shifts observed for some of the lines of crystalline ethylene bromide (see Table 1) might be interpreted as due to such a change in the molecular field on passing through the transition point. That we have found no appreciable change in frequency on fusion (see Table 1), would then be of particular interest, when we consider that the molecules are rotating in the liquid state as well as in the solid state above the transition point. The experimental error in the reading of each line is different according to the character of the line and consequently

Table 1. Frequency changes in some of the high frequency lines of ethylene bromide.

Crystal		Liquid
−40°C.	0°C.	
2848	2857	2859
3020	3013	3013

(5) Pauling, *Phys. Rev.*, **36** (1930), 430; see also Smyth, *Chem. Rev.*, **19** (1936), 329.

we cannot treat these small frequency shifts for all lines with the same accuracy, although the complete treatment would be desirable from the view-point of the modern theory of the liquid state (quasi-crystalline structure). In this connection we want to mention the existence of a very diffuse line of the frequency of 91 cm.$^{-1}$ observed in the liquid spectrum. At the present stage we cannot conclude that this line corresponds to the line of 49 cm.$^{-1}$ observed for the solid at 0°C., indicating the quasi-crystalline structure of the liquid. It is also probable that this line corresponds e.g. to the intermolecular vibration of a conglomerate of molecules existing only in the liquid state. In any case this line has frequency too low to be indentified with any of the internal vibration of ethylene bromide molecule as can easily be seen from our previous calculation.[2]

The spectrum of crystalline ethylene chloride at −40°C. has only one Raman line in the region of the unmodified line and the nature of this line is similar to that of the corresponding line of crystalline ethylene bromide at 0°C. Moreover, on fusion there have been observed no appreciable frequency shifts of the two hydrogen vibrations (2874 cm.$^{-1}$ of solid to 2874 cm.$^{-1}$ of liquid and 3005 cm.$^{-1}$ of solid to 3004 cm.$^{-1}$ of liquid) corresponding to the two bromide lines discussed above. These may suggest that the molecule of ethylene chloride exerts one dimensional rotation around the axis of the zigzag Cl–C–C–Cl chain at this temperature and also at considerably lower temperatures, since there was found no transition point in the thermal measurement by White and Morgan down to −95°C. We have then to consider that the potential hump restraining the said one dimensional rotation in the crystal is smaller for ethylene chloride than for ethylene bromide and the molecules of the former substance can exert rotation at lower temperatures than those of the latter.

One might doubt if the thermal energy at −95°C. can give rise molecular rotation for ethylene chloride, while it cannot cause rotation for ethylene bromide below −24°C. The alternative possibility is that the molecules of ethylene chloride are fixed in the lattice or performing only the oscillatory rotation around the equilibrium orientations (this should not be confused with the intramolecular oscillatory rotation with which we have been dealing[6]). It is conceivable that because of the difference in size between chlorine and bromine atoms the potential hump acting against the one dimensional rotation becomes so large in the crystal of ethylene chloride as to permit no rotation below the freezing point. It is obviously too early at the present stage to give decision between these

(6) Mizushima, Morino, and co-workers, *Physik. Z.*, **35** (1934), 905; **36** (1935), 600; **38** (1937), 459; *Sci. Papers Inst. Phys. Chem. Research* (Tokyo), **25** (1934), 159; **26** (1934), 1; **29** (1936), 63, 111, 188; **31** (1937), 296; **32** (1937), 33, 129, 220.

two alternative possibilities. The investigation of the Raman spectrum of ethylene iodide, which we have already begun, might throw light on this problem.

We have no intention of giving here a conclusive explanation for our experimental result. The object of the present paper is to report these very interesting observations and to suggest a probable explanation for them.

Experimental.

In the present investigation we used a spectrograph of higher luminocity and a mercury lamp of stronger radiation than in our previous measurement. This together with the use of Agfa Isopan ISS film considerably reduced the time of exposure. For the crystals the longest exposure in the present experiment amounted to 15 hours, which would correspond to an exposure of more than two hundred hours with our previous apparatus. In order to investigate the region of the unmodified line, it is important to avoid as much as possible all parasitic light and stray reflections from the face of the crystals. This condition was secured by using carefully distilled liquids, which was allowed to solidify to a uniform mass. As the filters we have used, according to the suggestion of Ananthakrishnan,[7] dilute as well as con-

Table 2. The Raman spectra of $C_2H_4Cl_2$.

Solid state (−40°C.)			Liquid state					
			Present authors			Ananthakrishnan		
66	(4b)	$k\pm$						
	v							
	v		125	(5b)	$e\pm, k\pm$	123	(4b)	D
			265	(5)	$e\pm, k, i$	263	(2)	P
302	(5)	e, k	300	(8)	$e\pm, k, i$	302	(8)	P
	v		411	(5)	$e\pm, k, i$	411	(3)	D
	v		654	(8)	$e\pm, k, i, f$	654	(10)	PP
	v		677	(6b)	$e\pm, k, i$	675	(3)	D
750	(10)	e, k, i, f	754	(10b)	$e\pm, k, i$	754	(15b)	P
	v		881	(4)	e, k	880	(1)	D
	v		943	(5)	$e, [k]$	940	(2)	P
992	(3)	e, k	989	(2)	e, k			
			1031	(2)	e, k			
1059	(3)	e, k	1052	(4)	e, k	1052	(1)	P
			1145	(3)	e, k	1144	($^1/_2$)	D
	v		1207	(5)	e, k	1206	(2)	D
1265	(2b)	k	1264	(3)	e, k	1262	(1)	D
1301	(5b)	k	1304	(6)	e, k	1302	(3)	P
			1393	(1)	e, k			
	v		1429	(6)	e, k	1429	(3)	D
1448	(2b)	e, k	1445	(4b)	e, k	1440	($^1/_2$)	D
			2844	(3)	e, k	2844	(1)	?
2874	(3)	e, k, i	2874	(4)	e, k	2872	(1)	P
2964	(10)	e, k, i	2957	(10)	e, k, i	2956	(12b)	PP
3005	(6)	e, k, i	3004	(8b)	e, k, i	3002	(4b)	D

(7) Ananthakrishnan, *Proc. Indian Acad. Sci.*, A, **5** (1937), 76.

centrated solutions of iodine in carbon tetrachloride, which proved to be quite useful for our present purpose.

The results of our Raman measurement are shown in Tables 2 and 3, in which there is listed for each observed line: first, its frequency in cm.$^{-1}$; second, in parenthesis, its intensity as obtained by visual estimation; third, the mercury lines exciting it. The letter b following the number indicating the intensity, signifies a broad line and v in the columns of the solid spectra means the disappearance of the corresponding liquid line undoubtedly established in the accuracy of the present measurement. For the sake of comparison the experimental values of Ananthakrishnan[8] obtained for liquid ethylene chloride and bromide are inserted in the following tables.

Table 3. The Raman spectra of $C_2H_4Br_2$.

Solid state (−40°C.)			Solid state (0°C.)			Liquid state					
						Present authors			Ananthakrishnan		
41	(4)	$k\pm$	49	(3b)	$k\pm$						
53	(3)	$k\pm$									
	v			v		91	(2b)	$e\pm, k\pm$	92	(2b)	
						132	(2)	e			
187	(7)	$e\pm, k+$	190	(7)	$e, k+$	190	(10)	$e\pm, k\pm$	189	(10)	P
	v			v		231	(3)	e	228	(1b)	P
						325	(1)	e	320	(0)	?
	v			v		355	(5)	e, k	358	(2)	D
						469	(1)	e, k	470	(0)	?
	v			v		551	(9)	$e\pm, k, i, f$	551	(8)	PP
	v			v		583	(6b)	$e\pm, k, i$	580	(2b)	D
656	(10)	e, k, i, f, g	657	(10)	e, k, i, f	660	(10b)	$e\pm, k, i$	659	(15b)	P
									790	(0)	?
						836	(2)	e	834	($^1/_2$)	D
						899	(3)	e, k	895	(1)	P
933	(0)	k	934	(1)	k	933	(2)	e, k	930	(1b)	P
						997	(0)	e			
						1019	(1)	e, k			
1057	(5)	e, k, i	1056	(5)	e, k	1053	(9)	e, k, i	1051	(6)	D
									1086	(??)	
1157	(1)	e				1169	(3)	e, k	1169	($^1/_2$)	D
									1187	(0)	D
1254	(8)	e, k, i	1250	(8b)	e, k	1255	(10b)	e, k	1256	(10b)	P
	v			v		1276	(3)	e, k	1295	(1s)	P
	v			v		1419	(3)	e, k	1419	(1)	D
1436	(3)	$[e], k$	1438	(3)	$[e], k$	1440	(5)	e, k	1436	(2)	D
2848	(2)	e, k	2857	(3)	e, k	2859	(4)	e, k	2852	(1)	PP
	v			v		2953	(8)	e, k, i	2950	(6)	PP
2968	(8)	e, k, i	2966	(10)	e, k, i	2972	(10)	e, k, i	2970	(8)	PP
3020	(2)	$e, [k]$	3013	(5)	e, k, i	3013	(4b)	$e, [k]$	3012	(2b)	D

We thank Prof. M. Katayama and Prof. I. Nitta for their valuable advices. We are indebted to Hattori-Hôkôkai for a grant in aid of this research.

(8) Ananthakrishnan, *Proc. Indian Acad. Sci.*, A, **5** (1937), 285.

Summary.

In the region of the unmodified line there have been observed for crystalline ethylene halides some Raman lines which correspond to motions of a molecule as a whole, but not to internal normal vibrations. For ethylene bromide a considerable change in these low frequency lines was observed between the spectrum at −40°C. and that at 0°C. and it is highly probable that this change is caused at the transition temperature (−24°C.) observed in the thermal measurement. An explanation for these experimental results was suggested to identify these lines with lattice frequencies and to regard the transition point as the temperature at which the one dimensional molecular rotation sets in.

Chemical Institute, Faculty of Science,
Tokyo Imperial University.

The Normal Vibrations of Ethylene Halides.

By Yonezo MORINO.

(Received December 27, 1937.)

In the preceding article[1] it was established that the Raman lines observed in the solid state correspond to the symmetric vibrations of the *trans*-form of $C_2H_4X_2$, while those disappearing upon solidification to the antisymmetric vibrations, etc. This fact is very useful for the assignment of the fundamental frequencies of ethylene halides.

In our previous paper[2] we calculated the normal frequencies of $C_2H_4X_2$ considering CH_2-group as one particle, because it was chiefly in the lower frequency region that we were interested. To treat mathematically C-H vibrations as well as their effects on chain frequencies, we must consider the molecule as a system of eight particles having eighteen

(1) S. Mizushima and Y. Morino, this Bulletin, **13** (1938), 182. See also S. Mizushima, Y. Morino, and S. Noziri, *Nature*, **137** (1936), 945; *Sci. Papers Inst. Phys. Chem. Research* (Tokyo), **29** (1936), 63.

(2) S. Mizushima and Y. Morino, *Sci. Papers Inst. Chem. Phys. Research* (Tokyo), **26** (1934), 1.

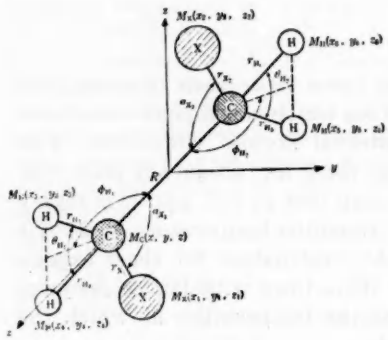

Fig. 1.

normal modes of vibrations. The equilibrium position of this system is the *trans*-form as shown in Fig. 1. It has the symmetry of C_{2h}, viz. one plane of symmetry and one centre of symmetry. The system makes a small vibration about this configuration. Let M_C, M_X, and M_H be the masses of carbon, halogen, and hydrogen atoms respectively, and x_i, y_i, z_i be their coordinates. The kinetic energy of this system T is easily separated as follows:

$$T = T_1 + T_2 + T_3 + T_4$$

where

$$T_1 = \frac{1}{4}M_C\left[(\dot{x}-\dot{x}')^2+(\dot{y}-\dot{y}')^2\right]+\frac{1}{4}M_X\left[(\dot{x}_1-\dot{x}_2)^2+(\dot{y}_1-\dot{y}_2)^2\right]$$
$$+\frac{1}{8}M_H\left[(\dot{x}_3+\dot{x}_4-\dot{x}_5-\dot{x}_6)^2+(\dot{y}_3+\dot{y}_4-\dot{y}_5-\dot{y}_6)^2+(\dot{z}_3-\dot{z}_4-\dot{z}_5+\dot{z}_6)^2\right],$$

$$T_2 = \frac{1}{4}M_C\left[(\dot{x}+\dot{x}')^2+(\dot{y}+\dot{y}')^2\right]+\frac{1}{4}M_X\left[(\dot{x}_1+\dot{x}_2)^2+(\dot{y}_1+\dot{y}_2)^2\right]$$
$$+\frac{1}{8}M_H\left[(\dot{x}_3+\dot{x}_4+\dot{x}_5+\dot{x}_6)^2+(\dot{y}_3+\dot{y}_4+\dot{y}_5+\dot{y}_6)^2+(\dot{z}_3-\dot{z}_4+\dot{z}_5-\dot{z}_6)^2\right],$$

$$T_3 = \frac{1}{4}M_C(\dot{z}-\dot{z}')^2+\frac{1}{4}M_X(\dot{z}_1-\dot{z}_2)^2$$
$$+\frac{1}{8}M_H\left[(\dot{x}_3-\dot{x}_4-\dot{x}_5+\dot{x}_6)^2+(\dot{y}_3-\dot{y}_4-\dot{y}_5+\dot{y}_6)^2+(\dot{z}_3+\dot{z}_4-\dot{z}_5-\dot{z}_6)^2\right],$$

and

$$T_4 = \frac{1}{4}M_C(\dot{z}+\dot{z}')^2+\frac{1}{4}M_X(\dot{z}_1+\dot{z}_2)^2$$
$$+\frac{1}{8}M_H\left[(\dot{x}_3-\dot{x}_4+\dot{x}_5-\dot{x}_6)^2+(\dot{y}_3-\dot{y}_4+\dot{y}_5-\dot{y}_6)^2+(\dot{z}_3+\dot{z}_4+\dot{z}_5+\dot{z}_6)^2\right].$$

The coordinates $x-x'$, $y-y'$, etc. belonging to the first part T_1 are totally symmetric, i.e. symmetric to the centre of symmetry as well as to the plane of symmetry. The coordinates $x+x'$, $y+y'$, etc. belonging to the second part T_2 are antisymmetric to the centre and symmetric

to the plane. The coordinates of the third part T_3 are symmetric to the centre and antisymmetric to the plane. The coordinates of the last part T_4 are antisymmetric both to the centre and to the plane. (See Table 1). It can be shown that the expression of the potential energy is also splitted into these four groups, although we assume the general quadratic form for it. The fundamental frequencies are thus separated into the four classes.

Table 1.

	Class I	Class II	Class III	Class IV
Centre of symmetry	sym.	antisym.	sym.	antisym.
Plane of symmetry	sym.	sym.	antisym.	antisym.
Coordinates of carbon atoms	$x-x'$ $y-y'$	$x+x'$ $y+y'$	$z-z'$	$z+z'$
halogen atoms	x_1-x_2 y_1-y_2	x_1+x_2 y_1+y_2	z_1-z_2	z_1+z_2
hydrogen atoms	$x_3+x_4-x_5-x_6$ $y_3+y_4-y_5-y_6$ $z_3-z_4-z_5+z_6$	$x_3+x_4+x_5+x_6$ $y_3+y_4+y_5+y_6$ $z_3-z_4+z_5-z_6$	$x_3-x_4-x_5+x_6$ $y_3-y_4-y_5+y_6$ $z_3+z_4-z_5-z_6$	$x_3-x_4+x_5-x_6$ $y_3-y_4+y_5-y_6$ $z_3+z_4+z_5+z_6$
Total number of coordinates	7	7	5	5
Conditions for translational motions		2		1
Conditions for rotational motions	1		2	
Number of normal coordinates	6	5	3	4
Selection rules for Raman-spectra	active	inactive	active	inactive
Selection rules for Infrared	inactive	active	inactive	active

The condition that the x-coordinate of the centre of gravity of the whole system is fixed, can be expressed by means of the coordinates belonging to Class II only:

$$M_C(\dot{x}+\dot{x}')+M_X(\dot{x}_1+\dot{x}_2)+M_H(\dot{x}_3+\dot{x}_5+\dot{x}_4+\dot{x}_6)=0\,.$$

The same holds for the y- and z-coordinates, thus we have

$$M_C(\dot{y}+\dot{y}')+M_X(\dot{y}_1+\dot{y}_2)+M_H(\dot{y}_3+\dot{y}_4+\dot{y}_5+\dot{y}_6)=0,$$

$$M_C(\dot{z}+\dot{z}')+M_X(\dot{z}_1+\dot{z}_2)+M_H(\dot{z}_3+\dot{z}_4+\dot{z}_5+\dot{z}_6)=0.$$

The conditions that the system is devoid of rotation are also given in a similar way. The number of the normal modes of vibrations belonging to each class is given by the difference between the number of the coordinates mentioned above and that of the conditions of this class. The vibrations of Classes I and III are active in the Raman effect, but inactive in the infrared. The vibrations of Classes II and IV are inactive in the Raman effect, but active in the infrared. These relations are summarized in Table 1.

It is very difficult to solve the secular equation for all the 18 frequencies. For the vibrations of Classes I and II, however, the solution can be obtained in the following way: For the potential energy of these classes we assume the following expression corresponding to a valence force system:

$$V=\frac{1}{2}k\Delta R^2+\frac{1}{2}k_X(\overline{\Delta r_{X_1}^2}+\overline{\Delta r_{X_2}^2})+\frac{1}{2}\delta_X r_X^2(\overline{\Delta\alpha_{X_1}^2}+\overline{\Delta\alpha_{X_2}^2})$$
$$+\frac{1}{2}k_H(\overline{\Delta r_{H_3}^2}+\overline{\Delta r_{H_4}^2}+\overline{\Delta r_{H_5}^2}+\overline{\Delta r_{H_6}^2})+\delta_H r_H^2(\overline{\Delta\phi_{H_1}^2}+\overline{\Delta\phi_{H_2}^2})+\frac{1}{2}\beta_H r_H^2(\overline{\Delta\theta_{H_1}^2}+\overline{\Delta\theta_{H_2}^2}),$$

where the notations are shown in Fig. 1.

In Class I, we have $\dot{x}=-\dot{x}'$, $\dot{y}=-\dot{y}'$, $\dot{x}_1=-\dot{x}_2$, $\dot{y}_1=-\dot{y}_2$, $\dot{x}_3=\dot{x}_4=-\dot{x}_5=-\dot{x}_6$, $\dot{y}_3=\dot{y}_4=-\dot{y}_5=-\dot{y}_6$, $\dot{z}_3=-\dot{z}_4=-\dot{z}_5=\dot{z}_6$, and $\Delta r_{X_1}=\Delta r_{X_2}$, $\Delta\alpha_{X_1}=\Delta\alpha_{X_2}$, $\Delta r_{H_3}=\Delta r_{H_4}=\Delta r_{H_5}=\Delta r_{H_6}$, $\Delta\phi_{H_1}=\Delta\phi_{H_2}$, $\Delta\theta_{H_1}=\Delta\theta_{H_2}$. Through complicated calculations similar to those given in our previous paper,[2] the secular equation which designates the six totally symmetric vibrations is found to be

$$\begin{vmatrix} A_{11}\lambda^2-k, & A_{12}\lambda^2, & A_{13}\lambda^2, & A_{14}\lambda^2, & A_{15}\lambda^2, & A_{16}\lambda^2, \\ 2A_{12}\lambda^2, & A_{22}\lambda^2-k_X, & A_{23}\lambda^2, & A_{24}\lambda^2, & A_{25}\lambda^2, & A_{26}\lambda^2, \\ 2A_{13}\lambda^2, & A_{23}\lambda^2, & A_{33}\lambda^2-\delta_X r_X^2, & A_{34}\lambda^2, & A_{35}\lambda^2, & A_{36}\lambda^2, \\ 2A_{14}\lambda^2, & A_{24}\lambda^2, & A_{34}\lambda^2, & A_{44}\lambda^2-2k_H, & A_{45}\lambda^4, & A_{46}\lambda^2, \\ 2A_{15}\lambda^2, & A_{25}\lambda^2, & A_{35}\lambda^2, & A_{45}\lambda^2, & A_{55}\lambda^2-4\beta_H r_H^2, & A_{56}\lambda^2, \\ 2A_{16}\lambda^2, & A_{26}\lambda^2, & A_{36}\lambda_2, & A_{46}\lambda^2, & A_{56}\lambda^2, & A_{66}\lambda^2-2\delta_H r_H^2, \end{vmatrix}=0,$$

where A_{ij} are the coefficients defined by the masses of the atoms and the geometrical form of the molecule by means of the following relations:

$$\begin{cases} A_{11} = \frac{1}{2}M + 2a^2\rho , \\ A_{22} = M_X + b_1^2\rho , \\ A_{33} = M_X r_X^2 + c_1^2\rho , \\ A_{44} = 2M_H + b_2^2\rho , \\ A_{55} = 2M_H r_H^2 + d^2\rho , \\ A_{66} = 2M_H r_H^2 \cos^2\frac{\theta_H}{2} + c_2^2\rho , \end{cases}$$

$$\begin{cases} A_{12} = -\frac{1}{2}M_X \cos\alpha_X + ab_1\rho , \\ A_{13} = \frac{1}{2}M_X r_X \sin\alpha_X + ac_1\rho , \\ A_{14} = -M_H \cos\frac{\theta_H}{2}\cos\phi_H + ab_2\rho , \\ A_{15} = M_H r_H \sin\frac{\theta_H}{2}\cos\phi_H + ad\rho , \\ A_{16} = M_H r_H \cos\frac{\theta_H}{2}\sin\phi_H + ac_2\rho , \end{cases}$$

$$\begin{cases} A_{23} = b_1c_1\rho , \\ A_{24} = b_1b_2\rho , \\ A_{25} = b_1d\rho , \\ A_{26} = b_1c_2\rho , \\ A_{34} = c_1b_2\rho , \\ A_{35} = c_1d\rho , \\ A_{36} = c_1c_2\rho , \\ A_{45} = b_2d\rho , \\ A_{46} = b_2c_2\rho , \\ A_{56} = c_2d\rho , \end{cases}$$

and

$$\begin{cases} M = M_C + M_X + 2M_H , \\ -1/\rho = MR^2 + 4\left(M_X r_X^2 + 2M_H r_H^2 \cos^2\frac{\theta_H}{2}\right) \\ \qquad -4R\left(M_X r_X \cos\alpha_X + 2M_H r_H \cos\frac{\theta_H}{2}\cos\phi_H\right) , \\ a = -M_X r_X \sin\alpha_X + 2M_H r_H \cos\frac{\theta_H}{2}\sin\phi_H , \\ b_1 = M_X R \sin\alpha_X , \\ b_2 = -2M_H R \cos\frac{\theta_H}{2}\sin\phi_H , \\ d = 2M_H r_H R \sin\frac{\theta_H}{2}\sin\phi_H , \\ c_1 = -M_X r_X (2r_X - R\cos\alpha_X) , \\ c_2 = 2M_H r_H \cos\frac{\theta_H}{2}\left(2r_H \cos\frac{\theta_H}{2} - R\cos\phi_H\right) . \end{cases}$$

Putting $M_C = 12$, $M_H = 1.008$, $M_X = 79.92$, $r_H = 1.08$ Å, $r_X = 2.05$ Å, $R = 1.54$ Å and $\alpha = 109°28'$ for ethylene bromide, it is found that the cross terms A_{14}, $A_{15} \cdots A_{35}$, A_{36} are smaller than A_{11}, $A_{12} \cdots$, owing to the fact that the mass of hydrogen is small compared with that of bromine atom. If we neglect these cross terms, we have

$$\begin{vmatrix} A_{11}\lambda^2 - k, & A_{12}\lambda^2, & A_{13}\lambda^2, \\ 2A_{12}\lambda^2, & A_{22}\lambda^2 - k_X, & A_{23}\lambda^2, \\ 2A_{13}\lambda^2, & A_{23}\lambda^2, & A_{33}\lambda^2 - \delta_X r_X^2, \end{vmatrix} = 0 \qquad (1),$$

$$A_{44}\lambda^2 - 2k_H = 0 \qquad (2),$$

$$A_{55}\lambda^2 - 4\beta_H r_H^2 = 0 \qquad (3),$$

$$A_{66}\lambda^2 - 2\delta_H r_H^2 = 0 \qquad (4).$$

Equation (1) gives the chain frequencies of X-(CH_2)-(CH_2)-X. It can be reduced to the solution of the four body problem,[2] if $M_C + 2M_H$ is put equal to M and the distance r_H to zero. This shows that our former treatment for the chain frequencies is sufficiently correct in this approximation, even if we take the vibrations of hydrogen atoms into consideration. The latter three equations give the frequencies of CH_2-group, viz. equation (2) gives the C-H valency frequency, equation (3) that of the deformation of H-C-H angle, and equation (4) that of the deformation of CH_2-group relative to C-C axis.

These three hydrogen frequencies as well as the three chain frequencies should be active in the Raman effect in solid ethylene bromide. The higher frequencies of ethylene bromide in the solid state 2968 cm.$^{-1}$, 1436 cm.$^{-1}$, and 1254 cm.$^{-1}$ are assigned to the C-H frequencies, while the lower frequencies 187 cm.$^{-1}$, 656 cm.$^{-1}$, and 1057 cm.$^{-1}$ to the chain frequencies. The line 2968 cm.$^{-1}$ is identified with the C-H valency vibration; the line 1436 cm.$^{-1}$ with the deformation of H-C-H angle, and the line 1254 cm.$^{-1}$ with the deformation of CH_2-group relative to C-C axis. This assignment is in conformity with the results of Ta-You Wu[3] for C_2H_4 and of Trumpy[4] for *trans*-$C_2H_2Cl_2$. Ta-You Wu assigned the line 1440 cm.$^{-1}$ of C_2H_4 to the deformation frequency of CH_2-group. Trumpy observed that the frequency 1260 cm.$^{-1}$ of *trans*-$C_2H_2Cl_2$ decreased to 992 cm.$^{-1}$ on the insertion of D in place of H, showing that this frequency

(3) Ta-You Wu, *J. Chem. Phys.*, **5** (1937), 392.
(4) B. Trumpy, *Nature*, **135** (1935), 764.

is the deformation frequency of C-H to C-C axis. For ethylene chloride the corresponding three lines 2964 cm.$^{-1}$, 1448 cm.$^{-1}$, and 1301 cm.$^{-1}$, are identified with the totally symmetric vibrations of CH_2-groups. The force constants are thus obtained to be

$$\begin{cases} k_H = 5.19 \times 10^5 & \text{dyne/cm.} \\ \beta_H = 0.607 \times 10^5 & ,, \quad \text{for ethylene bromide,} \\ \delta_H = 0.308 \times 10^5 & ,, \end{cases}$$

and

$$\begin{cases} k_H = 5.18 \times 10^5 & \text{dyne/cm.} \\ \beta_H = 0.618 \times 10^5 & ,, \quad \text{for ethylene chloride.} \\ \delta_H = 0.330 \times 10^5 & ,, \end{cases}$$

For the vibrations of Class II, we obtain the following secular equation:

$$\begin{vmatrix} B_{11}\lambda^2-k_X, & 0, & B_{13}\lambda^2, & B_{14}\lambda^2, & B_{15}\lambda^2, \\ 0, & B_{22}\lambda^2-\delta_X r_X^2, & B_{23}\lambda^2, & B_{24}\lambda^2, & B_{25}\lambda^2, \\ B_{13}\lambda^2, & B_{23}\lambda^2, & B_{33}\lambda^2-2k_H, & B_{34}\lambda^2, & 0, \\ B_{14}\lambda^2, & B_{24}\lambda^2, & B_{34}\lambda^2, & B_{44}\lambda^2-4\beta_H r_H^2, & 0, \\ B_{15}\lambda^2, & B_{25}\lambda^2, & 0, & 0, & B_{55}\lambda^2-2\delta_H r_H^2, \end{vmatrix} = 0,$$

where

$$\begin{cases} B_{11} = M_X(M_C+2M_H)/M, \\ B_{22} = r_X^2 M_X(M_C+2M_H)/M, \\ B_{33} = 2M_H - 4\cos^2\dfrac{\theta_H}{2} M_H^2/M, \\ B_{44} = 2r_H^2 M_H - 4r_H^2 \sin^2\dfrac{\theta_H}{2} M_H^2/M, \\ B_{55} = 2r_H^2 \cos^2\dfrac{\theta_H}{2} M_H(M_C+M_X)/M, \end{cases}$$

and

$$\begin{cases} B_{13} = -2\cos\dfrac{\theta_H}{2}(\cos\alpha_X\cos\phi_H - \sin\alpha_X\sin\phi_H) M_H M_X/M, \\ B_{14} = 2r_H \sin\dfrac{\theta_H}{2}(\cos\alpha_X\cos\phi_H - \sin\alpha_X\sin\phi_H) M_H M_X/M, \end{cases}$$

$$
\begin{cases}
B_{15} = 2r_H \cos\dfrac{\theta_H}{2}(\cos\alpha_X \sin\phi_H + \sin\alpha_X \cos\phi_H)M_H M_X/M\,, \\
B_{23} = 2r_X \cos\dfrac{\theta_H}{2}(\cos\alpha_X \sin\phi_H + \sin\alpha_X \cos\phi_H)M_H M_X/M\,, \\
B_{24} = -2r_X r_H \sin\dfrac{\theta_H}{2}(\cos\alpha_X \sin\phi_H + \sin\alpha_X \cos\phi_H)M_H M_X/M\,, \\
B_{25} = 2r_X r_H \cos\dfrac{\theta_H}{2}(\cos\alpha_X \cos\phi_H - \sin\alpha_X \sin\phi_H)M_H M_X/M\,, \\
B_{34} = 4r_H \cos\dfrac{\theta_H}{2}\sin\dfrac{\theta_H}{2} M_H^2/M\,.
\end{cases}
$$

Neglecting the cross terms, we have

$$B_{11}\lambda^2 - k_X = 0 \qquad (5),$$

$$B_{22}\lambda^2 - \delta_X r_X^2 = 0 \qquad (6),$$

$$B_{33}\lambda^2 - 2k_H = 0 \qquad (7),$$

$$B_{44}\lambda^2 - 4\beta_4 r_H^2 = 0 \qquad (8),$$

$$B_{55}\lambda^2 - 2\delta_H r_H^2 = 0 \qquad (9).$$

Equations (5) and (6) express the antisymmetric valency and deformation frequencies of C-Cl bond and are the same as those derived in the previous paper.[2] Equations (7), (8), and (9) are those of the CH_2-groups. These vibrations are forbidden in the Raman effect for the *trans*-form of the molecule, and can be assigned to the lines disappearing in the solid spectra, for in the solid state the molecules of ethylene halides are in the *trans*-configuration, while in the liquid state it considerably deviates from this stable configuration. From the force constants obtained for the vibrations of Class I, we get the values 2978 cm.$^{-1}$, 1445 cm.$^{-1}$, and 1260 cm.$^{-1}$ for these lines. Actually ethylene bromide has the lines 2953 cm.$^{-1}$, 1419 cm.$^{-1}$, and 1276 cm.$^{-1}$, which disappear in the solid state and are to be assigned to the frequencies calculated. For ethylene chloride the observed lines 1429 cm.$^{-1}$ and 1393 cm.$^{-1}$ must be assigned to the calculated frequencies 1465 cm.$^{-1}$ and 1417 cm.$^{-1}$ respectively. Though in the C-H valency frequency region we have no line which vanishes and is to be assigned to the calculated frequency 2984 cm.$^{-1}$, comparison of its spectra with those of bromide suggests that the line corresponding to this frequency might overlap that of a symmetric vibration. (See Table 2.)

Table 2. Antisymmetric C–H vibrations.

	$C_2H_4Cl_2$		$C_2H_4Br_2$	
	$\nu_{calc.}$ (cm.$^{-1}$)	$\nu_{obs.}$ (cm.$^{-1}$)	$\nu_{calc.}$ (cm.$^{-1}$)	$\nu_{obs.}$ (cm.$^{-1}$)
ν(C—H)	2984	(2957)?	2978	2953
δ(H-C-H)	1465	1429	1445	1419
$\delta(CH_2$-C)	1417	1393	1260	1276

We have discussed eleven frequencies so far. It is easily seen from Table 1 that the remaining seven frequencies must be C-H vibrations except a vibration corresponding to the internal rotation. Thus we get as much lower frequencies as those of the four body problem X-(CH_2)-(CH_2)-X, even though we take the motion of hydrogen atoms into consideration. The conclusion of the previous paper with regard to these chain frequencies of ethylene halides is, therefore, not essentially modified by the consideration of the motion of hydrogen atoms.

In conclusion, the author wishes to express his cordial thanks to Prof. M. Katayama and Prof. S. Mizushima for their kind guidance and encouragement throughout the course of this study.

Chemical Institute, Faculty of Science,
Imperial University of Tokyo.

Über die Intensitätsverteilung der Faserdiagramme.

Von Yukichi GO, Saburo NAGATA und Jiro KAKINOKI.

(Eingegangen am 15. Januar 1938.)

I. **Einleitung.** Für die Entstehung der Faserstrukturen sind allgemein zwei Gründe massgebend, nämlich das natürliche Wachstum und die mechanische Deformation.

Als Wachstumsfaserstrukturen kann man nennen die von allen organischen Pflanzenfasern, ferner von tierischen Haaren und Wolle und vielleicht noch die von mineralischen Fasern.

Demgegenüber ist die Faserstruktur bei der Naturseide, Seidenstramin, Kunstseide, Zellwolle und den dünnen Metallfasern auf Einflüsse der mechanischen Deformation zurückzuführen.

Aber auch die oben angegebenen Fasern haben nicht immer die einfache Faserstruktur, sondern es können auch Spiralfaserstruktur,[1] Ringfaserstruktur und ganz allgemein noch abweichende Strukturen verschiedenen Grades vorliegen.

Im Folgenden wird nun die Intensitätsverteilung bei Röntgenaufnahmen dieser verschiedenen Faserstrukturen besprochen.

Über die Beziehung zwischen der Orientierung der Kristallite und der Intensitätsverteilung von Röntgenfaserdiagrammen existiert bisher nicht viele Literatur. Nach der allgemeinen qualitativen Systematisierung von K. Weissenberg,[1][2][3] hat O. Kratky[4] zum ersten Mal einen quantitativen Ausdruck für die Äquator-Reflexe der Spiralfaserstruktur abgeleitet, als er den Deformationsmechanismus der Faserstoffe untersuchte. I. Sakurada und K. Hutino haben für den Fall der Ringfaserstruktur die Intensitätsverteilung nicht nur für die Äquator-Reflexe, sondern auch für die allgemeinen Reflexe quantitativ diskutiert. Der noch allgemeinere Fall, nämlich der allgemeinen Reflexe der verschiedenen Faserstrukturen, wurde im hiesigen Laboratorium untersucht.[6] Beinahe zur gleichen Zeit hat C. Matano nach eigener Rechnungsweise ebenfalls den allgemeinen Fall behandelt.[7]

---

(1) K. Weissenberg, *Z. Physik*, **8** (1921), 20.
(2) K. Weissenberg, *Ann. Physik*, **69** (1922), 421.
(3) K. Weissenberg, *Z. Krist.*, **61** (1925), 58.
(4) O. Kratky, *Kolloid-Z.*, **64** (1933), 213.
(5) I. Sakurada und K. Hutino, *Sci. Papers Inst. Phys. Chem. Research* (Tokyo), **24** (1934), 193.
(6) Y. Go, J. Kakinoki und S. Nagata, *Rept. Japan. Assoc. Adv. Sci.*, **12** (1937), 128.
(7) C. Matano, *J. Soc. Chem. Ind. Japan*, **39** (1936), 478.

II. Anwendung der Polanyi'schen Lagenkugel. Für die Diskussion des Faserdiagrammes ist bekanntlich die Anwendung der Polanyi'schen Lagenkugel[8] am bequemsten. Jeder Kristallit des Aggregates wird durch Parallelverschiebung in den Mittelpunkt einer Einheitskugel gebracht und die Durchstosspunkte seiner Achsen an der Kugeloberfläche werden aufgesucht. Die „Dichte" oder „Belegungsdichte", welche diese „Repräsentationspunkte" an einer bestimmten Stelle haben, ist ein Mass für die Häufigkeit der entsprechenden Achsenrichtung. Die Dichteverteilung dieser „Repräsentationspunkte" auf der Lagenkugel zeigt den Ordnungszustand der Kristallite im Aggregat.

Für die Ermittlung der Intensitätsverteilung längs des Debye-Scherrer-Kreises jedoch muss in erster Linie die Dichteverteilung der Netzebenenrepräsentationspunkte auf der Lagenkugel entlang dem Reflexionskreise untersucht werden.

III. Verhältnisse auf der Lagenkugel. Die Lagenkugel für die Diskussion der Intensitätsverteilung ist in Abb. 1 abgebildet. Die Röntgenstrahlen gehen durch S_0 nach O. Eine zu untersuchende ideale Spiralfaser befindet sich im Punkte O und ihre Faserachse OF steht senkrecht zur Richtung S_0O. Da die Kristallitachse OC der Faser, welche mit der Symmetrieachse OF einen Winkel φ bildet, um diese gleichmässig verteilt ist, bildet der geometrische Ort von C einen Kreis, welcher OF als seine Achse besitzt.

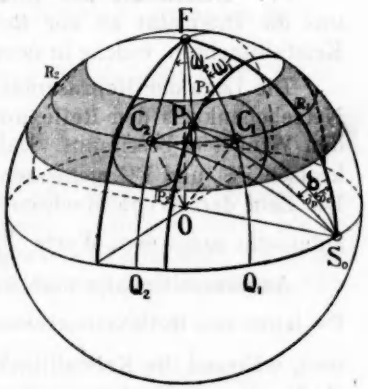

Abb. 1.

Die Normale von der Netzebene, welche bestimmten Netzebenenabstand „d" besitzt verteilt sich um OC herum gleichmässig mit dem bestimmten Winkel ρ. Der geometrische Ort der Repräsentationspunkte dieser Normalen bilden einen sogenannten „Netzebenenkreis" um die Achse OC.

Während die Kristallitachse OC um die Faserachse OF herum verteilt ist und ihre Repräsentationspunkte C folglich einen Kreis bilden, bestreicht der Netzebenenkreis eine Zone (auf der Abbildung schraffiert) auf der Lagenkugel. Alle Repräsentationspunkte der in Frage kommenden Netzebenen fallen also in diese Zone hinein. Diese Zone kann man die „Netzebenenzone" nennen.

(8) M. Polanyi, *Z. Physik*, **7** (1921), 149.

Im allgemeinen wenn die den bestimmten Netzebenenabstand „d" besitzende Netzebene die Röntgenstrahlen reflektiert, muss ihre Normale nach einer bestimmten Richtung gerichtet sein, welche die Bragg'sche Beziehung $n\lambda = 2d\sin\theta$ erfüllt. Der geometrische Ort der Repräsentationspunkte einer solchen Normale bildet einen sogenannten „Reflexionskreis" auf der Lagenkugel um die Achse OS_0, welche von dem Punkt S_0 den Abstand $90°-\theta$ besitzt.

Der Schnittpunkt von Reflexionskreis und Netzebenenkreis bildet einen Interferenzpunkt auf dem Debye-Scherrer-Kreis. Der Punkt P in Abb. 1 ist ein dieser Reflexionsstelle entsprechender Punkt auf der Lagenkugel.

Der Richtungswinkel δ einer Reflexionsstelle längs des Debye-Scherrer-Kreises wird auf der photographischen Platte von der Projektionslinie der Achse OF aus gemessen, und zwar von dem Punkte S_0 aus gesehen nach links als positiv. Dann ist der Winkel zwischen den beiden Hauptkreisen FS_0 und PS_0 kein anderer als δ.

IV. **Diskussion der Intensitätsverteilung.** Einerseits denken wir uns die Intensität an der Reflexionsstelle proportional der Anzahl der Kristallitachsen, welche in dem kleinen Bereich $d\delta$ ihren Einfluss ausüben.

Die Lage der Repräsentationspunkte C der Kristallitachse OC, deren Netzebenenkreis den Reflexionskreis im Punkte P schneidet, wird durch den Winkel ω bestimmt. Dabei ist ω der Winkel zwischen den Hauptkreisen FS_0 und FC, gemessen von F aus gesehen nach rechts als positiv. Die Zahl der Kristallitachsen ist dann proportional $d\omega$ und die gesuchte Intensität muss dem Werte $\frac{d\omega}{d\delta}$ proportional sein.

Andererseits kann man die Wanderungsgeschwindigkeit des Punktes P—längs des Reflexionskreises zwischen P_1 und P_2—mit $v = \frac{d\delta}{dt}$ annehmen, während die Kristallitachse OC mit der konstanten Geschwindigkeit $\frac{d\omega}{dt}$ = Konst. um ihre Achse rotiert. Nach der Beziehung $\frac{d\delta}{d\omega} \cdot \frac{d\omega}{dt} = \frac{d\delta}{dt}$ ist daher $\frac{d\omega}{d\delta} = \frac{1}{v}$. Also ist die gesuchte Intensität proportional $\frac{1}{v}$. Je schneller also der Punkt P längs des Reflexionskreises wandert, desto kleiner wird die Intensität der entsprechenden Reflexionsstelle im Diagramm. Unsere Aufgabe besteht nunmehr darin, den Wert von $\frac{d\delta}{d\omega}$ oder v auszurechnen. Der Winkel δ wird in zwei geteilt; δ_c ist derjenige zwischen den beiden Hauptkreisen CS_0 und FS_0, und δ_p der zwischen PS_0 und CS_0.

$$\delta = \delta_c \pm \delta_p \tag{1}$$

$$\therefore \quad \frac{d\delta}{d\omega} = \frac{d\delta_c}{d\omega} \pm \frac{d\delta_p}{d\omega}$$

Aus den drei sphärischen Dreiecken PCS_0, FCS_0 und CQS_0 (Q ist der Schnittpunkt eines zu OF senkrecht stehenden und durch den Punkt S_0 gehenden Hauptkreises SQ mit dem Hauptkreis FC) können die folgenden drei Gleichungen abgeleitet werden.

$$\cos\delta_p = (\cos\rho - \cos\beta\sin\theta)\Big/\sin\beta\cos\theta \tag{2},$$

$$\cos d_c = \cos\varphi\Big/\sin\beta \tag{3},$$

$$\cos\beta = \sin\varphi\cos\omega \tag{4},$$

wobei β der Winkel zwischen OC und OS_0 ist.

Aus diesen drei Grundbeziehungen folgt:

$$\frac{d\delta}{d\omega} = \frac{\sin\varphi}{(1-\sin^2\varphi\cos^2\omega)}\Big\{\cos\varphi\cos\omega \pm \mu\sin\omega\,(\sin\varphi\cos\omega\cos\rho - \sin\theta) \times (\cos^2\theta - \sin^2\varphi\cos^2\omega - \cos^2\rho + 2\cos\rho\sin\theta\sin\varphi\cos\omega)^{\frac{1}{2}}\Big\} \tag{5},$$

$\pm$ ist bestimmt nach (1): $\mu = +1$ wenn $\sin\delta_p \geqslant 0$ und $\mu = -1$ wenn $\sin\delta_p < 0$.

Da im allgemeinen jeder Interferenzpunkt P zu zwei Netzebenenkreisen (C_1 und C_2 in Abb. 1) gehören kann, so müssen beide bei der Rechnung berücksichtigt werden. Dementsprechend sind auch für ω zwei Werte ω_1 und ω_2 möglich und wird nach jedem einzelnen bestimmt, nämlich $v_1 = \frac{d\delta}{d\omega_1}$ und $v_2 = \frac{d\delta}{d\omega_2}$.

$$v_1 = \left(\frac{d\delta}{d\omega}\right)_{\omega=\omega_1} = \frac{A}{A^2-B_1^2}\left\{\cos\varphi\cdot B_1 + \kappa_1\frac{(\cos\rho B_1 - \sin\theta A)\sqrt{\sin^2\varphi\cdot A^2 - B_1^2}}{\sqrt{A^2\cos^2\theta - B_1^2 - A^2\cos^2\rho + 2\cos\rho\sin\theta\cdot A\cdot B_1}}\right\}$$

$$v_2 = \left(\frac{d\delta}{d\omega}\right)_{\omega=\omega_2} = (B_1 \text{ und } \kappa_1 \text{ sind durch } B_2 \text{ und } \kappa_2 \text{ zu ersetzen}).$$

Wobei
$$A = 1-\cos^2\delta\cos^2\theta$$
$$B_1 = \sin\theta\cos\rho - \cos\varphi\cos\delta\sin\theta\cos\theta + \cos\theta\sin\delta\sqrt{c}$$
$$B_2 = \sin\theta\cos\rho - \cos\varphi\cos\delta\sin\theta\cos\theta - \cos\theta\sin\delta\sqrt{c}$$
$$c = \sin^2\varphi - \cos^2\rho - \cos^2\theta\cos^2\delta + 2\cos\rho\cos\varphi\cos\theta\cos\delta$$
κ_1 und κ_2 sind $+1$ oder -1.

Die gesuchte Intensität ist nun:

$$I \propto \left|\frac{1}{v_1}\right| + \left|\frac{1}{v_2}\right| \tag{7}$$

Einige spezielle Fälle.

(A) Äquator-Reflexe der Spiralfaserstruktur $\rho = 90°$.

$$v_1 = \frac{A}{A^2-B_1^2}\left\{\cos\varphi B_1 + \frac{\sin\theta A\sqrt{\sin^2\varphi A^2-B_1^2}}{\sqrt{A^2\cos^2\theta-B_1^2}}\right\}$$
$$v_2 = \frac{A}{A^2-B_2^2}\left\{\cos\varphi B_2 - \kappa_2\frac{\sin\theta A\sqrt{\sin^2\varphi A^2-B_2^2}}{\sqrt{A^2\cos^2\theta-B_2^2}}\right\} \tag{8}$$

κ_1 ist hierbei immer -1 und nur κ_2 muss wie folgt bestimmt werden:

(1) wenn $\cos\delta < \tan\varphi\tan\theta$
wenn $\cos\delta \lesseqgtr \cos\varphi\sin\theta$, $\kappa_2 = \pm 1$
wenn $\cos\delta = \cos\varphi\sin\theta$, $v_2 = \infty$ unabhängig von κ_2

(2) wenn $\cos\delta = \tan\varphi\tan\theta$ . . . . . $v_2 = -\tan\varphi$ „ „ „ .

(3) wenn $\cos\delta > \tan\varphi\tan\theta$ . . . . . $\kappa_2 = -1$

(B) (i) Ringfaserstruktur (allgemeine Reflexe) $\varphi = 90°$.

$$v_{1,2} = \frac{A(\cos\rho B_{1,2} - \sin\theta A)}{\sqrt{A^2-B_{1,2}^2}} \times \left\{A^2\cos^2\theta - B_{1,2}^2 - A^2\cos^2\rho + 2\cos\rho\sin\theta A B_{1,2}\right\}^{-\frac{1}{2}} \tag{9}$$

(ii) Äquator-Reflexe der Ringfaserstruktur $\varphi = 90°$, $\rho = 90°$.

$$v_1 = v_2 = (1-\cos^2\delta\cos^2\theta)\Big/\cos\delta\sin\theta\cos\theta \tag{10}$$

Die Gleichungen (9) und (10) stimmen mit denjenigen überein, welche von Sakurada und Hutino abgeleitet wurden.

V. Systematisierung der verschiedenen Diagramm-Typen. Da die Intensität I nicht imaginär sein kann, kann

$$C = \sin^2\varphi - \cos^2\rho - \cos^2\theta\cos^2\delta + 2\cos\rho\cos\varphi\cos\theta\cos\delta$$

keinen negativen Wert haben und damit folgt:

$$\frac{\cos(\varphi-\rho)}{\cos\theta} \geqslant \cos\delta \geqslant \frac{\cos(\varphi+\rho)}{\cos\theta} \tag{11}$$

Unter Zugrundelegung dieser Bedingung kann man sämtliche möglichen Diagrammtypen systematisieren, wie es in der folgenden Tabelle 1 gezeigt wird.

Dabei scheiden von vornherein die zwei folgenden Fälle aus:

(1) Wenn $\theta > \rho + \omega$ ist, tritt kein Reflex auf.

(2) kann nicht 0 sein.

Tabelle 1.

1	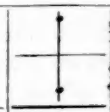	$\begin{cases}\rho=0\\ \theta=\varphi\end{cases}$ $\begin{cases}\varphi=0\\ \theta=\rho\end{cases}$ $\begin{cases}\rho<\varphi\\ \rho<90^\circ-\varphi\\ \theta=\varphi+\rho\end{cases}$ $\begin{cases}\rho=\varphi\\ \rho<90^\circ-\varphi\\ \theta=2\varphi\end{cases}$ $\begin{cases}\rho>\varphi\\ \rho<90^\circ-\varphi\\ \theta=\rho+\varphi\end{cases}$
2	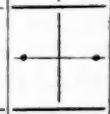	$\begin{cases}\rho=0\\ \varphi=90^\circ\end{cases}$ $\begin{cases}\rho=90^\circ\\ \varphi=0\end{cases}$
3	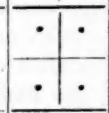	$\begin{cases}\rho=0\\ \varphi\neq 90^\circ\\ \theta<\varphi\end{cases}$ $\begin{cases}\varphi=0\\ \theta<\rho\neq 90^\circ\end{cases}$
4	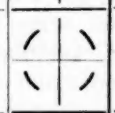	$\begin{cases}\rho<\varphi\\ \rho<90^\circ-\varphi\\ \theta<\varphi-\rho\end{cases}$ $\begin{cases}\rho>\varphi\\ \rho<90^\circ-\varphi\\ \theta<\rho-\varphi\end{cases}$
5		$\begin{cases}\rho<\varphi\\ \rho<90^\circ-\varphi\\ \theta\geq\varphi-\rho\\ \theta<\varphi+\rho\end{cases}$ $\begin{cases}\rho=\varphi\\ \rho<90^\circ-\varphi\\ \theta<2\varphi\end{cases}$ $\begin{cases}\rho>\varphi\\ \rho<90^\circ-\varphi\\ \theta\geq\rho-\varphi\\ \theta<\rho+\varphi\end{cases}$
6		$\begin{cases}\rho<\varphi\\ \rho=90^\circ-\varphi\\ \theta<\varphi-\rho\end{cases}$ $\begin{cases}\rho<\varphi=90^\circ\\ \theta<90^\circ-\rho\end{cases}$ $\begin{cases}\rho>\varphi\\ \rho=90^\circ-\varphi\\ \theta<\rho-\varphi\end{cases}$ $\begin{cases}\rho=90^\circ>\varphi\\ \theta<90^\circ-\varphi\end{cases}$
7		$\begin{cases}\rho<\varphi=90^\circ\\ \theta=90^\circ-\rho\end{cases}$ $\begin{cases}\rho<\varphi\\ \rho=90^\circ-\varphi\\ \theta\geq\varphi-\rho\end{cases}$ $\begin{cases}\rho<\varphi\neq 90^\circ\\ \rho>90^\circ-\varphi\\ \theta\geq 180^\circ-(\varphi+\rho)\end{cases}$ $\begin{cases}\rho<\varphi=90^\circ\\ \theta>90^\circ-\rho\end{cases}$ $\rho=\varphi=45^\circ$ $\begin{cases}\rho=\varphi\neq 90^\circ\\ \rho>90^\circ-\varphi\\ \theta\geq 180^\circ-2\varphi\end{cases}$
8		$\begin{cases}\rho<\varphi\neq 90^\circ\\ \rho>90^\circ-\varphi\\ \theta<\varphi-\rho\end{cases}$ $\begin{cases}90^\circ\neq\rho>\varphi\\ \rho>90^\circ-\varphi\\ \theta<\rho-\varphi\end{cases}$ $\rho=\varphi=90^\circ$ $\begin{cases}\rho>\varphi\\ \rho=90^\circ-\varphi\\ \theta\geq\rho-\varphi\end{cases}$ $\begin{cases}90^\circ\geq\rho>\varphi\\ \rho>90^\circ-\varphi\\ \theta\geq 180^\circ-(\varphi+\rho)\end{cases}$
9		$\begin{cases}\rho<\varphi\neq 90^\circ\\ \rho>90^\circ-\varphi\\ \theta\geq\varphi-\rho\\ \theta<180^\circ-(\varphi+\rho)\end{cases}$ $\begin{cases}\rho=\varphi\neq 90^\circ\\ \rho>90^\circ-\varphi\\ \theta<180^\circ-2\varphi\end{cases}$ $\begin{cases}90^\circ\neq\rho>\varphi\\ \rho>90^\circ-\varphi\\ \theta\geq\rho-\varphi\\ \theta<180^\circ-(\varphi+\rho)\end{cases}$

Diese Tabelle zeigt natürlich nur die typischen Formen der Diagramme, gibt dagegen keine Auskunft über die Intensitätsverhältnisse.

Alle diese Reflexions- bzw. Diagramm-Typen können ebenfalls abgeleitet werden ohne die Beziehung (11) anzuwenden, und zwar mit Hilfe einer einfachen Betrachtung der Lagenkugel. Dieses hat bereits früher K. Weissenberg getan. Einer der von K. Weissenberg beschriebenen Fälle muss aber hier korrigiert werden. Für den Fall $\rho > \varphi$ wurde von ihm ein Diagrammtypus besprochen, der durch eine Intensitätsverdopplung in der vertikalen Mittellinie charakterisiert war. Aber wie man in der Tabelle 1 deutlich sieht, existiert diese Möglichkeit nicht.

Eine experimentelle Bestätigung hierfür konnte wie folgt durchgeführt werden. Ein Steinsalzkristall wurde um eine Achse herum gedreht, welche ihrerseits nochmals mit dem Neigungswinkel $\varphi = 51°10'$ (dem Spiralwinkel entsprechend) um eine zweite Achse rotierte. Bestrahlt man diesen rotierenden Kristall senkrecht zur zweiten Drehachse, dann erhält man ein der idealen Spiralfaserstruktur entsprechendes Diagramm. Trotzdem die Reflexionen der Ebenen (111), (200) und (220) die Bedingung $\rho > \varphi$ erfüllen, tritt dabei keine Intensitätsverdopplung in der vertikalen Mittellinie auf. Ein schematisches Bild und die Winkelverhältnisse werden in Abb. 2 und Tabelle 2 gezeigt.

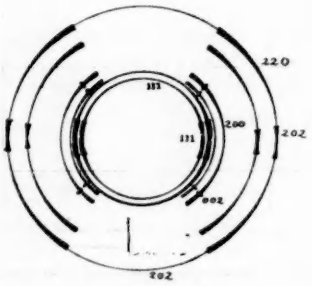

Abb. 2.

Tabelle 2.

		$\varphi=51°\ 10'$	$\lambda=Cu\ K_\alpha\ K_\beta$			
Index	λ	ρ	γ	δ_1	δ_2	Reflexe
111	α	54°41′	13°41′	0°	106°20′	
	β	54°41′	12°21′	0°	106°10′	
200	α	90°	15°51′	36°	144°	
	β	90°	14°18′	36°30′	143°30′	
002	α	0°	15°51′	49°20′	49°20′	
	β	0°	14°18′	49°40′	49°40′	
220	α	90°	22°42′	32°20′	147°40′	
	β	90°	20°42′	33°50′	146°10′	
202	α	45°	22°42′	0°	96°40′	
	β	45°	20°24′	0°	96°30′	

VI. Vergleich der Intensitätsformeln von verschiedenen Autoren. Jeder Autor hat nach eigenem Arbeitsprinzip die Verteilungsfunktionen ausgerechnet und ist zu verschiedenen Formeln gekommen, die aber beinahe gleiche Kurven zeigen. Diese Formeln müssen zunächst auf eine gleiche Bezeichnungsweise gebracht und dann zusammengestellt werden.

(1) *Spiralfaserstruktur.* (a) Allgemeine Reflexe.

(i) unsere Formel: $I \propto \left|\frac{1}{v_1}\right| + \left|\frac{1}{v_2}\right|$

$$v_{1,2} = \left(\frac{d\delta}{\delta\omega}\right)_{\omega_1,\,\omega_2} = \frac{A}{A^2-B_{1,2}^2}\left\{\cos\varphi\cdot B_{1,2} + \kappa_{1,2}\frac{(\cos\rho B_{1,2}-\sin\theta\cdot A)\sqrt{\sin\varphi\, A^2-B_{1,2}^2}}{\sqrt{A^2\cos^2\theta-B_{1,2}^2-A^2\cos^2\rho+2\cos\rho\sin\theta\cdot A\cdot B_{1,2}}}\right\}$$

$$A = 1-\cos^2\delta\cos^2\theta$$
$$B_1 = \sin\delta\cos\rho-\cos\varphi\cos\delta\sin\theta\cos\theta+\cos\theta\sin\delta\sqrt{c}$$
$$B_2 = \quad ,, \qquad\qquad ,, \qquad -\cos\theta\sin\delta\sqrt{c}$$
$$c = \sin^2\varphi-\cos^2\rho-\cos^2\theta\cos^2\delta+2\cos\rho\cos\varphi\cos\theta\cos\delta$$

(ii) Matano'sche Formel:

$$I \propto \frac{\sin\rho}{\sqrt{\sin^2\varphi-\cos^2\rho-\cos^2\theta\cos^2\delta+2\cos\theta\cos\rho\cos\varphi\cos\delta}}$$

$$\propto \frac{\sin\rho}{\sqrt{c}} \propto \frac{1}{\sqrt{c}} \quad (\sin\rho \text{ ist konstant bei einem bestimmten } \rho)$$

Die Matano'sche Formel ist viel einfacher als die von uns. Sie enthält nur den Ausdruck $\sqrt{c}$.

(b) Äquator-Reflexe. $\rho = 90°$.

(i) unsere Formel:

$$v_{1,2} = \frac{A}{A^2-B_{1,2}^2}\left\{\cos\varphi\cdot B_{1,2}-\kappa_{1,2}\cdot\frac{\sin\theta\cdot A\sqrt{\sin^2\varphi\, A^2-B_{1,2}^2}}{\sqrt{A^2\cos^2\theta-B_{1,2}^2}}\right\},$$

$$I \propto \left|\frac{1}{v_1}\right| + \left|\frac{1}{v_2}\right|.$$

(ii) Matano: $$I \propto \frac{1}{\sqrt{\sin^2\varphi-\cos^2\theta\cos^2\delta}}.$$

(iii) Kratky: $$I \propto \frac{\sin\varphi}{\sqrt{\sin^2\varphi-\cos^2\theta\cos^2\delta}} \propto \frac{1}{\sqrt{\sin^2\varphi-\cos^2\theta\cos^2\delta}}.$$

($\sin\varphi$ ist konstant bei einem bestimmten φ)

Hier stimmen die Formeln von Matano und Kratky überein.

(2) *Ringfaserstruktur.* (a) Allgemeine Reflexe.

(i) unsere Formel:

$$v_{1,2} = \frac{A(\cos\rho B_{1,2} - \sin\theta \cdot A)}{\sqrt{A^2 - B_{1,2}^2}} \times \left\{A^2\cos^2\theta - B_{1,2}^2 - A^2\cos^2\rho + 2\cos\rho\sin\theta A \cdot B_{1,2}\right\}^{-\frac{1}{2}},$$

$$I \infty \left|\frac{1}{v_1}\right| + \left|\frac{1}{v_2}\right|.$$

(ii) Matano: $$I \infty \frac{\sin\rho}{\sqrt{1-\cos^2\rho-\cos^2\theta\cos^2\delta}}.$$

(b) Äquator-Reflexe.

(i) unsere Formel: $$I \infty \frac{\cos\delta\sin\theta\cos\theta}{1-\cos^2\delta\cos^2\theta}.$$

(ii) Matano: $$I \infty \frac{1}{\sqrt{1-\cos^2\delta\cos^2\theta}}.$$

(iii) Kratky: $$I \infty \frac{1}{\sqrt{1-\cos^2\delta\cos^2\theta}}.$$

(iv) Sakurada u. Hutino: $$I \infty \frac{\cot\theta\cos\delta}{1+\cot^2\theta\sin^2\delta} = \frac{\cos\delta\sin\theta\cos\theta}{1-\cos^2\delta\cos^2\theta}.$$

Hier findet man zwei paarweise Übereinstimmungen, nämlich einerseits zwischen uns und Sakurada-Hutino, und andererseits zwischen Matano und Kratky.

Die zwei verschiedenen Funktionen sind in Abb. 3 graphisch dargestellt.

Die Kurven der Funktionen unterscheiden sich zu wenig von einander und auch die experimentelle Genauigkeit ist nicht gross genug, um die Richtigkeit der Funktionen einwandrei festzustellen.

Es ist also notwendig irgendeinen Fall herauszusuchen, bei dem die Funktionen schon qualitativ vershieden sind. Die Maximum- und Minimumpunkte der Funktionen wurden ausgerechnet und verglichen, aber leider findet man bei der Ringfaserstruktur in allen Fällen, und bei der Spiralfaserstruktur im Falle der Äquator-Reflexe keine Unterschiede. Nur bei den allgemeinen Reflexen der Spiralfaserstruktur ergibt sich die Möglichkeit einer Nachprüfung, da die Funktionen von uns und von Matano einen voneinander experimentell unterscheidbaren Minimumpunkt besitzen. Die Abb. 4 zeigt die Kurven für die Netzebene (021) der Cellulose; die ausgezogene Linie ist die nach unserer Funktion, die Gestrichelte Linie die nach Matano errechnete Kurve.

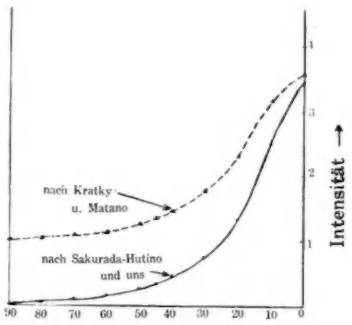

Abb. 3.

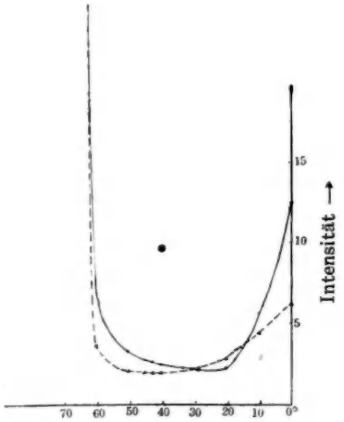

Abb. 4.

In unserer letzten Aufnahme konnten wir feststellen, dass die nach unserer Funktion errechnete Kurve mit dem experimentellen Ergebnis übereinstimmt.

VII. **Realisierung der verschiedenen Faserstrukturen durch Rotation des „Einkristalls"** Wie es schon im Paragraph V erklärt ist, kann man durch die doppelte Rotation des „Einkristalls" beliebige ideale Faserstrukturen realisieren. Hier zeigen wir das letzte Modell unserer Kamera und einige damit gemachte Aufnahmen.

Der Kristall K (Abb. 5) wird zunächst auf die Spitze einer Drehachse A gesetzt und mit einer konstanten Geschwindigkeit, welche durch einen kleinen synchronisierten Motor erzeugt wird, um eine bestimmte kristallographische Achse herum gedreht. Das ganze System lässt man dann nochmals um eine zweite Achse B (der Faserachse entsprechend) herum rotieren. Der Winkel φ zwischen den beiden Drehachsen A und B, welcher dem Spiralwinkel entspricht, ist beliebig regulierbar konstruiert. Durch die Blende S wird der Kristall senkrecht zur Achse B mit Röntgenstrahlen bestrahlt und das Diagramm wird auf einer flachen photographischen Platte oder einem zylindrisch gerollten Film F aufgenommen. Um längs des Debye-Scherrer-Kreises praktisch zu photometrieren, ist der zylindrisch gerollte Film geeignet, dessen Achse aber dabei mit dem Röntgenstrahlenbündel übereinkommen muss. Da das „Einkristall" der Cellulose selbst nicht hergestellt und daher auch nicht untersucht werden kann, so wird zur annäherungsweisen Realisierung beliebiger Faserstrukturen von

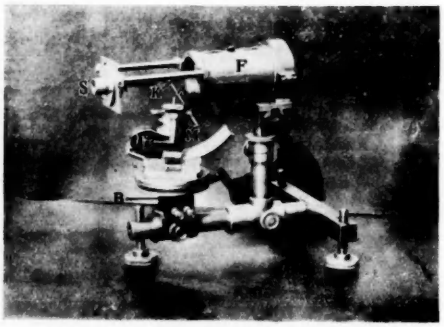

Abb. 5 Doppeldrehe-Kristall Kamera.

Abb. 6.

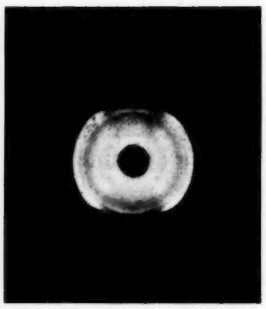

Abb. 7.

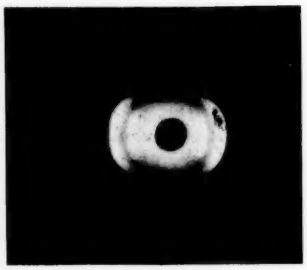

Abb. 8.

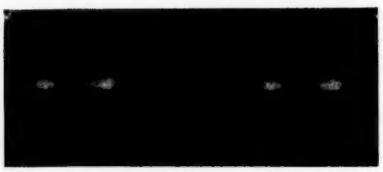

Abb. 9.

Cellulose die Ramiefaser benutzt, da diese den besten Parallelitätsgrad der Kristallite aufweist.

Natürlich ist es nicht notwendig, bei der Ramiefaser die Achse A rotieren zu lassen, weil sie schon axiale Symmetrie besitzt; ferner ist es auch nicht möglich, damit die ideale Spiralfaserstruktur zu realisieren, sondern nur die reale.

Abb. 6 und 7 zeigen die Spiralfaserdiagramme von NaCl und Cellulose ($\varphi = 45°$), welche mit unserer Einrichtung aufgenommen sind. Die Intensitätsverteilungskurven dieser beiden Aufnahmen sind in Abb. 10 dargestellt.

Abb. 8 zeigt das Diagramm der natürlichen Spiralfaser der Agave.

Abb. 9 ist das auf dem zylindrisch gerollten Film aufgenommene Spiralfaserdiagramm der Cellulose mit dem Spiralwinkel 60°.

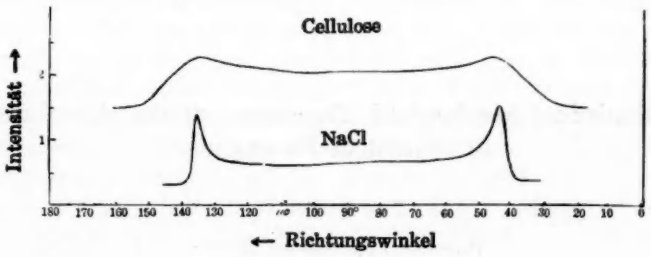

Abb. 10.

Schlussbetrachtung. Es wurde versucht, die Intensitätsverteilung des Faserdiagrammes quantitativ zu erfassen und eine allgemeine mathematische Funktion für die Intensitätsverteilung bei der idealen Spiralfaserstruktur zu finden. Eine solche Funktion schliesst die Intensitätsverteilung bei der Ringfaserstruktur und der einfachen Faserstruktur als Spezialfälle ein, und andererseits kann man sich das Diagramm der realen Faserstruktur aus einer Überlagerung vieler idealer Spiralfaserstrukturdiagramme zusammengesetzt denken.

Es wurde nun auf dem oben beschriebenen Wege eine Formel für die Intensitätsverteilung abgeleitet. Im Anschluss hieran konnte unter Zugrundelegung dieser Formel eine Systematisierung der verschiedenen möglichen Diagrammtypen vorgenommen werden.

Es wurde dann weiterhin ein genauer Vergleich unserer Formel mit den Formeln anderer Autoren vorgenommen. Hierbei zeigte es sich, dass die verschiedenen, auf verschiedenen Wegen erhaltenen Formeln von Kratky, Sakurada-Hutino, Matano und uns zwar sehr ähnlich sind, aber

doch kleine Abweichungen aufweisen. Für den praktischen Gebrauch—zum mindesten in den Fällen, wenn keine grösste Genauigkeit verlangt wird—ist die Benutzung der einfacheren und integriebaren Formel Matano's zu empfehlen.

Durch experimentelle Nachprüfung der nach Matano und uns errechneten Kurven in einem speziellen Fälle, in dem diese schon qualitativ verschieden sind, konnte gezeigt werden, dass die nach unserer Formel errechnete Kurve richtig ist.

Institut für Faserforschung,
Kaiserliche Universität zu Osaka.

On the Statistical Mechanical Treatment of the Absolute Rate of Chemical Reaction.

By Juro HORIUTI.

(Received December 20, 1937.)

By "chemical reaction" we understand simple rearrangements of chemical combinations among a group of atoms. It is the object of the present article to discuss in general the statistical method for treatment of the absolute reaction rate with a group of atoms having the following properties: (1) displacements of atoms take place adiabatically with regard to the electronic configuration; (2) classical mechanics holds for the motion of centres of gravity of atoms; (3) the group has more or less chance of interchanging energy with its surroundings at a definite temperature by interaction with radiation or with other material system; the interaction will be called "collision" in what follows; (4) the group can stably exist in the initial and the final state, which are distinctly different with each other in spacial relative configuration of atoms. Such a group of atoms will be called "chemical system" in what follows.

The rate constant of the reaction is now the probability with which the chemical system transits from the configuration of the initial state to that of final one per unit time. The transition and its probability will be treated with special reference to the configuration space, rather than

with reference to the phase space, since we are interested in the spacial rearrangements of atomic nuclei rather than in those of momenta. The representative point of our chemical system will thus move in the configuration space along a trajectory belonging to a definite energy state until interrupted by a collision and switched over to another trajectory. Time interval and the portion of trajectory marked off by two successive collisions will be called in what follows, "life time" and "free path" respectively. Further aspects of the motion of the representative point are those imposed by (4), i.e. the point may move about within either of two separate regions in the configuration space corresponding to the initial and the final state for a long time without traversing the critical regions intermediate between them. With this manner of representation the probability is now that with which a representative point escapes the initial region towards the final one. One may of course consider, if one prefers although it is not absolutely necessary, an assemblage of such points contained in the initial region, and use the terminology of the gas kinetic theory: the fraction of points out of the total contained in the initial region, which escape the latter per unit time, is the probability in question. It will be meant by the statistical equilibrium of the assemblage that the number of points contained in any assigned volume in the configuration space is proportional to the phase integral over the volume.

The probability will be dealt with for three different types of flow of points arising from different magnitudes of the free path. If the free path is small compared to the extension of the critical region and still less compared to that of the initial and the final regions, the representative point would, when situated at the critical regions, move back and forth and hesitate to reach either of regions. Even if it has once transited any fixed point on the critical region toward the final region, it would with almost equal probability, go back home as arrive at the destination and it is only with very small probability that one may expect it at the final region some time after the transition.

The assemblage of points, if it is at the distribution departing from that of statistical equilibrium, would thus flow with mass velocity less than that of thermal motion. Since momenta of points contained within any elementary volume, whose extention is larger than the free path, accord with Boltzmann's distribution because of sufficient collisions, the flow of points may be treated like diffusion if such volume is small enough.

According to (4) further, we have a steady flow in the neighbourhood of the critical region. In this case we may set up lines of flow and surfaces orthogonal to latters along which no resultant flow of points takes place. The main line of flow may duly be termed the "reaction co-

ordinate"[1][2] but the number of points which pass through the surface from the side of the initial region to that of the final region is by no means equal to that of the mass flow, the latter giving the reaction rate in this case.

This effect diminishes the reaction constant the more, the broader is the critical region measured along lines of flow and the more frequent are the collisions. So far as the latter frequency does not appreciably depend upon the temperature, the resulting depression is mainly imposed upon the temperature independent factor or the "collision factor" Z of the reaction constant $\mathfrak{k}$ as expressed by $\mathfrak{k} = Ze^{-\frac{U^*}{kT}}$ where U^* is the activation energy. The frequent occurrence of collisions in the present sense thus diminishes "collision factor".

This effect may account for the so-called slow reaction in the solution raised by Moelwyn-Hughes and Hinshelwood[3] where frequent collisions are expected.

In the other extreme case when the free path is large compared with the extension of both the initial and the final regions, the representative point, moving on a trajectory of a single energy state, is able to fly through both the regions over and over again without being hit by a collision. The reaction is completed by a timely collision when the representative point is just flying through the final region. This case was thoroughly discussed by Wigner from a different angle with special reference to the association reaction stabilised by three body collisions.[4]

The intermediate case is now that in which the free path is longer than the extension of the critical region but shorter than that of the initial and the final region. The representative point, when it has entered either of the regions, thus collides once at least and assumes an energy state in the region with a probability proportional to the Boltzmann factor but it traverses the critical region with one flight.

As to the manner of flow of points the following can be inferred. Suppose a surface S were stretched between the initial and the final region so that a point in the initial region has once at least to pass through it and that a large number of points exist in the initial region while none in the final region. The points which pass through the surface are those moving along trajectories which lead to the final region with a single pass through the surface or after once or many times passed in and out the

(1) Eyring, *J. Chem. Phys.*, **3** (1935), 107.
(2) Evans and Polanyi, *Trans. Faraday Soc.*, **31** (1935), 875.
(3) Moelwyn-Hughes and Hinshelwood, *J. Chem. Soc.*, **1932**, 230.
(4) Wigner, *J. Chem. Phys.*, **5** (1937), 720.

surface, and those moving on trajectories which pass the surface in and out without leading to the final region. The former group of points is assured of passage into the final region since none of them are struck out of their route in the critical region, the number of their passages per unit time being the point in question. If, on the other hand, the assemblage were at statistical equilibrium over the whole configuration space, the number of points in the initial region being the same as before, the total number of passages through the surface is increased by the number of in-and-out passages of trajectories which are traced by points coming from the final region: points from the final region which arrive at the initial region with a single pass through the surface contribute nothing to the total number since they do not encounter collisions within the critical region. The total number is thus the upper limit of that in question and the minimum value obtained by varying the surface is the best approximation. The minimum will give the exact number in question if it is the case that trajectories are not entangled within the critical region, which might be satisfied if the potential energy is not very complicated there. Such type of flow of points may be called "effusion". The reaction rate can be calculated as given below by counting the number of points falling on the surface S, and by minimizing the latter. The number is given by

$$-\frac{dN}{dt} = N\frac{\int^{S}\cdots\int c_1 e^{-\frac{\mu_1 c_1^2}{2kT}-\frac{E^*}{kT}} dq_2 dq_3 \cdots dq_n dp_1 dp_2 \cdots dp_n}{\int^{V}\cdots\int e^{-\frac{E}{kT}} dq_1 dq_2 \cdots dq_n dp_1 dp_2 \cdots dp_n} \qquad (1),$$

where $$E^* = E_K^* + U^*,$$

and $$E = \frac{1}{2}\mu_1 c_1^2 + E_K + U.$$

$q_1, q_2, \ldots, q_n$ are orthogonal curvilinear coordinates, q_1 being normal to the surface, n three times the number of nuclei of the chemical system, and p's conjugated momenta, while μ_1 and c_1 are respectively the reduced mass and the velocity associated with q_1. E is the total energy, E_K the kinetic energy in the degree of freedom 2, 3,..., n and U the potential energy where asterisks denote those quantities on surface S. Integration S is to be taken over whole S surface, over positive value of p_1 and over whole momentum space of remaining momenta and N the total number of representative points distributed over the region. Integration V is the phase integral of the initial region bounded by S. Integration over c_1 being carried through, the above equation becomes

$$-\frac{dN}{dt} = NkT \frac{\int^{S}\cdots\int e^{-\frac{E^*}{kT}} dq_2 dq_3 \cdots dq_n\, dp_2 dp_3 \cdots dp_n}{\int^{V}\cdots\int e^{-\frac{E}{kT}} dq_1 dq_2 \cdots dq_n\, dp_1 dp_2 \cdots dp_n} \qquad (2).$$

The integral in the numerator is nothing but the phase integral of the motion restricted on the surface S. A surface S_0 which minimizes the rate (2) will be called "critical surface". S_0 satisfies the condition:

$$\delta\int^{S}\cdots\int e^{-\frac{E^*}{kT}} dq_2 dq_3 \cdots dq_n\, dp_2 dp_3 \cdots dp_n = 0\,,$$

since $N\Big/\int^{V}\cdots\int e^{-\frac{E}{kT}} dq_1 dq_2 \cdots dq_n\, dp_1 dp_2 \cdots dp_n$ remains unchanged by shifting surface S, because of the statistical equilibrium of points over the configuration space. Integrating over p, the variation equation becomes

$$\int^{S}\cdots\int^{i=2,3,\cdots,n} \Pi \sqrt{2\pi\mu_i kT}\, e^{-\frac{U^*}{kT}}\left(-\frac{1}{kT}\frac{\partial U^*}{\partial q_1} + \sum^{i=2,3,\cdots,n}\frac{1}{\rho_i}\right)(\delta q_1)^* dq_2 dq_3 \cdots dq_n = 0,$$

or

$$\frac{1}{kT}\frac{\partial U^*}{\partial q_1} = \sum^{i=2,3,\cdots,n}\frac{1}{\rho_i} \qquad (3),$$

where μ_i's are reduced masses associated with i-th coordinates and ρ_i's principal radii of curvature.

The reaction rate can thus be calculated according to Eq.(2) by determining the critical surface by means of (3).

The present procedure will be discussed and exemplified in some special cases assuming the fulfilment of conditions for "effusion".

(i) Eq.(2) may be expressed in terms of partition functions by dividing both numerator and denominator throughout by h^n:

$$-\frac{dN}{dt} = N\frac{kT}{h}\frac{Q^*}{Q} \qquad (4),$$

where $$Q^* = \frac{1}{h^{n-1}}\int\cdots\int e^{-\frac{E^*}{kT}} dq_2 dq_3 \cdots dq_n\, dp_2 dp_3 \cdots dp_n\,,$$

and $$Q = \frac{1}{h^n}\int\cdots\int e^{-\frac{E}{kT}} dq_1 dq_2 \cdots dq_n\, dp_1 dp_2 \cdots dp_n\,.$$

This is formally equivalent to the equations given by Eyring,[1] Wigner,[4] Evans and Polanyi[2] but different from those in the nature of the surface S for counting the passage of points; the method of the latter authors is equivalent to reckon the passage through a surface $\frac{\partial U}{\partial q_1} = 0$. In a special case when $\frac{\partial U}{\partial q_1} = 0$ happens to be a Cartesian plane Eq. (3) is satisfied and hence the difference in the two procedures vanishes.

In such a case Eq. (2) assumes the familiar form of the expression for effusion,

$$-\frac{dN}{dt} = N\sqrt{\frac{kT}{2\pi\mu_1}} \frac{\int^S \cdots \int e^{-\frac{U^*}{kT}} dq_2 dq_3 \cdots dq_n}{\int^V \cdots \int e^{-\frac{U}{kT}} dq_1 dq_2 \cdots dq_n} \qquad (5),$$

integrating over associated momenta, $q_2, q_3, \ldots, q_n$ being now Cartesian coordinates. Integrals S and V give the area of the orifice and the volume of the containing vessel in the case of the effusion of real gas, where $U^* = U = \text{const.}$

(iia) The present procedure is applied to the association of two atoms, whose mutual potential energy $U(r)$ depending only on the distance r has no maximum. This is a case when the transition state method[1][2][4] can not be applied. Surface S is now $r_i > r > r_f$ in the six dimensional configuration space, where r_i and r_f are nuclear separations at the initial and at the final state respectively. Critical surface S_0 can be located by (3) that,

$$r = r_0,$$

where

$$\frac{1}{kT}\frac{\partial U^*}{\partial r_0} = \frac{2}{r_0} \qquad (6).$$

r_0 is such a distance that if two nuclei are destined to approach each other within r_0 they probably react, but not otherwise. This might be interpreted as the sum of collision radii of the two nuclei or when two atoms are identical as the collision diameter. It may be noted that r_0 depends on the temperature or on the mean relative velocity of the two nuclei. If, for instance, $U^*(r)$ is that of Coulomb attraction, the collision diameter is inversely proportional to the temperature.

(iib) If $U^*(r)$ has a maximum, the transition state method would reckon the passage of representative points through the surface $\frac{\partial U^*}{\partial r} = 0$, while the present one that through the surface $\frac{\partial U^*}{\partial r} = \frac{2kT}{r}$. Assuming

that $\frac{\partial U^*}{\partial r} = 0$ at $r = r_0' = 1\text{Å}$ and $-\frac{\partial^2 U^*}{\partial r^2} = 1 \sim 0.1$e.v./Å^2 in its neighbourhood, the ratio of the reaction rate v_T due to the transition state method to that due to the present procedure is calculated by Eq. (2) and Eq. (6)

$$\frac{v_T}{v} = \frac{r_0'^2}{r_0^2} e^{-\frac{U^*(r_0') - U^*(r_0)}{kT}} = 1.1 \sim 1.5 \quad \text{at} \quad 25°\text{C}.$$

The ratio is only trifling at room temperature but increases rapidly with increasing temperature.

Hokkaido Imperial University,
Sapporo.

The Mechanism of the Hydrogen Electrode Process. I. The Catalytic Mechanism.

By **Juro HORIUTI** and **Go OKAMOTO.**

(Received January 21, 1938.)

The elementary reaction underlying to the hydrogen electrode process such as the evolution of hydrogen at cathode or the consumption at anode may generally be formulated in the form,

$$2\text{H}^+\text{B} + 2\ominus \rightleftarrows \text{H}_2 + 2\text{B},$$

where B is the base of generalised sense due to Brönsted[1] and $\ominus$ the metal electron.

In the case when the two opposed processes are balanced we are dealing with the reversible hydrogen electrode. In the latter case hydrogen gas and the solution are catalytically interchanging their hydrogen atoms by way of the hydrogen electrode process. If further this is the only possibility of interchanging hydrogen atoms, the isotopic interchange reaction is simply a special case of the hydrogen electrode process, and we are enabled to observe the rate of electrode process in each direction at equilibrium by labelling it with a hydrogen isotope.

(1) Brönsted, *Rec. trav. chim.*, **42** (1923), 718.

The elementary process in question may take place through various possible intermediate states and any reaction step between successive intermediate states may possibly govern the rate, thus giving rise to various mechanisms.

Remembering that the elementary process of interest includes three acts i.e. neutralizations of two protons and the combination of them, all possible sequences of intermediate states can be schematically expressed as follows:

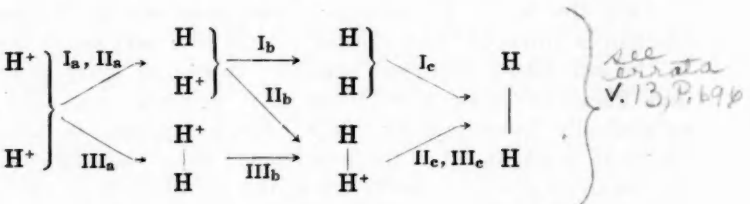

see errata V. 13, P. 696

where parentheses show two protons (or a hydrogen atom and a proton) which are statistically independent of each other and dashes two such ones combined somehow with each other.

I shows the sequence of intermediate states—to be called "reaction path" hereafter—in which two protons are independently neutralised and subsequently combined with each other to form a hydrogen molecule, II that in which one of protons is neutralised, combined with the second one to form a hydrogen molecule ion, the latter being subsequently neutralised to form a hydrogen molecule and III that in which two protons are combined with each other and are neutralised one after another to form a hydrogen molecule.

Any transitions from an intermediate state to another can possibly be the rate determining step thus giving rise to different mechanisms. In usual attempts to find out the mechanism it was customary to restrict oneself to the reaction path I and to pick up the rate determining step from the two alternatives (I_a and I_b are identical) with a hope that a single mechanism thus found might rule over all hydrogen electrode processes.

Tafel[2] in old days considered that I_c was the rate determining step. This concept has found a considerable support in experiments of Bonhoeffer,[3] who has found that the series of catalytic activity of several metals for the recombination of active hydrogen ran parallel with that of cathodic overvoltage.

(2) Tafel, *Z. physik. Chem.*, **50** (1905), 641.

(3) Bonhoeffer, *Z. physik. Chem.*, **113** (1924), 199.

Le Blanc[4] maintained against the former that it was the neutralisation of proton which governed the rate. This was later supported by Volmer[5] and Frumkin,[6] who on the basis of this mechanism accounted for the well known Tafel's empirical relation between cathodic current i and overvoltage η,

$$\log i = -\frac{\alpha F\eta}{RT} + \text{constant, where } 0 < \alpha < 1 .$$

On the basis of the same mechanism but in language of wave mechanics Gurney[7] and Fowler[8] have also arrived at the explanation of the interesting empirical relation. In use of heavy hydrogen Horiuti and Polanyi[9] have later found that hydrogen gas and water were catalytically interchanging their hydrogen atoms in the presence of platinum black and that the interchange rates were appreciably affected by the hydrogen ion concentration and by addition of salts. The result of experiments seemed to direct to the fact that the rate determining reaction was associated with the change of electric charge of the elementary system since the change of concentrations of hydrogen ions and salts was known to affect the potential across the double layer at the interface where reactants were situated. This being however only compatible with I_a (or I_b) as the rate determining step, the claimed mechanism for the hydrogen electrode process seemed for some time convincing so far as one adheres to the customary manner of treating the mechanism.

Following consideration would, however, reveal that the usual concept does not suffice to understand general features of the hydrogen electrode process. Since the rate with which the elementary system passes through an intermediate state must be equal or greater than the total reaction rate, any assigned intermediate state imposes an upper limit upon the reaction rate. Topley and Eyring[10] have thus found that the energy of the state of neutral atoms on the reaction path I, if they were free ones wandering about in the solution as supposed by Fowler[8] and Gurney,[7] was too high for a reasonable magnitude of the reaction rate. It follows then that metals of large adsorption energy may give rise to the reaction path I by sheltering free atoms at the state of lower energy while such metals of very small adsorption energy as mercury practically blocks up

(4) Le Blanc, "Abhandlungen der deutschen Bunsen-Gesellschaften," No. 3, Halle (1910).
(5) Volmer, *Z. physik. Chem.*, *A*, **150** (1930), 209.
(6) Frumkin, *Z. physik. Chem.*, *A*, **164** (1933), 121.
(7) Gurney, *Proc. Roy. Soc.* (London), A, **134** (1931), 137; **136** (1932), 378.
(8) Fowler, *Trans. Faraday Soc.*, **28** (1932), 368.
(9) Horiuti and Polanyi, *Nature*, **132** (1933), 819, 931; **133** (1934), 142.
(10) Topley and Eyring, *J. Chem. Phys.*, **2** (1934), 222.

the reaction path I. The reaction in this case must have managed another path to pass through, if it has occurred at all.

On the basis of the more basic concept advanced above and of experiments with several different hydrogen electrode processes, the present authors have previously suggested that the step I_c governed the rate of hydrogen electrode process with electrodes of Ni, Cu, Fe, Ag, Au, and Pb (in alkaline solution) and II_c that of Hg, Sn, and Pb (in acidic solution).[11]

The former in which the recombination of two chemisorbed atoms was the rate determining step was called the catalytic mechanism and the latter in which the neutralization of hydrogen molecule ion governed the rate was called the electrochemical mechanism.[12]

These assignments of mechanisms have since been confirmed from various angles in this laboratory. Experimental confirmations were given to conclusions on the behavior of the hydrogen electrode process derived from respective mechanisms. Some quantitative conclusions have thus been derived on respective rates of the governing reactions by virtue of the statistical mechanical method, which could nicely account for behaviors of hydrogen electrode processes.[13][14] Tafel's empirical relation was thus quantitatively accounted for in both cases of mechanisms with special reference to the mutual interaction of hydrogen atoms and protons situated on the surface of the catalyst.

It is the object of the present paper to put forward some of our recent experimental evidences for the catalytic mechanism with special reference to nickel electrode. Experimental evidences for the electrochemical mechanism will be presented in a separate paper by Hirota in conjunction with one of the present authors.

Under the assumption that the adsorbed hydrogen atoms are practically non-polar and that the hydrogen electrode processes comprise the isotopic interchange reaction in the above sense, conclusions will be derived from the catalytic mechanism and confirmed by experiments in the following three cases.

(1) The rate determining step of the catalytic mechanism being the transition between neutral states i.e. chemisorbed hydrogen atoms

(11) Horiuti and Okamoto, *Sci. Papers Inst. Phys. Chem. Research* (Tokyo), **28** (1936), 231.

(12) According to the recent study of Ikusima in this laboratory it is very probable that the electrochemical mechanism is operative on the hydrogen electrode of platinum at least in the neighbourhood of the reversible equilibrium. The result will be published in a near future.

(13) G. Okamoto, J. Horiuti, and K. Hirota, *Sci. Papers Inst. Phys. Chem. Research* (Tokyo), **29** (1936), 223.

(14) Hirota and Horiuti, to be published in a near future.

and hydrogen molecule, the change of electrical potential at the interface cannot affect the reaction rate. It follows that the isotopic interchange rate between heavy hydrogen gas and aqueous solution will be insensitive to the change of hydrogen ion concentration or to the addition of salts contrary to the case of a platinum catalyst for which the rate with N/10 HCl solution was found 100 times as large as that with 1 N KOH + 1 N KCl solution according to a recent result of Ikusima.[15]

This conclusion was experimentally investigated by the following procedure. 4% shifted hydrogen gas of 104 mm. pressure was shaken with several different aqueous solution in a suitable vessel in the presence of annealed nickel wire of 0.1 mm. diameter and of 3300 m. length at 100°C.

The following table shows the results of experiments carried out with one and the same catalyst changing the solution from time to time, the interchange reaction rate being expressed by the first order rate, $k = \frac{1}{t} \log \frac{x_0}{x_t}$, where x_0 and x_t are atomic fractions of deuterium in hydrogen gas respectively before and after the reaction and t time of

Catalysed interchange reaction with different solutions at 100°C.

No. of exp.	Solution	Initial D-percent. $100\,x_0$	Final D-percent. $100\,x_t$	Time of shaking t (hr.)	Reaction rate $k\left(=\frac{1}{t}\log_{10}\frac{x_0}{x_t}\right)$
1	Neutral water	4.42	2.15	6.08	0.051
2	,,	,,	2.27	6.30	0.046
3	,,	,,	1.89	7.23	0.051
4	$\frac{N}{1000}$ KOH	,,	1.78	6.17	0.064
5	,,	,,	1.85	6.00	0.063
6	,,	,,	1.85	6.00	0.063
7	$\frac{N}{1000}$ KOH + $\frac{N}{10}$ KCl	,,	2.17	7.70	0.040
8	,,	,,	2.46	6.00	0.043
9	,,	,,	2.43	6.17	0.042
10	$\frac{N}{1000}$ KOH	,,	1.67	5.97	0.070
11	,,	,,	1.93	6.00	0.060
12	,,	,,	1.69	6.38	0.065
13	Neutral water	,,	2.29	6.00	0.048
14	,,	,,	2.01	8.00	0.043

(15) To be published in a near future.

shaking. One sees that experiments Nos. 1, 2, 3, 13, and 14 give good check with the activity of the catalyst. No appreciable variation of reaction rate being observed here contrary to the case of platinum, the conclusion from the mechanism was amply justified by experiments.

(2) From the catalytic mechanism it is expected that the electrode current behaves peculiarly when the electrode potential is suddenly raised or lowered. An experiment which confirmed the above expectation was described in our previous communication[11] and employed as one of the basis of concluding the catalytic mechanism. Here will be presented in a more improved form the experiment and the argument which connect the behavior of electrode current with the mechanism.

Let an anodically polarised hydrogen electrode be at a steady state or an anode at a constant polarization be steadily consuming hydrogen gas to form Brönsted's base[1] giving rise to a constant anodic current. Assuming the catalytic mechanism the state of affairs can be expressed by the following scheme:

$$\frac{1}{2}H_2 \underset{\leftarrow i \rightarrow}{\overset{(\vec{I})}{\rightleftarrows}} K-H \underset{\leftarrow i \rightarrow}{\overset{(\vec{\Im})}{\rightleftarrows}} H^+-B + \ominus \qquad (1),$$

where $^1/_2H_2$ denotes gaseous state, K − H chemisorbed state and $H^+ - B$ ionised state. Length of arrows schematically corresponds the relative frequencies of elementary reactions, latters being expressed in terms of electric currents by $\vec{I}$, $\overleftarrow{I}$, $\vec{\Im}$, and $\overleftarrow{\Im}$. Longer arrows above thus correspond to the positive resultant current i and shorter ones on the left to the governing step of the catalytic atomisation. The same thing, when expressed by above quantities, is

$$i = \vec{I}_{(\theta)} - \overleftarrow{I}_{(\theta)} = \vec{\Im}_{(\theta,\,\eta)} - \overleftarrow{\Im}_{(\theta,\,\eta)} \qquad (2a),$$

and

$$\vec{I} \ll \vec{\Im} \qquad (2b).$$

$\vec{I}$ and $\overleftarrow{I}$ are independent of the electrode potential because of neutral reactants and resultants but depend in general upon the degree of saturation θ of the catalyst's surface with chemisorbed atoms, while $\vec{\Im}$ and $\overleftarrow{\Im}$ depending in general on the both.

From the above equations we have

$$\frac{\overleftarrow{\Im}}{\vec{\Im}} = 1 - \frac{i}{\vec{\Im}}.$$

But since $i < \vec{I}$, according to (2b),

$$i \ll \vec{\mathfrak{J}} .$$

Hence we have

$$\vec{\mathfrak{J}}(\theta_1, \eta_1) \fallingdotseq \overleftarrow{\mathfrak{J}}(\theta_1, \eta_1) ,$$

which expresses the partial equilibrium between adsorbed state and the ionised state.

If one changes η_1 suddenly to another value η_2 a new steady state is to be attained, being characterised by

$$\vec{\mathfrak{J}}(\theta_2, \eta_2) \fallingdotseq \overleftarrow{\mathfrak{J}}(\theta_2, \eta_2) .$$

θ_1 must now be readjusted to a new value θ_2 by removing or adding some hydrogen atoms to the chemisorbed state in order to attain the new steady state.

Since however,

$$\vec{I} > \overleftarrow{I} ,$$

we have by Eq.(2b)

$$\overleftarrow{I} \ll \vec{\mathfrak{J}} ,$$

and by Eq.(2a)

$$\vec{I} \ll \overleftarrow{\mathfrak{J}} ,$$

which show that the excess or the defect of θ is readjusted almost exclusively through ionization or neutralization respectively. Since latter acts are associated with the transposition of electricity, the sudden change of the electrode current thus inserts and additional current to the steady value.

Fig. 1a shows the expected behavior of the anodic current when the electrode potential is suddenly raised. By a similar reasoning it is inferred for the case when the ionization governs the rate that the sudden change of the electrode potential will result merely in an abrupt change of steady current as shown in Fig. 1b without the initial peak as in the case of 1a.

For the experimental confirmation of the above conclusions a hydrogen electrode was constructed with a thin nickel wire A of 0.1 mm. diameter and of 67 m. length (200 cm.^{2} of apparent area) which was sealed in a glass vessel of 170 c.c. capacity as shown in Fig. 2 together with 110 c.c. of N/10 KOH solution and hydrogen gas of 580 mm. Hg pressure.

The vessel was shaken lengthwise to assure a dissolution equilibrium and the hydrogen electrode of nickel was polarised against a platinised

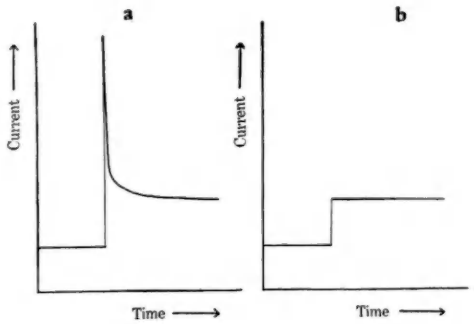

Fig. 1

Fig. 2

platinum wire P sealed in the vessel. Anodic and cathodic polarization were determined against a reference electrode R.

Over the whole range of electrode current (<0.2 microamp. cm.$^{-2}$) observed in the present experiment, the cathodic overvoltage was found to be negligible compared to the anodic one. This affords a sound basis to attribute observed aspects of current to the reaction at the anode. Moreover the diffusion of hydrogen gas toward the anode cannot be the governing process, for if it were the case, the thickness of the layer of solution adhered on the surface of the catalyst computed from the observed current, solubility of hydrogen gas and from the diffusion constant (10^{-5} cm.^{2}/sec.) amounts to the order of magnitude of 10 m., which is apparently impossible in our case. The genuine reaction rate at the anode in question could thus be observed by following the electrolytic current of the cell.

Actually the hydrogen electrode was kept at a fixed anodic polarization until a steady state was reached. The polarization was now suddenly raised by a small amount, the instantaneous current being followed by means of an oscillograph. Details of the experimental procedures and results are described in papers from this laboratory.[16]

The oscillograph record shows one of typical results of our observation. One sees that the theoretical conclusion is fully confirmed by the experiment.

(3) In the catalytic mechanism the rate of the electrode process at the steady state is governed by that of catalytic dissociation of hydrogen

(16) Okamoto, *J. Faculty Sci., Hokkaido Imp. Univ.*, Ser. III, Vol. II, No. 3 (1938), 116; Okamoto and Iijima, *Bull. Inst. Phys. Chem. Research* (Tokyo), **16** (1937), 1426 (printed in Japanese).

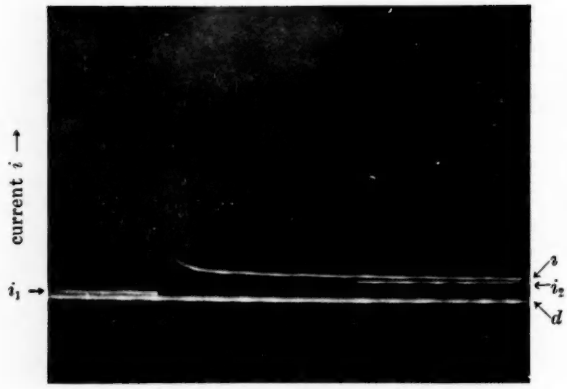

Fig. 3. Oscillograph record.

molecules or of its reversed process. By formulating the latter at a given condition one could obtain an expression for the electrode current. Along this line Hirota in conjunction with present authors[13] arrived at the following expressions for the reaction rates in respective directions:

$$\text{Catalytic atomization,} \qquad \vec{v} = KGe^{-\frac{\varepsilon^*_{H_2}}{RT}}\frac{n}{Q_{H_2}} \qquad \text{(3a)},$$

$$\text{Catalytic recombination,} \qquad \overleftarrow{v} = KGe^{-\frac{\varepsilon^*_{H_2}}{RT}}\frac{1}{P^2} \qquad \text{(3b)},$$

where G is the number of adjacent pairs of metal atoms per unit area at which the catalytic atomization or the recombination takes place, $\varepsilon^*_{H_2}$ minimum potential energy of HH at the activated state, n the number of hydrogen molecules per unit volume and

$$Q_{H_2} = \frac{(2\pi mkT)^{\frac{3}{2}}\,2\pi^2 IkT}{h^5 \sinh\dfrac{h\nu_{H_2}}{2kT}} \cdot e^{-\frac{\varepsilon_{H_2}}{RT}} \quad \text{(State sum of a hydrogen molecule)},$$

$$K = \frac{kT}{h}(1-\theta)^2 e^{-\frac{u^*\theta}{RT}} \sum_{j}^{1\text{-}5} \frac{1}{2}\left(\sinh\frac{h\nu^*_{H_2,\,j}}{2kT}\right)^{-1}, \quad \frac{1-\theta}{\theta} = \frac{\sqrt{\dfrac{Q_{H_2}}{n}}}{q} \cdot e^{\frac{F(\eta_1-\eta_0)}{RT}},$$

$$q = e^{-\frac{\varepsilon_H + u\theta}{RT}} \sum_{j}^{1-3} \frac{1}{2}\left(\sinh \frac{h\nu_{H,j}}{2kT}\right)^{-1}, \quad \text{and} \quad P = \sqrt{\frac{Q_{H_2}}{n}} \cdot e^{\frac{F(\eta-\eta_0)}{RT}}.$$

Other notations have following meanings: θ: degree of saturation of chemisorbed atoms. $\varepsilon_{H_2} = -109.12$ kcal.[17]: potential energy of hydrogen molecule at the equilibrium position. $\varepsilon_H = -60$ kcal.[18]: heat of adsorption of a hydrogen atom. η: electrode potential. η_0: potential of reversible hydrogen electrode. $\nu^*_{H_2,j} = 936, 687, 1704, 368, 626$ (cm.$^{-1}$)[13]: normal vibrational frequencies of HH at the activated state. $\nu_{H,j} = 417, 479, 1900$ (cm.$^{-1}$)[18]: normal vibrational frequencies of H at the adsorbed state. $\nu_{H_2} = 4417.2$ (cm.$^{-1}$)[17]: harmonic frequency of a hydrogen molecule. $I = 4.65 \times 10^{-41}$ (g. cm.^{2})[17]: moment of inertia of hydrogen molecule. $u = 5.65$ kcal.[11]: repulsive potential of an adsorbed hydrogen atom due to surrounding ones at $\theta = 1$. $u^* = 6.70$ kcal.[13]: repulsive potential of HH at the activated state due to the surrounding chemisorbed atoms at $\theta = 1$.

Steady anodic current i is now expressed by

$$i = 2\epsilon KG e^{-\frac{\varepsilon^*_{H_2}}{RT}}\left(\frac{n}{Q_{H_2}} - \frac{1}{P^2}\right) \qquad (4),$$

where ϵ is the elementary charge, two charges being conveyed by one act at catalytic atomisation or recombination.

Eqs. (3a) and (3b) could be checked respectively by observations of individual rates of atomisation and the recombination labelled by deuterium while (4) by direct observations of anodic currents. But since estimations of $\varepsilon^*_{H_2}$ and G are associated with a considerable inaccuracy, the experimental confirmation was made other way round in the present work i.e. G was inversely calculated from experimental data of the anodic current as well as from those of the isotopic interchange reaction and two values thus obtained were compared with each other and with Z, the number of available metal atoms per unit area for the chemisorption of hydrogen atoms. G from two sources should coincide with each other and be of the same order of magnitude with Z whichever lattice plane of the electrode were active, so far as the catalytic mechanism were actually operative.

---

(17) Jeppesen, *Phys. Rev.*, **44** (1933), 195.
(18) Horiuti and Polanyi, *Acta Physicochim. U.R.S.S.*, **2** (1935), 505.

Evaluating K, n/Q_{H_2} and P by data given above G could be determined from observations of the absolute value and of its temperature coefficient of the anodic current or of the interchange reaction rate. Details of the experiments are given in a separate paper from this laboratory.[16]

The results were

$$G = 4 \times 10^{12} \quad \text{from the anodic current,}$$

$$G = 2 \times 10^{12} \quad \text{from the interchange reaction.}$$

Z was, on the other hand, obtained from the following quantitative analysis of the result of experiments (2).

The instantaneous current i or the excess of the rate of ionization of chemisorbed hydrogen atoms over that of neutralization will be assumed to vary linearly with θ,
or

$$i = \epsilon Zk\theta + \text{const.},$$

where ϵ is the elementary charge and k a proportionality constant. Denoting with i_2 and θ_2 corresponding quantities at the steady state reached some time after the raise of the anodic polarization, the above equation is

$$i - i_2 = \epsilon Zk(\theta - \theta_2) \qquad (5).$$

On the other hand the time rate, $-Z\frac{d\theta}{dt}$, of the decrease of chemisorbed atoms can similarly be expressed by

$$-Z\frac{d\theta}{dt} = Zk(\theta - \theta_2) - \{v(\theta) - v(\theta_2)\} \qquad (6),$$

where $v(\theta)$ is the supply of chemisorbed atoms due to the excess of the rate of the catalytic atomization of hydrogen molecules over that of recombination. Neglecting the second member on the right,[19] Eq.(6) is integrated in the form,

---

(19) $\varepsilon v(\theta_1)$ and $\varepsilon v(\theta_2)$ are steady currents respectively before and after the polarization was raised. According to Eq.(4) however the rate of the catalytic atomization varies monotonously from $v(\theta_1)$ to $v(\theta_2)$ along with the decrease of θ or $v(\theta_1) < v(\theta) < v(\theta_2)$. It follows then that $v(\theta_2) - v(\theta)$, which is smaller than $v(\theta_2) - v(\theta_1)$, can be neglected in comparison with $zk(\theta - \theta_2)$, since as seen from the oscillograph record, the total variation of the steady current $i_2 - i_1 = \varepsilon\{v(\theta_2) - v(\theta_1)\}$ is only a small fraction of $i - i_2$, or of $\varepsilon zk(\theta - \theta_2)$ by Eq.(5), at earlier stage immediately after the sudden raise of the anodic potential.

$$\log \frac{\theta - \theta_2}{\theta_1 - \theta_2} = -kt ,$$

time of switching being the origin of t.

By Eq. (5) we have

$$\log \frac{i - i_2}{i_0 - i_2} = -kt \qquad (7),$$

where $$i_0 - i_2 = \epsilon Zk(\theta_1 - \theta_2) \qquad (8),$$

i_0 being the big initial current at $t = 0$.

Observed current was now analysed[20] according to Eq. (7) evaluating i_0 and k. From Eq. (8) we have immediately

$$Z = 2 \times 10^{12} ,$$

which is concordant with the forgoing two values of G affording another experimental support to the catalytic mechanism.

Hokkaido Imperial University,
Sapporo.

(20) According to a more detailed analysis, $i - i_2$ at the later stage is due to the outward diffusion of occluded hydrogen atoms in the metal. Cf. Reference (16).

The Mechanism of the Hydrogen Electrode Process. II. The Electrochemical Mechanism. The Existence of Hydrogen Molecule Ions on the Surface of the Electrode.

By Kozo HIROTA and Juro HORIUTI.

(Received January 21, 1938.)

Okamoto and one of the present authors[1] have previously suggested that it was the neutralization of hydrogen molecule ion adsorbed on the electrode-solution interface which governed the rate of the hydrogen electrode process on the mercury electrode. The proposed mechanism which was called the electrochemical mechanism has since been worked out and established by formulating the rate of the governing reaction by the statistical mechanical method, by deriving therefrom quantitative conclusions on the behavior of the hydrogen electrode process and by confirming latters by experimental data.[2] Especially Tafel's empirical relation[3] between electrolytic current i and the overvoltage η, i.e.

$$\log i = -0.5\frac{F\eta}{RT} + \text{const.},$$

and its range of validity was quantitatively derived from the theory.[2]

The present article deals with an experimental confirmation of one of direct conclusions from the theory i.e. the experimental verification of the existence of hydrogen molecule ion at the electrode-solution interface.

From the premise that the neutralization of hydrogen molecule ion is the slowest step it follows that hydrogen ions $(H^+)_{ads.}$ and hydrogen molecule ions $(HH^+)_{ads.}$ adsorbed on the interface must be at the partial equilibrium with each other and with ions H^+ in the bulk of the solution,

or $$(HH^+)_{ads.} \rightleftarrows (H^+)_{ads.} + H^+ + \ominus,$$

where $\ominus$ denotes metal electrons. Assuming the simple mass action law the electrical work required to transpose one mol of the reactant to the resultant is given by

(1) Horiuti and Okamoto, *Sci. Papers Inst. Phys. Chem. Research* (Tokyo), **28** (1936), 231.

(2) Hirota and Horiuti, to be published in a near future.

(3) Tafel, *Z. physik. Chem.*, **34** (1900), 200; **50** (1905), 649.

$$F\eta = -RT\ln\frac{n_{HH^+}}{n_{H^+}\cdot c_{H^+}} + \text{const.} \qquad (1),$$

from the condition that the total work should vanish at the equilibrium, where n_{HH^+} and n_{H^+} are respective numbers of the adsorbed elementary systems per unit area of the interface and c_{H^+} the concentration of H^+ in the bulk of the solution. It follows from Eq. (1)

$$\frac{n_{HH^+}}{n_{H^+}} \propto e^{-\frac{F\eta_i}{RT}} \qquad (2),$$

i.e. n_{HH^+} increases with negative polarization rapidly compared with n_{H^+}. By a more detailed statistical mechanical calculation taking the mutual interaction of $(HH^+)_{ads.}$ among themselves and with H^+ into account, $\frac{n_{HH^+}}{n_{H^+}}$ assumes the form,

$$\frac{n_{HH^+}}{n_{H^+}} = \kappa e^{-\frac{F\eta_i + u^{H^+}_{HH^+}\cdot\frac{n_{H^+}}{Z} - u^{HH^+}_{H^+}\cdot\frac{n_{HH^+}}{Z} + u^{HH^+}_{HH^+}\cdot\frac{n_{HH^+}}{Z}}{RT}} \qquad (3),$$

where κ is a constant independent of n_{HH^+}, n_{H^+} and of η.[4] Z is the

(4) In a separate work which will be published in a near future (Reference 2), the present authors have formulated and evaluated the constant κ with the result:

$$\kappa = Q_{HH^+}\Big/Q_{H^+}\cdot\sqrt{\frac{Q_{H_2}}{n}} = 1.0\times10^{-6}.$$

n is the number of hydrogen molecules per unit volume of the hydrogen gas of the hydrogen electrode to which the potential η_i is referred and Q_{H_2} the summation of states of a free hydrogen molecule expressed by

$$Q_{H_2} = \frac{(2\pi m_{H_2}kT)^{\frac{3}{2}}\,2\pi^2 I_{H_2}kT}{h^5\sinh\left(1-\frac{x}{2}\right)\cdot\frac{h\nu_0}{2kT}}\,e^{-\frac{\varepsilon^0_{H_2}}{kT}},$$

where m_{H_2} is the mass, I_{H_2} the moment of inertia, 6.21×10^{-41} g. cm.^{2}, ν_0 the harmonic frequency 4417.2 cm.$^{-1}$, x the anharmonicity constant 0.0297, and $\varepsilon^0_{H_2}$ the potential energy at the equilibrium position -109.12 kcal., numerical values being due to Jeppesen (*Phys. Rev.*, **44** (1933), 165).

Q_{H^+} and Q_{HH^+} are summation of states of respective elementary systems housed between a mercury atom and a water molecule at the interface being expressed by

$$Q_{H^+} = \int\frac{A^2}{h^2}\,\frac{1}{2}\left(\sinh\frac{h\nu_{H^+}}{2kT}\right)^{-1} e^{-\frac{\varepsilon_{H^+}}{kT}}\,d\sigma,$$

and

number of metal atoms per unit area of the metal surface and $u_{HH^+}^{H^+}$ is the potential exerted upon an adsorbed HH^+ by surrounding H^+ when $n_{H^+}=Z$. $u_{HH^+}^{HH^+}$ and $u_{H^+}^{HH^+}$ have similar meanings. $u_{HH^+}^{HH^+}$, for instance, was calculated by summing up quantum mechanical repulsive potentials[2] among HH^+ of interest and another HH^+ resting on one of surrounding metal atoms. Details of the calculation are left to the original paper.[2] Numerical values thus obtained are

$$u_{HH^+}^{HH^+} = 0.35 \text{ e.v.}, \quad u_{HH^+}^{H^+} = u_{H^+}^{HH^+} = 0.09 \text{ e.v.}$$

From the above result the followings can be deduced for the variation of population of HH^+ and H^+ with increasing cathodic potential.

At a sufficiently low cathodic potential charged particles at the interface consist almost exclusively of H^+. As the cathodic polarization is gradually increased, a point is reached when n_{HH^+} is no more negligible compared with n_{H^+}. From simplified Eq. (2) one sees that at room temperature a raise of cathodic polarization by 0.2 volts is sufficient to convert the ratio $\frac{n_{HH^+}}{n_{H^+}}$ from 10^{-2} to 10^2. Taking the mutual interaction of HH^+ and H^+ into account according to Eq. (3) another effect is expected at this turning point which can be subjected to an experimental verification.

Replacing the interface with the simplified model of Helmholtz's double layer and neglecting the concentration of negative ions on the cathode, the charge of the condenser $\epsilon(n_{H^+} + n_{HH^+})$ and its potential $\eta + \eta_0$ are related to each other by the formula,

$$-C(\eta+\eta_0) = \epsilon(n_{H^+}+n_{HH^+}) \qquad (4),$$

where η_0 is the absolute potential of the reference electrode, ϵ elementary charge and C the capacity of the double layer per unit area.

$$Q_{HH^+} = \int \frac{\sqrt{2\pi I_{HH^+} kT}}{h} \frac{1}{2^5} \prod_i^{1\cdots5} \left(\sinh \frac{h\nu_i}{2kT}\right)^{-1} e^{-\frac{\varepsilon_{HH^+}}{kT}} d\sigma ,$$

where $d\sigma$ is the elementary volume of the coordinate space of the water molecule's centre. Quantities in integrals, which are, in general, functions of σ, have the following meanings:

- A : the phase integral of the motion of H^+ perpendicular to the axis through the centres of the mercury atom and the water molecule.
- ν_{H^+} : the harmonic frequency of the vibration along the axis.
- ν_i : the normal vibrational frequencies of the hydrogen molecule ion housed between the mercury atom and the water molecule.
- I_{HH^+}: the moment of inertia of hydrogen molecule ion belonging to the single rotational degree of freedom around the $Hg-H_2O$ axis.
- ε_{H^+} and ε_{HH^+}: the potential energies at equilibrium positions.

The total amount of charge required to create a unit area of new surface, E, is given by[5]

$$E = \epsilon (n_{H^+} + 2n_{HH^+}) \qquad (5).$$

When H^+ at the interface is replaced by HH^+ the charge required to create a unit area would increase by Eq.(5), the charge of the condenser being assumed to remain constant. But since an increase of HH^+ is associated with more or less decrease of H^+ due to repulsion, the increase in E due to neutralization to form H^+ might possibly be overcompensated by the decrease of the number of adsorbed H^+. Assuming C to be 19 microfarads according to Frumkin,[6] E could be expressed as the function of η by solving Eqs. (3), (4), and (5) simultaneously as shown by the dotted line in Fig. 1. The ordinate gives the number of elementary charge required to create a unit area and the absissa polarization referred to the decinormal calomel electrode. As was expected the curve shows a marked dip at the polarization where $(H^+)_{ads.}$ are replaced by $(HH^+)_{ads.}$.

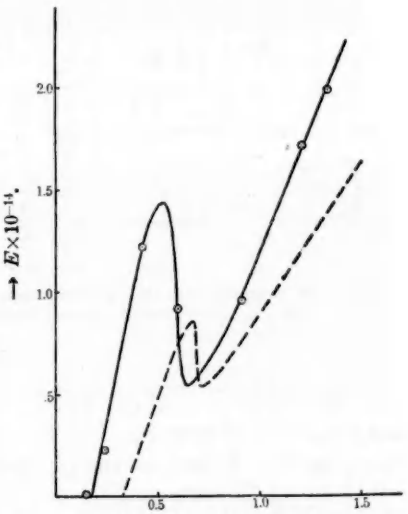

Fig. 1.

The above theoretical conclusion was subjected to an experimental investigation by the following procedure. Cathodically polarized mercury was slowly dropped into N/10 HCl solution, the current flowing was followed by an oscillograph and analysed to obtain the amount of charge E experimentally.

Fig. 2 shows the apparatus used. B is a burette of 60 cm. length and of 0.8 cm. diameter through its lower orifice of 0.3 mm. width mercury being dropped into the solution. S is a big mercury surface against which mercury drop is polarized at a constant potential. R is the switch which allows us to vary the potential stepwise. Solutions are combined with siphons packed with glass wool. The rate of dropping was varied from

(5) HH^+ requires another elementary charge for neutralization.
(6) Frumkin, *Z. physik. Chem.*, A, **164** (1933), 121.

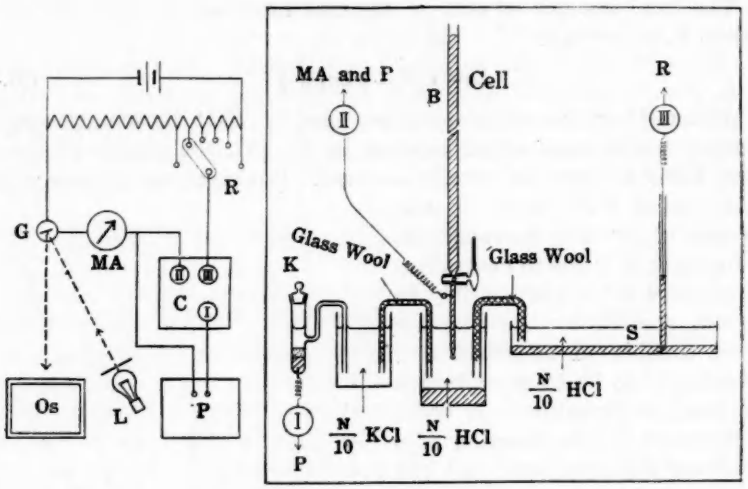

MA: Microammeter. Os: Oscillograph. P: Potentiometer. G: Galvanometer. C: Cell. K: Decinormal calomel electrode. L: Light source. R: Switch.

Fig. 2.

once per 2 sec. to once per 10 sec. Full size of a drop as determined by weighing was 0.0020 c.c. which was found independent of the rate of dropping but slightly of the polarization. Polarization was varied from -0.15 to -1.35 volts against decinormal calomel electrode at an interval of about 0.2 volts.

An oscillograph record was taken at a constant dropping rate but raising the polarization stepwise for every two or three drops. Here are shown two such ones taken both at 19°C. and respectively at the dropping rate once per 2.2 sec. and once per 7.1 sec. One sees that the current increases rapidly at first when a drop begins to grow but more and more slowly afterwards until the drop leaves the orifice when the current returns to the zero line to start a new course again.(7) Irregular discontinuities on the figure are due to switching from a polarization to another.

The record thus obtained being apparently contaminated with steady electrolytic currents the quantity of charge E in question was separated from the latter by the following analysis. The observed current at a given polarization and at a certain definite drop magnitude was plotted against the rate of increase of drop's area. The inclination of the straight line

(7) Instantaneous minus value of the current is due to the momentary diminution of the area after the mercury drop has been torn off at the orifice.

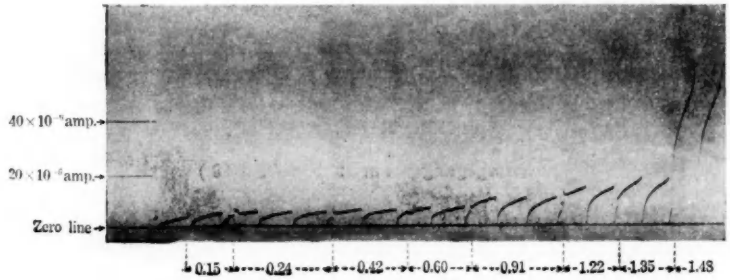

Fig. 3. Oscillograph record I. Dropping rate: Once per 7.1 sec.

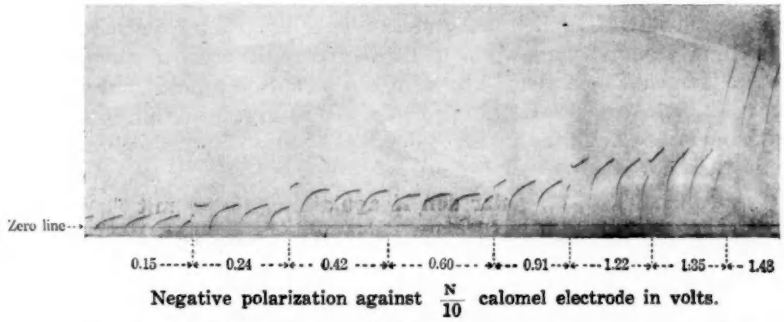

Fig. 4. Oscillograph record II. Dropping rate: Once per 2.2 sec.

gives the charge in question while its intercept at zero rate of increase of drop's area the electrolytic current which is a constant at a given polarization and at a definite surface area.

Experimental value of charge E expressed by the number of elementary charges per unit area was plotted against the polarization and shown by the full line in Fig. 1, the drop area being 0.159 cm.^{2} throughout.

One sees that the experiment satisfactorily confirms the strong dip on the theoretical curve derived from the claimed existence of hydrogen molecule ion at the interface. Quantitative disagreement would rather be shifted to the inaccuracy of *a priori* quantum mechanical calculation of interatomic potentials.

It is the pleasure of the present authors to express their sincere thanks to Professor M. Katayama for his valuable advices, his kind interests and encouragements throughout the forgoing three works.

Hokkaido Imperial University,
Sapporo.

Zur Kenntnis des Aufbaues thixotroper Systeme.

Von **Bunichi TAMAMUSHI.**

(Eingegangen am 22. Januar 1938.)

Freundlich[1] hat in seiner Monographie allgemeine Betrachtungen über die möglichen Ursachen der Thixotropie zusammengestellt. Bei der genannten Erscheinung handelt es sich sicherlich um die Wechselwirkung der abstossenden und anziehenden Kräfte zwischen den Teilchen der Sole oder Suspensionen, wenngleich die Meinungen über den feinen Mechanismus der Thixotropie auch noch divergieren. Bemerkenswert ist dabei der von Freundlich aufgestellte Zusammenhang zwischen Thixotropie und Koagulation, wonach die Thixotropie als Zwischenstufe von zwei extremen Zuständen, d.h. dem stabilen Solzustand einerseits und der vollkommenen Ausflockung anderseits, aufgefasst ist. Dieser bemerkenswerte Gedanke bedürfte jedoch noch weiterer experimenteller Unterstüztung.

Nun hat J. Russell,[2] der den Koagulationsprozess mit Suspensionen von einem englischen Ton (Oxford clay) untersucht hat, gefunden, dass sich die Koagulation mit sich vermehrender Elektrolytkonzentration in drei Typen A, B und C einteilen lässt, von denen A die partielle Koagulation mehr oder weniger lyophoben Charakters, B die thixotrope Gelatinierung und C die vollkommene Ausflockung lyophiler Natur darstellt. Eine ähnliche Erscheinung erkannte ich auch mit Suspensionen von einem Ton, der aus einem natürlichen japanischen Wasserstoffton durch Behandlung mit Natriumhydroxyd hergestellt wurde, indem man den Koagulationsprozess makroskopisch und ultramikroskopisch beobachtete. Diese Erfahrungen können im Grunde mit dem oben genannten Gedanken in Einklang gebracht werden.

Der untersuchte Natrium-Ton war thixotrop in seiner 10 prozentigen Suspension in destilliertem Wasser mit der Erstarrungszeit von etwa 6 Stunden. Durch Zusatz von 100–200 Millimol Natriumchlorid wird die Erstarrungszeit auf 15 Sekunden herabgesetzt, während die Suspensionen bei grösseren Elektrolytkonzentrationen unbeständig sedimentieren. Mit verdünnteren Suspensionen (0.4 und 2%) dieses Tons untersuchte man

(1) H. Freundlich, „Thixotropy" Actualités scientifiques et industrielles, No. 267, Paris (1935).

(2) J. L. Russell, *Proc. Roy. Soc.* (London), A, **154** (1936), 550.

die Koagulation unter Zusatz von NaCl, indem man das Sedimentvolumen nach einigen Tagen abliest und dann die Suspensionen durch ein neues Leitzsches Spaltultramikroskop beobachtet. Bei niedrigen Elektrolytkonzentrationen sedimentieren die Teilchen zum Teil, während die obere Flüssigkeit lange getrübt bleibt (partielle lyophobe Koagulation). Bei mittleren Elektrolytkonzentrationen (30–120 Millimol für 0.4 prozentige Suspension, und 15–60 Millimol für 2 prozentige Suspension), bilden die Teilchen mit den vielen Dispersionsmitteln eine uniforme, weiche, mehr oder weniger elastische Masse, wobei das Maximum des Sedimentvolumens aufgewiesen wird (thixotrope Gelatinierung). Bei höheren Elektrolytkonzentrationen flocken sich alle Teilchen in verhältnismässig kurzer Zeit vollkommen aus (lyophile Koagulation).

Noch einleuchtender war dieser Unterschied in den Typen der Koagulation im Feld des Ultramikroskops. Bei niederen Elektrolytkonzentrationen zeigen die Teilchen der Suspension lebhafte Brownsche Rotationsbewegung und teilweise noch Translationsbewegung. Mit steigender Elektrolytkonzentration werden diese Bewegungen allmählich schwächer, gleichzeitig sammeln sich die Teilchen zu Nebelflecken zusammen. In den optimalen Elektrolytkonzentrationen, wo das grösste Sedimentvolumen aufgewiesen ist, sieht man im Mikroskopfeld eine uniform ausgedehnte nebelartige Struktur, in der die Teilchen noch ganz schwache Brownsche Rotationsbewegung ausführen. Bei höheren Elektrolytkonzentrationen wird diese uniforme Struktur in mehrere irregular gebildete Flocken, die im Mikroskopfeld als dicke weisse Wolken glänzend erscheinen, umgewandelt, in denen die Teilchen bewegungslos dicht miteinander zusammenhalten. Im letzten Zustand sieht man jedoch noch einige Teilchen, die im Dispersionsmittel mehr oder weniger frei beweglich sind.

Ein analoges Verhalten findet man in denselben Ton-Suspensionen bei Zusatz von KCl, aber nicht bei Zusatz von $BaCl_2$ oder $AlCl_3$, in welchen letzteren Fällen die Koagulation in allen Elektrolytkonzentrationen fast gleichartig stattfindet, sodass sich kein merklicher Unterschied im Sedimentvolumen sowie im Flockungszustand erkennbar macht. Dies war auch der Fall, als man die Suspensionen von einem elektrodialysierten Wasserstoffton mit NaCl koagulieren liess. In allen diesen Fällen spielt sicherlich der Effekt der Entladung der Teilchen durch zugesetzte Ionen eine Hauptrolle, wobei die Teilchen überhaupt lyophob in dichte Packung eingepackt werden, welche gerade für das Entstehen der thixotropen Gelatinierung nachteilig ist. Die thixotrope Gelatinierung kommt also als eine Zwischenstufe des Koagulationsprozesses zustande, wobei die Teilchen zum Teil lyophob und zum Teil lyophil zu einer uniform gebildeten lockeren Struktur eingebaut sind.

Man könnte dann mit Freundlich[3] annehmen, dass die Thixotropie dadurch zutage tritt, dass die Teilchen in diesem Zustande in eine Gleichgewichtslage kommen, die einem schwachen Minimum der Potentialkurve der abstossenden und anziehenden Kräfte zwischen den Teilchen entspricht. Und zwar sind zwei Teilchen in dieser Gleichgewichtslage noch von einem mit ihrer Grösse vergleichbaren Abstande voneinander getrennt, welchen Abstand hindurch die anziehenden Kräfte wirken würden. Der durchschnittliche Abstand zwischen zwei Teilchen ist für den Fall der von Freundlich und Mitarbeitern[4] untersuchten 14 prozentigen Suspension von Bentonit, dessen Teilchengrösse im Mittel 0.1 μ ist, auf etwa 100 mμ geschätzt. Beinahe die gleichen Umstände gelten für die hier von mir untersuchten Ton-Suspensionen. Für den von mir früher untersuchten Fall der 33 prozentigen Kaolin-Suspensionen[5] bzw. Wasserstoffton-Suspensionen,[6] deren Teilchengrösse im Mittel 1 μ ist, ergibt sich der durchschnittliche Abstand gleich 1 μ, indem ein Teilchen etwa 10^{12} Wassermoleküle um sich trägt, unter Annahme, dass alle Teilchen für die Festigkeit des Systems verantwortlich sind. Die Anziehungskräfte, die in so grossem Abstande noch wirksam sind, kann man auf Grund der neuen quantenmechanischen Theorie der van der Waalsschen Kräfte begreifen.[7] Nach Kallmann und Willstätter,[8] welche versuchten die Londonsche Theorie auf kolloide Systeme zu übertragen, lassen sich die Kräfte zwischen zwei Teilchen folgendermassen ausdrücken: $U=\frac{16}{9}\pi^2 CN^2\left(\frac{r_0}{r}\right)^6$, worin r_0 den Teilchenradius und r den Abstand zwischen zwei Teilchen darstellt. Wie man sieht, ist dieser Ausdruck für einen bestimmten Wert von r_0/r unabhängig von der Teilchengrösse, und zwar für $r_0 \cong 2r$ wird diese Wechselenergie von der Grössenordnung einiger Zehntel Elektronvolt, die gerade gross genug, um das Zusammenhalten der Teilchen gegenüber der Temperaturbewegung aufrechtzuerhalten. Die grossen Teilchen können demnach bei relativ grossen Abständen noch mit Energie $>kT$ einander beeinflussen. Diese Schlussfolgerung macht eben die experimentellen Befunde, dass die Teilchen immer von Abständen, die ihrer Grösse vergleichbar sind, voneinander getrennt sind, verständlich. Dabei nimmt man allerdings an, dass der Typ der Koagulation mit der variierten Elektrolytkonzentration stetig von einem zum anderen übergeht, was an-

(3) H. Freundlich, „Thixotropy," S. 13, Paris (1935).
(4) H. Freundlich, O. Schmidt und G. Lindau, *Kolloid-Beihefte*, **36** (1932), 43.
(5) B. Tamamushi, *J. Chem. Soc. Japan*, **57** (1936), 132.
(6) B. Tamamushi, *Kolloid-Z.*, **79** (1937), 309.
(7) F. London, *Z. physik. Chem.*, B, **11** (1930), 222.
(8) H. Kallmann und M. Willstätter, *Naturwissenschaften*, **20** (1932), 952.

scheinend sowohl nach den Russellschen als auch nach meinen Erfahrungen berechtigt ist. Die Verwendung der neuerdings von Hamaker[9] formulierten Energiekurven soll demnach hier ausser Betracht gestellt werden.

Man beobachtete ferner eine hoch konzentrierte thixotrope Ton-Suspension (10%) unter Ultramikroskop und zwar im festen bzw. flüssigen Zustand. Im flüssigen Zustand, den man durch Hin- und Herbewegung der Gel in Quartzküvette mittels eines Handblasebalges erzielte, erkannte man deutlich Brownsche Rotationsbewegung der Teilchen, während sie nach dem Erstarren des Systems vollkommen bewegungslos wurden. Die Potentialenergie zwischen zwei ruhenden Teilchen übertrifft die kinetische Energie, aber sie muss jedoch genügend klein sein, damit die Struktur durch äusseren mechanischen Effekt leicht zerstört werden kann. Es handelt sich hier so zu sagen um ein stark gequelltes Gitter von sehr kleiner Gitterenergie.

Man stösst nun auf die Frage, ob die Teilchen im festen Zustand durch die Schicht des Dispersionsmittels einzeln voneinander getrennt sind, oder ob sie durch eine orientierte Anlagerung in einem dreidimensionalen Netzwerk, in welchem die Flüssigkeit durch die Netzarme in Kanälen oder in Tunneln gehalten wird, eingebaut sind. Auch wenn die Teilchen unter Ultramikroskop voneinander getrennt erscheinen, kann man nicht einfach daraufhin die erste Möglichkeit annehmen, da das Vorhandensein amikroskopischer Teilchen, die auch für die Thixotropie verantwortlich sind, nicht ausgeschlossen ist.

Rideal und Russell[10] schliessen sich lieber der zweiten Auffassung an, auf Grund der Tatsachen, (1) dass manchmal so verdünnte Sole, in denen man für die Dicke der angenommenen Lyosphere einen unbegreiflich grossen Wert gestatten muss, noch thixotrop sein können, und, (2) dass die thixotropen Sole im allgemeinen Teilchen enthalten, die anisometrisch sowie anisotrop sind.

Der erste Grund soll durch folgende Abschätzung anschaulich gemacht werden. Es sei hier angenommen, dass die Teilchen der Sole oder Suspensionen kugelförmig sind. Berechnet man die Zahl des Wassermoleküls, dessen Radius gleich 2.3×10^{-8} cm. gesetzt ist, die ein Teilchen durchschnittlich trägt, so ergibt sich Tabelle 1, worin einmal Lyosphere um die Teilchen und ein anderesmal dreidimensionales Netzwerk der Teilchen, in welchem die Flüssigkeit enthalten ist, angenommen ist.

(9) H. C. Hamaker, *Rec. trav. chim.*, **55** (1936), 1015; **56** (1937), 3, 727.
(10) E. K. Rideal und J. L. Russell, *Proc. Roy. Soc.* (London), A, **154** (1936), 540.

Tabelle 1.

Radius der Teilchen	Zahl des Wassermoleküle pro Teilchen					
	unter Annahme der Lyosphere		unter Annahme des dreidimensionalen Netzwerkes			
			Teilchen in einer Netzmasche			
	$r = r_0$	$r = \frac{1}{2} r_0$	4—5	10	40—50	100
1 mμ	6×10^{2}	2×10^{2}	2×10^{2}	10^{3}	2×10^{4}	10^{5}
10 mμ	6×10^{5}	2×10^{5}	2×10^{5}	10^{6}	2×10^{7}	10^{8}
100 mμ	6×10^{8}	2×10^{8}	2×10^{8}	10^{9}	2×10^{10}	10^{11}
1 μ	6×10^{11}	2×10^{11}	2×10^{11}	10^{12}	2×10^{13}	10^{14}
10 μ	6×10^{14}	2×10^{14}	2×10^{14}	10^{15}	2×10^{16}	10^{17}

Die Zahl der Wassermoleküle, die in der Netzwerkstruktur enthalten ist, ist also immer grösser als die in der Lyosphere, soweit eine Netzmasche mindestens aus 10 Teilchen besteht. Berechnet man ferner die Wassermoleküle pro Teilchen je nach der variierten Konzentration der Sole oder Suspensionen, indem man die Dichte des Teilchens gleich 2 setzt, so bekommt man die Ergebnisse der Tabelle 2, woraus man sieht, dass die grössere Zahl der Wassermoleküle bei geringeren Konzentrationen gerade nur durch die Netzwerkstruktur umfasst werden kann. Eine Lyosphere grösserer Dicke kann man allerdings nicht annehmen, soweit man für die Anziehungskräfte die Potentialenergie $>kT$ gestatten muss.

Tabelle 2.

Radius der Teilchen	Zahl der Wassermoleküle pro Teilchen je nach der Konzentration der Suspension			
	10%	1%	0.1%	0.01%
1 mμ	2.7×10^{3}	2.7×10^{4}	2.7×10^{5}	2.7×10^{6}
10 mμ	2.7×10^{6}	2.7×10^{7}	2.7×10^{8}	2.7×10^{9}
100 mμ	2.7×10^{9}	2.7×10^{10}	2.7×10^{11}	2.7×10^{12}
1 μ	2.7×10^{12}	2.7×10^{13}	2.7×10^{14}	2.7×10^{15}
10 μ	2.7×10^{15}	2.7×10^{16}	2.7×10^{17}	2.7×10^{18}

Es scheint demnach sehr berechtigt zu sein für thixotrope Systeme geringer Konzentrationen eine Struktur des dreidimensionalen Netzwerkes

anzunehmen, während eine Annahme der Lyosphere dabei unbefriedigend ist. Das sich die kugeligen Teilchen im Netzwerk linear einander anlagern werden, hat auch einen theoretischen Grund, welcher von Usher[11] angedeutet worden ist. Die neueren ultramikroskopischen Untersuchungen von Hauser und Reed[12] an Bentonit-Suspensionen sprechen auch für die Annahme der Strukturbildung des Netzwerkes.

Der zweite Grund, dass die Teilchen meistens anisometrisch und anisotrop sind, ist auch ohne Zweifel günstig für die Strukturbildung eines Netzwerkes oder einer Zone. Eine so orientierte Anlagerung der stark anisometrischen Teilchen könnte eventuell durch die regelmässige langsame Bewegung des Systems veranlasst werden, und dadurch wird das System schneller zur Erstarrung gebracht werden. Diese Erscheinung, die Rheopexy genannt ist, ist in der Tat zuerst von Freundlich und Juliusburger[13] z. B. bei thixotropen Gyps-Suspensionen und V_2O_5-Solen entdeckt worden. Immerhin müssen sich die Teilchen bei so orientierter Anlagerung in einem Gleichgewicht befinden, und sie müssen dabei locker, eventuell durch die Schicht des Dispersionsmittels getrennt, aneinander gebunden sein, sodass die Orientierung durch mechanischen Effekt leicht zerstört wird. Die Erstarrungszeit ist dann die Zeit, in der die einmal relaxierten Teilchen wieder zur Orientierung gebracht werden.

Wenn man nun die thixotrope Gelatinierung als Zwischenstufe der lyophoben und lyophilen Koagulation auffasst, so ergibt sich die Möglichkeit, dass das thixotrope System durch die Mischung von lyophoben und lyophilen Teilchen realisiert wird. Bary[14] deutete darauf hin, dass alle thixotropen Systeme eine Mischung von lyophoben und lyophilen Bestandteilen sind, wo die Gelatinierung durch die gegenseitige Orientierung dieser zwei Bestandteile zustande kommt.

Dass ein lyophobes, nicht thixotropes Material unter Zusatz eines lyophilen Materials thixotrop wird, ist in der Tat z. B. in der Rideal- und Russellschen Untersuchung[10] demonstriert worden, in welcher eine nicht thixotrope Quartz-Suspension bei Zusatz von einer sehr geringen Menge kolloidalen Aluminiumoxyds deutlich thixotrop gemacht werden konnte. Auch nicht thixotrope $BaSO_4$-Suspensionen werden durch Mischung mit Natrium-Ton thixotrop. Mit $BaSO_4$ allein, ist seine 30 prozentige Suspension weder thixotrop noch plastisch, während eine Mischung von 29.85 prozentigem $BaSO_4$ und 0.15 prozentigem Na-Ton in destilliertem Wasser

(11) Usher, *Proc. Roy. Soc.* (London), A, **125** (1929), 143.
(12) E. A. Hauser und C. E. Reed, *J. Phys. Chem.*, **41** (1937), 911.
(13) H. Freundlich und F. Juliusburger, *Trans. Faraday Soc.*, **31** (1935), 920.
(14) Bary, *Compt. rend.*, **196** (1933), 183.

bedeutende thixotrope und plastische Eigenschaften erwirbt.[15] Experimentiert man dabei mit gröberen Teilchen von $BaSO_4$ einerseits und mit feineren Teilchen anderseits, so tritt die Thixotropie bzw. Plastizität bei feineren Teilchen in stärkerem Masse auf. Hier erkennt man den Einfluss der Teilchengrösse auf die Thixotropie. Der Mechanismus, ob das lyophile Material durch nicht thixotrope lyophobe Teilchen adsorbiert wird, sodass sie genug Wasser um sich binden und demnach eine stark gelockerte Struktur bilden können, oder die beiden lyophilen und lyophoben Bestandteile durch eine orientierte Anlagerung zu einem Netzwerk eingebaut werden, kann doch von Fall zu Fall verschieden sein.

Um in den Mechanismus der Thixotropie weiter einzudringen, wäre es erwünscht Kenntnisse über die Mobilisierung bzw. Immobilisierung des Dispersionsmittels im flüssigen bzw. festen Zustande zu gewinnen, wozu wahrscheinlich die Messung des Dampfdrucks in den beiden Zuständen von Nutzen sein kann. Dieser von Herrn Professor Katayama freundlicherweise mündlich mitgeteilte Hinweis soll noch in Zukunft bearbeitet werden.

Zusammenfassung.

Auf Grund der Untersuchung des Koagulationsprozesses, die mit Suspensionen von einem Natrium-Ton durchgeführt wurde, ist festgestellt, dass die thixotrope Gelatinierung als Zwischenstufe von zwei extremen Zuständen, nämlich der partiellen lyophoben Koagulation einerseits und der vollkommenen lyophilen Ausflockung anderseits, auftritt.

Im Fall von konzentrierten thixotropen Suspensionen (grösser als etwa 10%), ist die Theorie der Lyosphere befriedigend, wobei man zwischen zwei Teilchen weitreichende van der Waalssche Kräfte annimmt. Dagegen bei thixotropen Systemen von geringeren Konzentrationen ist die Struktur eines dreidimensionalen Netzwerkes mit Recht annehmbar. Die Umstände, dass die Teilchen anisometrisch und anisotrop sind, begünstigen auch die Theorie der Strukturbildung eines orientierten Netzwerkes.

Dass ein thixotropes System durch Mischung von lyophilen und lyophoben Bestandteilen zu Tage tritt, wird demonstriert, indem man lyophoben nicht thixotropen $BaSO_4$-Suspensionen eine geringe Menge lyophilen Natrium-Ton zusetzt.

Nedzu Chemisches Laboratorium,
Musashi Hoch-Schule,
Itabashiku, Tokyo.

(15) Unveröffentliche Versuche von H. Sekiguchi.

See errata
V. 13, P. 69k

The Adsorption of Helium on Charcoal below 78°K., and Production and Thermometry of Low Temperatures.

see errata Vol. 13, P 694

By Eizo KANDA.

(Received January 17, 1938.)

The production of lower temperatures by pumping off the adsorbed gas at a low temperature was first tried by Simon.[1] Recently Keyes and his coworkers[2] indicated, in the process of liquefying hydrogen, the practicability of refrigeration at temperatures near 40°K. by desorption of the hydrogen adsorbed at 63°K. The present author intended to obtain various low temperatures between the triple point of hydrogen (14.0°K.) and the boiling point of helium (4.2°K.) without using the helium liquefying apparatus. The desorption of helium is an excellent method for this purpose, but the adsorption of this gas on charcoal at such low temperatures has scarcely been studied.[3] The author determined the adsorption of helium below 78°K. The temperature below 14°K. was determined with the helium gas thermometer, and the resistance thermometers of constantan and of manganin were calibrated.

Adsorption of Helium. Helium gas used in the adsorption experiment was imported from America and its quality was 95%. The gas used for the gas thermometer was obtained through heating the monazite sand over 750°C., the crude gas was purified through the adsorption on charcoal cooled by liquid nitrogen and by liquid hydrogen respectively. Charcoal at 21°K. adsorbs even the traces of admixed gases together with a small part of helium. The apparatus was very analogous to that of Fig. 1 used in the adsorption experiment.

Experiment on Adsorption. The apparatus is shown in Fig. 1. The activated charcoal is in C. The volume of the gas adsorbed was measured with the burette B. The low temperature was obtained by means of liquid hydrogen or solid hydrogen. The amount of the adsorbent was almost 5 g.

The volume of the helium adsorbed per gram of charcoal at various temperatures and pressures is shown in Table 1. The adsorption isotherms are shown in Fig. 2.

(1) Simon, *Physik. Z.*, **27** (1926), 790.
(2) Keyes, Gerry, and Hicks, *J. Am. Chem. Soc.*, **59** (1937), 1426.
(3) Dewar. *Ann. chim. phys.*, [8], **3** (1904), 5.

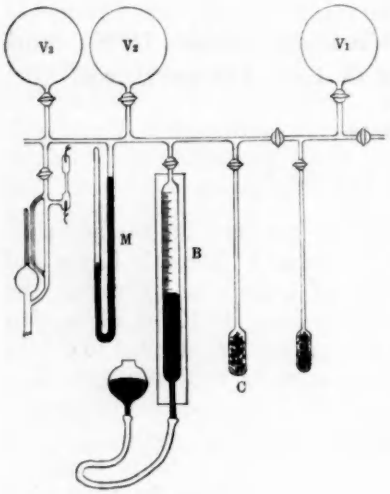

Fig. 1.

Table 1.

Press. (cm.) / Temp. (°K.)	30	50	76
78.1	4	6	11
53.5	12	15	26
21.3	108	150	180
15.0	192	255	300
12.9	244	310	360

The heat of sorption was determined preliminarily with an evaporation method. It amounts to 1.2 kcal. per mol helium and is much smaller than Dewar's value.[3] The value calculated from the adsorption isotherms according to Clapeyron-Clausius equation deviates largely from the observed value.

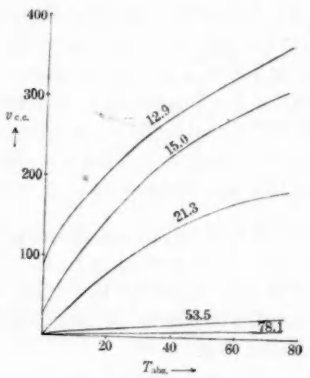

Fig. 2.

Production of Low Temperatures by Desorption. The apparatus was shown in Fig. 3.

Hydrogen or helium gas was introduced into C through V_2, and the charcoal in D was cooled by liquid hydrogen in the vessel B through the gaseous conduction. Helium gas was introduced into D through V_1 and was adsorbed on charcoal isothermally. After the saturation of adsorption was reached the gas for conduction in C was evacuated and the charcoal became adiabatic from the liquid hydrogen.

Adsorbed helium was pumped off as fast as possible. The temperature of the charcoal and the apparatus in D was lowered. In Fig. 3, G shows the bulb of the helium gas thermometer. The lowering of the

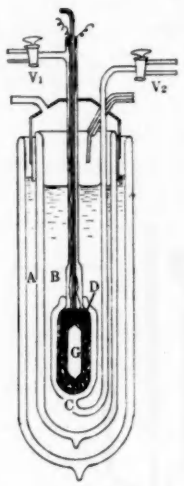

Fig. 3

temperature is dependent on (i) the dimension and adiabatic condition of the apparatus, (ii) the amount of charcoal, (iii) the amount of the adsorbed gas, (iv) the velocity of desorption, and (v) the initial temperature. In practice a large part of the heat of desorption was consumed against the thermal conduction from outward. The lowest temperature obtained in this trial was 5.8°K. To obtain any desired final temperature in certain apparatus containing the fixed amount of charcoal the author controlled the pressure of helium at which the adsorption took place. For example in an apparatus containing 17 g. of charcoal the various final temperatures reached are shown in Table 2. The initial temperature was 14.9°K.

The relation between the final temperature and the pressure at which the adsorption took place was shown in Fig. 4, where the amount of the charcoal was somewhat varied.

Table 2.

Pressure of helium (cm.)	Volume of adsorbed gas (l.)	Final temperature (°K.)
20	2.0	14.4
45	3.6	10.9
59	4.3	9.0
76	5.0	7.2
88	6.1	6.1

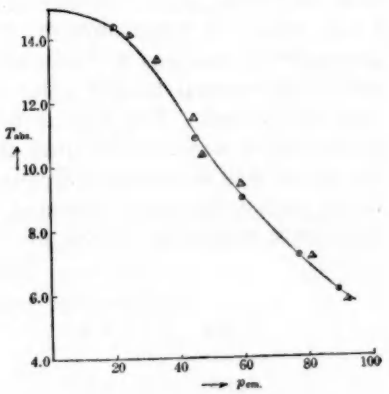

Fig. 4

Helium Gas Thermometer. The construction of the helium thermometer is very analogous to the hydrogen thermometer constructed by the present author,[4] but some modifications have been added. It is shown in Fig. 5. The thermometer bulb is of Pyrex glass and has a cylindrical cavity C in its centre for the resistance thermometer to be calibrated.

(4) Aoyama and Kanda, this Bulletin, **10** (1935), 472.

A is the adjustor of the mercury level having a thin iron plate and a screw.

The volume of the bulb V is 112.974 c.c. This volume, the capillary of the bulb, and the space of the mercury manometer have to be corrected for the thermal expansion. The linear expansion coefficient of the Pyrex glass is given in Table 3.

The temperature can be determined according to the equation:[4]

$$t = \frac{1}{\beta}\left[\frac{p_t V_0'}{p_0\left\{V_0 + \frac{V_s}{1+\beta t_s}\right\} - p_t \frac{V_s'}{1+\beta t_s}} - 1\right],$$

where V_s and t_s are the volume and the temperature of the dead space respectively, and p_0 is the pressure of the helium when the bulb is at 0°C. The pressure coefficient β of helium has a value $\beta = 0.00366072$.[5] To check the accuracy of the gas thermometer measurements the normal boiling point of hydrogen was determined. The vapour pressure tube of hydrogen was inserted into the cavity of the thermometer bulb and the whole was surrounded by liquid hydrogen. The equilibrium pressure in the vapour pressure tube and the temperature of the liquid hydrogen bath were measured (Table 4).

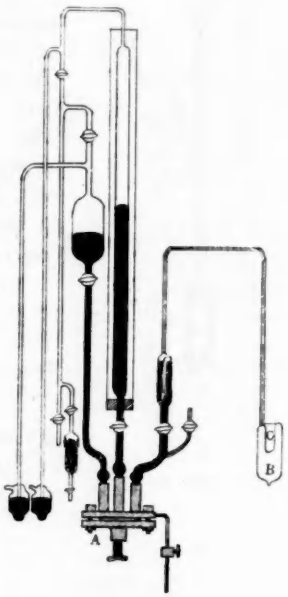

Fig. 5

Table 3.

T(°K.)	273	210	90	21
$\alpha \times 10^5$	0.35	0.30	0.10	0.05

Table 4.

p(mm.)	755.10	763.05	768.95	772.05
t(°C.)	−252.75	−252.72	−252.69	−252.68

(5) Keesom, Van der Horst, and Taconis, *Physica*, **1** (1933), 324.

The normal boiling point becomes −252.73°C. This is in good agreement with the values of other authors: Keesom, Bijl, and Van der Horst[6] −252.75°; Otto and Heuse[7] −252.78°; and Southard and Milner[8] −252.76°.

Calibration of Resistance Thermometer. The resistance thermometer is of a four lead type. The coil was set in the cylindrical cavity of the bulb of the gas thermometer and was buried by the charcoal. The results of calibration are shown in Table 5.

Table 5.

Constantan resistance thermometer. $R_0 = 49.150$

t (°C.)	R/R_0
−195.72	0.9945
−252.45	0.9728
−256.33	0.9687
−259.65	0.9637
−263.50	0.9544
−265.15	0.9487

Manganin resistance thermometer. $R_0 = 98.451$

t (°C.)	R/R_0
−194.98	0.9588
−252.66	0.9184
−254.95	0.9168
−257.32	0.9158
−259.81	0.9133
−262.40	0.9113
−264.51	0.9095
−266.59	0.9076
−267.33	0.9067

Both of constantan and manganin have very small temperature coefficients of electric resistance, but their resistances decrease monotonously down to the very low temperature near absolute zero. We can use them as thermometers for extreme low temperatures.

Summary.

The adsorption of helium on charcoal below to 78°K. was measured and the heat of sorption was determined. Systematical trials of the desorption method for the purpose of obtaining low temperatures without liquid helium were described. Resistance thermometers of manganin

(6) Keesom, Bijl, and Van der Horst, *Proc. Roy. Soc. Amsterdam*, **34** (1931), 78.
(7) Otto and Heuse, *Ann. Physik*, [5], **9** (1931), 486.
(8) Southard and Milner, *J. Am. Chem. Soc.*, **55** (1933), 4378.

and of constantan were calibrated with the helium gas thermometer down to 6°K.

The author wishes to express his sincere thanks to Prof. S. Aoyama who directed him throughout this work. He also wishes to express his heartful thanks to Prof. M. Katayama of Tokyo Imperial University who encouraged him incessantly. Thanks are also due to the Japan Society for the Promotion of Scientific Research for a grant.

Cryogenic Section, Research Institute
for Iron, Steel and Other Metals,
Tohoku Imperial University.